

**SYNTHESIS AND CHARACTERIZATION OF FUSED  
CONJUGATED MATERIALS FOR ORGANIC  
ELECTRONICS**

**GANAPATHY BALAJI**

**NATIONAL UNIVERSITY OF SINGAPORE  
2010**

**SYNTHESIS AND CHARACTERIZATION OF FUSED  
CONJUGATED MATERIALS FOR ORGANIC  
ELECTRONICS**

**GANAPATHY BALAJI**

*(M. Sc. Indian Institute of Technology - Madras, India)*

**A THESIS SUBMITTED  
FOR THE DEGREE OF DOCTOR OF PHILOSOPHY**

**DEPARTMENT OF CHEMISTRY  
NATIONAL UNIVERSITY OF SINGAPORE  
2010**

## ACKNOWLEDGEMENTS

I would like to express my sincere gratitude to my supervisor Prof. Suresh Valiyaveetil for his full support and constant encouragement.

I sincerely thank all the current and former members of the group for their cordiality and friendship. I thank Dr. Ani Deepti, Ankur, Anuradha, Asha, Ashok, Dr. Bindu, Colin, Elena, Dr. Fathima, Dr. Hairong, Haiyu, Dr. Gayathri, Dr. Jegadesan, Jhinuk, Dr. Jinu, Kirubakaran, Dr. Manoj, Narahari, Nizar, Dr. Nurmawati, Pradipta, Prasana, Ramakrishna, Dr. Rajeev, Dr. Sangita, Sajini, Dr. Santosh, Dr. Sathya, Dr. Sindhu, Dr. Sivamurugan, Sheeja, Thirumal, Dr. Velmurugan, Dr. Vetrichelvan, Yean Nee and Yiwei for all the good times in the lab and helping exchange knowledge skills. I also extend thanks to my Honour's students Jasmeet, Daisy, Dazril, Chan, and former Master's student Low shim for accompanying me in synthesis and for their cooperation.

I acknowledge the technical assistance provided by the staff of Chemical, Molecular and Materials Analysis Centre (CMMAC) for recording NMR, Mass spectrometry, Elemental Analyses and Thermal Analysis Laboratories at NUS. My sincere thanks to Madam Tan Geok Kheng for single crystal X-ray diffraction experiments and data refinement. I also extend my sincere thanks to Dr. Vijila and Mr. Tan Mein Jin of Institute of Materials Research and Engineering for their assistance in measuring the transport properties. I thank National University of Singapore for the scholarship.

My deepest gratitude to all my family members for their understanding, moral support and encouragement.

## TABLE OF CONTENTS

---

Acknowledgments	ii
Table of contents	iii
Summary	viii
List of Tables	xii
List of Figures	xiii
List of Schemes	xix
Abbreviations and Symbols	xxi

---

### Chapter 1

---

1.	General introduction	2
1.1.	Conjugated polymers: controlling the band gap	4
1.2.	Fused conjugated systems	7
1.2.1.	[ <i>n</i> ]acene systems	7
1.2.2.	Heteroacene systems	10
1.2.2.1.	Theinenoacene	12
1.2.2.2.	Thiophene-benzene annulated acenes	15
1.2.2.3.	Indolocarbazole	18
1.2.3.	Helicene and circulenes	22
1.2.4.	$\beta,\beta'$ -Bridged bithiophenes	26
1.2.5.	Ladder polymers	30

1.2.6.	Heteroacene polymers	35
1.2.7.	Other thiophene fused systems	36
1.3.	Aim and scope of the thesis	40
1.4.	References	42

---

## Chapter 2

---

2.1.	Introduction	50
2.2.	Experimental	51
2.2.1.	Materials and measurements	51
2.2.2.	Synthesis procedure	52
2.3.	Results and discussion	56
2.3.1.	Synthesis	56
2.3.2.	Single crystal X-ray structure and crystal packing	59
2.3.3.	Optical properties	61
2.3.4.	Electrochemical properties	63
2.4.	Conclusion	65
2.5.	References	67

---

## Chapter 3

---

3.1.	Introduction	70
3.2.	Experimental	71
3.2.1.	Materials	71
3.2.2.	Instrumentation	71

3.2.3.	Synthesis procedure	73
3.3.	Results and discussion	80
3.3.1.	Synthesis	80
3.3.2.	X-ray structure	81
3.3.3.	Optical properties	84
3.3.4.	Electrochemical properties	85
3.4.	Conclusion	89
3.5.	References	90

---

#### **Chapter 4**

---

4.1.	Introduction	93
4.2.	Experimental section	94
4.2.1.	Materials	94
4.2.2.	Instrumentation	95
4.2.3.	Synthesis procedure	96
4.3.	Results and discussion	99
4.3.1.	Synthesis	99
4.3.2.	Single crystal XRD	99
4.3.3.	Optical properties	100
4.3.4.	Electrochemical properties	103
4.3.5.	Electropolymerization	104

4.4.	Conclusion	107
4.5.	References	109

---

### Chapter 5

---

5.1.	Introduction	112
5.2.	Experimental	114
5.2.1.	Materials	114
5.2.2.	Spectroscopic characterization	114
5.2.3.	Synthesis procedure	116
5.3.	Result and discussion	120
5.3.1.	Synthesis	120
5.3.2.	X-ray crystal structure	120
5.3.3.	Optical properties	123
5.3.4.	Electrochemical properties	126
5.3.5.	Surface morphology	129
5.3.6.	Charge transport properties	131
5.4.	Conclusion	141
5.5.	Reference	143

---

### Chapter 6

---

6.1.	Introduction	147
6.2.	Experimental	149
6.2.1.	Materials and method	149

6.2.2.	Instrumentation	150
6.2.3.	Synthesis procedure	151
6.3	Results and discussion	155
6.3.1.	Synthesis	155
6.3.2.	Single crystal XRD	158
6.3.3.	Absorption properties	159
6.3.4.	Emission properties	162
6.3.5.	Acid-Base sensing	165
6.3.6.	Electrochemical properties	167
6.3.7.	Ionochromic effect of oligomers	170
6.3.8.	Amino acid sensing	173
6.3.9.	Charge mobility	174
6.3.10.	Electropolymerization	176
6.3.11.	Optical and electrical properties of polymers	179
6.4.	Conclusion	181
6.5.	References	183
<hr/>		
	Appendix	186
	List of Publications	195
<hr/>		



## *Summary*

The conjugated organic molecules emerged as a potential organic semiconducting material due to the presence of  $\pi$ -electrons and are extensively employed in organic electronics. Fused  $\pi$ -conjugated systems are an interesting class of conjugated systems due to their high solid-state ordering, higher stability, and better device performance. Over last 20 years, considerable research have been dedicated to synthesize new fused ring systems based on thiophene/pyrrole units with improved properties and processability. In this research effort, we introduce a series of dithieno[3,2-*b*]pyrrole, indolo[2,3-*a*]carbazole and thieno[3,4-*d*]imidazole based fused conjugated oligomers and polymers. The present thesis delineates the various aspects of these newly synthesized systems, such as solid-state packing, optical and electrochemical properties, thin film morphology, time-of-flight mobilities, sensing behavior, and electropolymerizations of the oligomers and the optoelectronic properties of the resultant polymers. The following section describes a detailed summary of each chapter in the thesis.

A detailed review of literature related to the discovery of conjugated systems with special emphasis to the fused ring compounds is given in *chapter one*. In addition the device performance of various heteroacenes and the synthesis and properties of dithieno[3,2-*b*]pyrrole and other fused thiophene systems are reviewed. Finally, a detailed scope and outline of the present thesis is also included.

The heteroatom analogue of [*n*]acenes called heteroacene is gaining increased attention in developing new materials for electronic applications. Most of the known heteroacenes are symmetrical in nature and only a few unsymmetrical heteroacenes are reported. In *chapter two*, a series of symmetrical and unsymmetrical

dibenzodithenopyrrole with varied *N*-substituents were synthesized and characterized. The crystal packing and the optoelectronic properties of symmetrical and unsymmetrical heteroacenes are compared and presented in this chapter.

The incorporation of heteroatoms into fused ring endows the stability to such systems. Hence, heteroacene opens up the possibility of synthesizing extended ladder oligomers. However, most of the reported heteroacenes are five units fused systems and only a few reports describe the synthesis and properties of extended heteroacenes. The *chapter three*, discuss the synthesis of a series of highly stable and soluble unsymmetrical and extended heteroacenes (seven units fused) containing thiophene and pyrrole units. Their packing behavior and optoelectronic properties are also discussed in detail.

In *chapter four*, indolo[2,3-*a*]carbazole-based heteroacenes containing thiadiazole units were synthesized and characterized. The change in photophysical and electrochemical properties upon incorporation of an acceptor moiety (benzothiadazole) in fused ring system was studied. The effect of thiadiazole fusion on the crystal packing of indolocarbazole unit was also unveiled. The unsubstituted compound was electropolymerized to yield the first electropolymerized polyindolocarbazole. The optoelectronic properties of the polyindolocarbazole were also studied.

Among the  $\pi$ -conjugated systems, for electronic applications oligomers possesses the advantage of well-defined structures and their accessibility in pure state. In recent days, dithieno[3,2-*b*]pyrrole based polymers are gaining significant attention in field effect transistor and photovoltaic applications. In *chapter five*, a series of highly fluorescent solution processable dithieno[3,2-*b*]pyrrole based oligomers were synthesized

and characterized. Their molecular ordering in solid state, photophysical and electrochemical properties along with their surface morphology were studied and compared with the parent compound. The mobilities of the charge carriers are studied by time-of-flight photoconductivity method. The temperature and field dependence of the transport properties are also explored.

In *chapter six*, a new series of thieno[3,4-*d*]imidazole based oligomers and polymers were synthesized. Poly(isothianaphene), poly(thienopyrazine), poly(thienothiophene) represents a group of low bandgap polymers constructed from thiophene. However, the material (electronics) aspect of the similar compound (thieno[3,4-*d*]imidazole) was not yet explored. Thienoimidazole skeleton resembles Biotin (Vitamin H), and hence are studied extensively for biological applications. In *chapter six*, we discuss the synthesis, solid state packing, photophysical, electrochemical properties and time-of-flight mobility of dithienothieno[3,4-*d*]imidazole-based oligomers. The metal ion and aminoacid sensing behavior of this versatile building block were explored in detail. These oligomers are also electropolymerized to result in low bandgap polymers. The photophysical and electrochemical properties of the polymers were also discussed.

Among the compounds discussed, the heteroacenes mentioned in chapter 2, 3 and 4 are potential candidate for OFET application. Among these heteroacenes thiadiazole fused indolo[2,3-*a*]carbazole based heteroacenes are expected to show better OFET mobility due to their close packing in solid state accompanied with high lying HOMO and good solubility. But, all these heteroacenes are not solution processable and their thin films need to be obtained only by chemical vapor deposition (CVD). On the other hand

oligomer DTP-PHE represented in chapter 5, is solution processable and the solution casted films showed highly crystalline grains of  $\mu\text{m}$  size. DTP-TPA is crystalline and also showed a good solid state quantum yield, indicating the potentiality of this compound towards organic light emitting field effect transistor (OLEFET) applications. DTP-FLU with reversible oxidation behavior and high solid state fluorescence is a potential material for OLED applications. Thieno[3,4-*d*]imidazole based polymers showed reduced bandgap, with broader absorption covering the entire visible spectrum can be expected to show promising performances in OPV devices.

## LIST OF TABLES

No.	TABLES	Page No.
<b>Table 1.1.</b>	Summary of FET mobilities and processing information of <i>p</i> -type heteroacenes	20
<b>Table 2.1.</b>	Photophysical and electrochemical properties of unsymmetrical and symmetrical heteroacenes	65
<b>Table 3.1.</b>	Photophysical and electrochemical properties of indolodithienopyrrole and diindolodithienopyrrole	88
<b>Table 4.1.</b>	Photophysical properties of thiadiazole fused indolocarbazoles recorded in THF	101
<b>Table 4.2.</b>	Electrochemical properties of thiadiazole fused indolocarbazoles derivatives recorded using cyclic voltammetry	103
<b>Table 5.1.</b>	Optical properties of DTP oligomers in solution and solid state	126
<b>Table 5.2.</b>	Electrochemical properties of DTP-oligomers recorded in dichloromethane containing 0.1 M <i>n</i> -Bu <sub>4</sub> NPF <sub>6</sub> as supporting electrolyte	128
<b>Table 5.3.</b>	Hole mobility of DTP-oligomers	134
<b>Table 5.4.</b>	Charge transport parameters of <b>DTP-FLU</b> calculated using Gaussian disorder model (GDM) and Correlated disorder model (CDM)	140
<b>Table 6.1.</b>	Photophysical properties of dithienothieno[3,4- <i>d</i> ]imidazole ( <b>T1-T7</b> )	164
<b>Table 6.2.</b>	The absorption and emission maxima of dithienothieno[3,4- <i>d</i> ]imidazoles upon addition of CF <sub>3</sub> COOH and NaOH in THF	166
<b>Table 6.3.</b>	Electrochemical properties of dithienothieno[3,4- <i>d</i> ]imidazole oligomers ( <b>T1-T7</b> )	169

<b>Table 6.4.</b>	Optoelectronic properties of electropolymerized dithienothieno[3,4- <i>d</i> ]imidazole polymers	181
-------------------	--	-----

---

### LIST OF FIGURES

---

No.	FIGURES	Page No.
<b>Figure 1.1.</b>	Chemical structure of some common $\pi$ -conjugated polymers	3
<b>Figure 1.2.</b>	Energy band structure of conjugated polymers emerging from the energetic splitting upon addition of an increasing number of atomic orbitals	5
<b>Figure 1.3.</b>	The quinoid form forces the rings to align in a planar conformation leading a low bandgap of 0.47 eV. The aromatic form allows the thiophene to rotate with a certain degree of rotational freedom results in bandgap of 2 eV	7
<b>Figure 1.4.</b>	Structure of reported [ <i>n</i> ]acene systems	8
<b>Figure 1.5.</b>	Possible degradation products of pentacene	10
<b>Figure 1.6.</b>	Structures of heteroacene compounds	11
<b>Figure 1.7.</b>	Structures thieno[ <i>n</i> ]acene based compounds	12
<b>Figure 1.8.</b>	Structure of thiophene-benzene annealed heteroacenes employed for FET application	15
<b>Figure 1.9.</b>	Structures of helicenes and circulenes	23
<b>Figure 1.10.</b>	Structures of $\beta, \beta'$ -bridged bithiophenes	26
<b>Figure 1.11.</b>	Chemical structures of heteroacene polymers	35

<b>Figure 1.12.</b>	Structure of thiophene, benzene annealed to thiophene system	36
<b>Figure 1.13.</b>	Aromatic resonance stabilization of isothianaphthene (ITN)	37
<b>Figure 1.14.</b>	Resonance structure of poly(isothianaphthene)	37
<b>Figure 1.15.</b>	5,7-di(2-thienyl)thieno[3,4- <i>b</i> ]pyrazine	39
<b>Figure 2.1.</b>	Structures of symmetric and unsymmetric heteroacenes	51
<b>Figure 2.2.</b>	Thermal ellipsoid plot and packing of <b>1a</b> (A), <b>1b</b> (B) and <b>2b</b> (C)	60
<b>Figure 2.3.</b>	UV-vis spectra of symmetric and unsymmetric heteroacenes	61
<b>Figure 2.4.</b>	The molecular structure of 5,6-dimethyldiindolo[3,2- <i>b</i> :4,5- <i>b'</i> ]thiophene ( <b>11</b> )	62
<b>Figure 2.5.</b>	Cyclic voltammogram of unsymmetric and symmetric heteroacenes recorded in dichloromethane containing 0.1 M <i>n</i> -Bu <sub>4</sub> NPF <sub>6</sub> as supporting electrolyte	64
<b>Figure 3.1.</b>	Structure of synthesized unsymmetric and extended heteroacenes	70
<b>Figure 3.2.</b>	Thermal ellipsoid plot of extended heteroacene ( <b>10a</b> ) (A). Phenyl group tilted from the heteroacene plane (B). Bowed nature of heteroacene backbone (C). Hydrogen atoms are removed for clarity	81
<b>Figure 3.3.</b>	Crystal packing of extended heteroacene ( <b>10a</b> ) in lattice (A). Thermal ellipsoid plot of dimer of <b>10a</b> (B)	82
<b>Figure 3.4.</b>	Thermal ellipsoid plot of unsymmetric heteroacene <b>9b</b> (A). Lateral view showing the bowed nature of	83

	heteroacene (B). Hydrogen atoms are removed for clarity	
<b>Figure 3.5.</b>	Packing of unsymmetrical heteroacene ( <b>9b</b> ) in crystal lattice (A). Hydrogen atoms are removed for clarity. Thermal ellipsoid plot of <b>9b</b> dimer (B)	84
<b>Figure 3.6.</b>	Normalized UV-vis absorption and emission spectra of extended diindolodithienopyrrole (A) and unsymmetric indolodithienopyrrole (B) recorded in THF	85
<b>Figure 3.7.</b>	Cyclic voltammogram of extended diindolodithienopyrrole and unsymmetric indolodithienopyrrole recorded in dichloromethane	86
<b>Figure 3.8.</b>	Repeated CV scan of <b>7a</b> using Pt as working electrode at scan rate of 100 mV/s	87
<b>Figure 4.1.</b>	Chemical structures of five isomers of indolocarbazole	93
<b>Figure 4.2.</b>	Structure of synthesized thiadiazole fused indolo[2,3- <i>a</i> ]carbazole based molecules	94
<b>Figure 4.3.</b>	Thermal ellipsoid plot of <b>5a</b> (A). Packing diagram of <b>5a</b> along <i>a</i> -axis. Hydrogen atoms removed for clarity (B)	100
<b>Figure 4.4.</b>	Normalized absorption spectra (A) and emission spectra (B) of thiadiazole fused indolocarbazole derivatives in THF	101
<b>Figure 4.5.</b>	Emission spectra of compound <b>4</b> in various solvents	102
<b>Figure 4.6.</b>	Cyclic voltammogram of thiadiazole-fused indolocarbazole based acenes	104
<b>Figure 4.7.</b>	Electro polymerization of <b>4</b> from acetonitrile solution at a scan rate of 100 mV/S (A). Linear relationship of increase in current with number scans (B)	105



<b>Figure 4.8.</b>	IR spectrum (A) and AFM image of (B) of electrodeposited polymers	106
<b>Figure 4.9.</b>	Cyclic voltamogram of polymer in monomer free acetonitrile with TBAPF <sub>6</sub> as supporting electrolyte (A). Solid state absorption spectra of electropolymerized polymer film (B)	107
<b>Figure 5.1.</b>	Molecular structures of synthesized DTP-oligomers	113
<b>Figure 5.2.</b>	Thermal ellipsoid plot of <b>DTP-TPA</b>	121
<b>Figure 5.3.</b>	Crystal packing along <i>a</i> -axis (A) and packing of two adjacent columns (B) of <b>DTP-TPA</b> . Hydrogen atoms are removed for clarity	122
<b>Figure 5.4.</b>	Normalized absorption spectra in solution state (THF) (A), in solid state (B) and emission spectra in solution state (THF) (C) and in solid-state (D) spectra of DTP oligomers	123
<b>Figure 5.5.</b>	CIE coordinate in film sample of <b>DTP-FLU</b> (x=0.2422, y=0.5019, z=0.2559)	125
<b>Figure 5.6.</b>	Cyclicvoltammogram of DTP oligomers in dichloromethane containing 0.1 M <i>n</i> -Bu <sub>4</sub> NPF <sub>6</sub> at the scan rate of 100 mV/s	127
<b>Figure 5.7.</b>	Tapping mode AFM images shows the surface morphology of the spin coated oligomers (A) <b>DTP-FLU</b> (10 μm × 10 μm) and (B) Magnified image of A (5 μm × 5 μm). (C) <b>DTP-PHE</b> (10 μm × 10 μm) and (D) Magnified image of C (5 μm × 5 μm), (E) the same sample after annealing at 60 <sup>0</sup> C for 20 minutes (10 μm × 10 μm) and (F) Magnified image of E (5 μm × 5 μm). (G) <b>DTP-CAR</b> (5 μm × 5 μm) and (H) <b>DTP-TPA</b> (1 μm × 1 μm)	130,131
<b>Figure 5.8.</b>	The linear plot of TOF hole transients for <b>DTP-PHE</b> (A) and <b>DTP-TPA</b> (B). The inset of A is the corresponding integrated plot of <b>DTP-PHE</b> and inset of B is the corresponding log-log plot of	133

	<b>DTP-TPA.</b> Variation of TOF hole mobility with applied electric field for <b>DTP-PHE</b> (C) and <b>DTP-TPA</b> (D), solid line is a linear fit with Pool-Frenkel equation	
<b>Figure 5.9.</b>	Linear plot of time-of-flight hole current transients for different applied voltage in DTP-FLU film at 298 K. The inset shows the corresponding double-logarithmic plot	134
<b>Figure 5.10.</b>	Linear plot of TOF photocurrent transients at various temperatures in <b>DTP-FLU</b> (Field: $2.7 \times 10^5$ V/cm)	135
<b>Figure 5.11.</b>	Poole–Frenkel plots of hole mobility in <b>DTP-FLU</b> at various temperatures	136
<b>Figure 5.12.</b>	Temperature dependence of mobilities at zero-field in <b>DTP-FLU</b>	137
<b>Figure 5.13.</b>	The slope of the field dependence of the logarithmic mobility <i>versus</i> $(\sigma/kT)^2$ for <b>DTP-FLU</b> , the solid line is a linear fit according to equation 5.1 (A). The slope of the field dependence of the logarithmic mobility <i>versus</i> $(\sigma/kT)^{3/2}$ , the solid line is a linear fit according to equation 5.2 (B)	139
<b>Figure 6.1.</b>	Chemical structure of the newly synthesized dithienothieno[3,4- <i>d</i> ]imidazole	149
<b>Figure 6.2.</b>	Thermal ellipsoid plot of <b>T7</b> (A), planar structure of <b>T7</b> (B) and its crystal packing (C)	158
<b>Figure 6.3.</b>	Normalized absorption spectra of dithienothienoimidazole ( <b>T1-T7</b> ) recorded in THF	160
<b>Figure 6.4.</b>	Thin film optical absorption spectra of dithienothienoimidazole ( <b>T1-T7</b> ) recorded in solid state	161
<b>Figure 6.5.</b>	Normalized emission spectra of dithienothienoimidazole ( <b>T1-T7</b> ) recorded in THF	162

<b>Figure 6.6.</b>	Emission spectra of <b>T7</b> oligomer in different solvents	163
<b>Figure 6.7.</b>	Absorption (A) and emission (B) spectra of <b>T1</b> upon addition of acid and base	165
<b>Figure 6.8.</b>	Cyclic voltammogram of dithienothieno[3,4- <i>d</i> ]imidazole oligomers ( <b>T1-T7</b> ) in dichloromethane containing 0.1M <i>n</i> -Bu <sub>4</sub> NPF <sub>6</sub> as supporting electrolyte at a scan rate of 100 mVs <sup>-1</sup>	168
<b>Figure 6.9.</b>	Visual features of <b>T7</b> (A) in THF upon addition of Ni(OAc) <sub>2</sub> (B), Cu(OAc) <sub>2</sub> (C) and Zn(OAc) <sub>2</sub> (D). ( <b>T7</b> and salt concentrations are $2.2 \times 10^{-5}$ M and $10 \times 10^{-3}$ M)	170
<b>Figure 6.10.</b>	Absorption spectra of the spectrophotometric titration of solution of <b>T7</b> ( $2.2 \times 10^{-5}$ M) with metal salts ( $1 \times 10^{-2}$ M) Cu <sup>2+</sup> (A), Ni <sup>2+</sup> (B), Zn <sup>2+</sup> (C) in THF. The fluorescence emission spectra of <b>T7</b> in THF with successive addition of Cu <sup>2+</sup> (D), Ni <sup>2+</sup> (E), Zn <sup>2+</sup> (F). The inset of (D, E and F) is the Stern–Volmer plot of linear range in the low quencher concentration regime	172
<b>Figure 6.11.</b>	Change in Absorption (A) and Fluorescence spectra (B) of <b>T7</b> in THF (□) with the addition of Cu(OAc) <sub>2</sub> (○) and with Cu(OAc) <sub>2</sub> and cystine (Δ). Inset: Fluorescence titration of <b>T7</b> containing Cu(OAc) <sub>2</sub> with cystine in THF	174
<b>Figure 6.12.</b>	Linear plot of TOF hole transient for different applied voltages and inset shows the corresponding integrated plot (A). Variation of TOF hole mobility with applied electric field, solid line is a linear fit according to Pool-Frenkel equation (B)	175
<b>Figure 6.13.</b>	Electropolymerization of thieno[3,4- <i>d</i> ]imidazole oligomers carried out at a scan rate of 100 mV/s, in dichloromethane containing 0.1 M TBAPF <sub>6</sub> as supporting electrolyte (A-E). Plot of current vs number of scans for the electropolymerization of thienoimidazole (F-J)	177,178

<b>Figure 6.14.</b>	Absorption spectra of electropolymerized polymer film over ITO surface	179
<b>Figure 6.15.</b>	Cyclic voltammogram of electropolymerized films of poly(thieno[3,4- <i>d</i> ]imidazole) in monomer free electrolyte at a scan rate of 100 mV/s	180

---

### LIST OF SCHEMES

---

No.	SCHEMES	Page No.
<b>Scheme 1.1.</b>	General synthesis of [ <i>n</i> ]acenes	9
<b>Scheme 1.2.</b>	Synthesis of fused thienoacene containing odd number of thiophene units	13
<b>Scheme 1.3.</b>	Synthesis of thienoacene containing even number of fused thiophene units	14
<b>Scheme 1.4.</b>	Synthesis of thiophene-benzene annulated heteroacenes	16
<b>Scheme 1.5.</b>	Synthesis route to indolo[3,2- <i>b</i> ]carbazole	19
<b>Scheme 1.6.</b>	Synthesis of heterohelicene	24
<b>Scheme 1.7.</b>	Synthesis of octathio[8]circulene	25
<b>Scheme 1.8.</b>	Classical route to <i>N</i> -functionalized dithieno[3,2- <i>b</i> :2',3'- <i>d</i> ]pyrroles	27
<b>Scheme 1.9.</b>	Efficient synthesis of soluble <i>N</i> -functionalized dithieno[3,2- <i>b</i> :2',3'- <i>d</i> ]pyrroles	28
<b>Scheme 1.10.</b>	Synthesis of ladder polyquinoxline	32
<b>Scheme 1.11.</b>	Synthesis of planarized ladder PPP	32

<b>Scheme 1.12.</b>	Synthesis of ladder PPP bridged by imine group	33
<b>Scheme 1.13.</b>	Synthesis of ladder-type polythiophene	34
<b>Scheme 1.14.</b>	Synthesis of 2,3-dihexylthieno[3,4- <i>b</i> ]pyrazine	38
<b>Scheme 2.1.</b>	Comparison of reactivity of 3-bromothiophene and 3-bromobenzo[ <i>b</i> ]thiophene under palladium catalyzed amination condition	57
<b>Scheme 2.2.</b>	Synthesis of unsymmetric heteroacene <b>1a</b> and <b>1b</b>	58
<b>Scheme 2.3.</b>	Synthesis of symmetrical heteroacene <b>2a</b> and <b>2b</b>	59
<b>Scheme 3.1.</b>	Synthesis of unsymmetrical and extended heteroacene	73
<b>Scheme 4.1.</b>	Synthesis of thiadiazole fused indolocarbazole derivatives	96
<b>Scheme 4.2.</b>	Synthesis of thiadiazole incorporated indolocarbazole polymer	105
<b>Scheme 5.1.</b>	Synthesis of DTP oligomers	119
<b>Scheme 6.1.</b>	Synthesis of target thienoimidazole based oligomers ( <b>T1-T7</b> )	157
<b>Scheme 6.2.</b>	Proposed reaction of <b>T1</b> with sodium hydroxide and trifluoroacetic acid	166
<b>Scheme 6.3.</b>	Schematic representation of fluorescence turn-off and turn-on sensing behavior of <b>T7</b> towards metal ions and $\alpha$ -amino acids	174
<b>Scheme 6.4.</b>	Electropolymerization of dithienothieno[3,4- <i>d</i> ]imidazole based oligomers	177

---

## ABBREVIATIONS AND SYMBOLS

---

$^1\text{H-NMR}$	Proton nuclear magnetic resonance
$^{13}\text{C-NMR}$	Carbon nuclear magnetic resonance
Å	Angstrom(s)
$\delta$	Chemical shift (in NMR spectroscopy)
$\Phi_{\text{F}}$	Fluorescence quantum yield
$\lambda$	Wavelength
$\theta$	Diffraction angle
$\mu\text{m}$	Micrometer
ca.	About
A	Acceptor
AFM	Atomic force microscopy
b	Broad
BLA	Bond length alteration
BuLi	Butyllithium
$\text{CHCl}_3$	Chloroform
CDM	Correlated disorder model
conc.	Concentrated
CV	Cyclic voltammetry
CP	Conjugated polymer
D	Donor
d	Doublet

DBA	Dibenzylideneacetone
DC	Direct current
dd	Double of doublet
DCM	Dichloromethane
DMF	Dimethylformamide
DMSO	Dimethylsulfoxide
DP	Degree of polymerization
DTP	Dithieno[3,2-b:2'3'- <i>d</i> ]pyrrole
DTPh	Dithieno[3,2-b:2'3'- <i>d</i> ]phosphole
DTS	Dithieno[3,2-b:2'3'- <i>d</i> ]silole
DTT	Dithieno[3,2-b:2'3'- <i>d</i> ]thiophene
EA	Ethyl acetate; Elemental analysis
EDOT	Ethylenedioxythiophene
$E_g$	Band gap
EI-MS	Electron impact - Mass spectrometry
$E_{\text{oxd}}$	Oxidation potential
$E_{\text{oxd}}^{\text{onset}}$	Oxidation onset potential
ESI-MS	Electron spray ionization - Mass spectrometry
EtOH	Ethanol
etc.	Et cetera
FAB-MS	Fast atom bombardment – Mass spectrometry
FT-IR	Infrared fourier transform

GDM	Gaussian disorder model
h	Hour(s)
HOMO	Highest occupied molecular orbital
Hz	Hertz
IC	Indolocarbazole
i.e.	That is (Latin id est)
ITO	Indium-tin-oxide
J	Coupling constant
KBr	Potassium bromide
K <sub>2</sub> CO <sub>3</sub>	Potassium carbonate
K <sub>sv</sub>	Stern-Volmer constant
LED	Light emitting diode
LUMO	Lowest unoccupied molecular orbital
m	Multiplet
m/z	Mass/Charge
MeOH	Methanol
mg	Milligram(s)
MHz	Mega hertz
mL	Milliliter(s)
mmol	Millimol
MW	Molecular weight
NBS	N-bromosuccinimide



NIR	Near infra red
nm	Nanometer
ns	Nanosecond
NMR	Nuclear magnetic resonance
OFET	Organic field effect transistor
OLED	Organic light emitting diode
OLEFET	Organic light emitting field effect transistor
OPV	Organic photovoltaics
OTS	Octadecyltrichlorosilane
PC	Polycarbazole
PCBM	Phenyl-C <sub>61</sub> -butyric acid methyl ester
Pd(0)P(Ph <sub>3</sub> ) <sub>4</sub>	Tetrakis(triphenylphosphine)palladium(0)
PF	Polyfluorene
PITN	Poly(iso-thianaphthene)
PL	Photoluminescence
PPP	Poly(p-phenylene)
PPV	Polyphenylenevinylene
PPY	Polypyrrole
PT	Polythiophene
QY	Quantum yield
q	Quartet
RT	Room temperature

s	Singlet; Second
t	Triplet
<sup>t</sup> Bu	Tertiary butyl
TOF	Time-of-flight
TMS	Tetramethylsilane
THF	Tetrahydrofuran
TLC	Thin layer chromatography
UV-vis	Ultra-violet visible spectroscopy
XRD	X-ray diffraction

---

# ***Chapter 1***

## ***Introduction***

## 1. General introduction

Organic electronics is a branch of electronics, which utilize organic materials (oligomers, polymers and dendrimers) for electronic applications. The semiconducting organic materials emerged as a promising candidate for electronic applications due to their delocalized  $\pi$ -electrons. The potential application of these molecules includes organic light emitting diodes (OLEDs), organic field effect transistors (OFETs), organic photovoltaic's (OPVs) and as chemical sensors.<sup>1</sup> Organic materials have proven useful in applications and some of them already entered into the consumer market (e.g., Sony's XEL-1 OLED television set, Konarka's power plastic products).

The term "organic semiconductors" is used to describe organic materials whose electronic conductivity spanning a broad range of  $10^{-9}$  to  $10^3 \Omega^{-1} \text{ cm}^{-1}$ . The conductivity study of organic materials dates back to 1906, with the discovery of photoconduction of solid anthracene.<sup>2</sup> In early 1950s, considerable amount of research was dedicated to understand the charge transport properties of semiconductors. In 1977, Allan J. Heeger, Alan, G. MacDiarmid and Hideki Shirakawa discovered the first evidence of high electrical conductivities in synthetic polyacetylene.<sup>3</sup> Since then, organic materials gained significant attention in electronic applications. Conjugated semiconducting polymers combine the optical and electronic properties of semiconductors with the advantage of easy processing and special mechanical properties. Unlike their inorganic counterpart, conjugated organic materials are solution processable and their properties can be tuned at the molecular level through molecular structure. Synthetic flexibility, ease of processing, (after attaching solubilizing side chains) and ability to tune the electronic and mechanical

properties to accomplish a desired function makes semiconducting organic materials attractive candidates for future applications in electronic devices.<sup>4</sup>

Research involving the synthesis of conjugated oligomers and polymers has gained significant attention in the past few years owing to considerable advantage over inorganic counterpart.<sup>5</sup> The development of new conjugated polymers and oligomers has been the focus of tuning the electronic properties of the semiconducting materials. Although polyacetylene was the first benchmark in this field, this material is not soluble in common organic solvents and not stable under ambient conditions, making it difficult to process and, consequently, incompatible for electronic devices. Variation of the conjugated backbone structure resulted in significant influence on the electronic properties of the polymers. Among the various conjugated polymers developed over the past 25 years poly(*p*-phenylene)s, poly(*p*-phenylenevinylene)s, polythiophenes, polypyrroles, polyanilines, polyfluorenes, and polycarbazoles attracted much attention (Figure 1.1).<sup>6</sup>

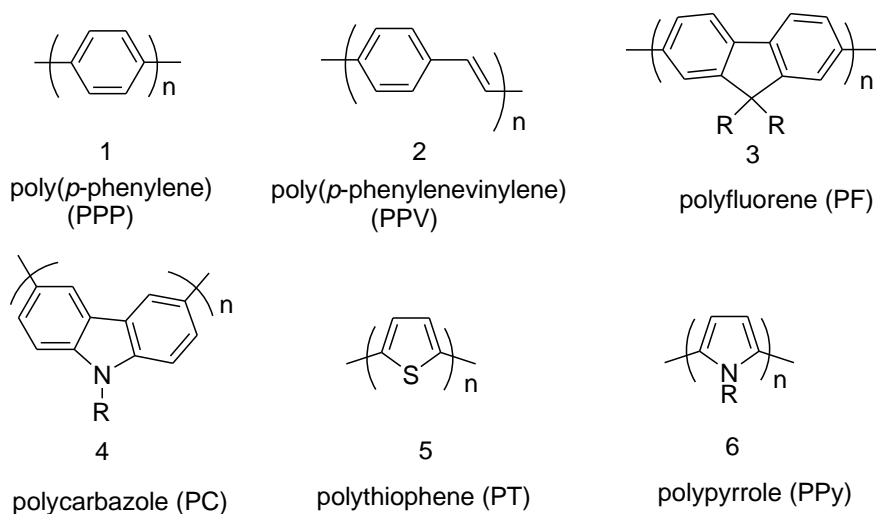


**Figure 1.1.** Chemical structure of some common  $\pi$ -conjugated polymers

The substituents in these polymers were also shown to influence its electronic properties. For example, a large number of polythiophenes with varying side chain structure have been synthesized and the structure-property relationship was investigated with a focus on its solubility, processability and the environmental stability. It is well understood that a small modification in the design of the polymeric backbone or the structure of the side chains can dramatically influence the characteristics of the polymer. Changes in the substituents are often made to make the materials more suitable for specific applications in polymer electronic devices.

Understanding the influence of geometry of molecules on their electronic properties, such as the electronic band gap and charge carrier mobility is imminent to fine-tune the properties. In particular, specific attention has been paid to the band gap energy as it is a crucial factor in tuning the intrinsic electronic and optical properties of the materials. Therefore, it is important to develop a correlation between the band gap energy and structure of semiconducting material.

### **1.1. Conjugated polymers: controlling the band gap**

Conjugated polymers have their electrons organized in bands rather than in discrete energy levels and their ground state energy bands are either totally filled or empty. The band structure of conjugated polymers originates from the interaction of the  $\pi$ -orbital's of the repeat unit throughout the main chain. This was explained by theoretical studies by comparing the calculated energy levels as a function of oligomer length for oligothiophenes with ( $n = 1 - 4$ ) and polythiophene.<sup>7</sup> Starting from a single thiophene unit, addition of each new repeat unit causes additional hybridization of the energy levels until the overlap of the energetic levels results in bands rather than discrete levels (Figure 1.2). As is

the case for inorganic semiconductors, the highest occupied band is called the valence band, while the lowest unoccupied band is called the conduction band, originating from the HOMO and the LUMO levels of the monomer units respectively, while the energy difference  $E_g$  is called the band gap. Due to the delocalization of  $\pi$ -electrons, conjugated polymers display semiconducting properties in their electro-neutral state and the ability to support the transport of charge carriers. When the molecular structure is considered, both oligomers and polymers show a narrow band gap (1.5 - 3.0 eV) representing a fruitful approach towards new materials for electronic applications.<sup>8</sup>

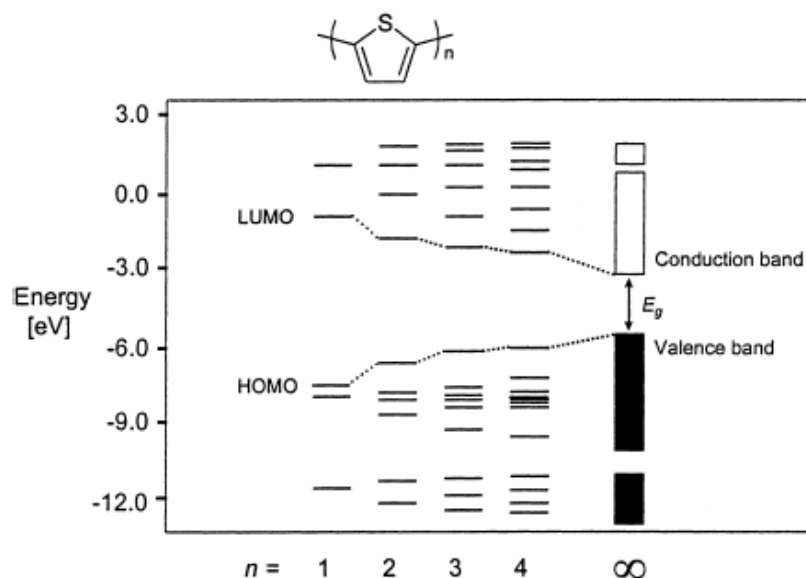


**Figure 1.2.** Energy band structure of conjugated polymers emerging from the energetic splitting upon addition of an increasing number of atomic orbitals. Adapted from reference (7)

The band gap energy can be engineered by the modification of macromolecular structure, a) towards small band gaps suitable for so-called synthetic metals or infrared emitting polymers, or b) towards a larger band gap for blue emitting polymers. By

changing structural features of the oligomer or polymer, such as the regioregularity or arrangement and distribution of the chromophoric units, it is possible to design a broad range of polymers with different band gap energies from a basic conjugated structure. Polythiophenes are one of the most prominent of the investigated examples; their band gap energy can be tuned throughout the whole UV-vis spectrum from UV to near IR (NIR) by varying the substituents attached in 3 and/or 4 - position of the thiophene ring, depending on the inductive/ mesomeric effects towards the main chain.<sup>9</sup>

In addition to the imminent influence of substituents, the so-called effective conjugation length is an important factor determining the electronic and electrochemical properties of organic semiconductors. Extended conjugation implies a narrow band gap in the resulting semiconducting polymer. Absorption maximum of a conjugated polymer is usually red-shifted with an increasing degree of polymerization (DP) up to a certain value above which no further red shift was observed. This threshold is described as the effective conjugation length. The convergence of the band gap energy for oligothiophenes was investigated by Bäuerle *et al* amongst others, and observed no further changes in the optical properties once the chain length had reached 16 repeating units.<sup>10</sup> The band gap is also dependent on the bond length alternation (BLA), which refers to the energy difference between single and double bonds.<sup>11</sup> As a result, polyaromatic polymers differ from their non-aromatic counterparts (CH)<sub>x</sub> as they have a non-degenerate ground state. The competing benzoic and quinoid energy states are energetically different and thus resulting in smaller resonance energy for the quinoid form (Figure 1.3). Stabilization of the quinoid resonance structure of conjugated



oligomers and polymers is of particular importance since it underlies a powerful strategy to synthesize low band gap polymers.

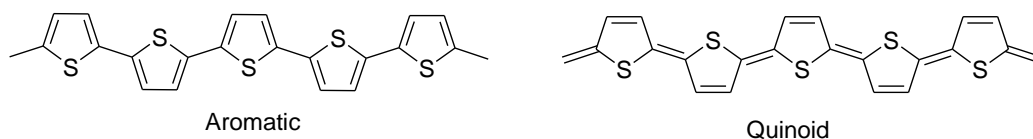


**Figure 1.3.** The quinoid form forces the rings to align in a planar conformation leading a low bandgap of 0.47 eV. The aromatic form allows the thiophene to rotate with a certain degree of rotational freedom results in bandgap of 2 eV

One of the factors determining the energy levels of conjugated materials is the rotation between neighboring aromatic units around the single bonds with its distinct influence on the effective conjugation length. The aromatic resonance state (ground state), often leads to a non-planar backbone leads to reduced overlap of the  $\pi$ -orbitals, proportional to the cosine of the twist angle ( $\theta$ ).<sup>12</sup> Second factor is the aromaticity of the monomeric units, which results in a competition between confinement of the  $\pi$ -electrons within the aromatic rings and delocalization along the  $\pi$ -conjugated chain.<sup>13</sup> Therefore, to obtain a low band gap energy, it is desirable to induce coplanarity of the building blocks along the  $\pi$ -conjugated chain, which can be achieved by an appropriate choice of substituents, fused ring systems, or the introduction of additional covalent bonds to rigidify the conjugated backbone in so-called step-ladder or ladder-type structures.

## 1.2. Fused conjugated systems

### 1.2.1. [*n*]acene systems

The construction of extended ladder conjugated systems (acenes) has been considered in early days to achieve low bandgap systems as it reduces the BLA and prevent the rotation between adjacent units and induce coplanarity. The oligomers of the

[*n*]acene series have been synthesized up to heptacene (Figure 1.4).<sup>14</sup> Examination of the bandgap and redox properties of compounds from naphthalene to heptacene suggests that increasing in chain length lead to reduction in bandgap.<sup>15</sup>

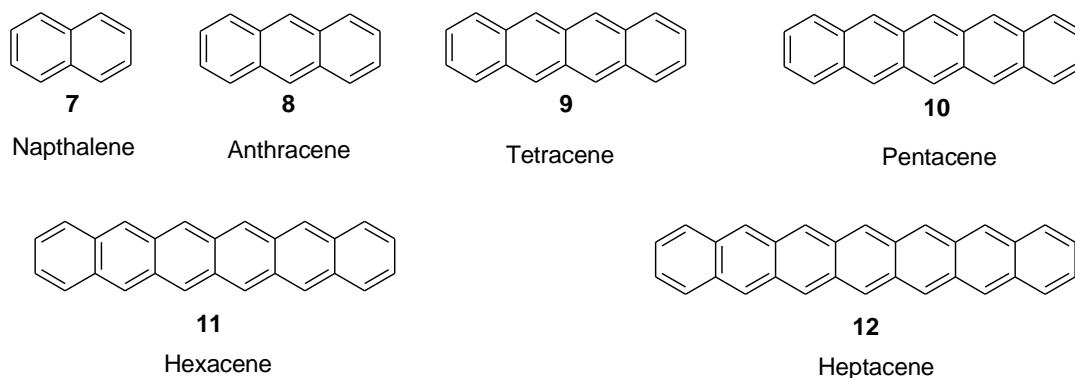
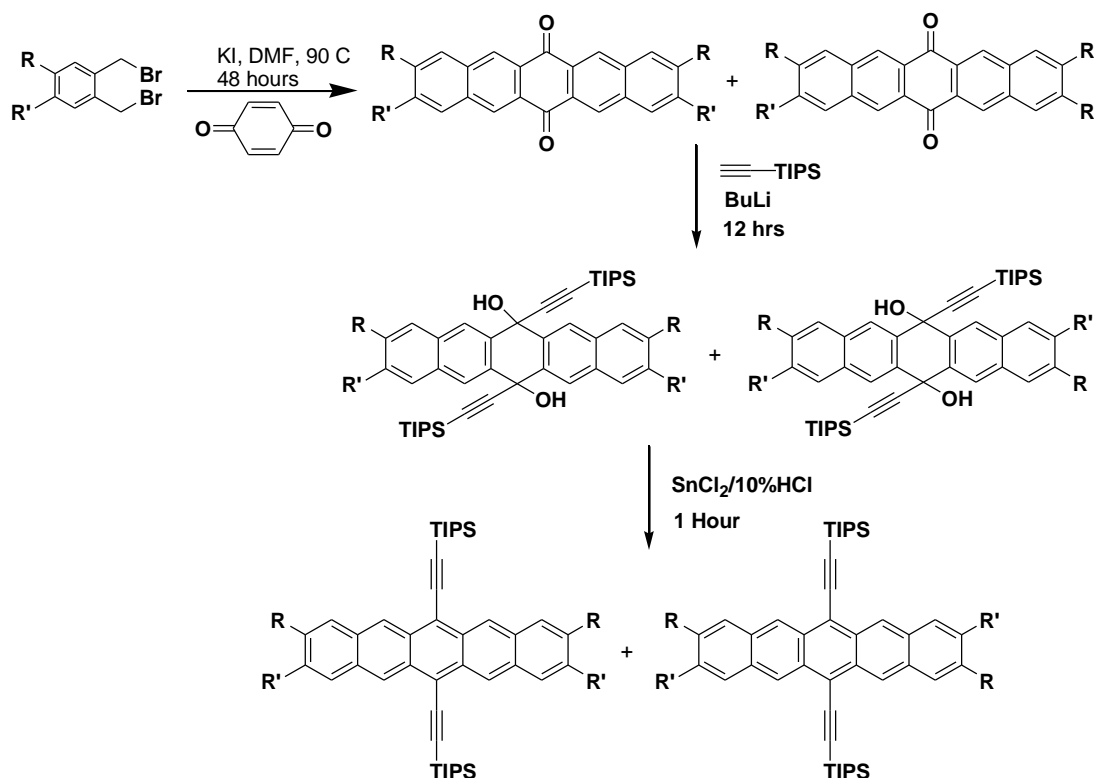


**Figure 1.4.** Structure of reported [*n*]acene systems

Acenes such as anthracene, tetracene, rubrene and pentacene are most commonly employed for OFET and OLED applications. Among all *p*-type materials investigated for OFET application, pentacene has shown the best performance. Acenes such as pentacene and rubrene are common benchmarks showing the field effect mobilities of  $>3 \text{ cm}^2\text{V}^{-1}\text{s}^{-1}$  with on-off current ratios of about  $10^8$ .<sup>16</sup> The high mobility of pentacene is due to high order in the crystalline film. The ordering is dominated by edge to face interaction leading to a closely packed “herring bone” arrangement.<sup>17</sup> When deposited over a substrate, the thin film of pentacene arranges with its long axis perpendicular to the substrate resulting in an interaction parallel to substrate. Fused [*n*]acene derivatives are generally synthesized by Diels-Alder reaction starting from  $\alpha,\alpha'$ -dibrominated *o*-xylene derivatives.<sup>18</sup> The Diels-Alder reaction and aromatisation to give a mixture of *syn* and *anti* 6-13 pentacenequinone derivatives. The mixture of pentacenequinones was then reacted with lithiated triisopropyl silyl acetylene without further separating to give the

diol. The target pentacene derivatives were obtained as *syn* and *anti* mixtures by reducing the diol with  $\text{SnCl}_2$  in 10%  $\text{HCl}$ .

**Scheme 1.1.** General synthesis of  $[n]$ acenes<sup>18</sup>



However, pentacene, rubrene and other higher  $[n]$ acenes are vulnerable to photo oxidation due to their high lying HOMO and narrow band gap. The decomposition pathway of pentacene includes endoperoxide formation (13) and butterfly dimerization (14) (Figure 1.5).<sup>19</sup> These acenes also suffers from poor solubility in most organic solvents which limits their processibility and hence its applications. Until now, heptacene remains the longest known member of the  $[n]$ acene series. Therefore, an ideal molecule for OFET device should have good solution processability, stability under ambient condition with high charge carrier mobility and better on-off ratios.

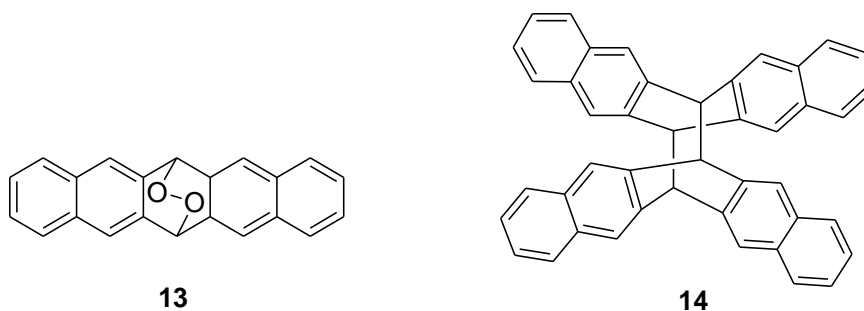


**Figure 1.5.** Possible degradation products of pentacene

### 1.2.2. Heteroacene systems

Heteroacenes are  $\pi$ -conjugated ladder molecules, with main group heteroatoms like N, S, O *etc.* embedded in the  $[n]$ acene structure (Figure 1.6).<sup>20</sup> The heteroacene possess rigid coplanar structures with enhanced  $\pi$ -conjugation leading to most desired properties such as high carrier mobility.<sup>21</sup> These heteroacenes show favorable close packing in solid state similar to pentacene with improved stability and solubility. Among the heteroatoms, the elements from group 13 to 16, such as B, N, Si, P, S and Se received increased attention.<sup>22</sup> The notable features of main group elements such as effective orbital interaction, diversity in coordination numbers and geometry helps to design new ladder type materials with unique functions and properties. Especially the orbital interaction is important in tuning the electronic properties of the materials.

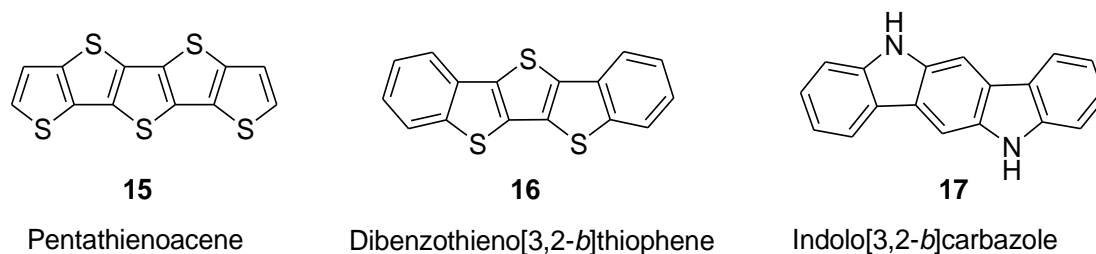


**Figure 1.6.** Structures of heteroacene compounds

The major advantage of the heteroacene is the presence of heteroatoms, which lowers the HOMO energy level to offer better stability and allow facile derivatization to tune the molecular organization.<sup>23</sup> In addition to the  $\pi$ -stacking expected for fused acene systems, the heteroacenes are expected to have additional secondary interactions such as hydrogen bonding and S-S interaction. Because of such interactions, densely packed solid structures, which are more advantageous for charge transport, are expected. Heteroacenes such as thieno[*n*]acenes,<sup>24</sup> thiophene-benzene annulated acenes<sup>25</sup> and pyrrole-based indolocarbazole<sup>26</sup> have been successfully synthesized and tested for OFET performance. Improved stability and solubility of heteroacene enabled the extension of ring fusion, which is limited in case of [*n*]acenes. This enables to understand the effect of ring fusion on solid state packing, optical and electrical properties. Katz and co-workers are the first to utilize this approach for enhancing the stability of pentacene by synthesizing the heterocyclic analogs with thiophene.<sup>20</sup> Since then, heteroacenes proved their potential in organic electronics and gained significant importance due to structural diversity. However, the synthesis of aromatic compounds with more than four rings poses a daunting synthetic challenge.

### 1.2.2.1. Theinenoacene

Compared to  $[n]$ acenes, thiophene based heteroacenes show interesting and favorable electronic and solid-state structure. The thiophene-based acenes have narrow HOMO-LUMO gaps owing to their large quinoid character. However, the condensed thiophene molecules show wide HOMO-LUMO gaps retaining their aromatic character. In crystal lattice, ladder thiophene compounds favor  $\pi$ -stacked structures in contrast to herringbone packing observed in acenes like pentacene. In fused thiophene compounds, the sulfur-sulfur contacts between the molecules in the adjacent stacks lead to close packed structure favorable for better device performance.

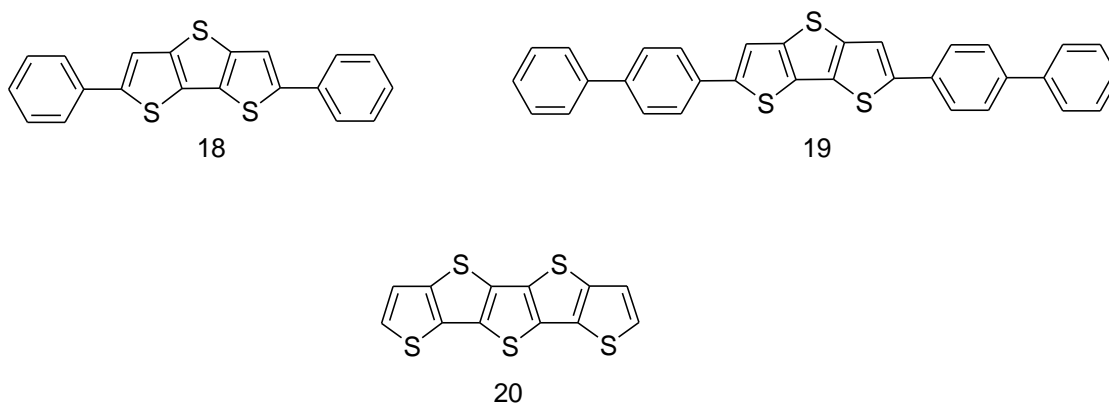
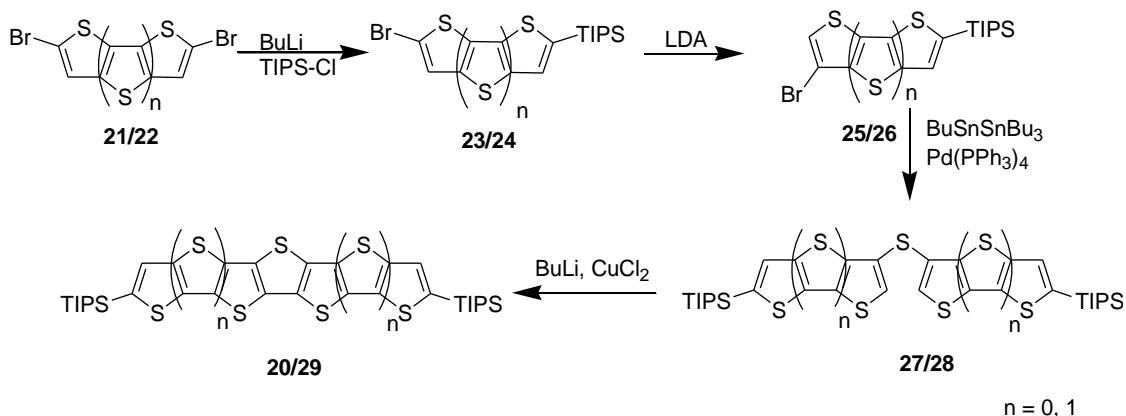


**Figure 1.7.** Structures thieno $[n]$ acene based compounds

Dithieno[3,2-*b*:2',3'-*d*]thiophene (DTT) is an interesting building block for constructing organic-semiconducting materials for OFET, OLED and organic light emitting field effect transistor (OLEFET) applications. Recently, a high performance and stable organic thin-film transistor based on phenyl and biphenyl substituted thienothiophene (18 and 19) was reported by Zhu and coworkers (Figure 1.7).<sup>27</sup> The thin film grown by vapor deposition showed a field effect mobility of  $0.42 \text{ cm}^2 \text{V}^{-1} \text{s}^{-1}$  with on-off ratio of  $5 \times 10^6$ . The shelf life of the device under ambient condition was also tested. The

device was found to be very stable with mobility remained the same even after two months.

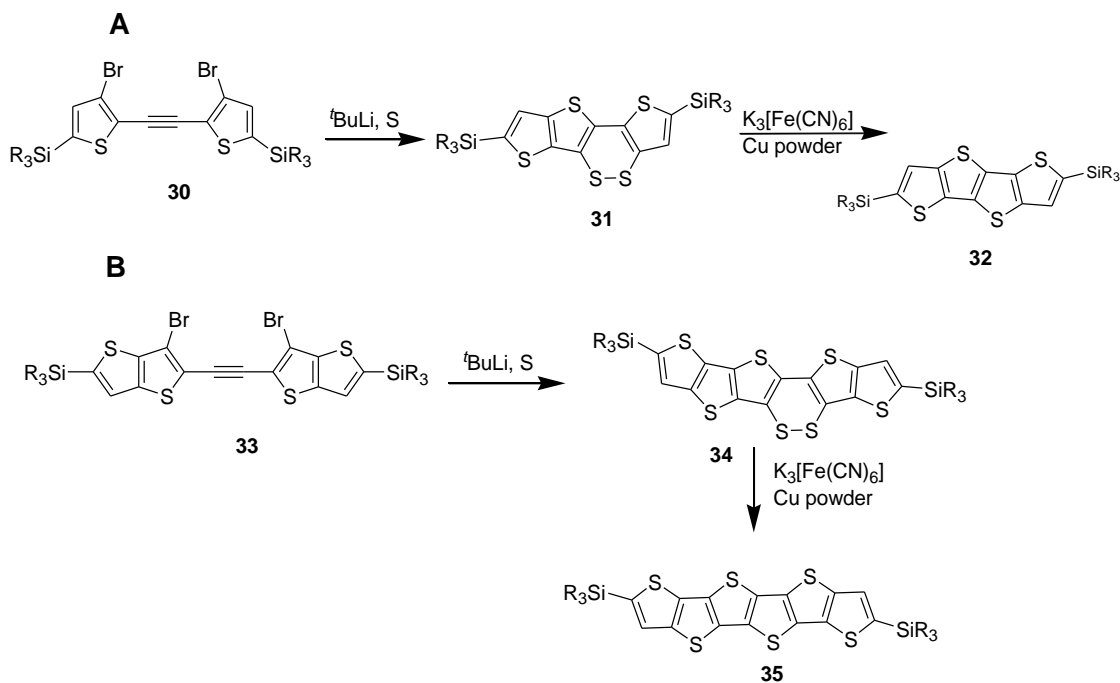
**Scheme 1.2.** Synthesis of fused thienoacene containing odd number of thiophene units<sup>28</sup>



Pentathienoacene (20) received special attention as it is considered as thiophene equivalent of pentacene. Matzger *et.al.* reported the effective synthesis and X-ray structure of this fused thiophene compound.<sup>28</sup> Thienoacenes containing odd number of thiophene units are synthesized in good yields from thienothiophene or dithienothiophene. Dibromothiophenes are mono-lithiated and quenched with triisopropylsilyl chloride (TIPS-Cl) to result in TIPS protection at  $\alpha$ -position (Scheme 1.2). The  $\beta$ -bromo substitution was achieved by halogen dance reaction using LDA. The sulfide compound was obtained by palladium catalyzed coupling using  $\text{Bu}_3\text{SnSnBu}_3$ . The oxidative ring closure using BuLi and cupric chloride resulted in highly soluble thienoacene. The crystal structure confirmed the planarity of this fused system similar to pentacene with a deviation less than 0.007(5) Å from the mean plane. In crystal lattice, molecules were found to show  $\pi$ -stacked structures with an intermolecular distance of 3.51 Å. The short sulfur-sulfur contact (3.55 Å) between the molecules led to the close packing in the solid state. Zhu and coworkers

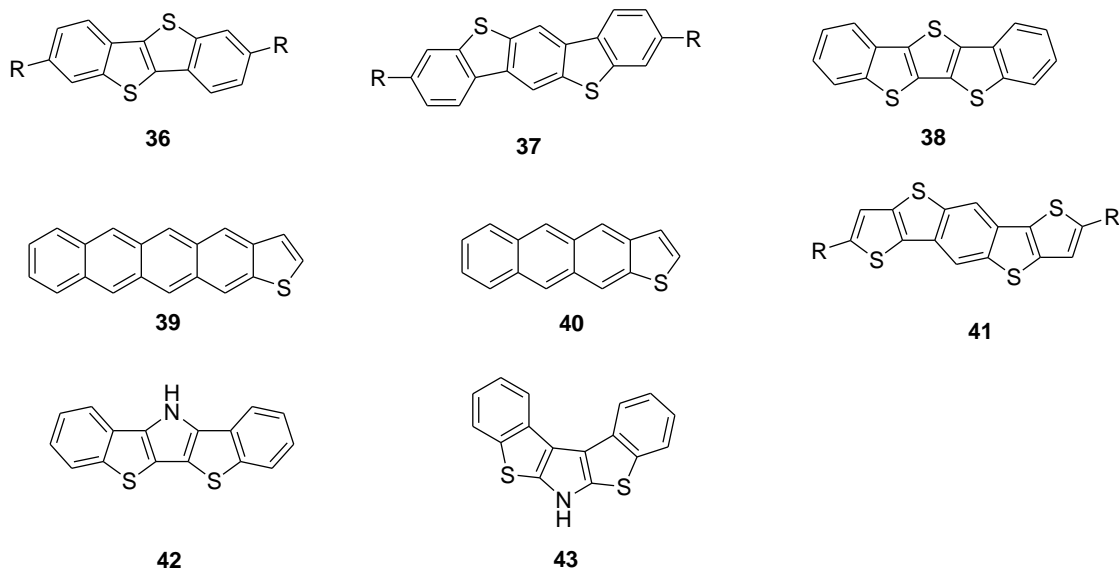
demonstrated the field-effect transistor property of condensed pentathienoacene.<sup>29</sup> The vapor deposited film showed a FET mobility of  $0.045 \text{ cm}^2\text{V}^{-1}\text{s}^{-1}$ . The synthesis, photophysical and electrochemical properties of extended thieno[*n*]acenes such as octathienoacene, hexathienoacene, pentathienoacenes were reported.<sup>30</sup> They are prepared by intramolecular double cyclization of bis(3-bromo-2-thienyl)-acetylenes (Scheme 1.3A). Thieno[3,2-*c*](1,2-dithiin) was obtained by lithium-halogen exchange reaction using the above mentioned acetylene compounds. The subsequent dechalcogenation using Cu nanoparticles afforded tetrathienoacene. Higher acenes are also prepared utilizing the same strategy (Scheme 1.3B). However, the device application of these interesting compounds is yet to be explored. The extended thienoacenes with alkyl substituent at  $\alpha$ -position in thienyl ring are soluble in common organic solvents. The presence of alkyl substituent at  $\alpha$ -position hinders the substitution and further extension of the fused system.

**Scheme 1.3.** Synthesis of thienoacene containing even number of fused thiophene units<sup>30</sup>



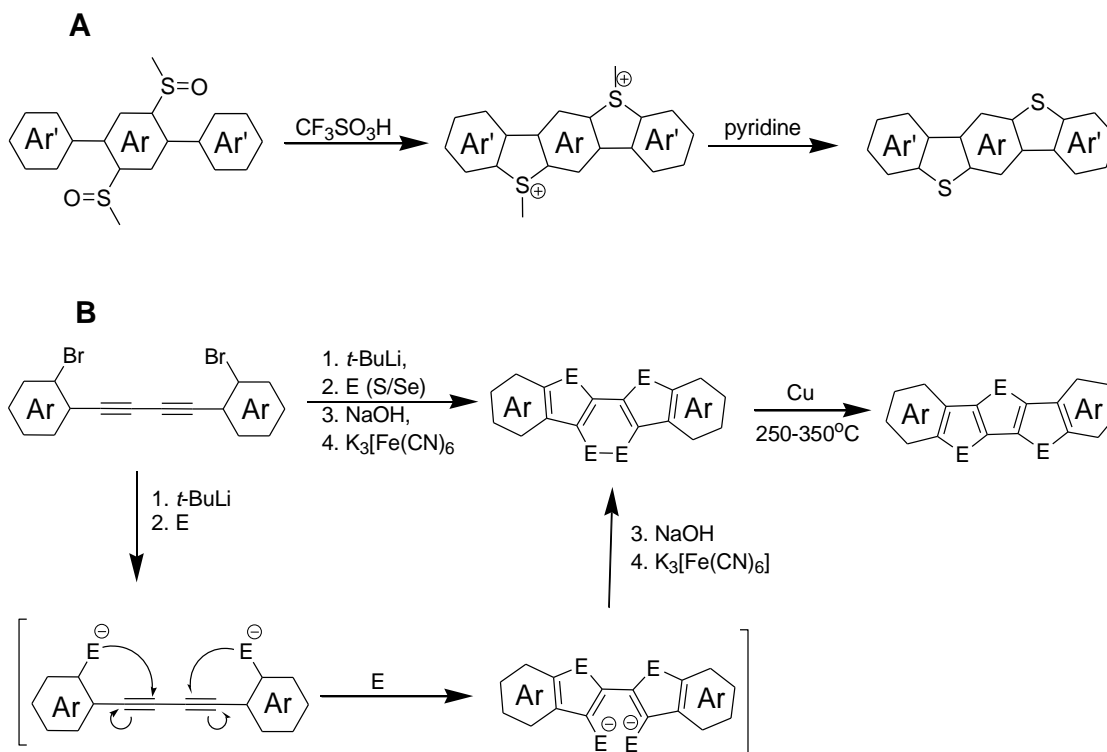


### 1.2.2.2. Thiophene-benzene annulated acenes



**Figure 1.8.** Structure of thiophene-benzene annealed heteroacenes employed for FET application

Fused benzene-thiophene molecules are the most common and promising heteroacene systems. Compared to thieno[*n*]acenes benzothioacenes are easy to synthesize, highly soluble and shows better performance in FET devices (Figure 1.8). Benzothienoacenes are generally synthesized by two methods. The first method involves the triflic acid induced electrophilic cyclization of 1-aryl-2-(methylsulfinyl)benzene (Scheme 1.4A).<sup>31</sup> This reaction lacks selectivity and results in mixture of products. Utilizing this method recently, Müllen and co-workers synthesized a series of extended diindolo[3,2-*b*:2',3'-*h*]benzo[1,2-*b*:4,5-*b'*]bis[1]benzothiophene (BIBBBT) with high regioselectivity.<sup>31</sup>

**Scheme 1.4.** Synthesis of thiophene-benzene annulated heteroacenes<sup>31,32</sup>


The second method involves intramolecular cyclization of bis(*o*-haloaryl)diacetylenes, via dilithiation followed by reaction with chalcogen elements, to result in heterole-1,2-dichalcogenin-heterole fused skeleton (Scheme 1.4B).<sup>32</sup> The dechalcogenation of the above compound with copper metal afforded a series of benzothiophene/benzoselenophene based heteroacene.

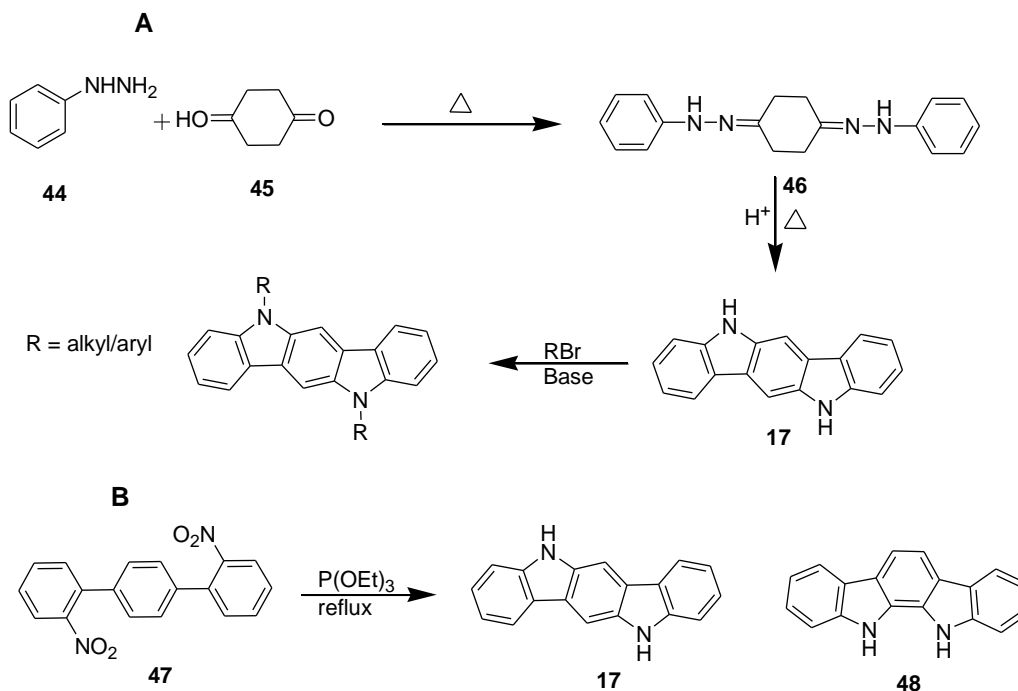
The highly soluble molecular semiconductors, 2,7-dialkyl[*I*]benzothieno[3,2-*b*]benzothiophenes (36) were synthesized and tested as an active layer in solution processed OFETs.<sup>33</sup> The OFET device showed typical *p*-channel FET response with FET mobility higher than  $1.0 \text{ cm}^2\text{V}^{-1}\text{s}^{-1}$  with an  $I_{\text{on}}/I_{\text{off}}$  ratio of  $\sim 10^7$ . Coplanar heteroacene benzo[1,2-*b*:4,5-*b'*]bis[*b*]benzothiophene (37) was synthesized and applied for OFET application.<sup>34</sup> The solution processed thin film showed a hole mobility up to  $0.01 \text{ cm}^2\text{V}^{-1}\text{s}^{-1}$ .

A similar system dibenzo[*d,d'*]thieno[3,2-*b*;4,5-*b'*]dithiophene (DBTDT) (38) was recently reported to show high FET mobility.<sup>35</sup> DBTDT showed crystal structure and packing similar to pentacene. However, unlike pentacene these compounds possess high ionization potential, higher stability and solubility. Thin film of DBTDT was obtained by the vapor deposition on octadecyltrichlorosilane (OTS) treated SiO<sub>2</sub>/Si substrate. The top contact device of the vapor deposited film gave mobilities up to 0.51 cm<sup>2</sup>V<sup>-1</sup>s<sup>-1</sup> with an on-off ratio larger than 10<sup>6</sup>.<sup>35</sup> Zhenan Bao and coworkers reported the first asymmetric linear acenes and employed them successfully in OFET devices.<sup>36</sup> The molecular design was based on the high dipole moment of asymmetric ladder structure, which promotes dense packing in solid state resulting in high mobility. Linear unsymmetrical pentacene derivative tetraaceno[2,3-*b*]thiophene (39) and tetracene derivative anthra[2,3-*b*]thiophene (40) were synthesized in two steps. The vapor deposited thin film of pentacene derivative, which was annealed for 60 minutes showed the best performance with the mobility of 0.47 cm<sup>2</sup>V<sup>-1</sup>s<sup>-1</sup> and an on-off ratio of 10<sup>6</sup>.<sup>36</sup> Very recently, Müllen and coworkers reported a high performance solution processed OFET with a FET mobility up to 1.7 cm<sup>2</sup>V<sup>-1</sup>s<sup>-1</sup>.<sup>37</sup> The OFET device was constructed by employing dithieno[2,3-*d*;2',3'-*d'*]benzo[1,2-*b*;4,5-*b'*]dithiophene (DTBDT) (41) as active layer. The highly soluble DTBDT with alkyl chains (linear or branched) in the molecular axis was synthesized in two steps. The crystal structure shows planar  $\pi$ -conjugated frame with alkyl chain  $\alpha$ - to thienyl groups lies outside the plane of ladder frame. The molecules are arranged *via*  $\pi$ -stacking with an interplanar distance of 3.68 Å. Short sulfur-sulfur interactions also accounts for the close packing in these molecules. The hexyl chain substituted DTBDT in solution processed OFETs produced the hole mobilities of 1.7 cm<sup>2</sup>V<sup>-1</sup>s<sup>-1</sup> and an on-off ratio of  $\sim 10^7$ .<sup>37</sup>

Thiophene and pyrrole fused thienopyrroles also showed good FET mobility. The first report on thienopyrrole based OFET device was reported by Daoben Zhu and coworkers. Both *syn* and *anti* isomers of dibenzothienopyrrole (42 and 43) were developed.<sup>38</sup> In the solid state *anti* isomer exhibit sandwiched herringbone structure. The OFET of *p*-channel device showed a better mobility for linear *syn* isomer over bent *anti* isomers. The *syn* isomers showed mobilities up to  $0.012 \text{ cm}^2\text{V}^{-1}\text{s}^{-1}$  with an on-off ratio of  $\sim 10^5$  at ambient conditions.

### 1.2.2.3. Indolocarbazole

Most of the amine-based semiconductors have low-lying HOMO and large bandgap. Although these materials are extensively studied for optoelectronic applications, most of them lead to low FET mobility, and is attributed to either poor molecular ordering or the lack of stabilization of the radical cation.<sup>39</sup> Pyrrole based indolo[3,2-*b*]carbazole is an appealing system for OFETs, due to their planar structure which enable to achieve higher structural order for charge transport. Indolo[3,2-*b*]carbazole based compounds are synthesized in good yields by a double Fischer indolization reaction (Scheme 1.5A). The Cadagon reductive ring closure route to achieve indolo[3,2-*b*]carbazole result in mixture of isomer with poor yields (Scheme 1.5B).<sup>40</sup> The substitution has dominant effect on the molecular self-organization and on the mobility of charge carriers. The oppositely positioned substituent affording stabilization to the radical cations, which affords high mobility. Ong *et.al.* demonstrated that the *N*-functionalized indolo[3,2-*b*]carbazoles are the high performing *p*-type semiconducting materials with good environmental stability.<sup>41</sup> High FET mobility was achieved by substituting 5,11 position of carbazole with phenyl groups which is capable of providing sufficient resonance stabilization to hole carriers.

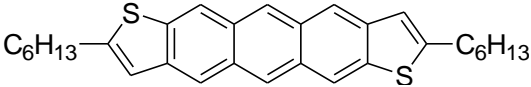
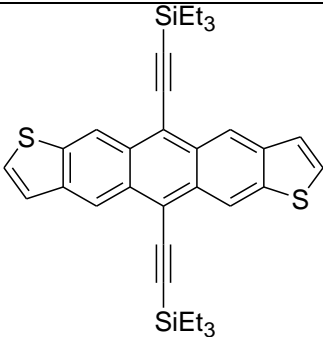
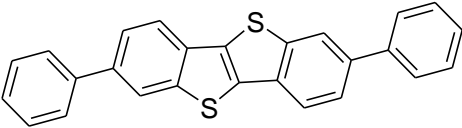
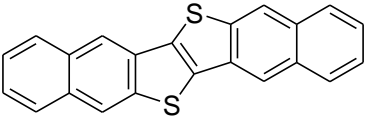
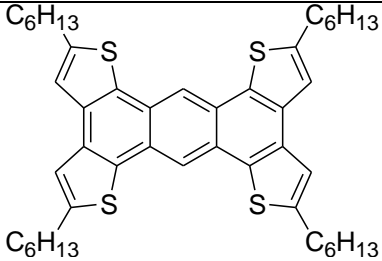
**Scheme 1.5.** Synthesis route to indolo[3,2-*b*]carbazole<sup>26</sup>

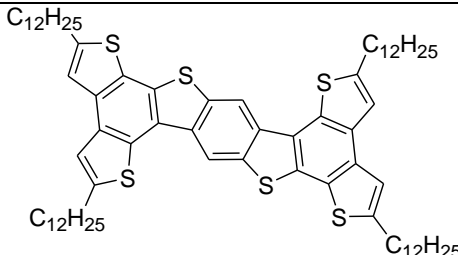
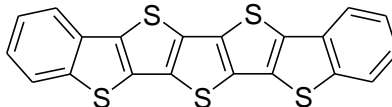
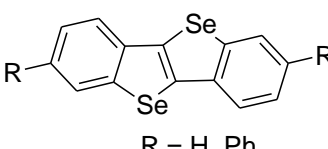
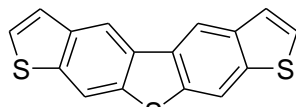
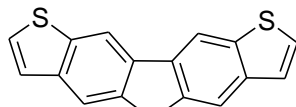
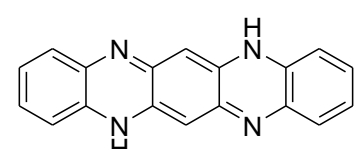
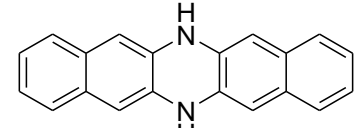
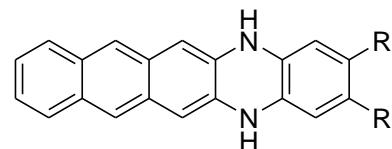
Under optimized conditions, these compounds showed excellent field-effect properties, with hole mobility up to  $0.12 \text{ cm}^2\text{V}^{-1}\text{s}^{-1}$  and current on/off ratio of  $10^7$ .<sup>41</sup> *N*-(4-hexylphenyl) substituted indolo[3,2-*b*]carbazole gave high FET mobility of  $0.14 \text{ cm}^2\text{V}^{-1}\text{s}^{-1}$  and current on-off ratio up to  $10^7$  when fabricated by vacuum deposition.<sup>42</sup> Leclerc *et.al.* synthesized a series of indolo[3,2-*b*]carbazole based compounds and studied the influence of side chains (alkyl, phenyl, thienyl substituents) on their solid-state packing.<sup>43</sup> The phenyl substituted material exhibited FET behavior with hole mobilities up to  $0.2 \text{ cm}^2\text{V}^{-1}\text{s}^{-1}$  with an on/off current ration higher than  $10^6$ .

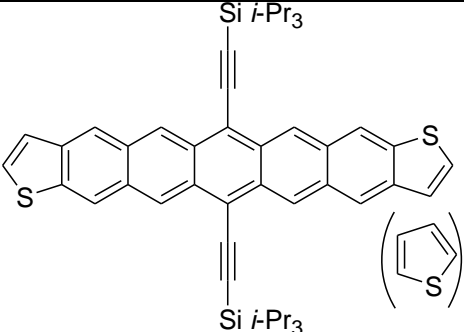
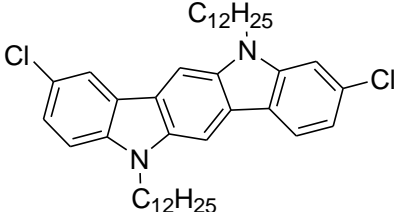
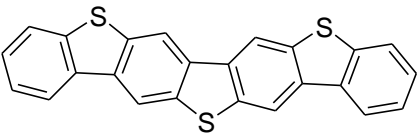
Heteroacenes are certainly a class of most promising materials for the fabrication of future OFETs. Good device stability, long lifetime and high mobility of heteroacenes are required to realize their benefits in practical applications (OFETs). The future looks promising as new and improved materials with better electronic properties are being

added to the arsenal of organic materials. Table 1.1 provides a summary of data for the *p*-type heteroacenes successfully employed for OFET application.

**Table 1.1.** Summary of FET mobilities and processing information of *p*-type heteroacenes

No.	Compounds	Processing method	$\mu$ ( $\text{cm}^2\text{V}^{-1}\text{s}^{-1}$ )	ref
1		Vacuum	0.15	44
2		Solution	0.1	45
3		Vacuum	2.0	46
4		Vacuum	2.9	47
5		Vacuum	0.012	48

6		Solution	0.01	49
7		Crystal	0.25 - 0.5	50
8	 <p>R = H, Ph</p>	Vacuum	0.31	51
9		Vacuum	0.011	52
10		Vacuum	0.12	52
11		Vacuum	0.02	53
12		Vacuum	$5 \times 10^{-5}$	54
13	 <p>R = H, CH<sub>3</sub></p>	Vacuum	$6 \times 10^{-3}$	54

14	 <p>The structure shows a central porphyrin ring with two trimethylsilyl ethynyl groups (<math>\text{Si } i\text{-Pr}_3</math>) at the top and bottom positions, and two thienyl groups at the left and right positions. A thienyl group is also shown in parentheses below the structure.</p>	Vacuum	$3 \times 10^{-5}$	55
15	 <p>The structure shows a phthalocyanine ring with two dodecyl groups (<math>\text{C}_{12}\text{H}_{25}</math>) on the nitrogen atoms and two chlorine atoms (<math>\text{Cl}</math>) on the benzene rings.</p>	Vacuum	0.085	56
16	 <p>The structure shows a phthalocyanine ring with four thienyl groups attached to the benzene rings.</p>	Vacuum	0.15	57

### 1.2.3. Helicene and circulenes

Helicenes *ortho*-fused polycyclic aromatic compounds in which benzene rings or other heteroaromatic compounds are angularly annulated to give helically shaped molecules (Figure 1.9).<sup>58</sup> The chemistry of helicenes has attracted continuing attention because of their unique structural, spectral, and optical features. Helicenes are significant for having chirality without the presence of asymmetric carbons and chiral centers. Helicenes chirality results from the non-superimposability of clockwise and counterclockwise helices. A resurgence in helicene chemistry occurred when Newman and Lednicer reported the synthesis of phenanthro[3,4-*c*]phenanthrene or hexahelicene, which displayed the stereotypical chirality due to steric overcrowding.<sup>59</sup> Since then,



several methods are reported for synthesizing helicenes. Today, the synthesis of helicenes with different lengths and substituents are possible.<sup>60</sup>

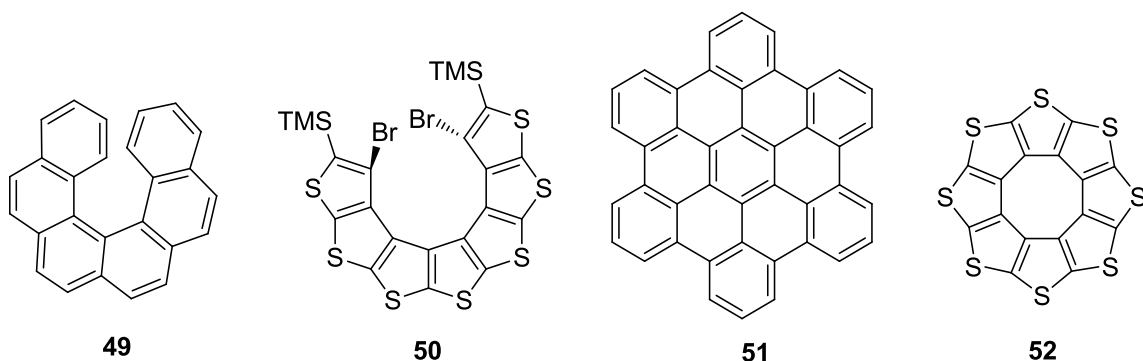


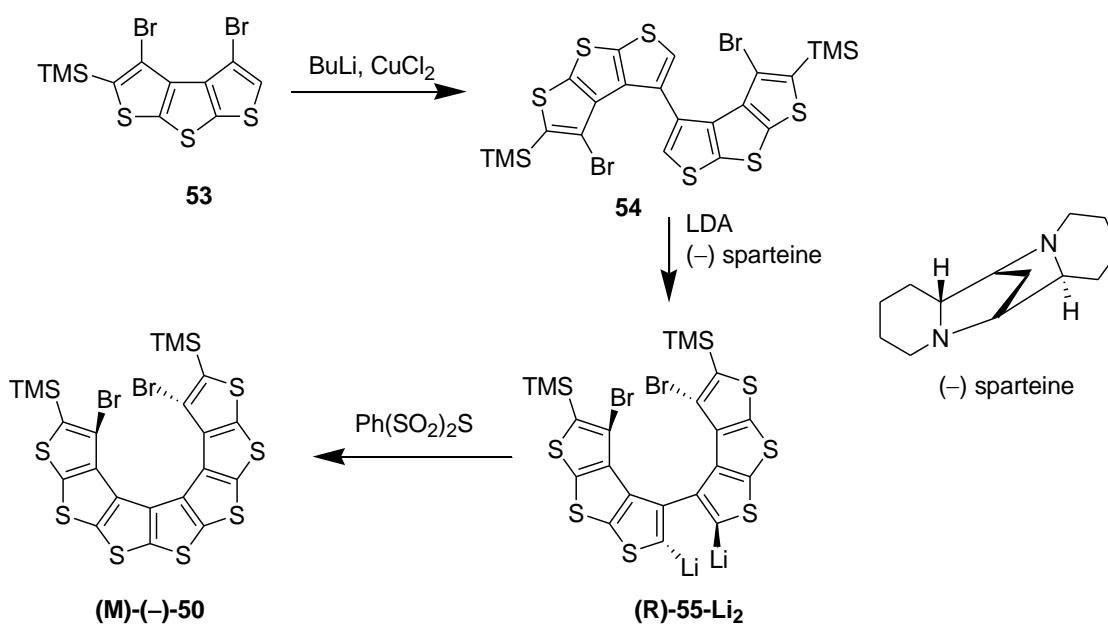
**Figure 1.9.** Structures of helicenes and circulenenes

Helicene molecules have enormous potential utility. Helicenes are foreseen to act as organic semiconductors, components of fast optical switches, asymmetric catalysts, and molecular actuators. Helicenes are potentially useful to the fields of nano-electronics, nano-mechanics, medicinal chemistry, and to the pharmaceutical industry. Due to their conjugated  $\pi$ -electron system, they can conduct electricity. The length of functionalized helicenes has been shown to be a function of pH, a quality that allows the molecule to stretch and contract, producing motion. To produce a significant amount of force as molecular actuators, it is desirable to produce polymeric helicenes that can develop a larger amount of motion and stretch larger distances. The electronic properties of organic semiconductors are a function of the purity of the compound, thus enantiomerically pure portions are needed.

Annulation of linear  $\beta$ -oligothiophenes gave helical carbon-sulfur  $(C_2S)_n$  oligomers for large values of  $n$  which reveal moderate curvature characteristic of helicenes. Such aesthetically pleasing structures are also associated with cross-conjugated  $\pi$ -systems for carbon-carbon frameworks. In the  $\beta$ -oligothiophenes all sulfur atoms are

positioned at the molecular periphery, facilitating multiple short intermolecular S...S contacts, which increase the effective dimensionality of the electronic structure and lead to enhanced transport properties. Rajca and co-workers with the successive asymmetric synthesis and resolution of helically annelated chiral  $\beta$ -heptathiophene **50** gave breakthrough in synthesis of such molecules (Scheme 1.6).<sup>61</sup>

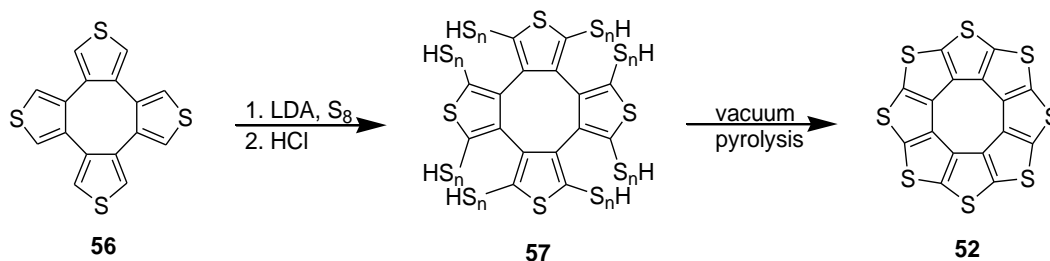
**Scheme 1.6.** Synthesis of heterohelicene<sup>61</sup>



Closed rings consisting of benzenes called circulenes. These compounds belong to a larger class of geodesic polyarenes. Whereas [5]circulene is bowl shaped [6]circulene is planar and [7]circulene has a unique saddle-shaped structure (compare to cone and partial cones in calixarene). The higher symmetry of such molecules (as compared to linear structures) is potentially more favorable for solid-state packing, although a practical advantage of this property is yet to be demonstrated. The discotic liquid crystalline derivatives of  $\pi$ -extended hexabenzocoronene (**51**) have been employed

as semiconductors in OFETs and photovoltaic cells and showed a hole mobility of up to  $10^{-3} \text{ cm}^2\text{V}^{-1}\text{s}^{-1}$ .<sup>62</sup> In the condensed, state it forms  $\pi$ -stacked columns with strong electronic coupling (and facile charge transport) along the column, but little or no electronic communication between the columns, which is responsible for pronounced one-dimensional charge transport. Introducing heteroatoms, such as S or Se, on the periphery of the circulene core, can induce intercolumnar interactions and, possibly, improve the charge-carrier mobility in such OSCs. The first all-heterocyclic octathio[8]circulene 52 (sunflower) has been recently synthesized (Scheme 1.7).<sup>63</sup> The treatment of 56 (obtained from 3,4-dibromothiophene) with LDA and sulfur resulted in complete sulfurization on thiophene rings and efficient formation of polythiolate which was acidified to yield polythiol (57). The vacuum pyrolysis of crude polythiol resulted in target circulene.

**Scheme 1.7.** Synthesis of octathio[8]circulene<sup>63</sup>



In the solid state and in thin films compound 52 packs in columns held together by close S...S contacts ( $\sim 3.25 \text{ \AA}$ ),<sup>64</sup> which could facilitate a 3D charge transport. Compound 52 can also be considered as a fused oligothiophene, thus establishing a structural similarity with linear thienoacenes, as well as a planar radialene. Recently, Peregichka *et.al.* demonstrated the *p*-type semiconducting behavior of sunflower

compound 52 in organic FETs. The highest hole mobility of  $9 \times 10^{-3} \text{ cm}^2 \text{V}^{-1} \text{s}^{-1}$  and on-off ratio of  $10^6$  was achieved for vapor deposited octathio[8]circulene.<sup>65</sup>

#### 1.2.4. $\beta, \beta'$ -Bridged bithiophenes

Annulation of bithiophene by bridging the  $\beta$  and  $\beta'$ -position with heteroatoms leads to useful building blocks for the construction of functional materials. The materials like dithieno[3,2-*b*:2'3'-*d*]thiophene (DTT) (58), dithieno[3,2-*b*:2'3'-*d*]silole (DTS) (59), dithieno[3,2-*b*:2'3'-*d*]phosphole (DTPh) (60) and dithieno[3,2-*b*:2'3'-*d*]pyrrole (61) belongs to this category and their structures are represented in Figure 1.10.<sup>66</sup>

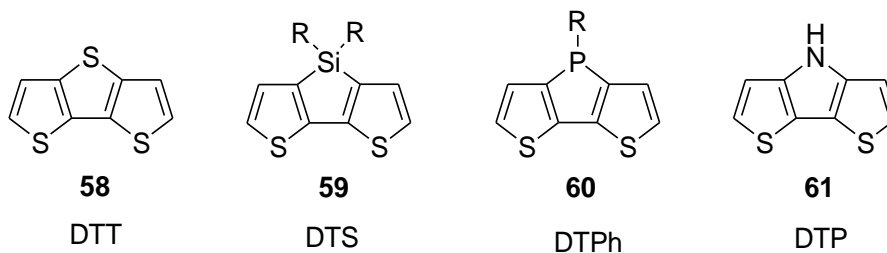
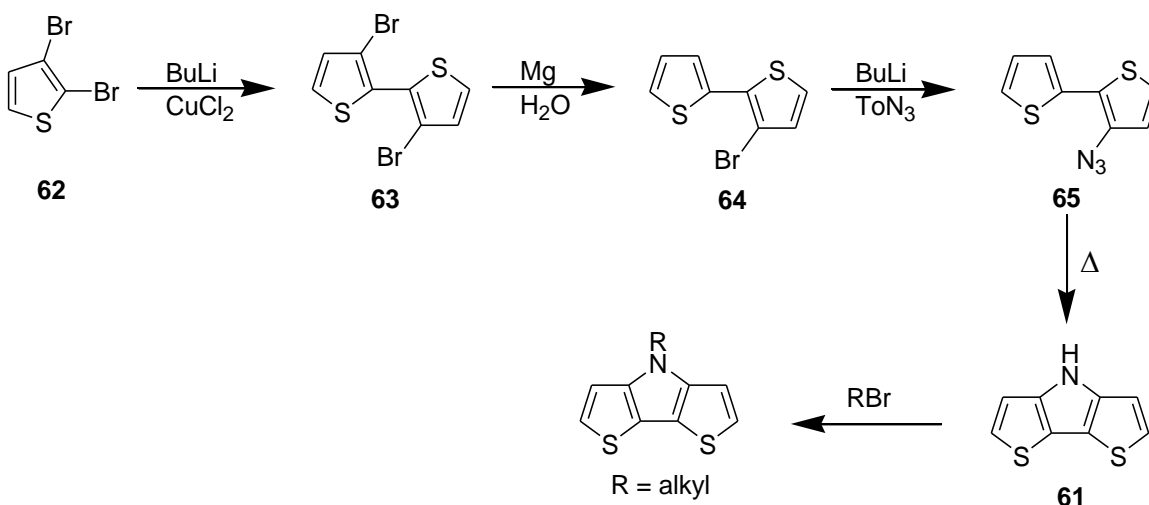


**Figure 1.10.** Structures of  $\beta, \beta'$ -bridged bithiophenes

Among the  $\beta, \beta'$ -bridged bithiophene systems DTT analogues have been developed as *p*-type semiconductors for OFETs. The fused nature of DTT promotes  $\pi$ -stacking, which is predicted to be a favorable motif for high charge transport in devices.<sup>67</sup> Until recently, far less attention was given to the related DTP, which are emerging as a useful structure for both molecular and polymeric materials.<sup>68</sup> Dithienopyrrole (DTP) contains a pyrrole fused tricyclic system similar to carbazole. The availability of pyrrole nitrogen for substitution (alkyl/aryl group) in DTP makes them superior to DTT in terms of solubility and tuning the properties (solid state, optical and electrochemical). DTPs are topic of current interest as native pyrrole and thiophene-based materials are well established in molecular electronics.<sup>69</sup> Although the first synthesis of

DTP dates back to 1983,<sup>70</sup> (Scheme 1.8) it was not until the early 1990's when the first investigations towards applications in molecular electronics of these materials occurred.<sup>71</sup> Electropolymerization studies of parent DTP system resulted in conducting polymers with poor solubility. The polymers are stable and showed electro-chromic behavior.<sup>72</sup>

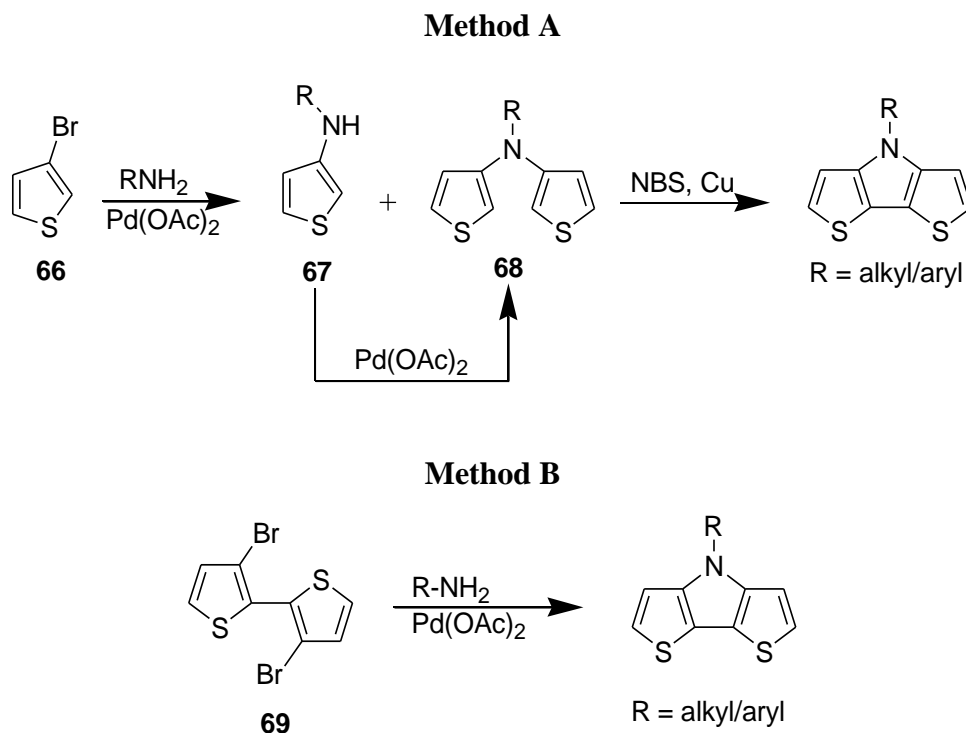
**Scheme 1.8.** Classical route to *N*-functionalized dithieno[3,2-*b*:2',3'-*d*]pyrroles<sup>70</sup>



Recently, new synthetic procedures towards *N*-functionalized DTP that provide necessary solubility for a successful application in molecular electronics and optoelectronics have been reported.<sup>73</sup> A few reports describe transition metal catalyzed routes to functionalized DTP (Scheme 1.9). The first approach involves the synthesis of DTP from 3-bromothiophene as starting material. 3-bromothiophene (66) was converted into the tertiary amine using a Buchwald-Hartwig reaction.<sup>74</sup> Since substantial amounts of mono-aminated product (67) was formed, only a second Buchwald-Hartwig reaction gave the desired tertiary amine (68) in good yields. The ring closure was performed by a one-pot, two-step reaction, which consists of bromination with NBS, followed by

Cu-mediated coupling.<sup>73a</sup> By the second route, DTP was synthesized using 3,3'-dibromobithiophene (69) and primary amines to build up the central pyrrole ring.<sup>73b</sup>

**Scheme 1.9.** Efficient synthesis of soluble *N*-functionalized dithieno[3,2-*b*:2',3'-*d*]pyrroles<sup>73</sup>



Ogawa and Rasmussen presented the first comprehensive study on the synthesis and optoelectronic properties including theoretical calculations in 2003.<sup>73a</sup> Structural investigations on the DTPs show that the fused-ring system is completely flat indicating a high degree of  $\pi$ -conjugation across the three ring-units. The dithieno[3,2-*b*]pyrrole exhibit a well-defined irreversible electrochemical oxidation processes and the frontier orbital's consist of the  $\pi$  and  $\pi^*$  transition. The photoluminescence quantum yields, however, are low ( $\Phi_{\text{PL}} = 0.28\%$ ). Rasmussen and co-workers reported a very high solution state quantum yield up to 65% for DTP-based oligomers and homopolymers (34 %).<sup>75</sup> However, the solid-state quantum yield of these materials, which is crucial for

optoelectronic application, was not reported. Recently, DTP based copolymers with fluorene showed a high quantum yield in solution as well as in solid state.<sup>76</sup> However, the OLED applications of DTP based materials are yet to be realized. Recently, DTP based copolymers are gaining significance and employed widely in electronic applications like OFETs and OPVs. DTP based copolymers with thiophene units leads to low band gap polymers, which are realized in OFET applications. The first field effect transistor property of DTP based material was reported by McCullough and co-workers.<sup>77</sup> They prepared a series of polymers containing *N*-alkyldithieno[3,2-*b*:2',3'-*d*]pyrroles and thiophene units using Stille coupling reaction. The thin film of these polymers prepared by solution processing showed highly disordered lamellar structure, which improved upon annealing. FET device fabricated out of these polymers showed an average mobility of  $0.13 \text{ cm}^2\text{V}^{-1}\text{s}^{-1}$ . Interestingly, the mobility of highly ordered annealed film show much lesser value than randomly ordered as-cast samples. Following the McCullough report, an independent work on *p*-channel FET mobilities of similar DTP-thiophene based copolymer was reported.<sup>78</sup> The bottom contact FET device of these polymers under ambient conditions exhibited good performance with a mobility up to  $0.11 \text{ cm}^2\text{V}^{-1}\text{s}^{-1}$  and current on-off ratio up to  $10^4$ . Very recently, *N*-alkyldithienopyrrole and bithiazole-based copolymer showed excellent FET performance with good air stability and solution processability.<sup>79</sup> A high FET mobility of  $0.14 \text{ cm}^2\text{V}^{-1}\text{s}^{-1}$  was achieved for the device without thermal annealing. Most of the devices fabricated using DTP based systems are hole transporting in nature. First electron transporting DTP based material was developed by Marder and co-workers.<sup>80</sup> DTP-perylene diimide based copolymers were synthesized and found to be electron transporting with electron mobilities of  $1.2 \times 10^{-3} \text{ cm}^2\text{V}^{-1}\text{s}^{-1}$ .

DTP being an electron rich monomer with lower ionization potential, when copolymerized with acceptor units leads to a low bandgap polymers with their absorption covering the entire visible and NIR region. Due to their low bandgap nature and higher stability, DTP based donor-acceptor (D-A) polymers are employed successfully in OPV applications.<sup>81</sup> A new D-A alternating copolymer of 2,6-DTP and 4,7-di(2'-thienyl)-2,1,3-benzothiadiazole resulted in a low bandgap of 1.46 eV. The photovoltaic device based on polymer:PCBM bulk heterojunction gave a power conversion efficiency of 2.18 %. The copolymer of DTP with 2,1,3-benzothiadiazole units resulted in NIR-absorbing materials with a bandgap of 1.72 eV.<sup>82</sup> The bulk heterojunction device constructed with polymer-PCBM blend showed the power conversion efficiency of 2.8%. Recently diketopyrrolopyrrole based DTP copolymers were reported to show good photovoltaic response.<sup>83</sup> The polymer with a band gap of 1.38 eV when blended with PCBM showed a power conversion efficiency of 1.12%. All these recent report on successful device application of DTP based compounds proves the potentially of this electron rich aromatic system as a promising candidate for future electronics.

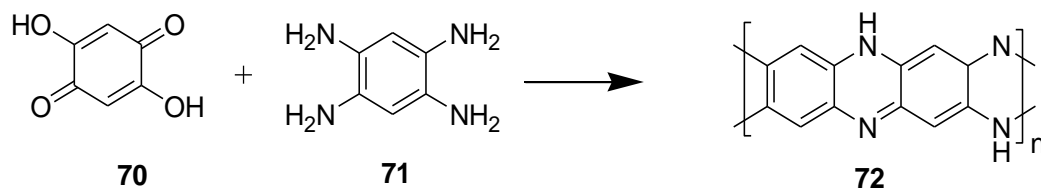
### 1.2.5. Ladder polymers

Ladder (ribbon) polymers consist of cyclic subunits, connected to each other by two links, which are attached to different sites of the respective subunits. Thus, ladder polymers have two independent strands of bonds, which are fused together regularly without merging to a single, or double bond or crossing each other. In the initial phase ladder polymers, was believed to make the polymers ideal candidates for applications requiring materials with high thermal, mechanical and chemical stability. This was rationalized by the fact that the molecular weight of ladder polymers obviously remains

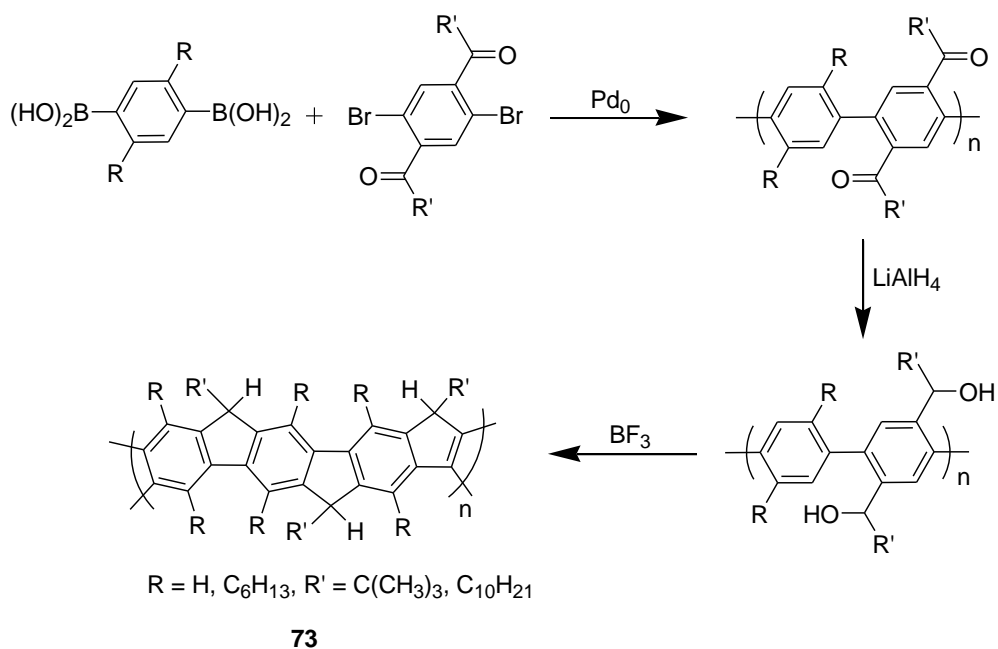


constant even if one or the other of the two strands breaks. However, it quickly turned out that, due to their poor solubility and infusibility, processing of these polymers was almost impossible. In the early 1970s poly(benzimidazobenzophenanthroline) (BBL), was synthesized and it was found to be readily processible into films using casting techniques.<sup>84</sup> In electronic aspect these polymers can be considered as 1D graphite ribbons, which will increase the dimensionality of polymers to overcome the effect of BLA and Peierls instability. Polyacenes is the most famous member of these series and subjected to numerous theoretical studies. However, polyacenes are highly unstable and hence their synthesis is difficult. The rigid polyphenanthrene based ladder polymer was synthesized by an electrophilic cyclization reaction. This polymer showed to show a large bandgap of 2.6 eV as predicted by the theoretical calculations.

Ladder-type polymers can be prepared by two main general strategies. The first employs the polymerization of multifunctional monomers in which both strands of the ladder structure are generated in a single reaction, while the second is based on the cyclization of a suitably substituted single stranded chain.<sup>85</sup> Polyquinoxalines (72) are probably one of the first class of ladder polymers to be investigated (Scheme 1.10).<sup>86</sup> These materials have been developed because of their high tensile strength and excellent thermal stability. Recently, their electronic properties have drawn renewed attention when it was suggested that the rigidity of the structure represented an interesting approach for the improvement of the electronic properties of the polymers with respect to electronic and nonlinear optical applications.<sup>9</sup>

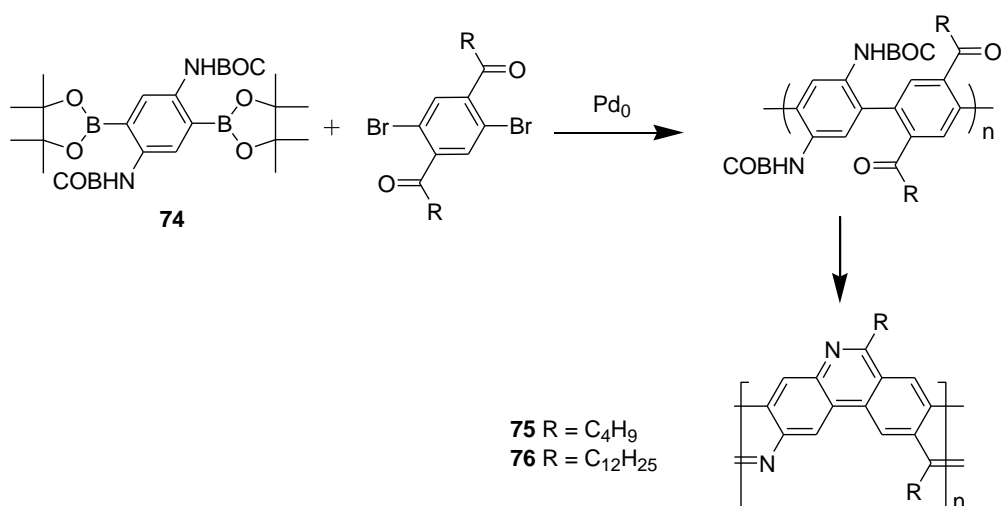
**Scheme 1.10.** Synthesis of ladder polyquinoxaline<sup>86</sup>

More conclusive results have been obtained concerning the preparation of ladder poly(*p*-phenylene) (PPP). The first fully planarized ladder PPP was synthesized in 1991 by Scherf and Müllen.<sup>87</sup> This polymer was obtained by Suzuki coupling of an aromatic dibromo diketone with an aromatic diboronic acid (Scheme 1.11). After polymerization, reduction of the keto groups afforded a polyalcohol which was readily converted into the ladder polymer 73 by Friedel-Crafts alkylation. The soluble polymer was obtained with a molecular weight  $M_n$  of 20 000 (about 45-50 phenylene units).

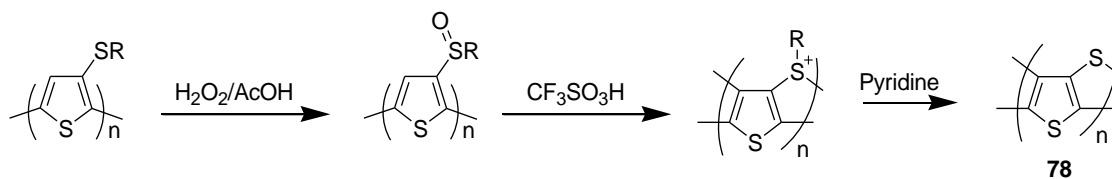
**Scheme 1.11.** Synthesis of planarized ladder PPP<sup>87</sup>

As shown by a study of the corresponding oligomers, for an equal number of benzene rings, fully bridged oligomers absorb at a considerably longer wavelength thus confirming that planarization significantly increases the effective conjugation. In fact, comparison of the optical spectra of PPP and of its ladder version has confirmed that the latter shows a smaller bandgap *i.e.* 2.70 vs 2.90- 3.20 eV for conventional PPP. Various topological isomers of ladder PPPs undergo low-energy losses by nonradiative decay and thus exhibit a high quantum efficiency of photoluminescence (>60%). Considered from a theoretical viewpoint and the calculated bandgaps were in the range of 2.40–2.50 eV, in good agreement with experiment.<sup>9</sup> Using a different approach, Tour *et al.* synthesized ladder PPPs in which consecutive phenyl rings are bridged by an imine group.<sup>88</sup> The polymers were synthesized by Pd(0)-catalyzed coupling of a dibromo diketone with a diboronic derivative of a protected diamine. After polymerization, treatment of the polymer with trifluoroacetic acid afforded the ladder polymers 75/76 (Scheme 1.12).

**Scheme 1.12.** Synthesis of ladder PPP bridged by imine group<sup>88</sup>



**Scheme 1.13.** Synthesis of ladder-type polythiophene<sup>89</sup>



The fused thiophene rings in these ladder polymers are considered almost coplanar, which is preferable for the band-gap reduction of  $\pi$ -conjugated materials. Tsuchida *et.al.* reported the first synthesis of linear ladder polythiophene (78) by polymer-analogous condensation of regioregular (head-to-tail) poly[3-(alkane-1-sulfinyl)-thiophene] (Scheme 1.13).<sup>89</sup> When compared with polythiophene, reduction of the bandgap was observed and is attributed to an increase in the quinonoid contribution to the electronic structure, which destabilized the HOMO and stabilized the LUMO. The smaller energy gap was supported by lower  $\pi$ - $\pi^*$  transition and smaller gap between cathodic and anodic potential. The geometric structures of the *p*-doped ladder-type polymer in the form of either polaron or bipolaron were calculated by adopting suitable boundary conditions to represent charged unit cells. The geometry relaxation process for the charged ladder-type backbone induces the appearance of a stronger quinonoidic character than that in the case of polythiophene, which suggests that the fused rings easily adopt quinonoid forms than thiophene rings. Calculated energetic aspects of the doping behavior and the paramagnetic resonance spectra of *p*-doped polymers revealed that the ladder-type polymer possesses polaron as the prevailing charged species, in contrast to many other  $\pi$ -conjugated polymers where bipolaron is the lowest-energy charge storage configuration.

### 1.2.6. Heteroacene polymers

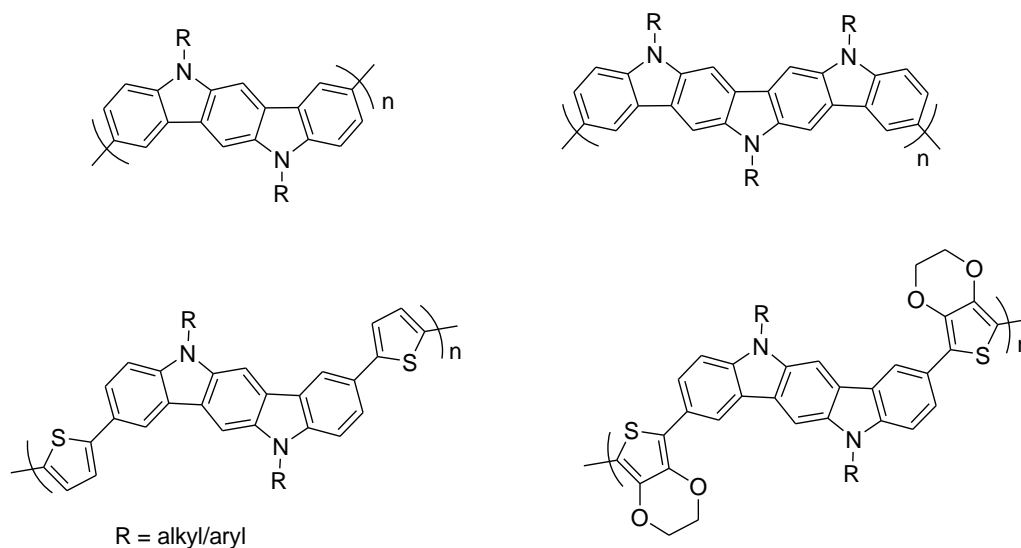


**Figure 1.11.** Chemical structures of heteroacene polymers

Heteroacenes are highly stable and soluble in common organic solvents with good device performance. It is interesting to include these heteroacenes into polymeric systems. Recently Leclerc and coworkers reported a series of heteroacene polymers based on indolocarbazole and diindolocarbazole based fused system using Zn-mediated dehalogenative coupling polymerization of dichloro derivatives (Figure 1.11).<sup>90</sup> The FET device performance of polyindolocarbazole was evaluated. The solution processable polymer showed a FET mobility of  $0.02 \text{ cm}^2\text{V}^{-1}\text{s}^{-1}$ , which is higher than that of corresponding monomer.<sup>91</sup> The better FET performance is attributed to the capability of the polymer to provide sufficient resonance stabilization to the ammonium radical cation be formed in the charge carrier transport process. The low-lying HOMOs and relatively large optical band gaps of poly(indolo[3,2-*b*]carbazole)s also rendered these semiconductors unusually stable under ambient conditions. Zotti and coworkers evaluated the influence of substitution pattern in homopolyindolocarbazoles and

polydiindolocarbazoles on their optoelectronic properties.<sup>92</sup> The copolymerizing bithiophene or BiEDOT copolymers with indolocarbazole resulted an increase in conductivity when compared with polyindolocarbazole. The presence of moderate electron-donating bithiophene units did not significantly affect the HOMO energy level, although it led to materials with lower band gaps. Therefore, one should be able to obtain low band-gap polymers where only the LUMO band is affected through the incorporation of electron-attracting units such as quinoxalines and benzothiazoles which could be useful to develop high efficient photovoltaic cells.

### 1.2.7. Other thiophene fused systems

Thiophene can be fused with aromatic or heteroaromatic units through their *b* or *c* face resulting in the fused conjugated thiophene systems (Figure 1.12).

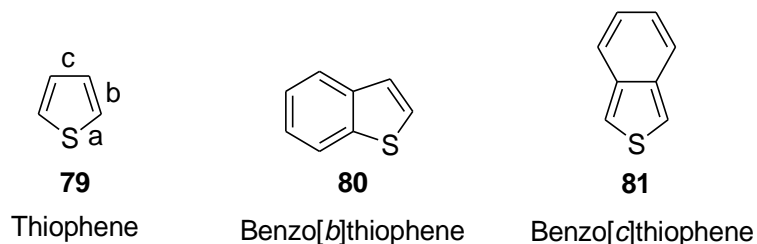


**Figure 1.12.** Structure of thiophene, benzene annealed to thiophene system

Thiophene annealed through *b* face results in the ladder  $\pi$ -conjugated heteroarene systems, which finds extensive application in OFET. Thiophene annealed through *c* face leads to thiophene monomers with stabilized quinoid states, which upon polymerization gave low bandgap polymers with potential application in OPV devices. Poly(isothianaphthene) (PITN) is the prototype of small bandgap polymers based on fused

thiophene.<sup>93</sup> The design was based on the idea that, after the fusion of thiophene and benzene, only one of them can accommodate aromatic sextet (Figure 1.13).

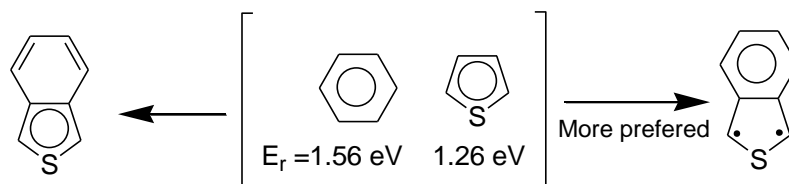


**Figure 1.13.** Aromatic resonance stabilization of isothianaphthene (ITN)

Based on the comparison of the aromatic resonance energy of thiophene (1.26 eV) and benzene (1.56 eV) it is more likely that benzene will have greater tendency to remain aromatic. Therefore, the limiting resonance forms C and D (Figure 1.14) is expected to be important and contribute in stabilizing the quinoid form of the polymer causing a bandgap of  $\sim 1$  eV, which is less by 1 eV than polythiophene (2 eV). As the double bond character of thiophene – thiophene linkages in polymers increases (less BLA) the quinoidal structure of thiophene becomes energetically more favorable. The more stable quinoidal structure is a result of the gain in aromaticity of the fused six-member ring. However, lacks of environmental stability of PITN reduce its practical applications. Though the quinoidal structure is stabilized to reduce BLA, the effective conjugation length is affected by the interaction of benzene H with adjacent units resulting in increased bandgap. Thus, the discovery of the low bandgap PITN, many compounds has been designed based on this fused ring system strategy.<sup>94</sup>

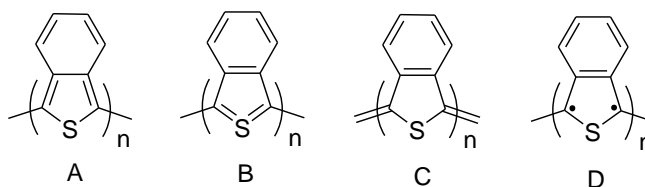
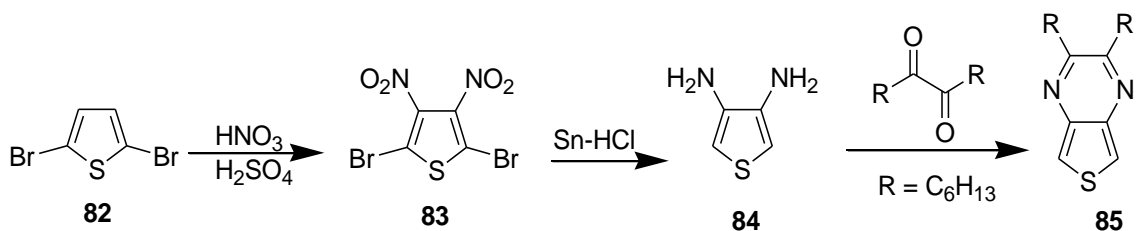


**Figure 1.14.** Resonance structure of poly(isothianaphthene)

The example of conjugated polymers utilizing the strategy above are those having thieno[3,4-*b*]pyrazine moiety.<sup>95</sup> These polymers were designed based on theoretical calculations of a bandgap prediction smaller than that of polyisothianaphene (0.7 eV vs 0.8 eV).

**Scheme 1.14.** Synthesis of 2,3-dihexylthieno[3,4-*b*]pyrazine<sup>95</sup>



Reduced steric interaction between adjacent monomer units was also expected, due to the replacement of carbon atoms by nitrogen atoms. The monomer 2,3-dihexylthieno[3,4-*b*]pyrazine was synthesized according to Scheme 1.14 and polymerized chemically using  $\text{FeCl}_3$  with a molecular weight cutoff of 3500. The electronic spectrum showed an absorption maximum at 875 nm (in  $\text{CHCl}_3$  solution) and at 915 nm for a solution cast film with a bandgap of 0.95 eV.<sup>95a</sup> Many of these polymers have been synthesized as precursors for low band gap polymers having absorptions in the red and near infrared regions.<sup>96</sup> Having low band gap and these specific absorptions, they are especially useful for the fabrication of solar cells.<sup>97</sup>

Another approach to achieve low bandgap is called the donor-acceptor systems. A strong electron-donor (D) and a strong electron acceptor (A) can interact and accommodate the charges that are associated with such mesomerism ( $\text{D-A} \leftrightarrow \text{D}^+=\text{A}^-$ ), thus they may result in an increased double bond character between these units.<sup>98</sup> The



interaction between the electron donor (D) and acceptor (A) moieties in an alternating donor–acceptor copolymer can result in the hybridization of the high-lying HOMO energy level of the donor and low-lying LUMO energy level of the acceptor, leading to a relatively small bandgap semiconductor.

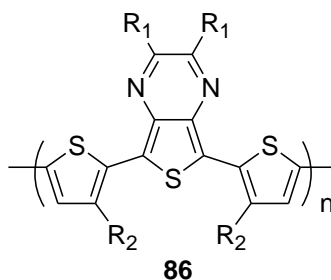


**Figure 1.15.** 5,7-di(2-thienyl)thieno[3,4-*b*]pyrazine<sup>99</sup>

An example of the strategy utilizing both fused rings and donor acceptor systems is illustrated in Figure 1.15. Martijn M. Wienk *et.al.* synthesized a high molecular weight low band gap polymers having alternating dithiophene and thieno-[3,4-*b*]pyrazine repeating units (86).<sup>99</sup> These polymers are soluble in most common organic solvents and can be easily processed into thin films, owing to the long alkoxy substituents on dithiophene or thieno[3,4-*b*]pyrazine moiety.<sup>99</sup> The insertion of a functional ring system into the middle of a trimeric precursor enables the construction of alternate donor and acceptor functionalities for the stabilization of unstable fused ring systems. Many systems based on thieno[3,4-*b*]pyrazine, thieno[3,4-*c*]thiophene, thieno[3,4-*b*]thiophene, thieno[3,4-*c*]thiadiazole and thieno[3,4-*b*]pyridine are synthesized utilizing this donor-acceptor and fused ring strategies and extensively applied for photovoltaic applications.<sup>100</sup> Substituted thienoimidazoles shows very interesting biological<sup>101</sup> and magnetic properties,<sup>102</sup> but their utility/application in material science has not been

explored. Hagan *et.al.* reported the bandgap of poly(thieno[3,4-*b*]imidazole) to be 0.85 eV, however no optical data were provided.<sup>103</sup>

It is well understood that the structure of the conjugated materials plays a dominant role in determining the properties of the materials. More research has been focused on developing new conjugated groups in order to understand their structure and function. The synthesis helps to determine the magnitude of  $\pi$ -conjugation and improve the device performance by eliminating the structural defects and planarization of the backbone. A large portion of the future research depends on synthesizing new materials that can be fabricated into electronic devices.

### 1.3. Aim and scope of the thesis

The focus of this work was to develop new fused conjugated heterocyclic systems containing sulfur and nitrogen atoms. The intention is to generate organic semiconducting oligomers and polymers based on new heterocyclic systems for organic field effect transistor (OFETs), organic light emitting diode (OLEDs) and organic photovoltaic (OPV) devices. In chapter 2, a series of symmetrical and unsymmetrical heteroacenes based on dithienopyrrole were synthesized. Their crystal packing, optical and electrochemical properties were studied and compared. In chapter 3, indole-fused indolodithienopyrrole and diindolodithienopyrrole based unsymmetrical and extended heteroacenes were synthesized and characterized. Highly stable and soluble extended (7-ring fused) heteroacenes was synthesized exploiting the stability afforded by the heteroatoms. It is noteworthy that the corresponding fused [*n*]acene (heptacene) is not very stable. In chapter 4, indolocarbazole based heteroacene was synthesized and characterized. Among the two linear isomers of indolocarbazole indolo[3,2-*b*]carbazole

was widely applied for OFET applications. The other linear isomer indolo[2,3-*a*]carbazole was found to have significant biological activity. However, its materials aspect was not explored. Here, we synthesized a series of thiadiazole (acceptor unit) fused indolo[2,3-*a*]carbazole based heteroacenes and studied their properties. In addition, the parent monomer was electro polymerized to afford a stable polymer. In chapter 5, a series of dithieno[3,2-*b*]pyrrole based oligomers were synthesized. Their solid-state structure, photophysical properties and electrochemical properties were studied in detail. The charge transport properties of the oligomers were investigated by time-of-flight photoconductivity technique. In chapter 6, a new series of thieno[3,4-*d*]imidazole based oligomers and polymers were synthesized. Poly(isothianaphthene), poly(thienopyrazine), poly(thienothiophene) represents the series of low bandgap polymers constructed from thiophene. However, the material (electronics) aspect of the similar compound (thienoimidazole) was not yet explored. Thienoimidazole skeleton resembles Biotin (Vitamin H), therefore thienoimidazole based compounds are extensively studied for biological application. In this chapter, we synthesized dithienothienoimidazole-based oligomers. Their solid state, photophysical and electrochemical properties are studied in detail. These oligomers are also electro polymerized to result in a low bandgap polymer with a bandgap of 1.6 eV. The photophysical and electrochemical properties of the polymers were also studied in detail.

## 1.4. References

---

- (1) Burroughes, J.H.; Bradley, D. D. C.; Brown, A. R.; Marks, R. N.; Mackay, K.; Friend, R. H.; Burns, P. L.; Holmes, A. B. *Nature* **1990**, *347*, 539. (b) Morin, J. F.; Beaupré, S.; Leclerc, M.; Lévesque, I.; D'Iorio, M. *Appl. Phys. Lett.* **2002**, *80*, 341. (c) Dimitrakopoulos, C. D.; Malenfant, P. R. L. *Adv. Mater.* **2002**, *14*, 99. (d) Winder, C.; Sariciftci, N. S. *J. Mater. Chem.* **2004**, *14*, 1077. (e) Grimsdale, A. C.; Chan, K. L.; Martin, R. E.; Jokisz, P. G.; Holmes, A. B. *Chem. Rev.* **2009**, *109*, 897. (f) Günes, S.; Neugebauer, H.; Sariciftci, N. S. *Chem. Rev.* **2007**, *107*, 1324. (g) Cheng, Y., -J.; Yang, S. -H.; Hsu, C., -S. *Chem. Rev.* **2009**, *109*, 5868.
- (2) Okamoto, Y.; Brenner, W. *Organic Semiconductors*. Reinhold Publishing Corporation: New York; 1964.
- (3) (a) Shirakawa, H.; Louis, E. J.; MacDiarmid, A. G.; Chiang, C. K.; Heeger, A. J. *Chem. Commun.* **1977**, 578. (b) Chiang, C. K.; Fincher, C. R. Jr., Park, Y. W.; Heeger, A. J.; Shirakawa, H.; Louis, E. J. *Phys. Rev. Lett.* **1977**, *39*, 1098.
- (4) Facchetti, A. *Materials Today* **2007**, *10*, 28.
- (5) (a) Coropceanu, V.; Cornil, J.; Da Silva, D. A.; Oliver, Y.; Silby, R.; Bredas, J. L. *Chem. Rev.* **2007**, *107*, 926. (b) Gholami, M.; Tykwinski, R. R. *Chem. Rev.* **2006**, *106*, 4997.
- (6) (a) Tour, J. M. *Chem. Rev.* **1996**, *96*, 537. (b) Van Hutten, P. F.; Krasnikov, V. V.; Hadziannou, G. *Acc. Chem. Res.* **1999**, *32*, 257. (c) Roncali, J. *Chem. Rev.* **1992**, *92*, 711. (d) Blouin, N.; Leclerc, M. *Acc. Chem. Res.* **2008**, *41*, 1110.
- (7) Salzner, U.; Lagowski, J. B.; Pickup, P. G.; Poirier, P. A. *Synth. Met.* **1998**, *96*, 177.
- (8) Thompson, B. C.; Kim, Y. G.; Reynolds, J. R. *Macromolecules* **2005**, *38*, 5359.
- (9) Roncali, J. *Chem. Rev.* **1997**, *97*, 173.
- (10) Bäuerle, P. *Adv. Mater.* **1992**, *4*, 102.
- (11) (a) Ajayaghosh, A. *Chem. Soc. Rev.* **2003**, *32*, 181. (b) Zhang Q. T.; Tour, J. M. *J. Am. Chem. Soc.* **1997**, *119*, 5065.
- (12) (a) Muliken, R. S.; Rieke, C. A.; Brown, W. G. *J. Am. Chem. Soc.* **1941**, *63*, 41. (b) Brédas, J. L.; Street, G. B.; Thémans, B.; André, J. M. *J. Chem. Phys.* **1985**, *83*, 1323.
- (13) Hernandez, V.; Castiglioni, C.; Del Zopo, M.; Zerbi, G. *Phys. Rev. B* **1994**, *50*, 9815.
- (14) Payne, M. M.; Parkin, S. R.; Anthony, J. E. *J. Am. Chem. Soc.*, **2005**, *127*, 8028.

- 
- (15) Simon, J.; Tournilhac, F.; André, J. J. *New. J. Chem.* **1987**, *11*, 383.
- (16) Klauk, H.; Halik, M.; Zschieschang, U.; Schmid, G.; Radlik, W. *J. Appl. Phys.* **2002**, *92*, 5259. (b) Sundar, V. C.; Zaumseil, J.; Podzorov, V.; Menard, E.; Willett, R. L.; Someya, T.; Gershenson, M. E.; Rogers, J. A. *Science* **2004**, *303*, 1644.
- (17) Dros, A. B.; Baas, J.; Meetsma, A.; De Boer, J. L.; Palstra, T. T. M. *Acta Cryst. C* **2001**, *57*, 939.
- (18) Swartz, C. R.; Parkin, S. R.; Bullock, J. E.; Anthony, J. E.; Mayer, A. C.; Malliaras, G. G. *Organic Letters* **2005**, *7*, 3163-3166
- (19) Clar, E. *Polycyclic Aromatic Hydrocarbons*. Academic Press: London; 1964, Vol. 1.
- (20) Laquindanum, J. G.; Katz, H. E.; Lovinger, A. J. *J. Am. Chem. Soc.* **1998**, *120*, 664.
- (21) Anthony, J. E. *Chem. Rev.* **2006**, *106*, 5028.
- (22) Fukazawa, A.; Yamaguchi, S. *Chem. Asian, J.* **2009**, *4*, 1386.
- (23) Baumgartner, T.; Réau, R. *Chem. Rev.* **2006**, *106*, 4681.
- (24) Li, X. -C.; Siringhaus, H.; Garnier, F.; Holmes, A. B.; Moratti, S. C.; Feeder, N.; Clegg, W.; Teat, S. J.; Friend, R. H. *J. Am. Chem. Soc.* **1998**, *120*, 2206.
- (25) (a) Laquindanum, J. G.; Katz, H. E.; Lovinger, A. J.; Dodabalapur, A. *Adv. Mater.* **1997**, *8*, 36. (b) Payne, M. M.; Parkin, S. R.; Anthony, J. E.; Kuo, C. -C.; Jackson, T. N. *J. Am. Chem. Soc.* **2005**, *127*, 4986.
- (26) Janosik, T.; Wahlstrom, N.; Bergman, J. *Tetrahedron* **2008**, *64*, 9159.
- (27) Sun, Y. M.; Ma, Y. Q.; Liu, Y. Q.; Lin, Y. Y.; Wang, Z. Y.; Wang, Y.; Di, C. A.; Xiao, K.; Chen, X. M.; Qiu, W. F.; Zhang, B.; Yu, G.; Hu, W. P.; Zhu, D. *Adv. Funct. Mater.* **2006**, *16*, 426.
- (28) Zhang, X.; Côté, A. P.; Matzger, A. J. *J. Am. Chem. Soc.* **2005**, *127*, 10502.
- (29) Xiao, K.; Liu, Y.; Zhang, W.; Wang, F.; Gao, J.; Qiu, W.; Ma, Y.; Cui, G.; Chen, S.; Zhan, X.; Yu, G.; Qin, J.; Hu, W.; Zhu, D. *J. Am. Chem. Soc.* **2005**, *127*, 13281.
- (30) Okamoto, T.; Kudoh, K.; Wakamiya, A.; Yamaguchi, S. *Chem. Eur, J.* **2007**, *13*, 548.
- (31) Gao, P.; Feng, X.; Yang, X.; Enkelmann, V.; Baumgarten, M.; Müllen, K. *J. Org. Chem.* **2008**, *73*, 9207.
- (32) Okamoto, T.; Kudoh, K.; Wakamiya, A.; Yamaguchi, S. *Org. Lett.* **2005**, *7*, 5301.

- 
- (33) Ebata, H.; Izawa, T.; Miyazaki, E.; Takimiya, K.; Ikeda, M.; Kuwabara, H.; Yui, T. *J. Am. Chem. Soc.* **2007**, *129*, 15732.
- (34) Gao, P.; Beckmann, D.; Tsao, H. N.; Feng, M.; Enkelmann, V.; Pisula, W.; Müllen. *Chem. Commun.* **2008**, 1548.
- (35) Gao, J. H.; Li, R. J.; Li, L. Q.; Meng, Q.; Jiang, H.; Li, H. X.; Hu, W. P. *Adv. Mater.* **2007**, *19*, 3008.
- (36) Tang, M. L.; Okamoto, T.; Bao, Z. *J. Am. Chem. Soc.* **2006**, *128*, 16002.
- (37) Gao, P.; Beckmann, D.; Tsao, H. N.; Feng, X.; Enkelmann, V.; Baumgarten, M.; Pisula, W.; Müllen, K. *Adv. Mater.* **2009**, *21*, 213.
- (38) Qi, T.; Guo, Y.; Liu, Y.; Xi, H.; Zhang, H.; Gao, X.; Liu, Y.; Lu, K.; Ku, C.; Yu, G.; Zhu, D.; *Chem. Commun.* **2008**, 6227.
- (39) Murphy, A. R.; Fréchet, M. J. *Chem. Rev.* **2007**, *107*, 1066.
- (40) Bouchard, J.; Wakim, S.; Leclerc, M. *J. Org. Chem.* **2004**, *69*, 5705.
- (41) Wu, Y.; Li, Y.; Gardner, S.; Ong, B. S. *J. Am. Chem. Soc.* **2005**, *127*, 614.
- (42) Wakim, S.; Buchard, J.; Simard, M.; Drolet, N.; Tao, Y.; Leclerc, M. *Chem. Mater.* **2004**, *16*, 4386.
- (43) Boudreault, P. T.; Wakim, S.; Blouin, N.; Simard, M.; Tessier, C.; Tao, Y.; Leclerc, M. *J. Am. Chem. Soc.* **2007**, *129*, 9125.
- (44) Laquindanum, J. G.; Katz, H. E.; Lovinger, A. J. *J. Am. Chem. Soc.* **1998**, *120*, 664.
- (45) Payne, M. M.; Parkin, S. R.; Anthony, J. E.; Kuo, C. C.; Jackson, T. N. *J. Am. Chem. Soc.* **2005**, *127*, 4986.
- (46) Yamamoto, T.; Takimiya, K. *J. Am. Chem. Soc.* **2007**, *129*, 2224.
- (47) Takimiya, K.; Ebata, H.; Sakamoto, K.; Izawa, T.; Otsubo, T.; Kunugi, Y. *J. Am. Chem. Soc.* **2006**, *128*, 12604.
- (48) Liu, W. J.; Zhou, Y.; Ma, Y.; Cao, Y.; Wang, J.; Pei, J. *Org. Lett.* **2007**, *9*, 4187.
- (49) Zhou, Y.; Liu, W. J.; Ma, Y.; Wang, H.; Qi, L.; Cao, Y.; Wang, J.; Pei, J. *J. Am. Chem. Soc.* **2007**, *129*, 12386.
- (50) Yamada, K.; Okamoto, T.; Kudoh, K.; Wakamiya, A.; Yamaguchi, S.; Takeya, J. *Appl. Phys. Lett.* **2007**, *90*, 072102(1)072102(3).

- 
- (51) Takimiya, K.; Kunugi, Y.; Konda, Y.; Ebata, H.; Toyoshima, Y.; Otsubo, T. *J. Am. Chem. Soc.* **2006**, *128*, 3044.
- (52) Wex, B.; Kaafarani, B. R.; Schoreder, R.; Majewski, L. A.; Burckel, P.; Grell, M.; Neckers, D. C. *J. Mater. Chem.* **2006**, *16*, 1121.
- (53) Ma, Y.; Sun, Y.; Liu, Y.; Gao, J.; Chen, S.; Sun, X.; Qiu, W.; Yu, G.; Cui, G.; Hu, W.; Zhu, D. *J. Mater. Chem.* **2005**, *15*, 4895.
- (54) Miao, Q.; Nguyen, T. -Q.; Someya, T.; Blanchet, G. B.; Nuckolls, C. *J. Am. Chem. Soc.* **2003**, *125*, 10284.
- (55) Morgenroth, F.; Berresheim, A. J.; Wagner, M.; Müllen, K. *Chem. Commun.* **1998**, 1138.
- (56) Li, Y.; Wu, Y.; Gardner, S.; Ong, B. S. *Adv. Mater.* **2005**, *17*, 849.
- (57) Siringhaus, H.; Friend, R. H.; Wang, C.; Leuninger, J.; Müllen, K. *J. Mater. Chem.* **1999**, *9*, 2095.
- (58) Torroba, T.; Gracia-Valverde, M. *Angew. Chem. Int. Ed.* **2006**, *45*, 8092.
- (59) (a) Newman, M. S.; Luts, W. B.; Lednicer, D. *J. Am. Chem. Soc.* **1955**, *77*, 3420. (b) Newman, M. S.; Lednicer, D. *J. Am. Chem. Soc.* **1956**, *78*, 4765.
- (60) Li, C.; Shi, J.; Xu, L.; Wang, Y.; Cheng, Y.; Wang, H. *J. Org. Chem.* **2009**, *74*, 408.
- (61) a) Miyasaka, M.; Rajca, A.; Pink, M.; Rajca, S. *J. Am. Chem. Soc.* **2005**, *127*, 13806. b) Rajca, A.; Miyasaka, M.; Pink, M.; Wang, H.; Rajca, S. *J. Am. Chem. Soc.* **2004**, *126*, 15211. c) Miyasaka, M.; Rajca, A.; Pink, M.; Rajca, S. *Chem. Eur. J.* **2004**, *10*, 6531.
- (62) Pisula, W.; Menon, A.; Stepputat, M.; Lieberwirth, I.; Kolb, U.; Tracz, A.; Siringhaus, H.; Pakula, T.; Müllen, K. *Adv. Mater.* **2005**, *17*, 684.
- (63) Chernichenko, K. Y.; Sumerin, V. V.; Shpanchenko, R. V.; Balenkova, E. S.; Nenajdenko, V. G. *Angew. Chem., Int. Ed.* **2006**, *45*, 7367.
- (64) Fujimoto, T.; Suizu, R.; Yoshikawa, H.; Awaga, K. *Chem.–Eur. J.* **2008**, *14*, 6053.
- (65) Dadvand, A.; Cicoira, F.; Chernichenko, K. Y.; Balenkova, E. S.; Osuna, R. M.; Rosei, F.; Nenajdenko, V. G.; Perepichka, D. F. *Chem. Commun.* **2008**, 5354.
- (66) Baumgarter, T. *Journal of Inorganic and Organometallic Polymers and Materials* **2005**, *15*, 389.

- (67) Roncali, J. In *Handbook of Conducting Polymers*, 2<sup>nd</sup> ed.; Stokheim, T. A., Elsenbaumer, R. L., Reynolds, J. R., Eds.; Marcel Dekker: New York, 1998; Chapter 12.
- (68) Rasmussen, S. C.; Straw, B. D.; Hutchison, J. E. In *Semiconducting Polymers: Applications, Synthesis and Properties*; Hsieh, B. R., Wei, Y.; Galvin, M., Eds.; ACS Symposium Series 735; American Chemical Society: Washington, DC, 1999; Chapter 21.
- (69) Mishra, A.; Ma, C -Q.; Bäuerle, P. *Chem. Rev.* **2009**, *109*, 1141.
- (70) Zanirato, P.; Spagnolo, P.; Zanardi, G. *J. Chem. Soc., Perkin Trans. 1* **1983**, 2551.
- (71) Berlin, A.; Pagani, G. A.; Sannicoló, F.; Schiavon, G.; Zotti, G. *Polymer*, **1991**, *82*, 1841.
- (72) Begiato, G.; Casalbore-Miceli, G.; Geri, A.; Berlin, A.; Pagani, P. *Synth. Met.* **1996**, *82*, 11.
- (73) (a) Ogawa, K.; Rasmussen, S. C. *J. Org. Chem.* **2003**, *68*, 2921. (b) Nozaki, K.; Takahashi, K.; Nakano, K.; Hiyama, T. Tang, H. -Z.; Fujika, M.; Yamaguchi, S.; Tamao, K. *Angew. Chem. Int. Ed. Engl.* **2003**, *42*, 2051. (c) Fujitsuka, M.; Sazo, T.; Sezaki, F.; Tanaka, K.; Watanabe, A.; Ito, O. *J. Chem. Soc., Faraday Trans.* **1998**, *94*, 3331.
- (74) Ogawa, K.; Radke, K. R.; Rothstein, S. D.; Rasmussen, S. C. *J. Org. Chem.* **2001**, *66*, 9067.
- (75) (a) Radke, K. R.; Ogawa, K.; Rasmussen, S. C. *Org. Lett.*, **2005**, *7*, 5253. (b) Mo, H.; Rasmussen, S. C. *Polym. Prepr.* **2007**, *48*, 61. (c) Ogawa, K.; Mo, H.; Radke, K. R.; Rasmussen, S. C. *Polym. Prepr.* **2007**, *48*, 40. (d) Ogawa, K.; Rasmussen, S. C. *Macromolecules*, **2006**, *39*, 1771.
- (76) Zhang, Wei, Li, J.; Zhang, B.; Qin, J. *Macromol. Rapid Commun.* **2008**, *29*, 1603.
- (77) Liu, J.; Zhang, R.; Sauv e, G.; Kwalewski, T.; McCullough, R. D. *J. Am. Chem. Soc.* **2008**, *130*, 13167.
- (78) Zhang, W.; Li, J.; Zou, L.; Zhang, B.; Qin, J.; Lu, Z.; Poon, Y. F.; Chan-Park, M. B.; Li, C. M. *Macromolecules* **2008**, *41*, 8953.
- (79) Liu, J.; Zhang, R.; Osaka, I.; Mishra, S.; Javier, A. E.; Smilgies, D.; Kowalewski, McCullough, R. D. *Adv. Funct. Mater.* **2009**, *19*, 1.
- (80) Zhan, X.; Tan, Z.; Zhu, E.; Li, Y.; Misra, R.; Grant, A.; Domercq, B.; Zhang, X.; An, Z.; Zhang, A.; Zhang, X.; Barlow, S.; Kippelen, B.; Marder, S. R. *J. Mater. Chem.* **2009**, *19*, 5794.



- (81) Zhou, E.; Nakamura, M.; Nishizawa, T.; Zhang, Y.; Wei, Q.; Tajima, K.; Yang, C.; Hashimoto, K. *Macromolecules* **2008**, *41*, 8302.
- (82) Yue, W.; Zhao, Y.; Shao, S.; Tian, H.; Xie, Z.; Geng, Y.; Wang, F. *J. Mater. Chem.* **2009**, *19*, 2199.
- (83) Zhou, E.; Yamakawa, S.; Tajima, K.; Yang, C.; Hashimoto, K. *Chem. Mater.* **2009**, *21*, 4055.
- (84) (a) Arnold, F. E.; Van Deusen, R. L. *J. Appl. Polym. Sci.* **1971**, 2035. (b) Sicree, A. J. Arnold, F. E.; Van Deusen, *J. Polym. Sci. Polym. Chem. Ed.* **1994**, *12*, 265.
- (85) Schlüter, A. -D. *Adv. Mater.* **1991**, *6*, 282.
- (86) Baumgarten, M.; Bunz, U.; Scherf, U.; Müllen, K. *In Molecular Engineering for Advanced Materials*; Becher, J., Schaumburg, K., Eds.; Kluwer Academic Publishers: Dordrecht, 1995; p 159.
- (87) Bohnen, A.; Koch, K.-H.; Lüttke, W.; Müllen, K. *Angew. Chem., Int. Ed. Engl.* **1990**, *29*, 525.
- (88) Tour, J. M.; Lamba, J. J. S. *J. Am. Chem. Soc.* **1993**, *115*, 4935.
- (89) Oyaizu, K.; Iwasaki, T.; Tukahara, Y.; Tachida, E. *Macromolecules* **2004**, *37*, 1257.
- (90) Blouin, N.; Michaud, A.; Wakim, S.; B. P. -L. T. Leclerc, M.; Vercelli, B.; Zecchin, S.; Zotti, G. *Macromol. Chem. Phys.* **2006**, *207*, 166.
- (91) Yuning, L.; Wu, Y.; Ong, B. S. *Macromolecules* **2006**, *39*, 6521.
- (92) Blouin, N.; Leclerc, M.; Vercelli, B.; Zecchin, S.; Zotti, G. *Macromol. Chem. Phys.* **2006**, *207*, 175.
- (93) (a) Wudl, F.; Kobayashi, M.; Heeger, A. J. *J. Org. Chem.* **1984**, *49*, 3382. (b) Meng, H. Wudl, F. *Macromolecules*, **2001**, *34*, 1810.
- (94) Rasmussen, S. C.; Pomerantz, M. *In Handbook of Conducting Polymers*, 3<sup>rd</sup> ed.; Stokheim, T. A., Reynolds, J. R., Eds.; CRC Press: Boca Raton, **2007**; Chapter 12.
- (95) (a) Pomerantz, M.; Chaloner-Gill, B.; Harding, L. O.; Tseng, J. J.; Pomerantz, W. J. *Chem. Soc. Chem. Commun.* **1992**, 1672. (b) Pomerantz, M.; Chaloner-Gill, B.; Harding, L. O.; Tseng, J. J.; Pomerantz, W. *Synth. Met.* **1993**, *55*, 960.
- (96) (a) Zhang, F.; Perzon, E.; Wang, X.; Mammo, W.; Andersson, M. R.; Inganäs, O. *Adv. Funct. Mater.* **2005**, *15*, 745. (b) Thomas, K. R. J.; Lin, J. T.; Tao, Y., -T.; Chuen, C., -H. *Adv. Mater.* **2002**, *14*, 822. (c) Shahid, M.; Ashraf, R. S.; Klemm, E.; Sensfuss, S. *Macromolecules* **2006**, *39*, 7844.

- 
- (97) Petersen, M. H.; Hagemann, O.; Nielsen, K. T.; Jørgensen, M.; Krebs, F. C. *Sol. Energy Mater. Sol. Cells* **2007**, *91*, 996.
- (98) van Mullekom, H. A. M.; Vekemans, J. J. M.; Havinga, E. E.; Meijer, E.W. *Material Science and Engineering* **2001**, *32*, 1.
- (99) Wienk, M. M.; Turbiez, M. G. R.; Struijk, M. P.; Fonrodona, M.; Janssen, R. A. J. *Appl. Phys. Lett.* **2006**, *88*, 153511.
- (100) Qin, Y.; Kim, J. Y.; Frisbie, C. D.; Hillmyer, M. A. *Macromolecules* **2008**, *41*, 5563.
- (101) (a) Beil, W.; Staar, U.; Sewing, K., -F. *Eur.J. Pharmacol.* **1990**, *187*, 455-77. (b) Nimmesgern, H.; Weidmann, K.; Lang, H,-J.; Ripeel, R.; Herling, A. W. (Hoechst Aktiengesellschaft). Application: 218386, 1990. (c) (20) Lang, H.-J.; Heinelt, U.; Wirth, K.; Licher, T. (Aventis Pharma Deutschland GmbH). Application: US 2005/0075385 A1, 2005.
- (102) Nagashima, H.; Inoue, H.; Yoshinoka, N. *Polyhedron* **2003**, *22*, 1823.
- (103) Hagan, A. J.; Moratti, S. C.; Sage, I. C. *Synth. Met.* **2001**, *119*, 147.

## *Chapter 2*

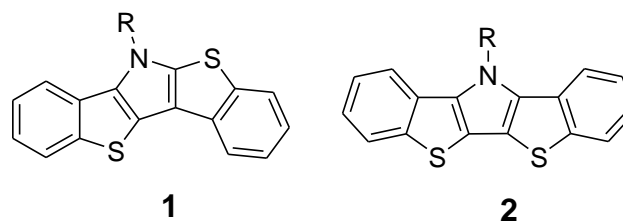
# *Symmetric and Unsymmetric Dibenzothienopyrroles*

*Publication from the chapter:*

**Balaji, G.;** Valiyaveetil, S. “*Synthesis and Properties of Symmetric and Unsymmetric Dibenzothienopyrroles*”, *Org. Lett.* **2009**, *11*, 3358-3361.

## 2.1. Introduction

Key advantages of using organic materials for electronic applications are their easy accessibility in pure form, tunability of properties and easy fabrication.<sup>1</sup> Acenes such as pentacene<sup>2</sup> are common benchmarks in the field of organic electronics with a high mobility of  $\sim 3 \text{ cm}^2 \text{ V}^{-1} \text{ s}^{-1}$ . However, pentacene and other higher acenes suffer from low environmental stability and poor solubility in common organic solvents which limits their practical applications.<sup>3</sup> Heteroacenes are  $\pi$ -conjugated ladder molecules, with heteroatoms (e.g., N, S, O *etc.*) incorporated into the structures.<sup>4</sup> Some heteroacenes such as thieno[*n*]acenes<sup>5</sup>, pyrrole based indolocarbazole<sup>6</sup> and thiophene-benzene annulated acene<sup>7</sup> have been successfully tested for application as organic field effect transistors (OFETs). Most of the heteroacenes reported in the literature are thiophene based symmetrical systems.<sup>8</sup> Unsymmetrical heteroacenes provide an inherent advantage of having a high dipole moment which is expected to provide dense packing and better transport properties.<sup>9</sup> Synthetic strategies for a highly extended  $\pi$  system possessing more than four aromatic rings are limited.<sup>10</sup> Moreover, synthesis of unsymmetrical heteroacenes is challenging owing to the requirement of selective reaction conditions or a long synthetic route. Heteroacenes containing more than two different heteroatoms have also been reported<sup>11</sup> though only a few unsymmetrical heteroacenes are known.<sup>9,12</sup> In this regard unsymmetrical heteroacenes **1**, and symmetrical heteroacenes **2** were synthesized (Figure 2.1).<sup>13</sup> Their properties, along with their molecular organization in the crystal lattice are studied in detail.



R = (a) *n*-butyl, (b) 4-hexylphenyl

**Figure 2.1.** Structures of symmetric and unsymmetric heteroacenes

## 2.2. Experimental

### 2.2.1. Materials and measurements

All reactions were carried out under inert atmosphere (Nitrogen or Argon), unless specified otherwise. All reagents were purchased from Aldrich, Fluka or Merck and used without further purification unless otherwise stated. All reactions were carried out with freshly distilled anhydrous solvents under inert atmosphere. Toluene was dried over calcium hydride and distilled under nitrogen atmosphere. 3-bromothionaphene, 2,3-dibromothionaphene, *n*-butyl bromide, butyl amine, and 4-hexylaniline were purchased from Aldrich. Chromatography was performed using silica gel (230-400 mesh). NMR spectra  $^1\text{H}$  (300 MHz) were collected on a Bruker AMX 300 spectrometer. All NMR data was calibrated with solvent signals and peak multiplicity was indicated as follows: s = singlet, d = doublet, t = triplet, dd = doublet of doublet, m = multiplet, b = broad. The UV-vis spectra were measured in chloroform solution on a Shimadzu UV-1601 PC spectrophotometer. Cyclic voltammetric measurements were performed in  $\text{CH}_2\text{Cl}_2$  containing 2.0 mM of substrate and 0.1 M of *n*- $\text{Bu}_4\text{NPF}_6$  as supporting electrolyte at a scan rate between  $100 \text{ mVs}^{-1}$ . The counter and working electrodes were Pt wires, and the reference electrode was Ag/AgCl. The potentials are calibrated with ferrocene/ferrocenium

redox couple (0.46 V vs Ag/AgCl). Onset value of the oxidation wave of the substrate ( $E_{\text{ox}}^{\text{onset}}$ ) was used to calculate HOMO energy level, using the relation  $E_{\text{HOMO}} = -(4.38 + E_{\text{ox}}^{\text{onset}})$ . LUMO levels were calculated from  $E_{\text{HOMO}}$  and optical band gap ( $E_g$ ). Single crystals of acene compounds suitable for structural analysis were obtained by recrystallization from chloroform. The X-ray crystal structure analysis was made on a Rigaku AFC-7 (Mo  $K\alpha$  radiation,  $\lambda = 0.71069 \text{ \AA}$ , graphite monochromator,  $T = 296 \text{ K}$ ,  $2\theta_{\text{max}} = 55.0^\circ$ ) or a Rigaku Rapid-IP (Mo  $K\alpha$  radiation,  $\lambda = 0.71069 \text{ \AA}$ , graphite monochromator,  $T = 296 \text{ K}$ ,  $2\theta_{\text{max}} = 55.0^\circ$ ).

### 2.2.2. Synthesis procedure

**General procedure for amination of heteroaryl halides:** Amine (1.5 mmol), palladium acetate (34 mg, 0.15 mmol), tri-tert-butylphosphine tetrafluoroborate (44 mg, 0.15 mmol)  $\text{NaO}^t\text{Bu}$  (6 mmol) were measured and mixed with 30 ml of toluene. 3-bromo-benzo[*b*]thiophene (0.32 g, 1.5 mmol) was added to the mixture, stirred and refluxed. After 3 hours, another equivalence of palladium acetate (34 mg, 0.15 mmol), tri-tert-butylphosphonium tetrafluoroborate (44 mg, 0.15 mmol) and 3-bromo-benzo[*b*]thiophene (0.32 g, 1.5 mmol) were added and allowed to reflux for another 2 hours. After this, reaction mixture was cooled water was added and extracted with ethyl acetate ( $3 \times 50 \text{ ml}$ ). Organic layer was dried over anhydrous sodium sulfate and concentrated under reduced pressure. The crude product was purified by chromatography over neutral alumina with 1% hexane/ethyl acetate as eluent.

***N*-Butyl-*N*-(2'-benzo[*b*]thienyl)-benzo[*b*]thiophene (7a):** Yellow viscous liquid (40%)  
 $^1\text{H NMR}$  (300 MHz,  $\text{CDCl}_3$ ,  $\delta$ , ppm): 7.99 (b, 2H), 7.85 (t,  $J = 6.9 \text{ Hz}$ , 2H), 7.62 (s, 1H), 7.54-7.41 (b, 5H), 3.13 (t,  $J = 7.23 \text{ Hz}$ , 2H), 1.43 (m, 2H), 1.14 (m, 2H), 0.82 (m, 3H).

$^{13}\text{C}$  NMR (75.4 MHz,  $\text{CDCl}_3$ ,  $\delta$ , ppm): 139.7, 139.2, 139.9, 138.3, 134.9, 129.5, 126.4, 124.7, 124.6, 124.5, 123.8, 123.4, 122.7, 122.7, 121.1, 112.5, 47.6, 32.7, 19.8, 13.7; MS (EI) 337 ( $\text{M}^+$ ); Anal. Calcd for  $\text{C}_{20}\text{H}_{19}\text{NS}_2$ : C, 71.17; H, 5.67; N, 4.15; S 19.00. Found: C, 71.79; H, 5.01; N 4.94; S 17.74.

***N*-(4-Hexylphenyl)-*N*-(2'-benzo[*b*]thienyl)-benzo[*b*]thiophene (7b):** Red solid (45%)

$^1\text{H}$  NMR (300 MHz,  $\text{CDCl}_3$ ,  $\delta$ , ppm): 7.95 (d,  $J = 7$  Hz, 1H), 7.87 (dd,  $J = 8$  Hz, 2H), 7.6 (d,  $J = 8$  Hz, 1H), 7.53 (s, 1H), 7.41-7.30 (m, 4H), 6.97 (d,  $J = 8.3$  Hz, 2H), 6.65 (d,  $J = 8.4$  Hz, 2H), 2.51 (t,  $J = 7.71$  Hz, 2H), 1.3 (b, H), 0.89 (b, 3H);  $^{13}\text{C}$  NMR (75.4 MHz,  $\text{CDCl}_3$ ,  $\delta$ , ppm): 143.5, 140.2, 138, 137.7, 136, 134.3, 132.4, 129, 128.3, 126.9, 124.8, 124.8, 124.6, 124.3, 124.1, 123.3, 123, 122.8, 122.6, 115.7, 35.1, 31.7, 31.6, 29, 22.6, 14.1; MS (EI) 441 ( $\text{M}^+$ ) Anal. Calcd for  $\text{C}_{28}\text{H}_{27}\text{NS}_2$ : C, 76.15; H, 6.16; N, 3.17; S 14.52. Found: C, 76.9; H, 5.91; N 3.74; S 14.74.

**General procedure for synthesis of unsymmetrical heteroacene (1a and 1b):** To a solution of tertiary amine (4.4 mmol) in 70 ml of THF at  $-14$  °C was added (5.6 ml, 9 mmol) of 1.6 M solution of BuLi in *n*-hexane. The mixture was stirred for 2 hours and cannula transferred to a vigorously stirred solution of  $\text{CuCl}_2$  (1.32 g, 10 mmol) in 70 ml of THF and allowed to stir at room temperature. After 6 h, resultant mixture was quenched with 50 ml of water and extracted with hexane ( $3 \times 50$  ml) and dried with sodium sulfate and concentrated in vacuum. The crude product was adsorbed over silica gel and subjected to chromatography with hexane as eluent.

***N*-Butyl-dibenzothieno[2,3-*b*: 2',3'-*d*]pyrrole (1a):** (White solid) 20% yield;  $^1\text{H}$  NMR (300 MHz,  $\text{CDCl}_3$ ,  $\delta$ , ppm): 7.92-7.78 (m, 4H), 7.49-7.4 (m, 2H), 7.31-7.25 (m, 2H), 4.43 (t,  $J = 7$  Hz, 2H), 2.04 (m, 2H), 1.5 (m, 2H), 1 (t,  $J = 7$  Hz, 3H);  $^{13}\text{C}$  NMR (75.4 MHz,

CDCl<sub>3</sub>, δ, ppm): 141, 139.4, 137.9, 135.7, 131.4, 127.2, 125, 124.5, 124.3, 123.6, 122.5, 122.3, 120.7, 118.1, 117.1, 115.2, 48.6, 32.2, 20.2, 13.7; MS (ESI) 335 (M<sup>+</sup>); Anal. Calcd for C<sub>20</sub>H<sub>17</sub>NS<sub>2</sub>: C, 71.6; H, 5.11; N, 4.18; S 19.12. Found: C, 71.79; H, 5.01; N 4.14; S 18.74.

***N*-(4-Hexylphenyl)dibenzothieno[2,3-*b*: 2',3'-*d*]pyrrole (1b):** 35% yield; <sup>1</sup>H NMR (300 MHz, CDCl<sub>3</sub>, δ, ppm): 7.94-7.87 (m, 2H), 7.77 (d, J = 8 Hz, 1H), 7.61 (d, J = 8.4 Hz, 2H), 7.51-7.41 (m, 4H), 7.32 (d, J = 1.14 Hz, 1H), 7.29-7.23 (m, 2H), 2.76 (t, J = 7.56 Hz, 2H), 1.8-1.7 (m, 2H), 1.47-1.37 (b, 6H), 0.94 (t, J = 7 Hz, 3H); <sup>13</sup>C NMR (75.4 MHz, CDCl<sub>3</sub>, δ, ppm): 143.2, 141.1, 140.2, 137.7, 136.4, 135.7, 131.3, 129.8, 127.2, 125.1, 124.6, 124.3, 124, 123.6, 123, 122.7, 120.9, 119.1, 118.4, 116.7, 35.7, 31.7, 31.3, 29.1, 22.6, 14.1; MS (EI) 439 (M<sup>+</sup>); Anal. Calcd for C<sub>28</sub>H<sub>25</sub>NS<sub>2</sub> : C, 76.5; H, 5.73; N, 3.19; S, 14.59. Found: C, 76.45; H, 5.77; N, 3.14; S, 14.62.

**3,3'-Dibromo-[2,2']bi[benzo[*b*]thiophenyl (9):** This compound was synthesized from 2,3-dibromobenzo[*b*]thiophene. *n*-Butyl lithium (1.6 M in hexane) (12.8 ml, 20.5 mmol) was added to a solution of 2,3-dibromobenzo[*b*]thiophene (5 g, 17.12 mmol) in 100 ml of dry THF at -78 °C under nitrogen. After one hour reaction mixture was warmed to -30 °C and maintained at the same temperature for 15 minutes. The mixture was transferred to a vigorously stirred solution of CuCl<sub>2</sub> (3.2 g, 24 mmol) in 70 ml of THF and allowed to stir at room temperature for 12 hours. Reaction mixture was quenched with ice water and extracted with ethyl acetate; combined organic layer was washed with brine solution and dried over anhydrous sodium sulfate. The solvent was removed under reduced pressure and the residue was purified by column chromatography on silica gel with hexane as eluent to give purple brown solid. Yield 90%. All spectroscopic data matches well with



the reported values.<sup>19</sup> <sup>1</sup>H NMR (300 MHz, CDCl<sub>3</sub>, δ, ppm): 7.92 (d, *J* = 7.59 Hz, 2H), 7.85 (d, *J* = 7.53 Hz, 2H), 7.5 (m, 2H). MS (EI) 422 (M<sup>+</sup>).

**Synthesis of heteroacene (10):** To a solution **9** (0.3 g, 0.711 mmol) in 3ml of toluene, potassium carbonate (0.29 g, 2.13 mmol) and tertiary butyl carbamate (0.1 g, 0.85 mmol) were added. Under a current of nitrogen *N,N'*dimethylethylenediamine (18 mg, 0.21 mmol) and copper iodide (0.13g, 0.71 mmol) were added and stirred at 125 °C for 12 hours. The reaction mixture was cooled and after usual work up was subjected to column chromatography on silica with hexane as eluent to afford a white solid. Yield 25%; <sup>1</sup>H NMR (300 MHz, acetone-d<sub>6</sub>, δ, ppm): 12.02 (s, 1H), 7.96 (d, *J* = 13.39 Hz, *J* = 7.89 Hz, 4H), 7.44 (t, *J* = 7.71 Hz, 2H), 7.33 (t, *J* = 7.47 Hz, 2H); <sup>13</sup>C NMR (75.4 MHz, acetone-d<sub>6</sub>, δ, ppm): 141.1, 137.3, 127.4, 124.4, 124, 123.4, 118.8, 114.5; MS (EI) 279 (M<sup>+</sup>); Anal. Calcd for C<sub>16</sub>H<sub>9</sub>NS<sub>2</sub>: C, 68.79; H, 3.25; N, 5.01; S 22.95, Found: C, 68.51; H, 3.10; N, 5.02; S, 19.24.

**Synthesis of compound 2a:** To a solution of **10** (84mg, 0.31 mmol) in 5ml of acetone sodium hydroxide (36 mg, 0.9 mmol) and *n*-bromobutane (84 mg, 0.61 mmol) were added and refluxed. After four hours reaction mixture was cooled and extracted with ethylacetate dried over anhydrous sodium sulfate and concentrated under vacuum. The residue was purified by column chromatography over silica with hexane as eluent. (White solid) Yield : 60%; <sup>1</sup>H NMR (300 MHz, CDCl<sub>3</sub>, δ, ppm): 7.88 (d, *J* = 13.03 Hz, *J* = 8.01 Hz, 4H), 7.42 (t, *J* = 7.17 Hz, 2H), 7.3 (t, *J* = 7.58 Hz, 2H), 4.79 (t, *J* = 7.41 Hz, 2H), 2.08-2 (m, 2H), 1.59-1.51 (m, 2H), 1 (t, *J* = 7.32 Hz, 3H); <sup>13</sup>C NMR (75.4 MHz, CDCl<sub>3</sub>, δ, ppm): 141.9, 137.8, 127.5, 124.5, 124.4, 123.1, 118.8, 114.6, 47.3, 33.3, 20.1, 13.9; MS (ESI) 335 (M<sup>+</sup>); Anal. Calcd for C<sub>20</sub>H<sub>17</sub>NS<sub>2</sub>: C, 71.6; H, 5.11; N, 4.18; S 19.12. Found: C, 71.65; H, 5.10; N 4.25; S 18.24.

**Synthesis of compound 2b:** To a solution of **9** (0.2 g, 0.47 mmol) in 10 ml of toluene at room temperature tri(*tert*-butyl)phosphonium tetrafluoroborate (22 mg, 0.095 mmol), sodium *tert*-butoxide (140 mg, 1.42 mmol) and [Pd<sub>2</sub>(dba)<sub>3</sub>] (55mg, 0.095 mmol) were added and heated to 125 °C under nitrogen for 5 hours. Reaction mixture was extracted with ethyl acetate and dried over anhydrous sulfate. Solvent was removed under vacuum and residue was purified by column chromatography on silica with hexane as eluent to afford colorless powder. Yield 55%. <sup>1</sup>H NMR (300 MHz, CDCl<sub>3</sub>, δ, ppm): 7.83 (d, J = 7.71 Hz, 2H), 7.55 (d, J = 8.07 Hz, 2H), 7.45 (d, J = 8.07 Hz, 2H), 7.24-7.09 (m, 6H), 2.81 (t, J = 7.56 Hz, 2H), 1.83-1.73 (m, 2H), 1.5-1.35 (b, 6H), 0.92 (t, J = 5.64 Hz, 3H). <sup>13</sup>C NMR (75.4 MHz, CDCl<sub>3</sub>, δ, ppm): 144.3, 141.8, 138.1, 135.8, 129.7, 127.7, 127.4, 124.2, 124, 123.4, 119.1, 115.3, 35.8, 31.7, 31.2, 29, 22.6, 14.1. MS (EI) 439 (M<sup>+</sup>); Anal. Calcd for C<sub>28</sub>H<sub>25</sub>NS<sub>2</sub>: C, 76.5; H, 5.73; N, 3.19; S, 14.59. Found: C, 76.1; H, 5.7; N, 3.45; S, 15.01.

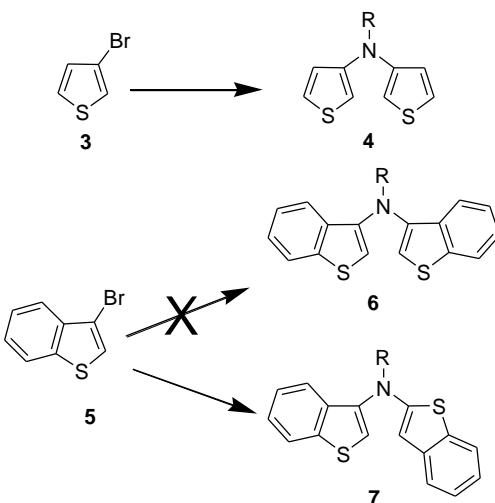
## 2.3. Results and discussion

### 2.3.1. Synthesis

Palladium catalyzed amination of 3-bromothiophene **3** with alkyl or aryl amine resulted in *N*-alkyl-*N*-(3'-thienyl)-3-aminothiophene (**4**).<sup>14</sup> Under identical conditions, 3-bromobenzo[*b*]thiophene (**5**) failed to give *N*-alkyl-*N*-(3'-benzo[*b*]thienyl)-3-aminobenzo[*b*]thiophene (**6**) but yielded *N*-alkyl-*N*-(2'-benzo[*b*]thienyl)-3-aminobenzo[*b*]thiophene **7** (Scheme 2.1). This unexpected reactivity formed the basis for the synthesis of unsymmetrical heteroacenes. When 3-bromobenzo[*b*]thiophene, was treated with half an equivalent of alkyl or aryl amine, **7a** or **7b** was obtained in 40 - 45% yield along with 3,3'-bibenzo[*b*]thiophene (20 - 30%) and 3-aminobenzo[*b*]thiophene (10 - 15%) (Scheme 2.2). A stepwise procedure also resulted in the same rearranged product **7**, possibly due to

the rearrangement of *N*-functionalized 3-aminobenzo[*b*]thiophene under the coupling conditions (in the catalytic cycle). The 3,3'-dibenzo[*b*]thiophene was obtained from the oxidative coupling of **5**.<sup>14</sup> Reactions involving aryl amine resulted in higher yields due to the absence of a competing  $\beta$ -elimination pathway.<sup>14a</sup> Isolation of *N*-functionalized-3-aminobenzo[*b*]thiophene in one pot as well as in step wise reaction suggest that the *N*-functionalized-3-aminobenzo[*b*]thiophene undergo rearrangement under coupling conditions. Palladium catalyzed mono-amination of 3-bromobenzo[*b*]thiophene is well established<sup>15</sup> whereas di-amination was not reported. The rearrangement of a similar system, 3-bromo-2-nitrobenzo[*b*]thiophene was known for aromatic nucleophilic substitution with amines.<sup>16</sup>

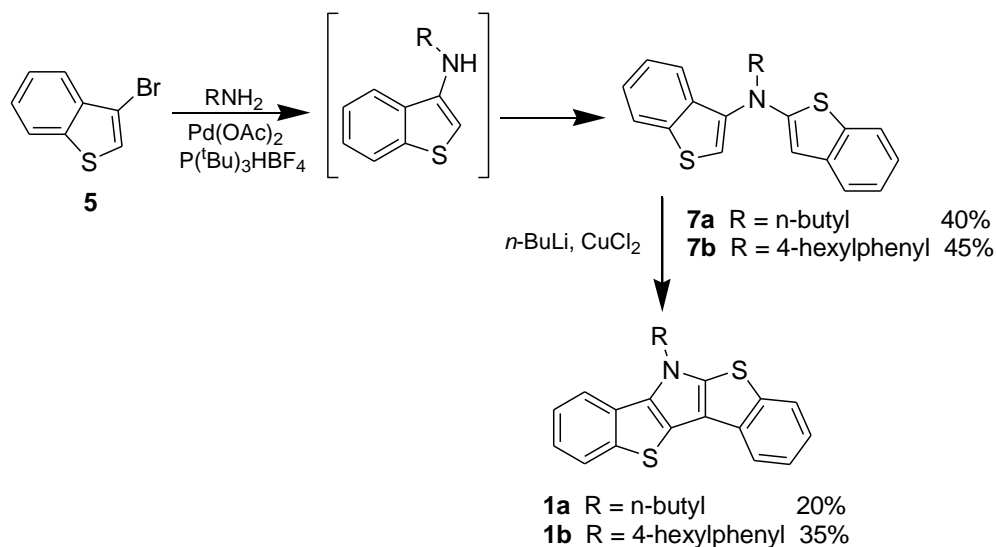
**Scheme 2.1.** Comparison of reactivity of 3-bromothiophene and 3-bromobenzo[*b*]thiophene under palladium catalyzed amination condition



Since the Pd(OAc)<sub>2</sub>/P(<sup>*t*</sup>Bu)<sub>3</sub> catalyst system was successful in the amination of 3-bromothiophene, initially the same catalyst was used for the amination of 3-bromobenzo[*b*]thiophene.<sup>14</sup> Other catalysts such as Pd<sub>2</sub>(dba)<sub>3</sub>/±BINAP,

$\text{Pd}_2(\text{dba})_3/\text{P}(\text{tBu})_3$ ,  $\text{Pd}(\text{OAc})_2/\pm\text{BINAP}$ ,  $\text{Pd}(\text{OAc})_2/\text{PCy}_3$  were also employed and only product **7** was obtained, but in lower yield.

**Scheme 2.2.** Synthesis of unsymmetric heteroacene **1a** and **1b**

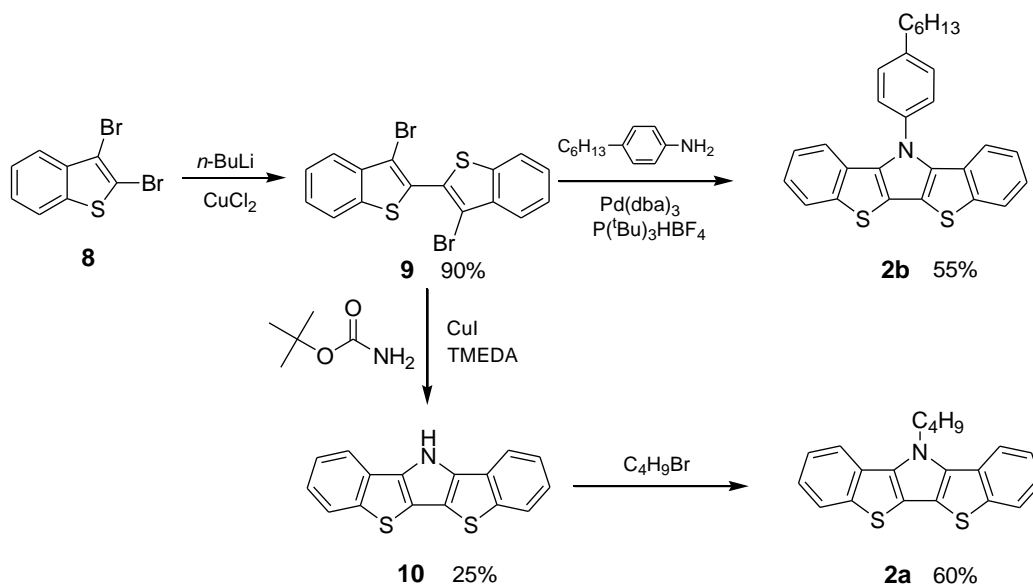


Toluene and *o*-xylene were employed as solvents for the amination reaction and both solvents yielded the same amination products without significant difference in yield. The target compounds **1a** and **1b** were synthesized *via* cyclization of **7**, using butyl lithium and anhydrous cupric chloride.

As the palladium catalysed amination reaction resulted in rearranged product, symmetrical heteroacenes were prepared by a different synthetic approach. Symmetrical heteroacenes **2a** and **2b** were synthesized from 2,3-dibromobenzo[*b*]thiophene **8**. The synthetic route leading to these compounds is represented in Scheme 2.3. Compound **9**<sup>17</sup> was synthesized from 2,3-dibromobenzo[*b*]thiophene by treatment with BuLi followed by addition of anhydrous  $\text{CuCl}_2$ . Herein, pyrrole fusion was achieved by employing a recently reported amidation procedure.<sup>18</sup> Cyclization proceeded with concomitant hydrolysis and gave **10** in 25 % yield. Heteroacene **10** was then alkylated with butyl

bromide to yield **2a**. Compound **2b** was synthesized by palladium catalyzed double *N*-arylation of 4-hexylaniline with 3,3'-dibromo-[2,2']bibenzo[*b*]thiophene **9**.<sup>19</sup> It is notable that our entire synthetic route leading to five ring fused systems involves only two steps. The synthesized heteroacenes were characterized by NMR spectroscopy (<sup>1</sup>H and <sup>13</sup>C), elemental analysis and X-ray crystallography. These compounds are soluble in common organic solvents such as hexane, chloroform, toluene, ethyl acetate and methanol.

**Scheme 2.3.** Synthesis of symmetrical heteroacene **2a** and **2b**



### 2.3.2. Single crystal X-ray structure and crystal packing

Single crystals of compounds **1a**, **1b** and **2b** suitable for single crystal X-ray diffraction studies were obtained by slow evaporation from a chloroform solution. The crystal packing of symmetric and asymmetric heteroacene are compared. Structural analysis indicated that these heteroacenes are planar and their molecular packing in the crystal lattice is shown in Figure 2.2. The bond length of N-C(Ph) in unsymmetric compound **1b** is similar (1.43 Å) to symmetric compound **2b** (1.44 Å). The pendant

phenyl group in **1b** and **2b** are twisted by an angle of  $46.7^\circ$  and  $81.8^\circ$ , with respect to the acene plane. This may be due to unymmetrical electron cloud distribution in **1b** or steric factor arising from ortho hydrogen atoms of the terminal benzene rings in **2b**. Heteroacene **1a** packs in an edge-to-face manner, leading to a sandwiched herringbone arrangement with a distance of  $3.54 \text{ \AA}$  between sandwiched molecules.

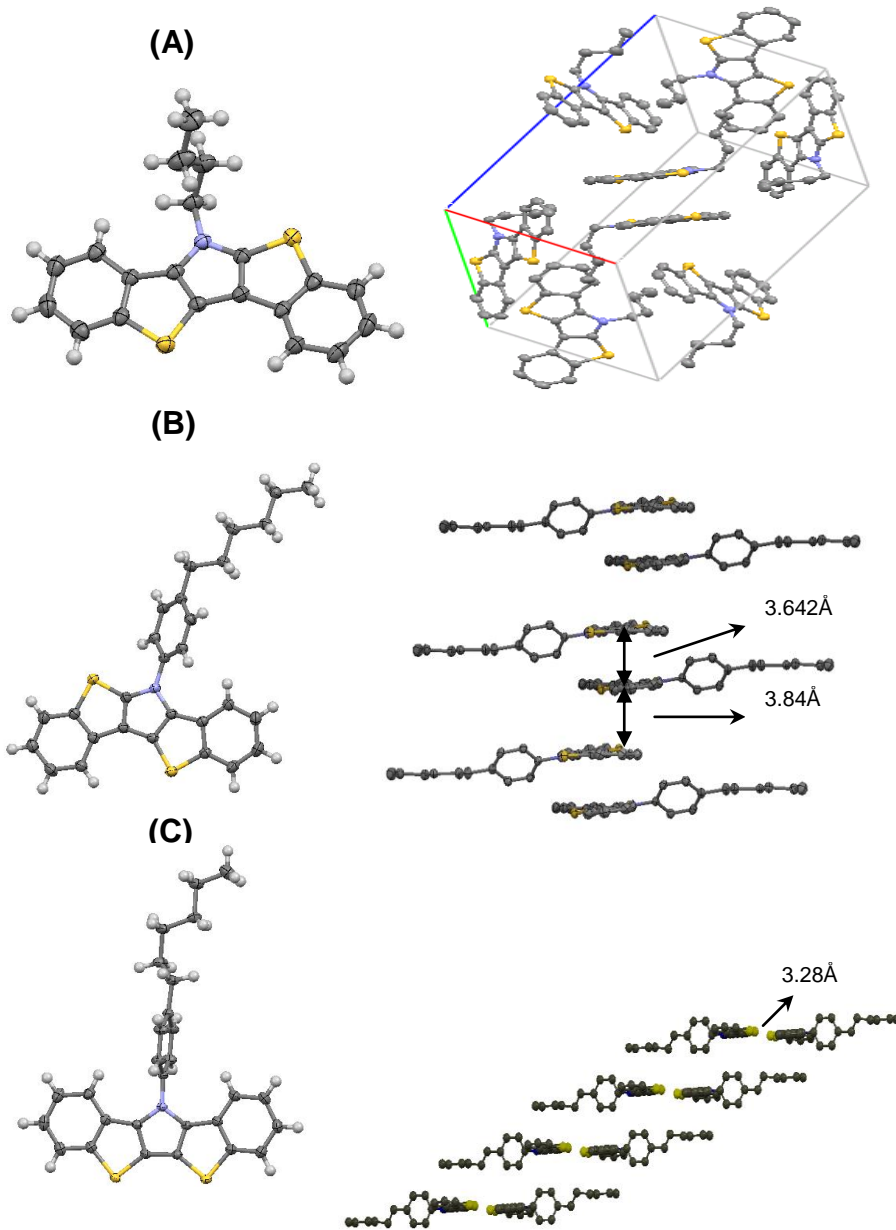


**Figure 2.2.** Thermal ellipsoid plot and packing of **1a** (A), **1b** (B) and **2b** (C)

In the case of **1b**, molecules form a  $\pi$ -stacked dimers which interact with other dimers of adjacent column by  $S\cdots H$  (2.87 Å) interaction. The sulfur atom *anti* to the pyrrole nitrogen is involved in this interaction. The molecular packing, which is a critical parameter to consider for applications,<sup>20</sup> is influenced by the substituents on the nitrogen atom of the pyrrole ring. In the case of symmetrical molecule **2b**, a molecular dimer is formed by short  $S\cdots S$  contacts (3.3 and 3.6 Å). Such dimers are well separated by a pendant phenyl group and the alkyl chain attached to it. In short, packing in the symmetrical acene (**2**) is mainly effected by  $S\cdots S$  contact whereas in the case of an unsymmetrical acene (**1a,b**) it is dominated by  $S\cdots H$  interaction.

### 2.3.3. Optical properties

The UV-vis spectrum of unsymmetrical and symmetrical heteroacenes are given in Figure 2.3 and the values are tabulated in Table 2.1, and compared with diindolothiophene<sup>21</sup> (Figure 2.4).

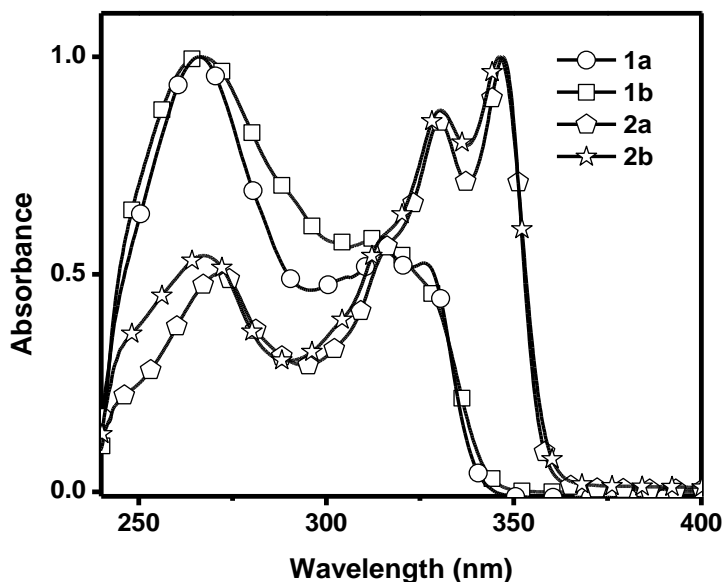


**Figure 2.3.** UV-vis spectra of symmetric and unsymmetric heteroacenes

The absorption spectra of dilute solution of unsymmetrical compounds showed similar absorption properties with  $\lambda_{\max}$  at 266 nm and 323 nm and an absorption onset at 343 nm. Both the compounds (**1a** and **1b**) possess similar absorption characters, indicating the absence of any pronounced effect of substitution at central pyrrole ring. The symmetrical compounds showed absorption peaks at 263 nm and 326 nm with an absorption onset at 360 nm. The absorption peak at lower wavelength region (around 260 nm) corresponds to benzo[*b*]thiophene unit, whereas the peak at higher wavelength (< 300 nm) corresponds to the  $\pi$ - $\pi^*$  transition of heteroacene unit. The peak around 260 nm is pronounced for unsymmetrical compounds suggesting the hindered conjugation. The absorption maxima of symmetrical heteroacenes are red shifted compared to those of unsymmetrical heteroacenes indicating a better conjugation/delocalization in compound **2** compared to compound **1**. This can be attributed to the nonlinear structure of **1** which is expected to reduce the effective conjugation. The conjugation in **1a** and **1b** goes through the sulfur lone pair as the thienyl rings are linked 2,3 whereas in **2a** and **2b** the thienyl rings are linked 2,2 which gives better conjugation.

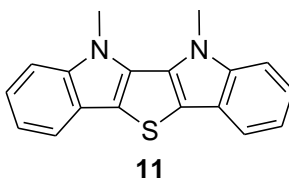


**Figure 2.4.** The molecular structure of 5,6-dimethyldiindolo[3,2-*b*:4,5-*b'*]thiophene (**11**)<sup>11</sup>

The absorption spectra of dilute solution of compound **1** and **2** showed a blue-shift in absorption relative to **11**. In case of compound **11**, the fused ring skeleton is similar to **2**, but has different composition of heteroatoms. The blue shift in absorption of **2**



compared to **11** is attributed to the higher sulfur content of **2** which tends to widen the HOMO-LUMO gap induced by LUMO destabilization.<sup>22</sup> The bandgap of the synthesised compounds are estimated from the absorption onset. The band gap of the heteroacenes were found to be 3.62 eV and 3.44 eV for **1** and **2** respectively. The relatively lower band gap of **2** compared to **1** also suggests a better delocalization of  $\pi$ -electrons in **2**. Such semiconductors with large band gaps, are suitable for fabricating transparent OTFT circuits which are used for optoelectronic devices requiring transparency.<sup>23</sup>

#### 2.3.4. Electrochemical properties

Electrochemical properties of the compounds **1** and **2**, were investigated using cyclic voltammetry with Ag/AgCl as the reference electrode. The cyclic voltammogram of acenes are given in Figure 2.5 and the values are listed in Table 2.1. All heteroacenes exhibit similar electrochemical behaviors with reversible oxidation waves. Compound **1a** showed an oxidation peak maximum at 1.19 V with an onset potential around 0.87 V, whilst **1b** showed an oxidation peak at 1.17 V with an oxidation onset of 0.94 V. The oxidation peaks of **2a** and **2b** were found at 1.14 and 1.25 V. HOMO energy level of **1a** and **1b** calculated from the oxidation onset potential using the empirical formula  $E_{\text{HOMO}} = -(E_{\text{ox}}^{\text{onset}} + 4.38) \text{ eV}$ <sup>24</sup> are comparable (-5.25 eV and -5.32 eV). As the reduction peaks are out of our scan range, the LUMO energy levels are calculated from the HOMO energy level and the optical band gap. In the produced heteroacenes, the substitution has little effect on HOMO and LUMO energy levels. However, it should be noted that **2b** has a relatively higher oxidation potential and lowest HOMO and LUMO energy levels. This can be due to the sufficient resonance stabilization to injected hole carriers due to aryl substitution. Unlike symmetrical compound **2b**, unsymmetrical compound **1b** is not

influenced considerably by an aryl substituent which may be due to lesser delocalization caused by the twisted backbone of **1**. All synthesised heteroacenes posseses low lying HOMO energy levels and larger band gap than pentacene ( $E_{\text{HOMO}} = -4.6$  eV,  $E_g = 2.21$  eV),<sup>25</sup> indicating their stability under ambient conditions.

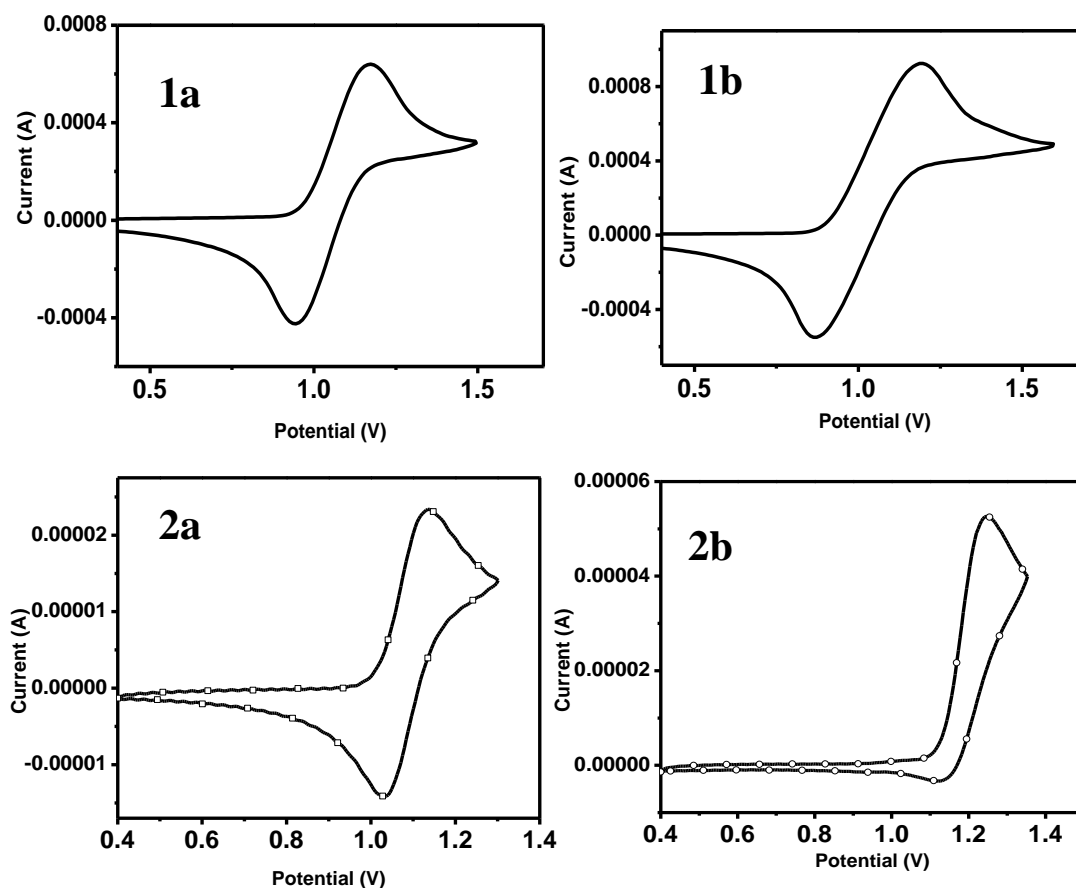


**Figure 2.5.** Cyclic voltammogram of unsymmetric and symmetric heteroacenes recorded in dichloromethane containing 0.1 M  $n\text{-Bu}_4\text{NPF}_6$  as supporting electrolyte

**Table 2.1.** Photophysical and electrochemical properties of unsymmetrical and symmetrical heteroacenes

Compounds	$\lambda_{\text{max}}^{\text{a}}$ (nm)	$E_{\text{g}}^{\text{b}}$ (eV)	$E_{\text{HOMO}}^{\text{c}}$ (eV)	$E_{\text{LUMO}}^{\text{d}}$ (eV)
<b>1a</b>	266, 323	3.62	-5.25	-1.63
<b>1b</b>	266, 323	3.62	-5.32	-1.7
<b>1c</b>	263, 326, 346	3.44	-5.39	-1.95
<b>2a</b>	263, 326, 346	3.44	-5.51	-2.07
<b>2b<sup>f</sup></b>	344, 353 <sup>e</sup>	3.3	-5.29	-1.99

<sup>a</sup>Measured in a dilute THF solution. <sup>b</sup>Estimated from the onset of absorption spectra ( $E_{\text{g}} = 1240/\lambda_{\text{onset}}$ ). <sup>c</sup>Calculated using the empirical relation  $\text{HOMO} = -(4.38 + E_{\text{ox}}^{\text{onset}})$ . <sup>d</sup>Calculated from  $E_{\text{g}}$  and  $E_{\text{HOMO}}$ . <sup>e</sup>Measured in dilute  $\text{CH}_2\text{Cl}_2$  solution. <sup>f</sup>From reference 11.

## 2.4. Conclusion

In summary, we report a new series of ladder-type heteroacene containing thiophene and pyrrole units (thienopyrrole). Both symmetrical and unsymmetrical compounds are synthesized in just two-steps and their properties are compared in detail. The unsymmetrical heteroacenes are synthesised by utilizing the Palladium catalyzed amination as key step, which resulted in a rearranged product. Symmetrical heteroacenes are synthesised by utilizing copper catalyzed amidation reaction as key step. All these compounds are highly stable and soluble in common organic solvents. Crystal packing of symmetrical and unsymmetrical compounds are compared. The packing in symmetrical heteroacene is mainly effected by S...S contact, whereas in the case of an unsymmetrical

acene packing is dominated by S-H interaction. Low lying HOMO energy levels, indicaties good stability of these compounds under ambient condition. Investigation of their physical properties and electrochemical properties suggests that these molecules are potential candidates for applications in OFET.

## 2.5. References

- 
- (1) (a) Sheats, J. R. *J. Mater. Res.* **2004**, *19*, 1974. (b) Gundalch, D. J.; Nichols, J. A.; Zhou, L.; Jackson, T. N. *Appl. Phys. Lett.* **2002**, *8*, 2925. (c) Hepp, A.; von Malm, N.; Schmechel, R.; von Seggern, H. *Synth. Met.* **2003**, *138*, 201.
- (2) (a) Kalauk, H.; Halik, M.; Zschieschang, U.; Schmikd, G.; Radlik, W.; Weber, W. *J. Appl. Phys.* **2002**, *92*, 5259. (b) Kelley, T. W.; Boardman, L. D.; Dunbar, T. D.; Muyres, D. V.; Pellerite, M. J.; Smith, T. P. *J. Phys. Chem. B* **2003**, *107*, 5877. (c) Lin, Y. Y.; Gundlach, D. J.; Nelson, S. F.; Jackson, T. N. *IEEE Electron Device Lett.* **1997**, *18*, 606.
- (3) (a) Maliakal, A.; Raghavachar, K.; Katz, H.; Chandross, E.; Siegrist, T. *Chem. Mater.* **2004**, *16*, 4980. (b) Coppo, P.; Yeates, S. G. *Adv. Mater.* **2005**, *17*, 3001. (c) Meng, H.; Bendikov, M.; Mitchello, G.; Helgeson, R.; Wudl, F.; Bao, Z.; Siegrist, T.; Kloc, C. H. *Adv. Mater.* **2003**, *15*, 1090. (d) Yamada, M.; Ikemoto, I.; Kuroda, H.; *Bull. Chem. Soc. Jpn.* **1998**, *61*, 1057.
- (4) Laquindanum, J. G.; Katz, H. E.; Lovinger, A.; *J. Am. Chem. Soc.* **1998**, *120*, 664.
- (5) (a) Li, X.-C.; Sirringhaus, H.; Garnier, F.; Holmes, A. B.; Moratti, S. C.; Feeder, N.; Clegg, W.; Teat, S. J.; Friend, R. H. *J. Am. Chem. Soc.* **1998**, *120*, 2206. (b) Xiao, K.; Liu, Y.; Qi, T.; Zhang, W.; Wang, F.; Gao, J.; Qiu, W.; Ma, Y.; Cui, G.; Chen, S.; Zhan, X.; Yu, G.; Qin, J.; Hu, W.; Zhu, D. *J. Am. Chem. Soc.* **2005**, *127*, 13281.
- (6) (a) Wu, Y.; Li, Y.; Gardner, S.; Ong, B. S. *J. Am. Chem. Soc.* **2005**, *127*, 614. (b) Boudreault, P. L. T.; Wakim, S.; Blouin, N.; Simard, M.; Tessier, C.; Tao, Y.; Leclerc, M. *J. Am. Chem. Soc.* **2007**, *129*, 9125.
- (7) (a) Anthony, J. E.; *Chem. Rev.* **2006**, *106*, 5028. (b) Laquindanum, J. G.; Katz, H. E.; Lovinger, A. J.; Dodabalapur, A. *Adv. Mater.* **1997**, *8*, 36. (c) Takimiya, K.; Kunugi, Y.; Konda, Y.; Niihara, N.; Otsubo, T. *J. Am. Chem. Soc.* **2004**, *126*, 5084. (d) Sirringhaus, H.; Friend, R. H.; Wang, C.; Leuninger, J.; Mullen, K. *J. Mater. Chem.* **1999**, *9*, 2095. (e) Payne, M. M.; Parkin, S. R.; Anthony, J. E.; Kuo, C.-C.; Jackson, T. N. *J. Am. Chem. Soc.* **2005**, *127*, 4986. (f) Takimiya, K.; Ebata, H.; Sakamoto, K.; Izawa, T.; Otsubo, T.; Kunugi, Y. *J. Am. Chem. Soc.* **2006**, *128*, 12604. (g) Takimiya, K.; Kunugi, Y.; Konda, Y.; Ebata, H.; Toyoshima, Y.; Otsubo, T. *J. Am. Chem. Soc.* **2006**, *128*, 3044. (h) Yamamoto, T.; Takimiya, K. *J. Am. Chem. Soc.* **2007**, *129*, 2224.
- (8) (a) Ebata, H.; Izawa, T.; Miyazaki, E.; Takimiya, K.; Ikeda, M.; Kuwabara, H.; Yui, T. *J. Am. Chem. Soc.* **2007**, *129*, 15732. (b) Pietrangelo, A.; Maclachlan, M. J.; Wolf, M. O.; Patrick, B. O. *Org. Lett.* **2007**, *9*, 3571.
- (9) Bredas, J. L.; Beljonne, D.; Coropceanu, V.; Cornil, J. *Chem. Rev.* **2004**, *104*, 4971.

- (10) (a) Okamoto, T.; Kudoh, K.; Wakamiya, A.; Yamaguchi, S. *Org. Lett.* **2005**, *7*, 5301. (b) Okamoto, T.; Kudoh, K.; Wakamiya, A.; Yamaguchi, S. *Chem. –Eur. J.* **2007**, *13*, 548. (c) Valiyev, F, Hu, W. S.; Chen, H. Y.; Kuo, M. Y.; Chao, I.; Tao, Y. T. *Chem. Mater.* **2007**, *19*, 3018.
- (11) Qi, T.; Qiu, W.; Guo, Y.; Liu, Y.; Xi, H.; Zhang, H.; Gao, X.; Liu, Y.; Lu, K.; Ku, C.; Yu, G.; Zhu, D. *J. Org. Chem.* **2008**, *73*, 4638.
- (12) (a) Tang, M. L.; Okamoto, T.; Bao, Z. *J. Am. Chem. Soc.* **2006**, *128*, 16002. (b) Kawaguchi, K.; Nakano, K.; Nozaki, K. *Org. Lett.* **2008**, *10*, 1199.
- (13) Qi, T.; Guo, Y.; Liu, Y.; Xi, H.; Zhang, H.; Gao, X.; Liu, Y.; Lu, K.; Ku, C.; Yu, G.; Zhu, D. *Chem. Commun.* **2008**, 6227.
- (14) (a) Ogawa, K.; Radke, K. R.; Rothstein, S. D.; Rasmussen, S. C. *J. Org. Chem.* **2001**, *66*, 9067. (b) Ogawa, K.; Rasmussen, S. C. *J. Org. Chem.* **2003**, *68*, 2921.
- (15) Hooper, M. W.; Utsunomiya, M.; Hartwig, J. F. *J. Org. Chem.* **2003**, *68*, 2861.
- (16) Guerrers, F.; Salerno, L.; Lamartina, L.; Spinelli, D. *J. Chem. Soc. Perkin Trans. I.* **1995**, 1243.
- (17) (a) Dahlmann, U.; Neidlein, R. *Helv. Chim. Acta.* **1997**, *80*, 111. (b) Gao, J.; Li, R.; Li, L.; Meng, Q.; Jiang, H.; Li, H.; Hu, W. *Adv. Mater.* **2007**, *19*, 3008.
- (18) Martin, R.; Larsen, C. H.; Cuenca, A.; Buchwald, S. L. *Org. Lett.* **2007**, *9*, 3379.
- (19) Nozaki, K.; Takahashi, K.; Nakano, K.; Hiyama, T.; Tang, H. Z.; Fujiki, M.; Yamaguchi, S.; Tamao, K. *Angew. Chem. Int. Ed.* **2003**, *42*, 2051.
- (20) (a) Gundlach, D. J.; Nichols, J. A.; Zhou, L.; Jackson, T. N. *Appl. Phys. Lett.* **2002**, *80*, 2925. (b) Hepp, A.; von Malm, N.; Schmechel, R.; von Seggern, H. *Synth. Met.* **2003**, *138*, 201.
- (21) Gao, P.; Beckmann, D.; Tsao, H. N.; Feng, X.; Enkelmann, V.; Pisula, W.; Müllen, K. *Chem. Commun.* **2008**, 1548.
- (22) Zhang, X.; Matzger, A. J. *J. Org. Chem.* **2003**, *68*, 9813.
- (23) Nomura, K.; Ohta, H.; Ueda, K.; Kamiya, T.; Hirano, M.; Hosono, H. *Science* **2003**, *300*, 1269.
- (24) (a) Li, Y.; Ding, J.; Day, M.; Tao, Y.; Lu, J.; D'iorio, M. *Chem. Mater.* **2004**, *16*, 2165. (b) Leeuw, D. M.; Simenon, M. M. J.; Brown, A. R.; Einerhand, R. E. F. *Synth. Met.* **1987**, *53*. (c) Cui, Y.; Zhang, X.; Jenekhe, S. A. *Macromolecules* **1999**, *32*, 3824.
- (25) Meng, H.; Bendikov, M.; Mitchell, G.; Helgeson, R.; Wudl, F.; Bao, Z.; Siegrist, T.; Kloc, C.; Chen, C. H. *Adv. Mater.* **2003**, *15*, 1090.

## *Chapter 3*

# *Unsymmetric Indolodithienopyrrole and Extended Diindolodithienopyrroles*

*Publication from the chapter:*

**Balaji, G.;** Phua, D. I.; Shim, W. L.; Valiyaveetil, S. “Synthesis and Characterization of Unsymmetric Indolodithienopyrrole and Extended Diindolodithienopyrrole”, *Org. Lett.* **2010**, *12*, 232.

### **3.1. Introduction**

The incorporation of heteroatoms has been part of an ongoing effort to prepare new [*n*]acene analogues, known as heteroacenes, with improved device performances.<sup>1</sup> These heteroatoms with low HOMO level offer stability to devices.<sup>2</sup> Furthermore, easy functionalization on the heteroatoms (e.g., N, P, Si) allows for facile derivatization<sup>3</sup> and incorporation of the substituents designed to tune the molecular organization and solubility.<sup>4</sup> Heteroacenes are expected to possess better organic field effect transistor (OFET) performance<sup>5</sup> due to secondary interactions such as hydrogen bonding,  $\pi$ -stacking, and sulfur–sulfur (S $\cdots$ S) interactions originating from the high polarizability of sulfur electrons in thiophene rings.<sup>6</sup> Thiophene-based dithieno[3,2-*b*:2',3'-*d*]pyrrole (DTP) represents a promising class of semiconducting materials because of their fused-rigid backbone and good molecular planarity.<sup>7</sup> Thiophene- and pyrrole-based symmetrical heteroacenes were also successfully tested for OFET applications.<sup>8</sup> Most of the reported heteroacenes (five rings fused) are symmetrical in nature.<sup>9</sup> Only a few unsymmetrical heteroacenes<sup>10</sup> and extended heteroacenes have been reported.<sup>11</sup> In this regard, a series of unsymmetrical indolodithienopyrroles and the extended (seven-ring fused) diindolodithienopyrroles were synthesized. Their photophysical and electrochemical properties along with their molecular organization in crystal lattice are presented in this study. The structures of the synthesised heteroacenes are given in Figure 3.1.

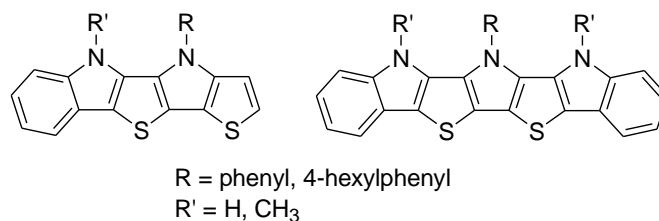


**Figure 3.1.** Structure of synthesized unsymmetric and extended heteroacenes

### 3.2. Experimental



### 3.2.1. Materials

*N*-Bromosuccinimide was recrystallized using hot water. All other chemicals and reagents were purchased from commercial suppliers (Sigma-Aldrich, and Merck) and used without further purification. Solvents used for spectroscopic measurements were spectrograde. Tetrahydrofuran (THF) was distilled from sodium. All reactions were monitored by thin-layer chromatography carried out on silica gel plates. Preparative separations were performed by column chromatography on silica gel grade 60 (0.040 – 0.063 mm) from Merck. 2,2'-Bithiophene, 4-hexylaniline, aniline and 2-nitrophenylboronic acid, triethyl phosphate were purchased from Aldrich and used without further purification.

### 3.2.2. Instrumentation

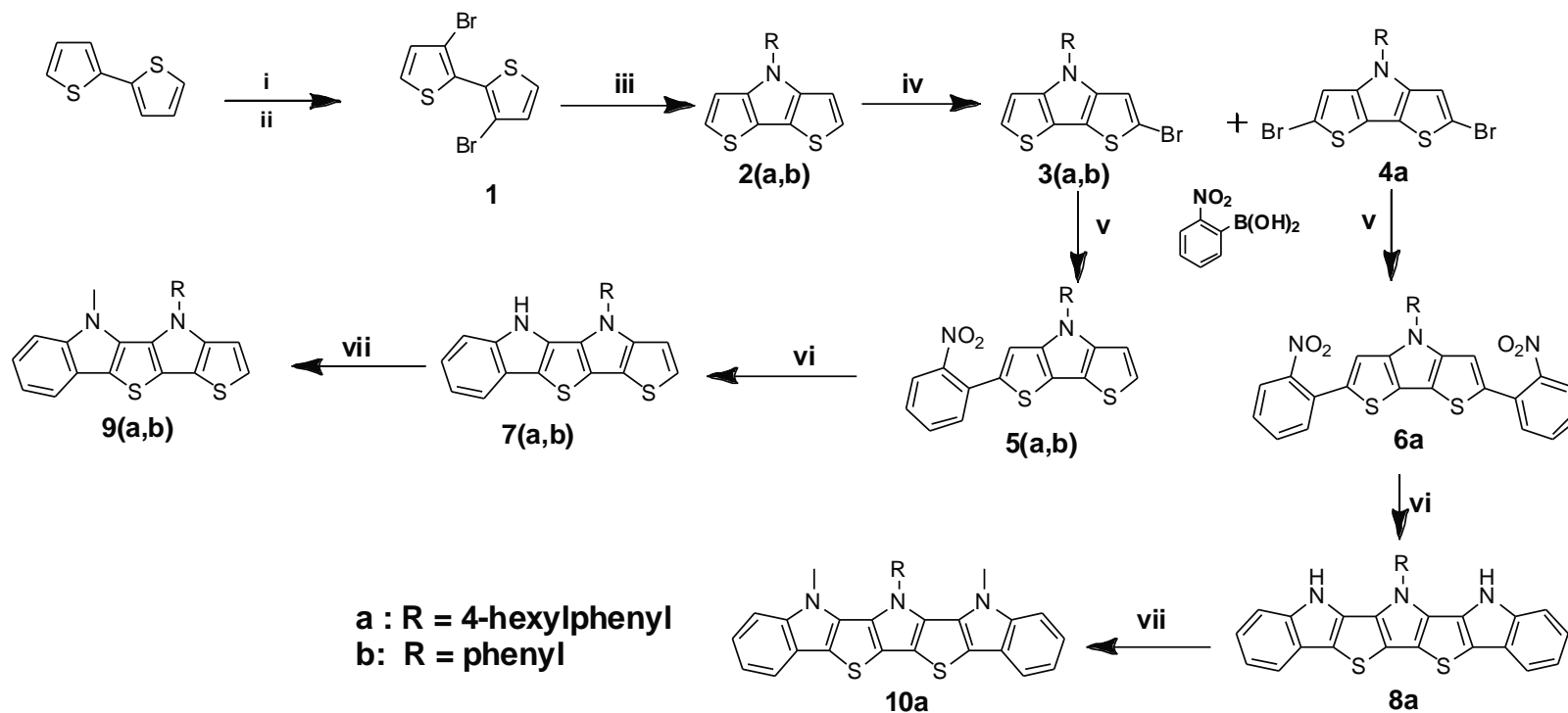
<sup>1</sup>H NMR spectra were recorded on Bruker ACF300 (300 MHz) spectrometer. The chemical shifts are reported in ppm and referenced to the residual solvent peak. s = singlet, d = doublet, dd = doublet of doublet, t = triplet, m = multiplet, b = broad. EI mass spectra were obtained on a Finnigan MAT 95XL-T mass spectrometer. Absorption spectra were recorded on Shimadzu UV-1601PC UV-vis spectrophotometer. THF was used as solvent for all the target molecules under room temperature. The concentration of each sample was adjusted so that the maximum absorbance of the solution is lower than 0.1 at the absorption maxima. Fluorescence emission spectra were recorded on Shimadzu RF-5301PC spectrofluorophotometer. The compounds were excited at the wavelength corresponding to individual absorption maximum of the first electronic transition. Solution state photoluminescence quantum yields were recorded using quinine sulfate (0.1 M H<sub>2</sub>SO<sub>4</sub>) as standard.<sup>12</sup>

The electrochemical behavior of the heteroacenes was investigated by cyclic voltammetry (CV). The cyclic voltammograms were recorded with a computer controlled CHI Electrochemical Analyzer/Workstation CHI 600C at a constant scan rate of 100 mV/s. Measurements were performed in an electrolyte solution of 0.1 M tetrabutylammonium hexafluorophosphate ( $n\text{-Bu}_4\text{NPF}_6$ ) dissolved in degassed dichloromethane. An undivided three-electrode configuration cell was used with Pt wire as working and counter electrode, and Ag/AgCl as the reference electrode. The potentials are calibrated with ferrocene/ferrocenium redox couple (0.47 V). Onset value of the oxidation wave ( $E_{\text{ox}}^{\text{onset}}$ ) was used to calculate HOMO energy level, using the relation  $E_{\text{HOMO}} = -(4.38 + E_{\text{ox}}^{\text{onset}})$ . The LUMO levels were calculated from  $E_{\text{HOMO}}$  and optical energy level gap ( $E_g$ ). Concentration of samples was 5 mg/mL in THF.

Single crystals of acene compounds suitable for structural analysis were obtained by recrystallization from the mixture of hexane and dichloromethane. The X-ray crystal structure analysis was made on a Rigaku AFC-7 (Mo  $K\alpha$  radiation,  $\lambda = 0.71069 \text{ \AA}$ , graphite monochromator,  $T = 296 \text{ K}$ ,  $2\theta_{\text{max}} = 55.0^\circ$ ) or a Rigaku Rapid-IP (Mo  $K\alpha$  radiation,  $\lambda = 0.71069 \text{ \AA}$ , graphite monochromator,  $T = 296 \text{ K}$ ,  $2\theta_{\text{max}} = 55.0^\circ$ ).

### 3.2.3. Synthesis procedure

**Scheme 3.1.** Synthesis of unsymmetrical and extended heteroacene<sup>a</sup>



<sup>a</sup>Reagents and conditions: (i) Br<sub>2</sub>, CHCl<sub>3</sub>, CH<sub>3</sub>COOH; (ii) Zn, HCl, CH<sub>3</sub>COOH, C<sub>2</sub>H<sub>5</sub>OH; (iii) Pd<sub>2</sub>(dba)<sub>3</sub>, P(<sup>t</sup>Bu)<sub>3</sub>.HBF<sub>4</sub>, NaO<sup>t</sup>Bu, toluene, aniline/4-hexylaniline, reflux; (iv) NBS, AcOH, CHCl<sub>3</sub>; (v) THF, 2 M K<sub>2</sub>CO<sub>3</sub>, Pd(PPh<sub>3</sub>)<sub>4</sub>, 60°C; (vi) P(OEt)<sub>3</sub>, 1,2-dichlorobenzene, reflux; (vii) DMF, NaOH, CH<sub>3</sub>I, RT, 24 h.

**General procedure for Buchwald coupling reaction<sup>11c</sup> – synthesis of compounds 2a and 2b:** To a 250 ml two-neck round-bottom flask, under nitrogen atmosphere, toluene, Pd<sub>2</sub>(dba)<sub>3</sub> catalyst (0.71 mmol) and P(<sup>t</sup>Bu)<sub>3</sub>HBF<sub>4</sub> ligand (0.71 mmol) were added. The base NaO<sup>t</sup>Bu (21.3 mmol) and compound **1** (7.1 mmol) were then added consecutively. After five minutes, arylamine (9.94 mmol) was added and the reaction mixture was allowed to stir at 125°C for 6 hours. Reaction mixture was allowed to cool to room temperature and extracted with ethyl acetate/brine. The collected organic layer was dried over anhydrous sodium sulfate, filtered and concentrated under reduced pressure. The crude product was purified by column chromatography to give desired compound **2**. The spectroscopic data matches well with the reported values.<sup>11c</sup>

**2a:**<sup>11c</sup> Yellow solid (Yield 65%). TLC (Solvent 100% Hexane) R<sub>f</sub> = 0.77; <sup>1</sup>H NMR (300 MHz, CDCl<sub>3</sub>, ppm) δ = 7.49 (d, *J* = 8.22 Hz, 2H), 7.33 (d, *J* = 8.22 Hz, 2H), 7.16 (s, 4H), 2.69 (t, *J* = 7.73 Hz, 2H), 1.69 (m, 2H), 1.37 (m, 6H), 0.92 (t, *J* = 6.72 Hz, 3H). HRMS *m/z* [M<sup>+</sup>] calcd for C<sub>20</sub>H<sub>21</sub>NS<sub>2</sub> 339.115, found 339.1113.

**2b:**<sup>11c</sup> Yellow solid (Yield 64%). TLC (Solvent 100% Hexane) R<sub>f</sub> = 0.64; <sup>1</sup>H NMR (300 MHz, CDCl<sub>3</sub>, ppm) δ = 7.56 (m, 4H), 7.33 (t, *J* = 7.08, 1H), 7.18 (s, 4H). HRMS *m/z* [M<sup>+</sup>] calcd for C<sub>14</sub>H<sub>9</sub>NS<sub>2</sub> 255.0176, found 255.0184.

**General procedure for bromination of DTP – synthesis of compounds 3(a, b) and**

**4a:** To a 250 ml two-neck round-bottom flask covered with aluminum foil, compound **2** (3.1 mmol), glacial acetic acid (20 ml) and CHCl<sub>3</sub> (20 ml) were added. Reaction mixture was stirred under nitrogen atmosphere with the temperature maintained at 4 °C. After 5 - 10 minutes, *N*-bromosuccinimide (NBS) (0.66 g, 3.72 mmol) was added in portions over 2 minutes. Reaction mixture was stirred at 4 °C for 1.5 hours, and subsequently at room

temperature for ½ hr. After completion of reaction mixture was extracted with CHCl<sub>3</sub> twice (2 × 50 ml) and washed with saturated NaHCO<sub>3</sub> solution. The collected organic layer was dried over anhydrous sodium sulfate. The solvent was removed under reduced pressure and the crude product was purified by column chromatography to give monobromo DTP (**3**) and dibromo DTP (**4**). Dibromo DTP was also synthesized in high yield of 77% by carrying out the reaction with excess (2.5 equ.) of NBS.

**3a:** Orange-white flakes (Yield 47%). TLC (Solvent 100% Hexane) R<sub>f</sub> = 0.88; <sup>1</sup>H NMR (300 MHz, CDCl<sub>3</sub>, ppm) δ = 7.43 (d, *J* = 8.37 Hz, 2H, Ph-**H**), 7.32 (d, *J* = 8.37 Hz, 2H, Ph-**H**), 7.19 (s, 1H, Th-**H**), 7.16 (d, *J* = 5.25 Hz, 1H, Th-**H**), 7.11 (d, *J* = 5.28 Hz, 1H, Th-**H**), 2.68 (t, *J* = 7.89 Hz, 2H, Ph-**CH**<sub>2</sub>), 1.68 (m, 2H, -**CH**<sub>2</sub>), 1.35 (m, 6H, -**CH**<sub>2</sub>), 0.91 (t, *J* = 6.9, 3H, -**CH**<sub>3</sub>). <sup>13</sup>C NMR (75.4 MHz, CDCl<sub>3</sub>, ppm) δ = 143.2, 141.6, 141.3, 137, 129.7, 128.8, 123.7, 122.5, 116.6, 115.6, 112.1, 110, 35.5, 31.8, 31.4, 29, 22.7, 14.2. HRMS *m/z* [M<sup>+</sup>] calcd for C<sub>20</sub>H<sub>20</sub>NBrS<sub>2</sub> 417.0221, found 417.0211.

**3b:** Orange-white flakes (Yield 45%). TLC (Solvent 100% Hexane) R<sub>f</sub> = 0.84; <sup>1</sup>H NMR (300 MHz, CDCl<sub>3</sub>, ppm) δ = 7.52 (m, 4H, Ar-**H**), 7.37 (m, 1H, Ar-**H**), 7.21 (s, 1H, Th-**H**), 7.18 (d, *J* = 5.25 Hz, 1H, Th-**H**), 7.14 (d, *J* = 5.28 Hz, 1H, Th-**H**). <sup>13</sup>C NMR (75.4 MHz, CDCl<sub>3</sub>, ppm) δ = 143.2, 141.5, 139.4, 129.9, 126.4, 123.9, 122.8, 117, 115.6, 112.1, 110.1. HRMS *m/z* [M<sup>+</sup>] calcd for C<sub>14</sub>H<sub>8</sub>NBrS<sub>2</sub> 332.9282, found 332.9293.

**4a:** Orange yellow flakes (Yield 77%). TLC (Solvent 100% Hexane) R<sub>f</sub> = 0.9; <sup>1</sup>H NMR (300 MHz, CDCl<sub>3</sub>, ppm) δ = 7.38 (d, *J* = 8.37 Hz, 2H, Ph-**H**), 7.32 (d, *J* = 6.72 Hz, 2H, Ph-**H**), 7.15 (s, 2H, Th-**H**), 2.67 (t, *J* = 7.7 Hz, 2H, Ph-**CH**<sub>2</sub>), 1.66 (m, 2H, -**CH**<sub>2</sub>), 1.34 (m, 6H, -**CH**<sub>2</sub>), 0.90 (t, *J* = 6.9 Hz, 3H, -**CH**<sub>3</sub>); <sup>13</sup>C NMR (75.4 MHz, CDCl<sub>3</sub>, ppm) 141.9,

140.9, 136.6, 129.9, 127.4, 122.8, 115.4, 110.3, 35.5, 31.7, 31.4, 29, 22.6, 14.1; HRMS  $m/z$   $[M]^+$  calcd for  $C_{20}H_{19}NBr_2S_2$  496.9305, found 496.9324.

**General procedure for Suzuki coupling – synthesis of compounds 5a, 5b and 6a:** To a 250 ml two-neck round-bottom flask, THF, compound **3** or **4**, 2-nitrophenylboronic acid, and  $K_2CO_3$  were added. The flask was evacuated and back-filled with nitrogen. The catalyst tetrakis(triphenylphosphine)palladium(0) was added and heated at 60 °C overnight. The reaction mixture was cooled to room temperature and extracted with ethyl acetate/brine. The extracted organic layer was collected and dried over anhydrous sodium sulfate. The solvent was removed under reduced pressure. The crude, brown solid product was washed with hexane to remove the non-polar side products and the remaining solid was dried at pump. Products **5a** and **5b** were carried on to next step without further purification. Product of **4a** was purified by column chromatography to afford **6a** as brown solid (Scheme 3.1).

**5a:** THF (25 ml), compound **3a** (662 mg, 1.59 mmol), 2-nitrophenylboronic acid (318 mg, 1.91 mmol),  $K_2CO_3$  (35 ml, 2 M),  $Pd(PPh_3)_4$  (128 mg, 0.11 mmol).

**5b:** THF (40 ml), compound **3b** (1.1 g, 3.3 mmol), 2-nitrophenylboronic acid (660 mg, 3.95 mmol),  $K_2CO_3$  (30 ml, 2 M),  $Pd(PPh_3)_4$  (267 mg, 0.23 mmol).

**6a:** THF (20 ml), compound **4a** (1g, 2.01 mmol), 2-nitrophenylboronic acid (869 mg, 5.15 mmol),  $K_2CO_3$  (30 ml, 2 M),  $Pd(PPh_3)_4$  (232 mg, 0.2 mmol).

The crude product was purified by column chromatography to afford product **6a** as brown solid (1.01 g, 87%). TLC (Solvent 10% ethyl acetate : 90% hexane)  $R_f$  = 0.5;  $^1H$  NMR (300 MHz,  $CDCl_3$ ,  $\delta$ , ppm) 7.76 (dd,  $J_1$  = 8.04 Hz,  $J_2$  = 0.9 Hz, 2H, Ph-**H**), 7.61

(m, 4H, Ph-**H**), 7.46 (m, 4H, Ph-**H**), 7.32 (d,  $J = 8.4$  Hz, 2H, Ph-**H**), 7.16 (s, 2H, Th-**H**), 2.67 (t,  $J = 7.73$  Hz, 2H, Ph-**CH**<sub>2</sub>), 1.65 (m, 2H, -**CH**<sub>2</sub>), 1.34 (m, 6H, -**CH**<sub>2</sub>), 0.9 (t,  $J = 6.66$  Hz, 3H, -**CH**<sub>3</sub>); <sup>13</sup>C NMR (75.4 MHz, CDCl<sub>3</sub>,  $\delta$ , ppm) 149.4, 143.9, 141.7, 136.7, 135.3, 132.3, 131.9, 129.8, 129.1, 128.5, 124, 122.8, 117.7, 112.3; HRMS  $m/z$  [M]<sup>+</sup> calcd for C<sub>32</sub>H<sub>27</sub>O<sub>4</sub>N<sub>3</sub>S<sub>2</sub> 581.1443, found 581.1438.

**General procedure for Cadogan cyclization – synthesis of compounds 7a, 7b and 8a:**

To a 100 ml two-neck round-bottom flask kept under nitrogen atmosphere, compound **6**, triethyl phosphite and 1,2-dichlorobenzene were added. Reaction mixture was heated under reflux at 160 °C for 24 hours. Solvent and excess triethyl phosphite was removed under reduced pressure. The crude product was purified by column chromatography to give desired compound **7**.

**7a:** Compound **5a** (500 mg, 1.09 mmol), triethyl phosphite (8 ml), 1,2-dichlorobenzene (3 ml). Yellow solid (160 mg, 35%). TLC (Solvent 5% ethyl acetate : 95% hexane)  $R_f = 0.48$ ; <sup>1</sup>H NMR (300 MHz, CDCl<sub>3</sub>, ppm)  $\delta = 7.93$  (s, 1H, N-**H**), 7.7 (m, 1H), 7.57 (d,  $J = 8.4$  Hz, 2H, Ph-**H**), 7.45 (d, 2H,  $J = 8.4$  Hz, Ph-**H**), 7.4 (m, 1H, Th-**H**), 7.22 – 7.14 (m, 4H), 7.15 (m, 2H, Ph-**H**), 2.75 (t, 2H, Ph-**CH**<sub>2</sub>), 1.74 (m, 2H, -**CH**<sub>2</sub>), 1.39 (m, 6H, -**CH**<sub>2</sub>), 0.94 (t,  $J = 6.9$  Hz, 3H, -**CH**<sub>3</sub>); <sup>13</sup>C NMR (75.4 MHz, CDCl<sub>3</sub>, ppm)  $\delta = 142.3, 141.7, 139.7, 137.2, 130.2, 128.7, 128, 123.5, 123.3, 122.6, 122.3, 120.3, 119.1, 118.6, 118.1, 118, 112, 111.9, 35.6, 31.7, 31.4, 29.1, 22.6, 14.1$ ; HRMS  $m/z$  [M]<sup>+</sup> calcd for C<sub>26</sub>H<sub>24</sub>N<sub>2</sub>S<sub>2</sub> 428.1381, found 428.1373.

**7b:** Compound **5b** (1.1 g, 2.92 mmol), triethyl phosphite (10 ml), 1,2-dichlorobenzene (3 ml). Orange-yellow solid (340 mg, 34%). TLC (Solvent 5% ethyl acetate : 95% hexane)  $R_f = 0.22$ ; <sup>1</sup>H NMR (300 MHz, acetone-d<sub>6</sub>, ppm)  $\delta = 10.19$  (s, 1H, N-**H**), 7.78 (m, 2H,

Ph-**H**), 7.68 (m, 3H, Ph-**H**), 7.49 (m, 2H, Ph-**H**), 7.37 (d,  $J = 5.25$  Hz, 1H, Th-**H**), 7.26 (d,  $J = 5.25$  Hz, 1H, Th-**H**), 7.16 (m, 2H, Ph-**H**);  $^{13}\text{C}$  NMR (75.4 MHz,  $\text{CDCl}_3$ , ppm) 143.1, 139.7, 139.6, 130.4, 130.1, 128.6, 128, 126.7, 123.5, 123.5, 122.7, 122.5, 122.4, 120.4, 118.9, 118.3, 118, 111.9; HRMS  $m/z$   $[\text{M}]^+$  calcd for  $\text{C}_{20}\text{H}_{12}\text{N}_2\text{S}_2$  344.0442, found 344.0437.

**8a**: Compound **6a** (135 mg, 0.23 mmol), triethyl phosphate (2 ml), 1,2-dichlorobenzene (3 ml). Brown solid (42 mg, 35%). TLC (Solvent 20% ethyl acetate : 80% hexane)  $R_f = 0.70$ ;  $^1\text{H}$  NMR (300 MHz,  $\text{DMSO-d}_6$ , ppm)  $\delta = 10.76$  (s, 2H, N-**H**), 7.64 (m, 8H, Ph-**H**), 7.15 (m, 4H, Ph-**H**), 2.81 (t,  $J = 7.8$  Hz, 2H, Ph-**CH}\_2**), 1.80 (m, 2H, -**CH}\_2**), 1.50 (m, 2H, -**CH}\_2**), 1.38 (m, 4H, -**CH}\_2**), 0.93 (t,  $J = 7$  Hz, 3H, -**CH}\_3**);  $^{13}\text{C}$  NMR (75.4 MHz,  $\text{DMSO-d}_6$ ,  $\delta$ , ppm) 141.4, 140.9, 136.1, 131.2, 128.6, 128.2, 123.2, 122.8, 122.2, 120, 117.5, 116.5, 113.4, 35.4, 31.6, 31.1, 29.2, 22.5, 14.4; HRMS  $m/z$   $[\text{M}]^+$  calcd for  $\text{C}_{32}\text{H}_{27}\text{N}_3\text{S}_2$  517.1646, found 517.1646.

**General procedure for alkylation – synthesis of compounds 9a, 9b and 10a**: In a 100 ml round-bottom flask, compound **7** was dissolved in DMF. To the solution, NaOH and iodomethane were added. Reaction mixture was stirred at room temperature for 24 hours. Reaction mixture was extracted with diethyl twice ( $2 \times 50$  ml). Organic layer was dried over anhydrous sodium sulfate. The excess solvent was removed under reduced pressure. Crude product was purified by column chromatography to give desired compound.

**9a**: Compound **7a** (134 mg, 0.31 mmol), DMF (6 ml), NaOH (38 mg, 0.94 mmol), iodomethane (67 mg, 0.47 mmol). Pale yellow solid (100 mg, 70%). TLC (Solvent 5% ethyl acetate : 95% hexane)  $R_f = 0.65$ ;  $^1\text{H}$  NMR (300 MHz, acetone- $\text{d}_6$ ,  $\delta$ , ppm) 7.66 (m, 3H, Ar-**H**), 7.54 (d,  $J = 8.37$  Hz, 2H, Ar-**H**), 7.37 (d,  $J = 8.22$  Hz, 1H, Ar-**H**), 7.32 (d,  $J =$



5.10 Hz, 1H, Th-**H**), 7.22 (m,  $J = 7.07$  Hz,  $J = 1.17$  Hz, 1H, Ar-**H**), 7.14 (m,  $J = 7.65$  Hz,  $J = 1.14$  Hz, 1H, Ar-**H**), 6.93 (d,  $J = 5.25$  Hz, 1H, Th-**H**), 3.25 (s, 3H, N-**CH<sub>3</sub>**), 2.77 (t,  $J = 7.23$  Hz, 2H, Ph-**CH<sub>2</sub>**), 1.75 (m, 2H, -**CH<sub>2</sub>**), 1.38 (m, 6H, -**CH<sub>2</sub>**), 0.92 (t,  $J = 7.08$ , 3H, -**CH<sub>3</sub>**);  $^{13}\text{C}$  NMR (75.4 MHz,  $\text{CDCl}_3$ , ppm)  $\delta = 146, 143.7, 141.6, 138.3, 131.8, 131.1, 129.7, 126.9, 123.2, 121.8, 119.6, 117.9, 117.4, 111.9, 109.8, 108.4, 35.6, 32.9, 31.7, 31.4, 28.8, 22.6, 14.1$ ; HRMS  $m/z$   $[\text{M}]^+$  calcd for  $\text{C}_{27}\text{H}_{26}\text{N}_2\text{S}_2$  442.1537, found 442.1538.

**9b**: Compound **7b** (150 mg, 0.44 mmol), DMF (10 ml), NaOH (52 mg, 1.31 mmol), iodomethane (93 mg, 0.65 mmol). Pale yellow solid (109 mg, 70%). TLC (Solvent 5% ethyl acetate : 95% hexane)  $R_f = 0.48$ ;  $^1\text{H}$  NMR (300 MHz, acetone- $d_6$ , ppm)  $\delta = 7.7$  (m, 6H, Ph-**H**), 7.38 (d,  $J = 8.22$  Hz, 1H, Ph-**H**), 7.33 (d,  $J = 5.25$  Hz, 1H, Th-**H**), 7.23 (t,  $J = 7.07$ , 1H, Ph-**H**), 7.15 (t,  $J = 7.16$ , 1H, Ph-**H**), 6.95 (d,  $J = 5.25$ , 1H, Th-**H**), 3.26 (s, 3H, N-**CH<sub>3</sub>**);  $^{13}\text{C}$  NMR (75.4 MHz,  $\text{CDCl}_3$ ,  $\delta$ , ppm) 145.9, 141.6, 140.8, 131.5, 130.9, 130.7, 129.9, 128.8, 128.5, 126.9, 123.4, 123.3, 121.9, 119.6, 117.9, 117.7, 111.9, 109.8, 68.2. HRMS  $m/z$   $[\text{M}]^+$  calcd for  $\text{C}_{21}\text{H}_{14}\text{N}_2\text{S}_2$  358.0598, found 358.0603.

**10a**: Compound **8a** (135 mg, 0.29 mmol), DMF (10 ml), NaOH (35 mg, 0.87 mmol), iodomethane (123 mg, 0.87 mmol). Brown solid (88 mg, 56%). TLC (Solvent 10% ethyl acetate : 90% hexane)  $R_f = 0.7$ ;  $^1\text{H}$  NMR (300 MHz, acetone- $d_6$ , ppm)  $\delta = 7.92$  (d,  $J = 8.4$  Hz, 2H, Ph-**H**), 7.67 (d,  $J = 8.04$  Hz, 4H, Ph-**H**), 7.36 (d,  $J = 8.04$  Hz, 2H, Ph-**H**), 7.17 (m, 4H, Ph-**H**), 3.10 (s, 6H, N-**CH<sub>3</sub>**), 2.89 (t,  $J = 7.56$  Hz, 2H, Ph-**CH<sub>2</sub>**), 1.8 (m, 2H, -**CH<sub>2</sub>**), 1.41 (m, 6H, -**CH<sub>2</sub>**), 0.95 (t,  $J = 6.98$  Hz, 3H, -**CH<sub>3</sub>**);  $^{13}\text{C}$  NMR (75.4 MHz,  $\text{CDCl}_3$ ,  $\delta$ , ppm) 146.1, 139.7, 138.3, 133.3, 130.2, 130.2, 130, 121.8, 119.5, 117.9, 117.8, 35.7, 31.8, 31.7, 31.5, 28.7, 22.7, 14.1; HRMS  $m/z$   $[\text{M}]^+$  calcd for  $\text{C}_{34}\text{H}_{31}\text{N}_3\text{S}_2$  545.1959, found 545.1968.

### 3.3. Results and discussion

#### 3.3.1. Synthesis

The synthetic route leading to the unsymmetrical and extended heteroacene is presented in Scheme 3.1. The palladium-catalyzed ( $\text{Pd}_2(\text{dba})_3/\text{P}^t\text{Bu}_3$ ) amination of 3,3'-dibromo-2,2'-bithiophene **1** with excess (1.4 equiv) aniline/4-hexyl aniline afforded DTP in 60% yield. Only aryl substituents were incorporated, as the alkyl-substituted bromo-DTPs are unstable.<sup>13</sup> It was postulated that the presence of CH group  $\alpha$  to N in the *N*-alkyl derivatives plays a role in the decomposition of the brominated product. The dibromination of DTP was carried out by following the reported procedure.<sup>13</sup> Monobromination of DTP was achieved by the addition of 1.2 equiv of *N*-bromosuccinimide (NBS) under nitrogen atmosphere. Reactions were unsuccessful under normal conditions and led to decomposed products as indicated by the presence of black insoluble particles. By applying an inert nitrogen atmosphere throughout the reaction, decomposition was avoided, and compound **5** was obtained in a reasonable yield (45%). The dibrominated product **4** was also isolated in this reaction along with the unreacted starting material **2**. Suzuki coupling of **3a**, **3b** and **4a** was carried out with 2-nitrophenyl boronic acid (NBA) to obtain compounds **5a**, **5b** and **6a**, respectively. Suzuki coupling of 2,2'-dibromo-*N*-phenyldithienopyrrole resulted in an insoluble product. Hence the synthesis of **8b** and **10b** becomes unfeasible. The thienopyrrole-based, heteroacenes were prepared by reductive Cadogan cyclization.<sup>14</sup> Refluxing the compounds **5** and **6** with excess of triethyl phosphite and 1,2-dichlorobenzene for 24 hours resulted in the target compound **7** and **8** respectively, in around 35% yield. *N*-Methyl products **9** and **10**, were obtained by reacting **7** and **8** with iodomethane.

Structures of the synthesized compounds were confirmed by  $^1\text{H}$  NMR,  $^{13}\text{C}$  NMR and high-resolution mass spectrometry.

### 3.3.2. X-ray structure

Single crystals of **9b** and **10a** suitable for single-crystal X-ray analysis were obtained by slow evaporation from a mixture of hexane and dichloromethane at room temperature. Extended heteroacene **10a** is not planar, it deviates  $13.4^\circ$  from planarity (Figure 3.2).

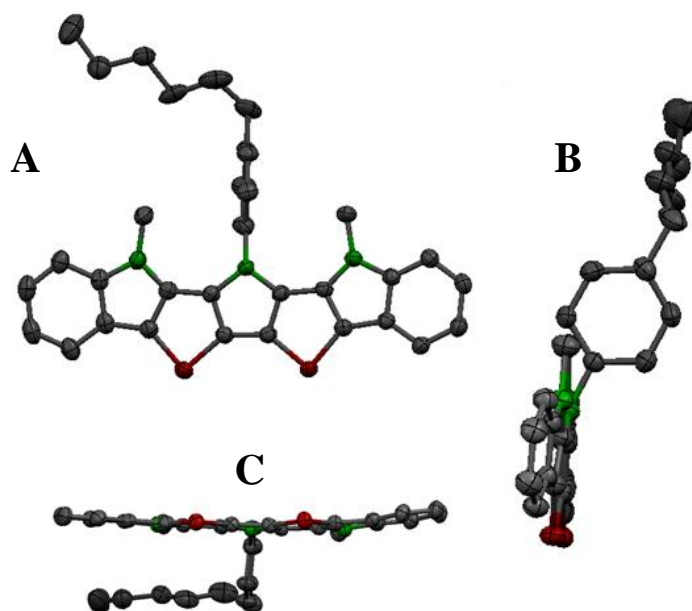


**Figure 3.2.** Thermal ellipsoid plot of extended heteroacene (**10a**) (A). Phenyl group tilted from the heteroacene plane (B). Bowed nature of heteroacene backbone (C). Hydrogen atoms are removed for clarity

The phenyl ring attached to the pyrrole ring is twisted by an angle of  $84.6^\circ$  with respect to the acene core. This pendant phenyl group is tilted from the plane of molecule possibly due to the steric hindrance imposed by the adjacent methyl groups (Figure 3.2).

In the crystal lattice, **10a** forms  $\pi$ -stacked dimers that are rotated by  $180^\circ$  to each other. The distance between these, dimers was found to be around  $3.34 \text{ \AA}$ , which equals the sum of van der Waals radii of carbon atoms (Figure 3.3A).

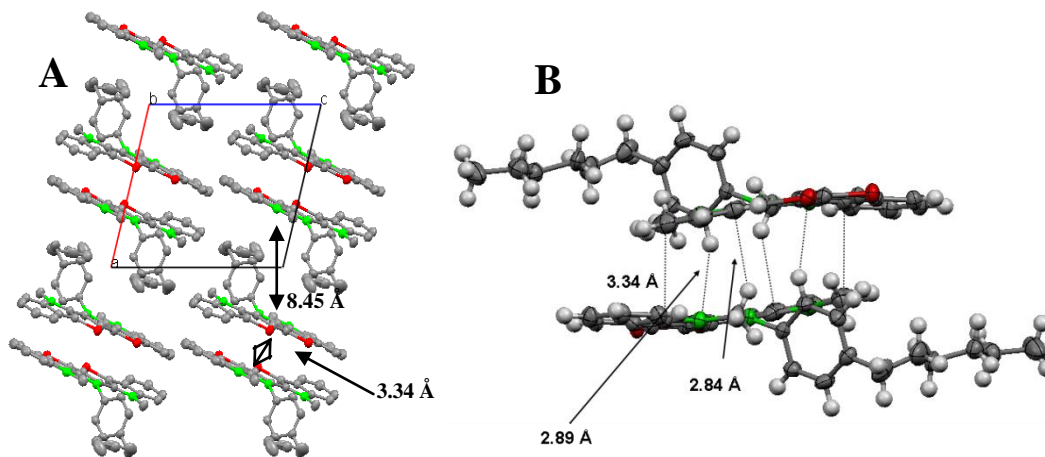


**Figure 3.3.** Crystal packing of extended heteroacene (**10a**) in lattice (A). Thermal ellipsoid plot of dimer of **10a** (B)

The existence of  $\text{C-H}\cdots\pi$  interactions between hydrogen atoms of the methyl group with a  $\pi$  cloud of the adjacent molecule also accounts for the close interactions in these dimers ( $2.84 \text{ \AA}$ ) (Figure 3.3). These dimers interact with other dimers in the lattice through  $\text{C-H}\cdots\text{S}$  interaction between pendant phenyl group of one dimer with the  $\pi$ -backbone of another dimer ( $2.89 \text{ \AA}$ ). As a consequence of this interaction, the fused  $\pi$ -backbones (dimer) are well separated from other dimers by a distance of  $8.45 \text{ \AA}$ . Though there exists a short  $\text{S}\cdots\text{S}$  contact ( $3.34 \text{ \AA}$ ) between the molecules of adjacent column, a less densely packed structure of **10a** was obtained. Similar to **10a**, compound **9b** was also not strictly planar, as it deviates  $12^\circ$  from planarity (Figure 3.4).

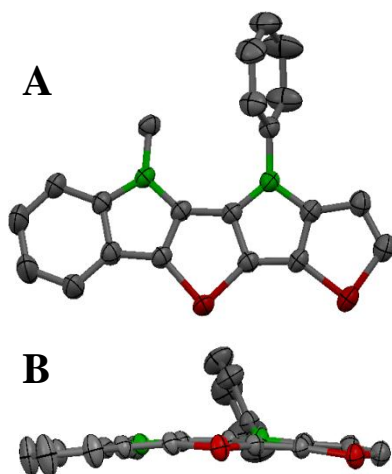


**Figure 3.4.** Thermal ellipsoid plot of unsymmetric heteroacene **9b** (A). Lateral view showing the bowed nature of heteroacene (B). Hydrogen atoms are removed for clarity

The phenyl group attached to the pyrrole ring is twisted by an angle of  $64^\circ$  with respect to the acene core. In **9b**, molecule pack in an edge-to-face manner leading to the sandwiched herringbone packing with the herringbone angle of  $60^\circ$  along the  $a$ -axis (Figure 3.5A). Such packing mode favors two-dimensional electronic interactions in the solid, which is advantageous for better charge carrier mobility.<sup>7a</sup> The molecule **9b** form dimers with an antiparallel, slipped cofacial arrangement, presumably to minimize dipolar interactions and the steric effect imposed by the pendant phenyl ring. Within each dimer, the molecules are held together by short C-H $\cdots$  $\pi$  contacts of 2.76 Å between the pendant phenyl ring and the acene core (Figure 3.5B). The molecules in these dimers are 3.6 Å apart at the shortest intermolecular distance. The S $\cdots$ S interactions of 3.5 Å between the molecules from adjacent columns are also dominant (shown in Figure 3.5A).

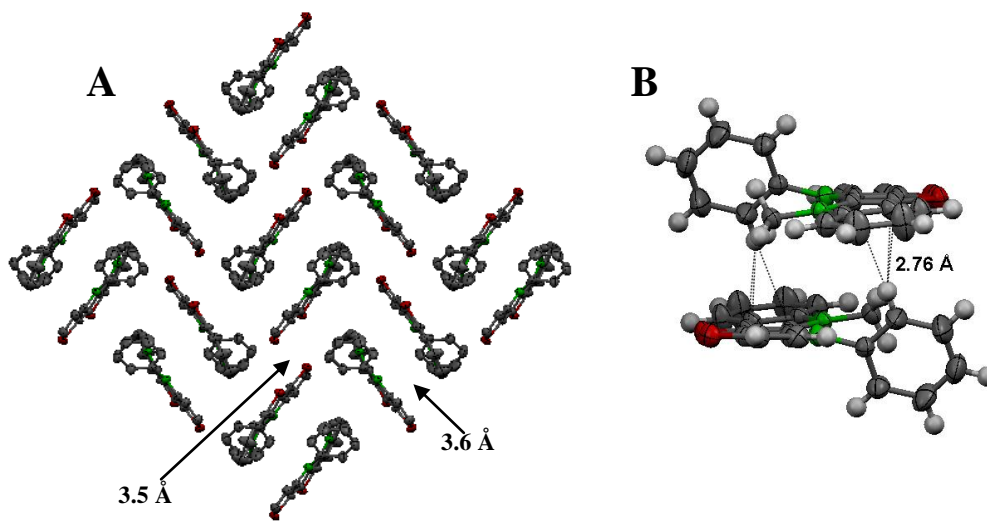


**Figure 3.5.** Packing of unsymmetrical heteroacene (**9b**) in crystal lattice (A). Hydrogen atoms are removed for clarity. Thermal ellipsoid plot of **9b** dimer (B)

### 3.3.3. Optical properties

Absorption and emission spectra of heteroacenes are depicted in Figure 3.6 and the spectral characteristics are summarized in Table 3.1. Absorption spectra of extended heteroacenes **8a** and **10a** shows similar spectral characteristics (Figure 3.6A) illustrating the insignificant effect of alkyl substituent on the electronic states of these compounds. All unsymmetrical heteroacenes showed similar absorption properties with  $\lambda_{\text{max}}$  around 340 nm and absorption onset at 370 nm (Figure 3.6B). It is noteworthy that the absorption spectra of the compounds are featured with several vibronic peaks, characteristics of fused ring systems with well-defined electronic states. The optical band gap estimated from the onset of UV-vis absorption is identical for both **8a** and **10a** (i.e. ca. 3.02 eV). Interestingly, **8a** and **10a** possess a larger band gap compared to

diindolocarbazole (2.73 eV).<sup>11e</sup> An identical band gap value of 3.35 eV is obtained for all unsymmetrical heteroacenes. The fluorescence spectra are virtually the mirror image of absorption spectra, indicating a rigid planar system.<sup>15</sup> The fluorescence quantum yield ( $\Phi_f$ ) of all compounds were measured in THF using quinine sulfate in 0.1 M sulfuric acid as standard. The solution state quantum yield of extended fused ring compounds are found to be 18%, whereas the unsymmetrical compounds have a quantum yield of around 5%.

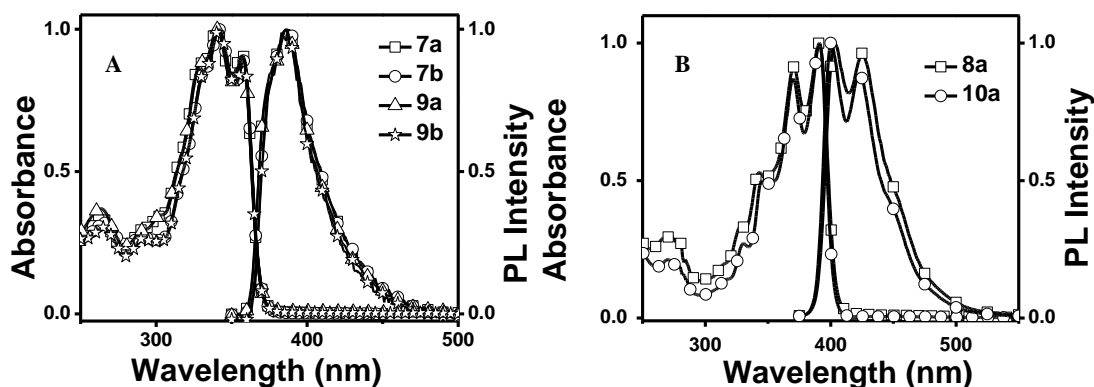


**Figure 3.6.** Normalized UV-vis absorption and emission spectra of extended diindolodithienopyrrole (A) and unsymmetric indolodithienopyrrole (B) recorded in THF

### 3.3.4. Electrochemical properties

Electrochemical properties of the compounds were investigated with cyclic voltammetry performed using  $\text{Ag}/\text{Ag}^+$  as the reference electrode (Figure 3.7). The cyclic voltammogram of **8a** and **10a** showed two quasi-reversible oxidation peaks around 0.6 and 1.2 V. Unlike extended heteroacene, oxidation process in unsymmetrical compound is irreversible.

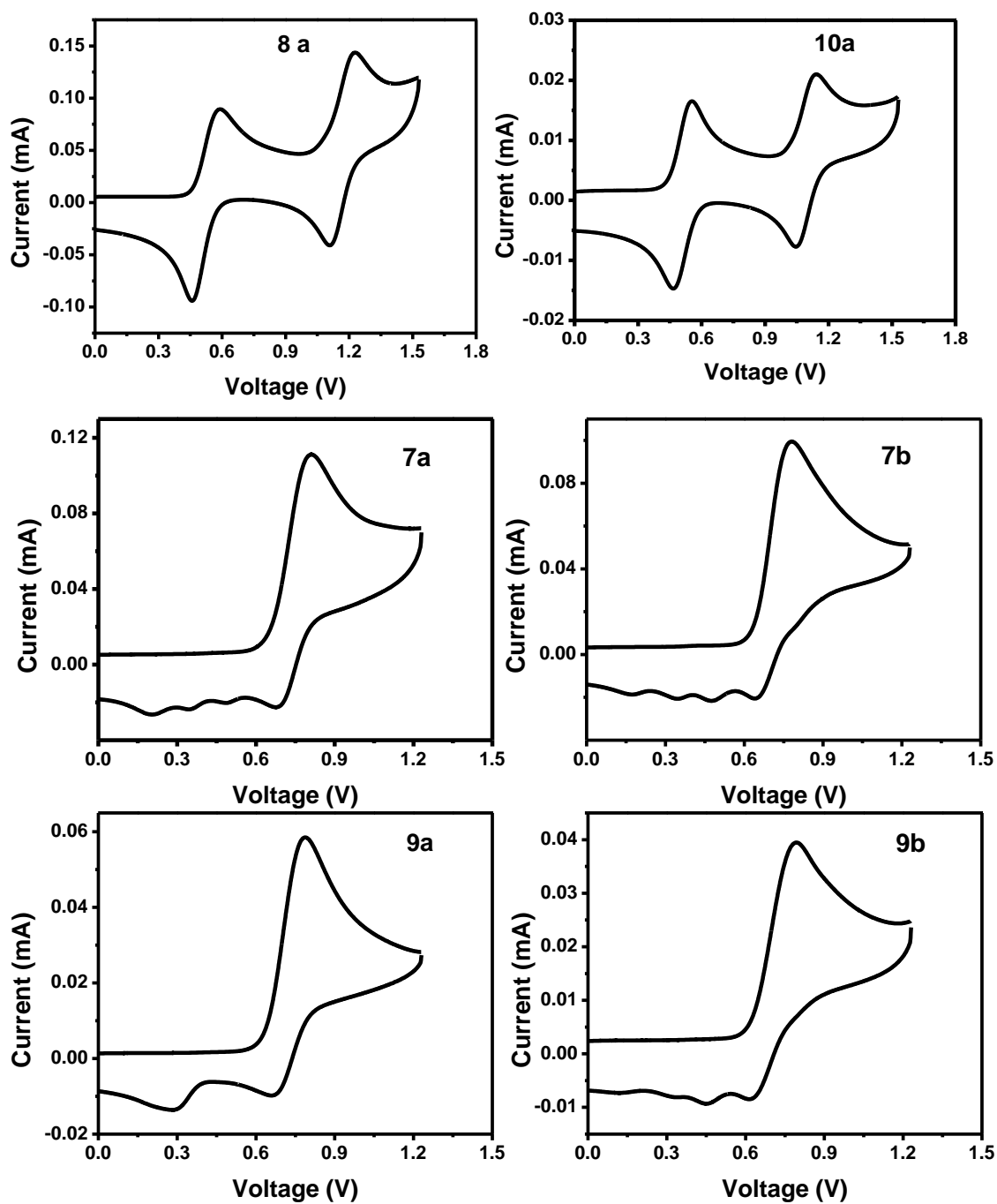


**Figure 3.7.** Cyclic voltammogram of extended diindolodithienopyrrole and unsymmetric indolodithienopyrrole recorded in dichloromethane



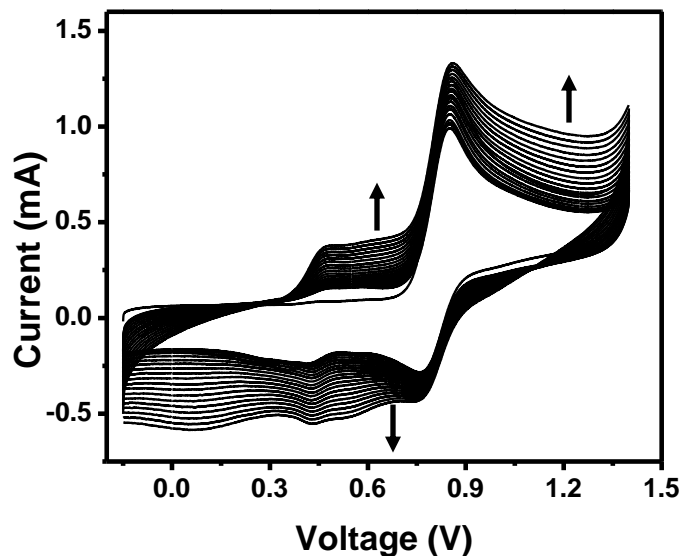


**Figure 3.8.** Repeated CV scan of **7a** using Pt as working electrode at scan rate of 100 mV/s

Unsymmetrical heteroacenes **7a**, **7b**, **9a** and **9b** showed irreversible oxidation with peak potential around 0.8 V. Oxidation potential gradually shifted to lower potential with increase in peak current during repeated anodic scans (Figure 3.8). This can be attributed to the presence of unblocked electroactive unit (thiophene end) which can undergo oxidative coupling under electrochemical conditions. The HOMO energy level was calculated from the oxidation onset potential using the empirical formula  $E_{\text{HOMO}} = - (E_{\text{ox}}^{\text{onset}} + 4.38) \text{ eV}$ .<sup>16</sup> As we were unable to observe any reduction within our scan range, LUMO energy level was empirically calculated from the HOMO energy level and optical band gap (absorption edges in UV-vis spectra). All unsymmetrical compounds showed an oxidation onset potential around 0.7 V, which corresponds to HOMO energy levels of -5.01 eV. The smaller band gap of extended ring compounds (**8a** and **10a**) compared to the unsymmetrical systems are consistent with extension of  $\pi$ -conjugation. The HOMO energy level in these compounds is significantly lower than that reported for

pentacene (ca. -4.4 eV).<sup>17</sup> The low-lying HOMO and relatively large band gap afford environmental stability to these molecules. Electrochemical data and energy levels are summarized in Table 3.1.

**Table 3.1.** Photophysical and electrochemical properties of indolodithienopyrrole and diindolodithienopyrrole

compound	$\lambda_{\text{Abs}}$ (nm)	$\lambda_{\text{Em}}^{\text{a}}$ (nm)	$\Phi_{\text{F}}^{\text{b}}$ (%)	Band gap <sup>c</sup> (eV)	$E^{\text{d}}_{\text{oxid}}$ (V)	HOMO <sup>e</sup>	LUMO <sup>f</sup>
8a	391, 370, 343, 329, 273	425, 403	18	3.02	0.59, 1.23	-4.84	-1.82
10a	391, 370, 345, 330, 270	423, 400	18	3.02	0.56, 1.14	-4.82	-1.8
7a	357, 341, 264	386	6	3.35	0.81	-5.04	-1.69
7b	357, 340, 264	386	4	3.35	0.78	-5.01	-1.66
9a	358, 342, 291, 265	387	6	3.35	0.79	-5.01	-1.66
9b	357, 342, 290, 265	388	4	3.35	0.79	-5.01	-1.66

<sup>a</sup>The sample was excited at absorption maximum. <sup>b</sup>Solution state quantum yield in THF calculated with quinine sulfate as standard. <sup>c</sup>Optical band gap estimated from onset of absorption. <sup>d</sup>Onset potentials (vs Ag/AgCl) calculated from cyclic voltammetry: 0.1 M *n*-Bu<sub>4</sub>NPF<sub>6</sub> in acetonitrile, Pt as working electrode under the scan rate of 100 mVs<sup>-1</sup>. <sup>e</sup>Calculated using the relationship  $E_{\text{HOMO}} = -(E_{\text{onset}}^{\text{ox}} + 4.38)$ . <sup>f</sup>Derived from optical band gap and HOMO.

### 3.4. Conclusion

In conclusion, we synthesised a new class of heteroacenes (unsymmetrical and extended) containing thiophene and pyrrole units. These acenes are stable at ambient conditions and soluble in common organic solvents. Unsymmetrical heteroacene packs in sandwich herringbone manner leading to densely-packed structures. The extended heteroacene is bowed and leads to a less densely packed structure due to the phenyl substitution of central pyrrole ring and the alkyl chain attached to it. Low lying HOMO levels indicates the superiority of these molecules compared to pentacene in terms of stability.

### 3.5. References

---

- (1) (a) Yamamoto, T.; Takimiya, K. *J. Am. Chem. Soc.* **2007**, *129*, 2224. (b) Wex, B.; Kaafarani, B. R.; Schroeder, R.; Majewski, L. A.; Burckel, P.; Grell, M.; Neckers, D. C. *J. Mater. Chem.* **2006**, *16*, 1121. (c) Cicoira, F.; Santato, C.; Melucci, M.; Favaretto, L.; Gazzano, M.; Muccini, M.; Barbarella, G. *Adv. Mater.* **2006**, *18*, 169. (d) Li, X.-C.; Sirringhaus, H.; Garnier, F.; Holmes, A. B.; Moratti, S. C.; Feeder, N.; Clegg, W.; Teat, S. J.; Friend, R. H. *J. Am. Chem. Soc.* **1998**, *120*, 2206.
- (2) (a) Payne, M. M.; Parkin, S. R.; Anthony, J. E.; Kuo, C. C.; Jackson, T. N. *J. Am. Chem. Soc.* **2005**, *127*, 4986. (b) Li, Y. N.; Wu, Y. L.; Gardner, S.; Ong, B. S. *Adv. Mater.* **2005**, *17*, 849. (c) Wakim, S.; Bouchard, J.; Simard, M.; Drolet, N.; Tao, Y.; Leclerc, M. *Chem. Mater.* **2004**, *16*, 4386.
- (3) (a) Anthony, J. E. *Chem. Rev.* **2006**, *106*, 5028. (b) T. Baumgartner, R. Réau, *Chem. Rev.* **2006**, *106*, 4681.
- (4) Winkler, M.; Houk, K. N. *J. Am. Chem. Soc.* **2007**, *129*, 1805.
- (5) (a) Gao, P.; Beckmann, D.; Tsao, H. N.; Feng, X.; Enkelmann, V.; Pisula, W.; Müllen, K. *Chem. Commun.* **2008**, 1548. (b) Tang, M. L.; Okamoto, T.; Bao, Z. *J. Am. Chem. Soc.* **2006**, *128*, 16002. (c) Wex, B.; Kaafarani, B. R.; Kirschbaum, K.; Neckers, D. C. *J. Org. Chem.* **2005**, *70*, 4502. (d) Xiao, K.; Liu, Y.; Qi, T.; Zhang, W.; Wang, F.; Gao, J.; Qiu, W.; Ma, Y.; Cui, G.; Chen, S.; Zhan, X.; Yu, G.; Qin, J.; Hu, W.; Zhu, D. *J. Am. Chem. Soc.* **2005**, *127*, 13281. (e) Li, Y. N.; Wu, Y. L.; Gardner, S.; Ong, B. S. *Adv. Mater.* **2005**, *17*, 849.
- (6) (a) Coropceanu, V.; Cornil, J.; da Silva Filho, D. A.; Olivier, Y.; Silbey, R.; Brédas, J.-L. *Chem. Rev.* **2007**, *107*, 926. (b) Lemaur, V.; da Silva Filho, D. A.; Coropceanu, V.; Lehmann, M.; Geerts, Y.; Piris, J.; Debije, M. G.; van de Craats, A. M.; Senthilkumar, K.; Siebbeles, L. D. A.; Warman, J. M.; Brédas, J.-L.; Cornil, J. *J. Am. Chem. Soc.* **2004**, *126*, 3271. (c) Barbarella, G.; Zambianchi, M.; Bongini, A.; Antolini, L. *Adv. Mater.* **1993**, *5*, 834.
- (7) (a) Zanirato, P.; Spagnolo, P.; Zanardi, G. *J. Chem. Soc. Perkin Trans I.* **1983**, 2551. (b) Berlin, A.; Zotti, G.; Schiavon, G.; Zecchin, S. *J. Am. Chem. Soc.* **1998**, *120*, 13453. (c) Ogawa, K.; Rasmussen, S. C. *J. Org. Chem.* **2003**, *68*, 2921.
- (8) Qi, T.; Guo, Y.; Liu, Y.; Xi, H.; Zhang, H.; Gao, X.; Liu, Y.; Lu, K.; Du, C.; Yu, G.; Zhu, D. *Chem. Commun.* **2008**, 6227.
- (9) (a) Gao, P.; Feng, X.; Yang, X.; Enkelmann, V.; Baumgarten, M.; Müllen, K. *J. Org. Chem.* **2008**, *73*, 9207. (b) Ebata, H.; Izawa, T.; Miyazaki, E.; Takimiya, K.; Ikeda, M.; Kuwabara, H.; Yui, T. *J. Am. Chem. Soc.* **2007**, *129*, 15732. (c) Pietrangelo, A.; MacLachlan, M. J.; Wolf, M. O.; Patrick, B. O. *Org. Lett.* **2007**, *9*, 3571.

- (10) (a) Kawaguchi, K.; Nakano, K.; Nozaki, K. *Org. Lett.* **2008**, *10*, 1199. (b) Tang, M. L.; Okamoto, T.; Bao, Z. *J. Am. Chem. Soc.* **2006**, *128*, 16002. (c) Balaji, G.; Valiyaveetil, S. *Org. Lett.* **2009**, *11*, 3358.
- (11) (a) Gao, P.; Feng, X.; Yang, X.; Enkelmann, V.; Baumgarten, M.; Müllen, K. *J. Org. Chem.* **2008**, *73*, 9207. (b) Sonnlag, M.; Strohmriegl, P. *Tetrahedron* **2006**, *62*, 8103. (c) Sirringhaus, H.; Friend, R. H.; Wang, C.; Leuninger, J.; Müllen, K. *J. Mater. Chem.* **1999**, *9*, 2095. (d) Okamoto, T.; Kudoh, K.; Wakamiya, A.; Yamaguchi, S. *Org. Lett.* **2005**, *7*, 5301. (e) Wakim, S.; Bouchard, J.; Blouin, N.; Michaud, A.; Leclerc, M. *Org. Lett.* **2004**, *6*, 3413. (f) Zhang, X.; Côté, A. P.; Matzger, A. J. *J. Am. Chem. Soc.* **2005**, *127*, 10502. (g) Payne, M. M.; Odom, S. A.; Parkin, S. R.; Anthony, J. E. *Org. Lett.* **2004**, *6*, 3325. (h) Payne, M. M.; Parkin, S. R.; Anthony, J. E. *J. Am. Chem. Soc.* **2005**, *127*, 8028.
- (12) Croby, G. A.; Demas, J. N. *J. Phys. Chem.* **1971**, *75*, 991.
- (13) Odom, S. A.; Lancaster, K.; Beverina, L.; Lefler, K. M.; Thompson, N. J.; Coropceanu, V.; Bredas, J.; Marder, S. R.; Barlow, S. *Chem. Eur. J.* **2007**, *13*, 9637.
- (14) Cadogan, J. I. G. *Synthesis* **1969**, 11.
- (15) Belletete, M.; Wakim, S.; Leclerc, M.; Durocher, G. *J. Mol. Struct.: THEOCHEM* **2006**, *760*, 147-152.
- (16) (a) Li, Y.; Ding, J.; Day, M.; Tao, Y.; Lu, J.; D'iorio, M. *Chem. Mater.* **2004**, *16*, 2165. (b) Leeuw, D. M.; Simenon, M. M. J.; Brown, A. R.; Einerhand, R. E. F. *Synth. Met.* **1997**, *87*, 53. (c) Cui, Y.; Zhang, X.; Jenekhe, S. A. *Macromolecules* **1999**, *32*, 3824.
- (17) Kahn, A.; Koch, N.; Gao, W. *J. Polym. Sci. B, Polym. Phys.* **2003**, *41*, 2529.

## ***Chapter 4***

# ***Thiadiazole Fused Indolo[2,3-a]carbazole Based Oligomers and Polymer***

***Publication from the chapter:***

**Balaji, G.;** Shim, W. L.; Parameswaran, M.; Valiyaveetil, S. “*Thiadiazole Fused Indolo[2,3-a]carbazole Based Oligomers and Polymer*”, *Org. Lett.* **2009**, *11*, 4450-4453.

#### 4.1. Introduction

Over the years, development of conjugated materials for the applications in organic electronics involves several common groups such as oligothiophenes,<sup>1</sup> oligofluorenes,<sup>2</sup> polycyclic aromatic compounds<sup>3</sup> and fused heterocyclic aromatic compounds.<sup>4</sup> In particular, fused-ring aromatic compounds exhibit good  $\pi$ -stacking and highly-ordered molecular structure, which are beneficial for the efficient charge transport. Hence, for electronic applications, molecules of high planarity with optimum band gap, close packing and good solubility are desired. Among the conjugated systems, fused heterocyclic aromatic compounds (heteroacenes) containing nitrogen atom showed a diverse range of applications, in biology, fabrication of new electronic devices and anion sensing.<sup>5</sup> In electronic applications, heteroacenes demonstrated improved properties of the highly ordered acene molecules.<sup>6</sup> Among the five indolocarbazole isomers,<sup>5</sup> (Figure 4.1) indolo[3,2-*b*]carbazole has been explored extensively for electronic applications.<sup>7</sup>

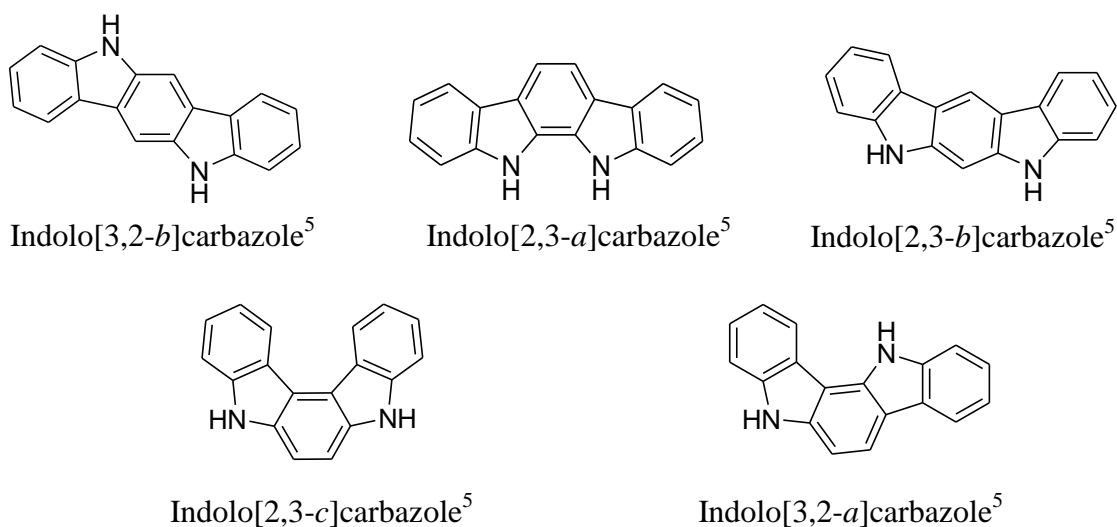


**Figure 4.1.** Chemical structures of five isomers of indolocarbazole<sup>5</sup>

Extensive studies on indolo[2,3-*a*]carbazoles based compounds are illustrated in biological applications such as protein kinase inhibitor,<sup>8</sup> antimicrobial agents<sup>9</sup> and as a ligand for aromatic hydrocarbon receptors (AhR).<sup>10</sup> Indolo[2,3-*a*]carbazole and its derivatives are also efficient sensors for anionic guest species, such as  $F^-$ ,  $Cl^-$ ,  $PhCO_2^-$ ,  $H_2PO_4^-$  and  $HSO_4^-$ .<sup>11</sup> But the material aspects of this isomer of indolocarbazole is poorly explored. In this regard, thiadiazole (acceptor moiety) fused indolo[2,3-*a*]carbazole (donor moiety) based new heteroacenes were synthesised. Their photophysical, electrochemical properties along with their packing in the crystal lattice were studied. Structures of the synthesised compounds are depicted in Figure 4.2.

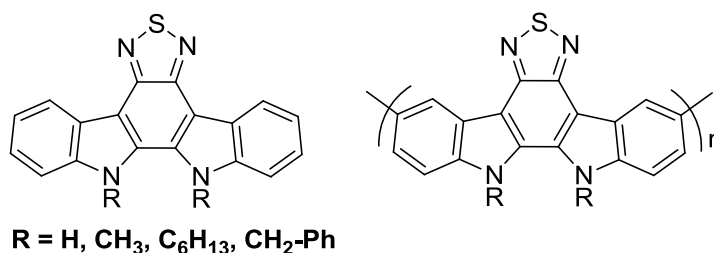


**Figure 4.2.** Structure of synthesized thiadiazole fused indolo[2,3-*a*]carbazole based molecules

## 4.2. Experimental section

### 4.2.1. Materials

All reactions were carried out under nitrogen atmosphere in oven-dried flask. All chemicals and reagents were purchased from commercial suppliers (Sigma-Aldrich, Merck, and Strem) and used without further purification. All reactions were carried out with freshly distilled anhydrous solvents under inert atmosphere. THF was distilled over sodium under nitrogen atmosphere. The reaction progress was monitored by thin-layer



chromatography (TLC). Chromatography was performed using silica gel (230-400 mesh) purchased from Merck. 2,1,3-benzothiadiazole, 2-nitrophenylboronic acid, triethyl phosphite were purchased from Aldrich. Compound **2** was synthesized from 2,1,3-benzothiadiazole by following the literature procedure.<sup>12</sup>

#### 4.2.2 Instrumentation

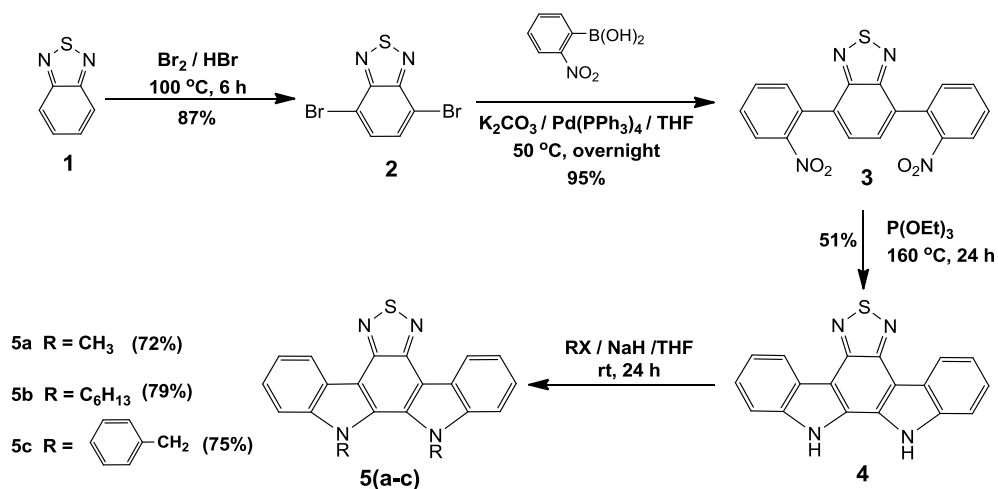
<sup>1</sup>H NMR spectra were recorded with Bruker ACF 300 (300 MHz) spectrometer. All NMR data was calibrated with solvent signals and peak multiplicity was indicated as follows: s = singlet, d = doublet, t = triplet, dd = doublet of doublet, m = multiplet, b = broad. Mass spectra were acquired by Micromass VG7035 double focusing mass spectrometer of high resolution. Cyclic voltammetric measurements were performed in CH<sub>2</sub>Cl<sub>2</sub> containing 1.0 mM of substrate and 0.1 M of Bu<sub>4</sub>NPF<sub>6</sub> as supporting electrolyte at a scan rate between 100 mVs<sup>-1</sup>. The counter and working electrodes were Pt wires, and the reference electrode was Ag/AgCl. The potentials are calibrated with ferrocene/ferrocenium redox couple (0.48 V vs Ag/AgCl). Onset value of the oxidation wave of the substrate ( $E_{\text{ox}}^{\text{onset}}$ ) was used to calculate HOMO energy level, using the relation  $E_{\text{HOMO}} = -(4.38 + E_{\text{ox}}^{\text{onset}})$ . LUMO levels were calculated from  $E_{\text{HOMO}}$  and optical band gap ( $E_g$ ). Electropolymerization was carried by using cyclic voltammetry (CV). A three-electrode system was used with indium-tin oxide (ITO) coated glass plate as working electrode, Pt wire as counter electrode and Ag/AgCl as reference electrode. Polymerization was performed in an acetonitrile solution containing 0.1 M of Bu<sub>4</sub>NPF<sub>6</sub> as supporting electrolyte. A 2.0 mM solution of monomer was used for polymerization at a scan rate of 100 mVs<sup>-1</sup>. Polymerization was achieved by repetitive scanning of anodic potential. Single crystals of acene compounds suitable for structural analysis were

obtained by recrystallization from chloroform. The X-ray crystal structure analysis was made on a Rigaku AFC-7 (Mo  $K\alpha$  radiation,  $\lambda = 0.71069 \text{ \AA}$ , graphite monochromator,  $T = 296 \text{ K}$ ,  $2\theta_{\text{max}} = 55.0^\circ$ ) or a Rigaku Rapid-IP (Mo  $K\alpha$  radiation,  $\lambda = 0.71069 \text{ \AA}$ , graphite monochromator,  $T = 296 \text{ K}$ ,  $2\theta_{\text{max}} = 55.0^\circ$ ).

### 4.2.3. Synthesis procedure

Synthesis scheme towards the target compounds are represented in Scheme 4.1

**Scheme 4.1.** Synthesis of thiadiazole fused indolocarbazole derivatives



**Synthesis of compound 3:** To a 500ml of two-necked round-bottomed flask was added compound **2** (3g, 10.2 mmol), 2-nitrophenylboronic acid (4.95 g, 29.7 mmol) and aqueous  $\text{K}_2\text{CO}_3$  (90 ml, 2M). The flask was evacuated and back-filled with nitrogen. 100 ml of THF was added. Reaction mixture was stirred and heated at  $50^\circ\text{C}$ . The catalyst  $\text{Pd}(\text{PPh}_3)_4$  (1.18 g, 1.02 mmol) was added and reaction was allowed to run overnight. The solution was cooled to room temperature and ethyl acetate was added and washed with water thrice. The extracted organic layer was dried over anhydrous sodium sulphate. The

solvent was evaporated under reduced pressure. The resulting dark brown solid was washed with hexane (250 ml  $\times$  6) and finally dried under vacuum to afford product **3** as fine grey solid (3.68 g, 95%). TLC (Solvent 20% ethyl acetate: 80% hexane)  $R_f = 0.35$ ;  $^1\text{H}$  NMR (300 MHz,  $\text{CDCl}_3$ ,  $\delta$ , ppm) 8.17 (d,  $J = 7.23$  Hz, 1H, Ar-**H**), 7.78 (m, 1H, Ar-**H**), 7.70 (s, 1H, Ar-**H**), 7.66 (m, 2H, Ar-**H**);  $^{13}\text{C}$  NMR (75.4 MHz,  $\text{CDCl}_3$ ,  $\delta$ , ppm) 133.2, 132.6, 132.1, 131.8, 129.6, 128.6, 128.4, 128, 124.9; HRMS  $m/z$   $[\text{M}]^+$  calcd for  $\text{C}_{18}\text{H}_{10}\text{O}_4\text{N}_4\text{S}$  - 378.0423, found 378.0434.

**Synthesis of compound 4:** To a 50 ml two-neck round-bottomed flask under nitrogen atmosphere was added compound **3** (1 g, 2.65 mmol), triethyl phosphite (14 ml) and 1,2-dichlorobenzene (5 ml). Reaction mixture was heated at reflux for 24 hours under nitrogen atmosphere. Reaction mixture was cooled and concentrated under reduced pressure. The crude product was finally purified by column chromatography to give desired compound **4** as a yellow solid (420 mg, 51%). TLC (2:3, ethyl acetate / hexane)  $R_f = 0.54$ ;  $^1\text{H}$  NMR (300 MHz, acetone- $d_6$ ,  $\delta$ , ppm) 11.23 (s, 2H, N-**H**), 8.63 (m, 2H, Ar-**H**), 7.76 (m, 2H, Ar-**H**), 7.45 (m, 4H, Ar-**H**);  $^{13}\text{C}$  NMR (75.4 MHz, acetone- $d_6$ ,  $\delta$ , ppm) 149, 138.1, 128.9, 124.2, 124, 121.1, 121, 111.9, 108.8; HRMS  $m/z$   $[\text{M}]^+$  calcd for  $\text{C}_{18}\text{H}_{10}\text{N}_4\text{S}$  - 314.0626, found 314.0625.

**Synthesis of compound 5(a-c):** To a 100 ml round bottom flask, compound **4** (100 mg, 0.318 mmol), dry THF (10 ml) and alkyl bromide (0.796 mmol) were added. To this reaction mixture (61 mg, 2.54 mmol) NaH (60% in mineral oil) was added and stirred at room temperature for 24 hours. After 24 hours, reaction mixture was quenched carefully by addition of water and extracted with chloroform (3  $\times$  20 ml). The collected organic layer was dried over anhydrous sodium sulphate and evaporated under reduced pressure.

Crude product was purified by column chromatography to get corresponding alkyl derivative.

**Compound 5a:** Orange yellow solid (78 mg, 72%). TLC (1:4, ethyl acetate:hexane)  $R_f = 0.45$ ;  $^1\text{H}$  NMR (300 MHz,  $\text{CDCl}_3$ ,  $\delta$ , ppm) 8.76 (d,  $J = 7.56$  Hz, 2H, Ar-**H**), 7.55 (m, 6H, Ar-**H**), 4.30 (s, 6H, N-**CH**<sub>3</sub>);  $^{13}\text{C}$  NMR (75.4 MHz,  $\text{CDCl}_3$ ,  $\delta$ , ppm) 125, 122.2, 122, 110.5, 36.6 (Even after 50,000 scans only five carbon signals appeared); HRMS  $m/z$   $[\text{M}]^+$  calcd for  $\text{C}_{20}\text{H}_{14}\text{N}_4\text{S}$  - 342.0939, found 342.0945.

**Compound 5b:** Yellow solid (121 mg, 79%); TLC (1:4, ethyl acetate / hexane)  $R_f = 0.94$ ;  $^1\text{H}$  NMR (300 MHz,  $\text{CDCl}_3$ ,  $\delta$ , ppm) 8.77 (d,  $J = 4.77$  Hz, 2H, Ar-H), 7.65 (d,  $J = 7.23$  Hz, 2H, Ar-H), 7.50 (m, 4H, Ar-H), 4.67 (t,  $J = 7.58$  Hz, 4H, Ar-**CH**<sub>2</sub>), 1.67 (m, 4H, -**CH**<sub>2</sub>), 1.05 (m, 12H, -**CH**<sub>2</sub>), 0.70 (t,  $J = 6.9$  Hz, 6H, - **CH**<sub>3</sub>);  $^{13}\text{C}$  NMR (75.4 MHz,  $\text{CDCl}_3$ ,  $\delta$ , ppm) 149.4, 141.7, 132.6, 125.9, 124.7, 122.2, 112.6, 111.9, 48.6, 31.1, 29, 26.3, 22.3, 13.8; HRMS  $m/z$   $[\text{M}]^+$  calcd for  $\text{C}_{30}\text{H}_{34}\text{N}_4\text{S}$  - 482.2504, found 482.2509.

**Compound 5c:** Yellow solid (118 mg, 75%). TLC (1:9, ethyl acetate / hexane)  $R_f = 0.6$ ;  $^1\text{H}$  NMR (300 MHz,  $\text{CDCl}_3$ , ppm)  $\delta = 8.82$  (d,  $J = 7.71$  Hz, 2H, Ar-**H**), 7.47 (t,  $J = 7.71$  Hz, 2H, Ar-**H**), 7.37-7.28 (m, 8H, Ar-**H**), 7.17 (d,  $J = 8.22$  Hz, 3H, Ar-**H**), 6.94 (d,  $J = 6.09$  Hz, 4H, Ar-**H**), 5.43 (s, 4H, Ar-**CH**<sub>2</sub>);  $^{13}\text{C}$  NMR (75.4 MHz,  $\text{CDCl}_3$ ,  $\delta$ , ppm); 149.2, 142, 136, 132, 128.8, 127.5, 125.7, 125.2, 125.1, 122.5, 122.1, 112.4, 111.7, 51.6; HRMS  $m/z$   $[\text{M}]^+$  calcd for  $\text{C}_{32}\text{H}_{22}\text{N}_4\text{S}$  - 494.1565, found 494.1578.

### 4.3. Results and discussion

#### 4.3.1. Synthesis

Scheme 4.1 displays the synthesis route towards the newly synthesised indolocarbazole derivatives. Benzothiadiazole (**1**) was treated with 2.4 fold excess of bromine under acidic condition to give 4,7-dibromo-2,1,3-benzothiadiazole (**2**) in good yield, 87%.<sup>12</sup> Suzuki coupling of compound **2** was carried out with 2-nitrophenylboronic acid (2-NBA) to get the compound **3**. Purification of the product was accomplished by washing the crude solid with hexane to achieve quantitative yield of compound **3**. Compound **4** was obtained *via* reported procedure of reductive Cadogan ring closure reaction,<sup>13</sup> where compound **3** in 1,2-dichlorobenzene was refluxed with triethyl phosphite for 24 hours. Target molecule **4** in 51% yield was isolated after purification by column chromatography. A few derivatives of compound **4** with various *N*-alkyl chain substituents (i.e. CH<sub>3</sub>, C<sub>6</sub>H<sub>13</sub> and CH<sub>2</sub>Ph) were prepared by alkylation with corresponding alkyl halides (**5a-c**). Longer alkyl chain increased the solubility of these indolocarbazoles in common organic solvents such as ethyl acetate, chloroform, dichloromethane, THF and acetone. The synthesized compounds were characterized using <sup>1</sup>H and <sup>13</sup>C NMR and high resolution mass spectrometry.

#### 4.3.2. Single crystal XRD

Among the synthesized molecules, **5a** was analyzed by single crystal X-ray diffraction technique. A solution containing **5a** in ethyl acetate was evaporated slowly at room temperature to yield single crystals of **5a** (Figure 4.3).

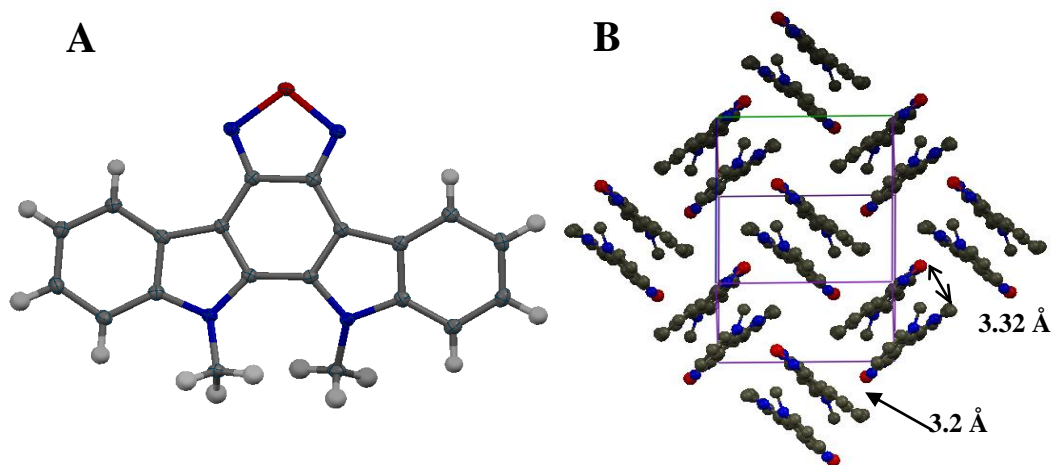


**Figure 4.3.** Thermal ellipsoid plot of **5a** (A). Packing diagram of **5a** along *a*-axis. Hydrogen atoms removed for clarity (B)

Compound **5a** exhibits sandwiched herringbone type packing with molecules existing as anti co-facial dimers with herringbone angle of  $89^\circ$ . This arrangement facilitates two-dimensional electronic transport, which is advantageous for better charge carrier mobility.<sup>14</sup> In addition; short intermolecular distance of  $3.32 \text{ \AA}$  in dimer indicates strong  $\pi$ - $\pi$  interactions. Such close contact is good as compared to the intermolecular distance ( $3.45 \text{ \AA}$ ) reported for planar indolo[3,2-*b*]carbazole derivatives.<sup>15</sup> Short N-S contact of  $3.2 \text{ \AA}$  was observed between the edge-to-face interacting **5a** molecules, leading to a close packed structure.

### 4.3.3. Optical properties

The UV-vis absorption and emission spectra of the oligomers in solution (tetrahydrofuran) are shown in Figure 4.4.

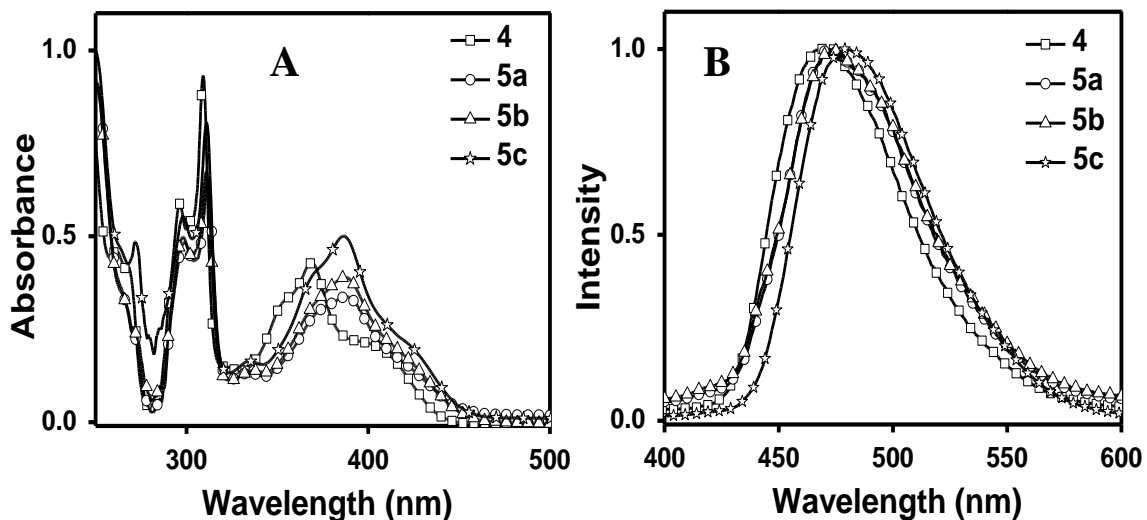


**Figure 4.4.** Normalized absorption spectra (A) and emission spectra (B) of thiadiazole fused indolocarbazole derivatives in THF

All spectra display multiple maxima in the UV region, featuring typical fused-ring systems with more defined electronic states.<sup>16</sup> The absorption maximum of alkyl-substituted derivatives (**5a-c**) is red-shifted as compared to the parent molecule **4**.

**Table 4.1.** Photophysical properties of thiadiazole fused indolocarbazoles recorded in THF

compound	$\lambda_{\text{abs}}$ (nm)	$\lambda_{\text{em}}$ (nm)	Stoke's shift (nm)	$\Phi_{\text{F}}$ (%)
<b>4</b>	368, 309, 296, 247	469	101	8
<b>5a</b>	387, 311, 298, 249	472	85	10
<b>5b</b>	387, 311, 298, 249	473	86	10
<b>5c</b>	386, 311, 298, 250	481	95	9

Leclerc *et al.* reported similar phenomena in their work on carbazole-based ladder compounds.<sup>16</sup> Emission maximum of all derivatives are in the blue-green region with  $\lambda_{\text{max}}$  centered around 475 nm. Interestingly all derivatives exhibit large Stoke's shifts which are unexpected for fused ring systems (Table 4.1). The wavelength of emission also showed a strong dependence on solvent (Figure 4.5). Such a larger Stoke's shift and solvent dependent emission indicates the effective intramolecular charge transfer (ICT) in the excited state between thiadiazole unit and indolocarbazole unit.<sup>17</sup> It is observed that the substituents on the N-atom have marginal effect on the optical properties of these compounds. The fluorescense quantum yield of heteroacenes are recorded in THF with quinine sulfate in 0.1 M H<sub>2</sub>SO<sub>4</sub> as standard.

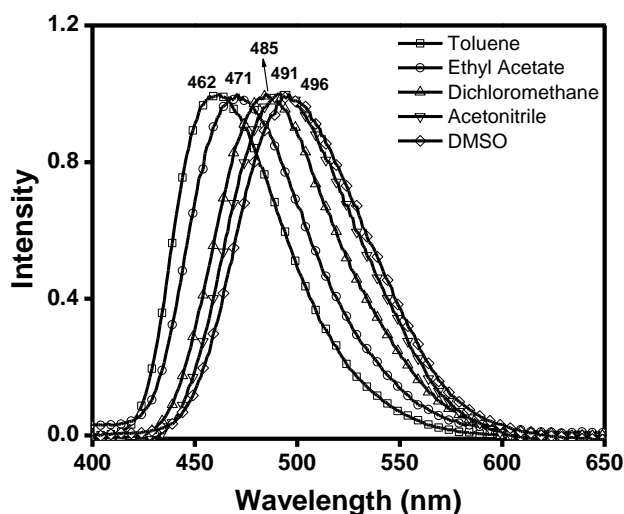


**Figure 4.5.** Emission spectra of compound **4** in various solvents

The fluorescence quantum yields ( $\Phi_F$ ) of all the compounds are relatively low. Such low  $\Phi_F$  values relative to indolo[3,2-*b*]carbazole may be due to an increase in the non-radiative intersystem crossing caused by the heavy atom (sulfur). The optical band gap estimated from the onset of UV-vis absorption for these derivatives are within the



range of ca. 2.7 - 2.8 eV. Some of the reported indolo[3,2-*b*]carbazole-based molecules show optical band gap between ca. 2.86 - 2.95 eV.<sup>18</sup>

#### 4.3.4. Electrochemical properties

Cyclic voltammetry (CV) was performed to investigate the redox properties of the new ladder molecules in dry dichloromethane (Figure 4.6). Oxidation peaks of **4**, **5a**, **5b** and **5c** were found to be 1.25, 1.3, 1.34 and 1.35 V (Table 4.2).

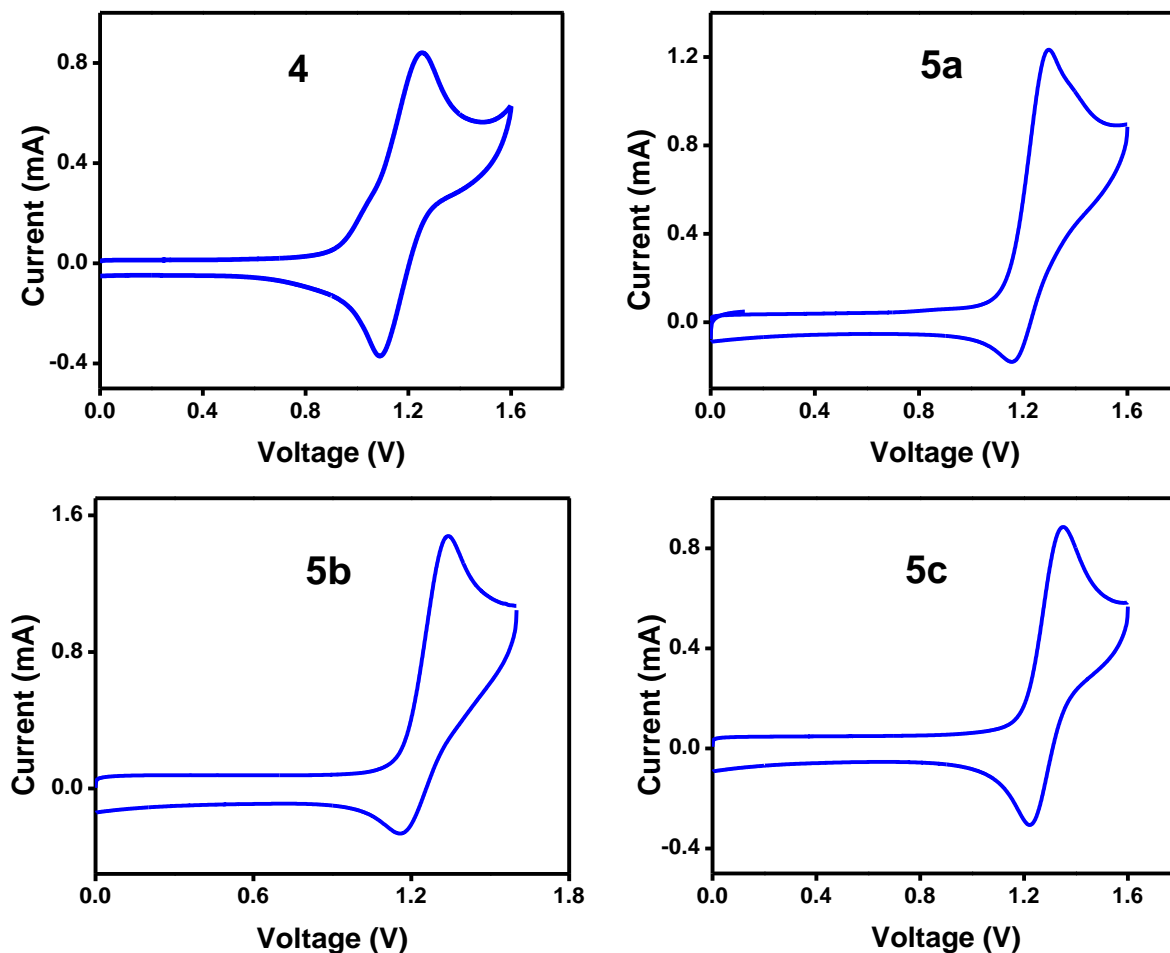
**Table 4.2.** Electrochemical properties of thiadiazole fused indolocarbazoles derivatives recorded using cyclic voltammetry

compound	$E_{\text{oxid}}^{\text{a}}$ (V)	HOMO <sup>b</sup> (eV)	$E_{\text{g}}^{\text{c}}$ (eV)	LUMO <sup>d</sup> (eV)
4	1.25	-5.39	2.8	-2.59
5a	1.3	-5.49	2.75	-2.74
5b	1.34	-5.33	2.74	-2.79
5c	1.35	-5.57	2.72	-2.85
poly4	-	-5.29	2.4	-3.14 <sup>e</sup>

<sup>a</sup>versus Ag/AgCl electrode in 0.1 M Bu<sub>4</sub>NPF<sub>6</sub> in acetonitrile, Pt as working electrode under the scan rate of 100 mVs<sup>-1</sup>. <sup>b</sup>Calculated using the relationship  $E_{\text{HOMO}} = -(E_{\text{oxi}}^{\text{onset}} + 4.38)$ . <sup>c</sup>Optical band gaps estimated from the onset position of absorption spectra. <sup>d</sup>Derived from optical band gap and HOMO. <sup>e</sup>Derived from reduction onset from cyclic voltammetry.

All alkyl substituted derivatives showed higher oxidation potential than the parent compound **4**. HOMO energy levels of ladder compounds are estimated by the oxidation onset using the relationship  $E_{\text{HOMO}} = -(E_{\text{onset}}^{\text{ox}} + 4.38)$  eV.<sup>19</sup> HOMO levels of -5.39, -5.49, -5.53, and -5.57 below vacuum level were estimated for the compounds **4**, **5a**, **5b** and **5c**,

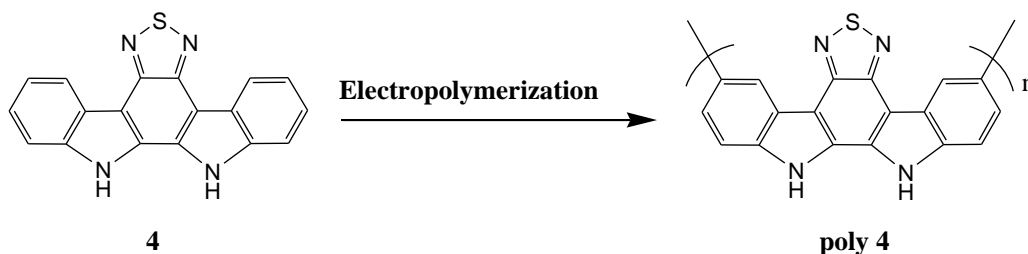
respectively. It can be noted that the synthesized compounds have low lying HOMO as compared to pentacene ( $E_{\text{HOMO}} = -4.6 \text{ eV}$ )<sup>20</sup> and indolo[3,2-*b*]carbazoles ( $E_{\text{HOMO}} = -5.12 \text{ eV}$ ).<sup>4c</sup>



**Figure 4.6.** Cyclic voltammogram of thiadiazole-fused indolocarbazole based acenes

#### 4.3.5. Electropolymerization

Electropolymerizations of compound **4** was carried out in acetonitrile containing 0.1M TBAPF<sub>6</sub> as supporting electrolyte at a scan rate of 100 mV/s. Polymer was formed synthesized electrochemically (Scheme 4.2) by repetitive scanning of anodic potential in the range of 0.2 V to 1.5 V. Indium tin oxide (ITO) was used as working electrode and Ag/AgCl as reference electrode (Figure 4.7A).

**Scheme 4.2.** Synthesis of thiadiazole incorporated indolocarbazole polymer

The growth of polymer is indicated by gradual increase of current during the potential cycles (Figure 4.7B). Polymerization occurred smoothly and resulted in yellow-brown colored, uniform deposits of polymer on the working electrode. Electrodeposited polymers showed a homogenous coating and strong adhesion to the electrode. The deposited polymer film was dedoped electrochemically, washed with acetonitrile to remove monomer and supporting electrolyte. The resulted polymer film was highly stable under normal conditions. To best of our knowledge, compound **4** is the first indolocarbazole-based material that undergoes electropolymerization.

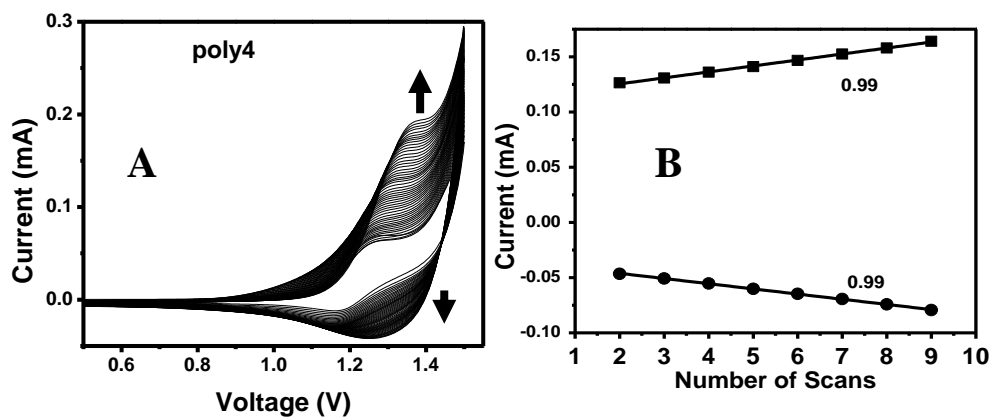


**Figure 4.7.** Electro polymerization of **4** from acetonitrile solution at a scan rate of 100 mV/S (A). Linear relationship of increase in current with number scans (B)

The resulted polymer was insoluble in most of the common solvents such as THF, DMF, DMSO, and  $\text{CHCl}_3$ . Poor solubility of this polymer hindered the structural characterization by NMR and molecular weight determination; therefore, the electrodeposited polymer was removed from ITO electrode surface and analyzed using infrared spectroscopy (IR) (Figure 4.8A). The IR spectrum (KBr disc) of the polymers showed a strong peak at  $3433\text{ cm}^{-1}$  corresponding to N-H stretching vibration. The other peaks at  $2915\text{ cm}^{-1}$  and  $1630\text{ cm}^{-1}$  corresponds to aromatic C-H stretching and aromatic C=C stretching respectively. The appearance of the new peak at  $848\text{ cm}^{-1}$  corresponds to the C-H out-of-plane bending vibrations of 1,2,3,4-substituted aromatic units. The possible structure of the polymer is represented in Scheme 4.2.

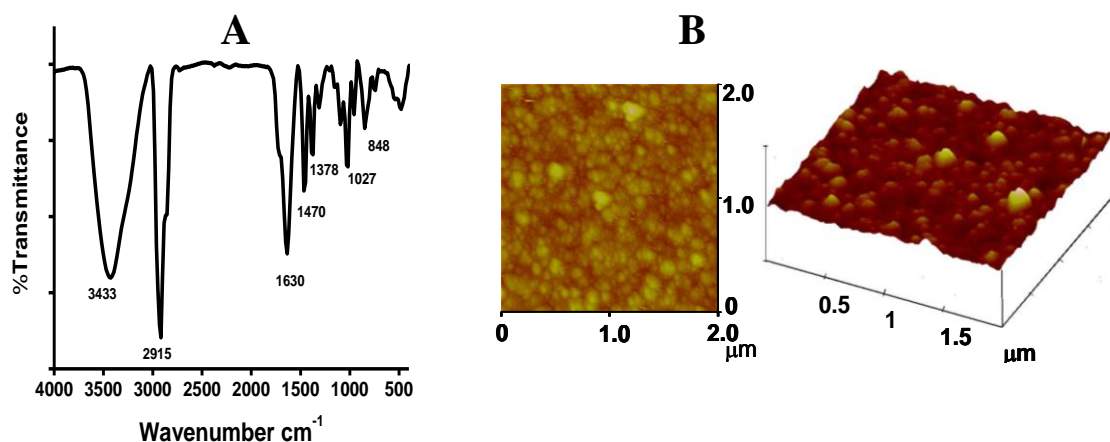


**Figure 4.8.** IR spectrum (A) and AFM image of (B) of electrodeposited polymers

The surface morphology of the **poly 4** was studied using atomic force microscopy (AFM). The experiment was performed at room temperature using a commercial AFM Nanoscope IV (Dimension 3100, Digital Instruments) in the tapping mode. The results showed uniform deposition of polymer over ITO surface (Figure 4.8B).

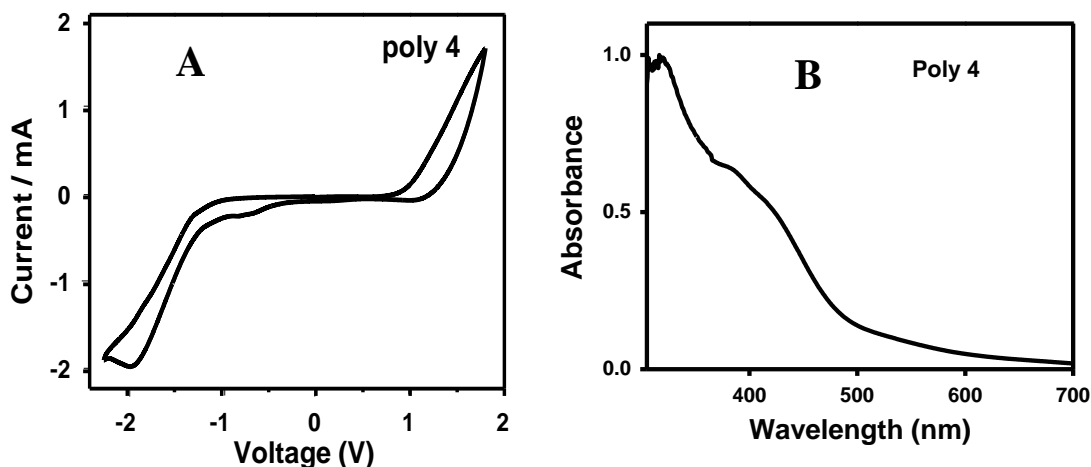


**Figure 4.9.** Cyclic voltamogram of polymer in monomer free acetonitrile with TBAPF<sub>6</sub> as supporting electrolyte (A). Solid state absorption spectra of electropolymerized polymer film (B)

Figure 4.9A represents the CV of the polymers deposited on ITO electrode recorded from monomer free acetonitrile solution. The polymer showed two broad reversible oxidation peaks with the oxidation potentials at 0.5 V and 0.85 V. The absorption spectrum of the polymer film was also recorded (Figure 4.9B). The UV-vis spectra showed a broad absorption peak characteristic of polymeric system with an optical band gap of 2.4 eV. The lower oxidation potential of polymers compared to monomer **4** (1.25 V) and reduction in band gap are consistent with extension of  $\pi$ -conjugation in polymer. The electrochemical properties of the polymer are also summarized in Table 4.2.

#### 4.4. Conclusion

Benzothiadiazole incorporated indolocarbazole derivatives are synthesized in three steps by utilizing Cadagon reduction as key step. The synthesized molecules are stable and soluble in common organic solvents. Single crystal X-ray diffraction study

showed a sandwiched herringbone arrangement for **5a**, which is advantageous for charge transport. Benzothiadiazole fusion leads to a close packing of indolocarbazole systems in the crystal lattice. It is observed that the solubility of these molecules can be tuned without affecting their opto-electronic properties. BTD fusion decreases both HOMO and LUMO energy levels of the system. The decrease in HOMO energy leads to the oxidative stability, therefore the strategy of BTD fusion can be utilized to stabilize unstable fused ring systems. The unsubstituted compound was electropolymerized to give the first electropolymerized poly-indolocarbazole. Due to their rigid structure, close packing (in crystalline state) and high stability these materials are potential candidate for OFET application.

## 4.5. References

---

- (1) (a) Barbarella, G.; Favaretto, L.; Zanelli, A.; Gigli, G.; Mazzeo, M.; Anni, M.; Bongini, A. *Adv. Funct. Mater.* **2005**, *15*, 664. (b) Oliveira, M. A. D.; Duarte, H.; Pernaut, J.; Almeida, W. B. D. *J. Phys. Chem. A* **2000**, *104*, 8256. (c) Parakka, J. P.; Jeevarajan, J. A.; Jeevarajan, A. S.; Kispert, L. D.; Cava, M. P. *Adv. Mater.* **1996**, *8*, 54.
- (2) (a) Yasuda, T.; Fujita, K.; Tsutsui, T. *Chem. Mater.* **2005**, *17*, 264. (b) Belletete, M.; Beaupre, S.; Bouchard, J.; Blondin, P.; Leclerc, M.; *J. Phys. Chem. B* **2000**, *104*, 9118.
- (3) (a) Afzali, A.; Dimitrakopoulos, C. D.; Breen, T. L. *J. Am. Chem. Soc.* **2002**, *124*, 8812. (b) Pisula, W.; Menon, A.; Stepputat, M.; Lieberwirth, I.; Kolb, U.; Tracz, A.; Sirringhaus, H.; Pakula, T.; Müllen, K. *Adv. Mater.* **2005**, *17*, 684.
- (4) (a) Sun, Y.; Liu, Y.; Ma, Y.; Di, C.; Wang, Y.; Wu, W.; Yu, G.; Hu, W.; Zhu, D. *Appl. Phys. Lett.* **2006**, *88*, 242113. (b) Sun, Y.; Ma, Y.; Liu, Y.; Lin, Y.; Wang, Z.; Wang, Y.; Di, C.; Xiao, K.; Chen, X.; Qiu, W.; Zhang, B.; Yu, G.; Hu, W.; Zhu, D. *Adv. Funct. Mater.* **2006**, *16*, 426. (c) Wu, Y.; Li, Y.; Gardner, S.; Ong, B. S. *J. Am. Chem. Soc.* **2005**, *127*, 614.
- (5) Janosik, T.; Wahlstrom, N.; Bergman, J.; *Tetrahedron* **2008**, *64*, 9159.
- (6) (a) Anthony, J. E. *Chem. Rev.* **2006**, *106*, 5028. (b) Boudreault, P. L. T.; Wakim, S.; Blouin, N.; Simard, M.; Tessier, C.; Tao, Y.; Leclerc, M. *J. Am. Chem. Soc.* **2007**, *129*, 9125. (c) Qi, T.; Guo, Y.; Liu, Y.; Xi, H.; Zhang, H.; Gao, X.; Liu, Y.; Lu, K.; Ku, C.; Yu, G.; Zhu, D. *Chem. Commun.* **2008**, 6227.
- (7) (a) Li, U.; Ong, B. S.; Wu, Y.; Liu, P. (Xerox Corporation, USA). Application: US 2007/0112167 A1, 2007. (b) Li, U.; Ong, B. S.; Wu, Y.; Liu, P. (Xerox Corporation, USA). Application: US 2007/0112172 A1, 2007.
- (8) (a) Kase, H.; Iwahashi, K.; Matsuda, Y. *J. Antibiot.* **1986**, *39*, 1059. (b) Kase, H.; Iwahashi, K.; Nakanishi, S.; Matuda, Y.; Yamada, K.; Takahashi, M.; Murakata, C.; Sato, A.; Kaneko, M. *Biochem. Biophys. Res. Commun.* **1987**, *142*, 436.
- (9) (a) Sezaki, M.; Sasaki, T.; Nakazawa, T.; Takeda, U.; Iwata, M.; Watanabe, T. *J. Antibiot.* **1985**, *38*, 1437. (b) Yasuzawa, T.; Iida, T.; Yoshida, M.; irayama, N.; Takahashi, M.; Shirahata, K.; Sano, H. *J. Antibiot.* **1986**, *39*, 1072.
- (10) Rannug, U.; Rannug, A.; Sjöberg, U.; Li, H.; Westerholm, R.; Bergman, J. *Chem. Biol.* **1995**, *2*, 841.

- 
- (11) (a) Curiel, D.; Cowley, A.; Beer, P. D. *Chem. Commun.* **2005**, 2, 236. (b) Wang, T.; Bai, Y.; Ma, L.; Yan, X.-P. *Org. Biomol. Chem.* **2008**, 6, 1751.
- (12) Mancilha, F. S.; Neto, B. A. D.; Lopes, A. S.; Moreira Jr. P. F.; Quina, F. H.; Goncalves, R. S.; Dupont, J. *Eur. J. Org. Chem.* **2006**, 4924.
- (13) Bouchard, J.; Wakim, S.; Leclerc, M. *J. Org. Chem.* **2004**, 69, 5705.
- (14) Ebata, H.; Miyazaki, E.; Yamamoto, T.; Takimiya, K. *Org. Lett.* **2007**, 9, 4499.
- (15) (a) Wakim, S.; Bouchard, J.; Simard, M.; Drolet, N.; Tao, Y.; Leclerc, M. *Chem. Mater.* **2004**, 16, 4386. (b) Liu, H.; Tao, X.; Yang, J.; Yan, Y.; Ren, Y.; Zhao, H.; Xin, Q.; Yu, W.; Jiang, M. *Crystal Growth & Design* **2008**, 8, 259.
- (16) (a) Belletete, M.; Blouin, N.; Boudreault, P. T.; Leclerc, M.; Durocher, G.; *J. Phys. Chem. A* **2006**, 110, 13696. (b) Belletete, M.; Wakim, S.; Leclerc, M.; Durocher, G. *J. Mol. Struct.: THEOCHEM* **2006**, 760, 147.
- (17) Neto, B. A. D.; Lopes, A. S. A.; Ebeling, G.; Goncalves, R. S.; Costa, V. E. U.; Quina, F. H.; Dupont, J. *Tetrahedron* **2005**, 61, 10975.
- (18) Kawaguchi, K.; Nakano, K.; Nozaki, K. *J. Org. Chem.* **2007**, 72, 5119.
- (19) (a) Li, Y.; Ding, J.; Day, M.; Tao, Y.; Lu, J.; D'iorio, M. *Chem. Mater.* **2004**, 16, 2165. (b) Leeuw, D. M.; Simenon, M. M. J.; Brown, A. R.; Einerhand, R. E. F. *Synth. Met.* **1997**, 87, 53. (c) Cui, Y.; Zhang, X.; Jenkhe, S. A. *Macromolecules* **1999**, 32, 3824.
- (20) Meng, H.; Bendikov, M.; Mitchell, G.; Helgeson, R.; Wudl, F.; Bao, Z.; Siegrist, T.; Kloc, C.; Chen, C. *Adv. Mater.* **2003**, 15, 1090.



## *Chapter 5*

# *Synthesis and Hole-transporting Properties of Highly Fluorescent N-Aryl Dithieno[3,2-b:2',3'-d]pyrrole Based Oligomers*

### *Publication from the chapter:*

1. **Balaji, G.**; Parameswaran, M.; Jin, T. M.; Vijila, C.; Furong, Z.; Valiyaveettil, S. “*Synthesis and Hole-transporting Properties of Highly Fluorescent N-aryl Dithieno[3,2-b:2',3'-d]pyrrole Based Oligomers*”. *J. Phys. Chem. C*. **2010**, *114*, 4628.
2. Parameswaran, M.; **Balaji, G.**; Jin, T. M.; Vijila, C.; Vadukumpully, S.; Furong, Z.; Valiyaveettil, S. “*Charge Transport Studies in Fluorene - Dithieno[3,2-b:2',3'-d]pyrrole Oligomer using Time-of-Flight Photoconductivity Method*”, *Org. Electron.*, **2009**, *10*, 1534-1540.

## 5.1. Introduction

Organic materials in electronic applications overcome many of the drawbacks of silicon technology such as expensive fabrication, difficulty in tuning the properties and processability.<sup>1</sup> Generally, organic  $\pi$ -conjugated low molecular weight oligomers or highly defined polymers are used for such applications.<sup>2</sup> The advantage of oligomeric systems over the polymeric counterpart is their well defined structures, high purity and high processability. Oligomers are processable by either vacuum sublimation or solution casting.<sup>3</sup> Among the  $\pi$ -conjugated materials, oligo and polythiophenes are used in many of the optoelectronic applications such as organic light emitting diodes (OLEDs),<sup>4</sup> organic field effect transistors (OFETs),<sup>5</sup> and organic photovoltaics (OPVs).<sup>6</sup>

Fused thiophene systems like dithienothiophene,<sup>7</sup> cyclopentadithiophene<sup>8</sup> and dithienopyrrole<sup>9</sup> are interesting due to their fused nature, enhanced  $\pi$ -conjugation<sup>10</sup> and hence used in various applications.<sup>11</sup> Dithieno[3,2-*b*]pyrrole contains a pyrrole fused planar tricyclic system, similar to carbazole. It is known that such molecules offer better electron donating properties than carbazole due to their lower ionization potential.<sup>12</sup> Dithieno[3,2-*b*]pyrrole based copolymers with acceptor units leads to low band gap materials, which are realized in OPV<sup>13</sup> and OFET<sup>14</sup> applications.

Unfunctionalized and *N*-functionalized dithieno[3,2-*b*]pyrrole molecule showed a very low quantum yield of ~0.008% and 0.1% respectively, which is attributed to the spin-orbit coupling due to the heavy atom effect of sulfur on the thiophene ring.<sup>15</sup> Therefore dithieno[3,2-*b*]pyrrole molecules with higher quantum yield, and better transport property is crucial for its extensive material applications. Rasmussen and co-workers reported a high solution state quantum yield, up to 65% for dithieno[3,2-*b*]pyrrole

based oligomers.<sup>16</sup> Dithieno[3,2-*b*]pyrrole based copolymers also showed a high quantum yield in solution as well as in solid state.<sup>17</sup> In order to develop a better dithieno[3,2-*b*]pyrrole based fluorophore *N*-aryl dithieno[3,2-*b*]pyrrole is an interesting building block than *N*-alkyl dithieno[3,2-*b*]pyrrole, as the high frequency mode of relaxation which could promote the internal conversion in alkyl analogue is absent in *N*-aryl dithieno[3,2-*b*]pyrrole.

In this regard, we synthesized dithieno[3,2-*b*]pyrrole based oligomers with high quantum yield and studied their charge carrier mobility in detail. Four new oligomers were synthesized with dithieno[3,2-*b*]pyrrole core incorporated with fluorene (DTP-FLU), triarylamine (DTP-TPA), benzene (DTP-PHE) and carbazole (DTP-CAR) groups. Their photophysical, electrochemical, surface morphology and transport properties along with single crystal X-ray studies (of **DTP-TPA**) are presented. Molecular structures of the synthesized molecules are shown in Figure 5.1.

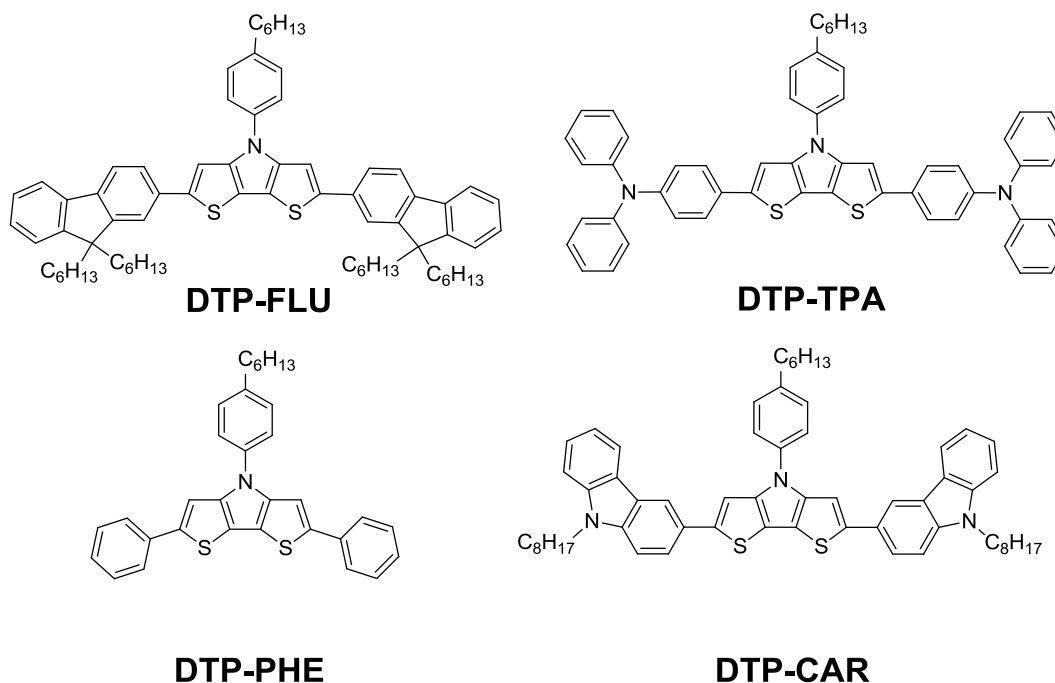


**Figure 5.1.** Molecular structures of synthesized DTP-oligomers

## 5.2. Experimental

### 5.2.1. Materials

All reactions were carried out under inert atmosphere ( $N_2$  or Ar), unless specified otherwise. All reagents were purchased from Aldrich, Fluka or Merck and used without further purification unless otherwise stated. All reactions were carried out with freshly distilled anhydrous solvents under inert atmosphere. Tetrahydrofuran (THF) was purified via distillation over sodium under nitrogen atmosphere. 2-2'-Bithiophene, *N*-bromosuccinimide (NBS), 2-bromofluorene, carbazole, benzene boronic acid, 4-(*N,N*-diphenylamino)phenyl boronic acid were purchased from Aldrich. NBS was recrystallized from hot water. *N*-(4-Hexylphenyl)-2,6-dibromodithieno[3,2-*b*;2',3'-*d*]pyrrole was prepared following the literature procedure.<sup>18</sup>

### 5.2.2. Spectroscopic characterization

$^1H$  (300 MHz) and  $^{13}C$  (75.4 MHz) NMR spectra were recorded on a Bruker AMX 300 spectrometer. Mass spectra were acquired by Micromass VG7035 double focusing mass spectrometer of high resolution. Single-crystal X-ray diffraction measurement was conducted on Bruker-AXS Smart Apex CCD single-crystal diffractometers. Unit dimensions were acquired with least-square refinements and all structures were solved by SHELXL-97. The UV-vis spectra were measured on Shimadzu UV-1601 PC spectrophotometer and fluorescence measurements were carried out on RF-5301PC Shimadzu spectrofluorophotometer. Solution state photoluminescence quantum yields were recorded using quinine sulfate (0.1 M  $H_2SO_4$ ) as standard.<sup>19</sup> The solid-state quantum yield was determined using an integrating sphere (Lab Sphere Com) with He-Cd laser (325 nm; 11 mW) as an excitation source. The surface morphology was studied

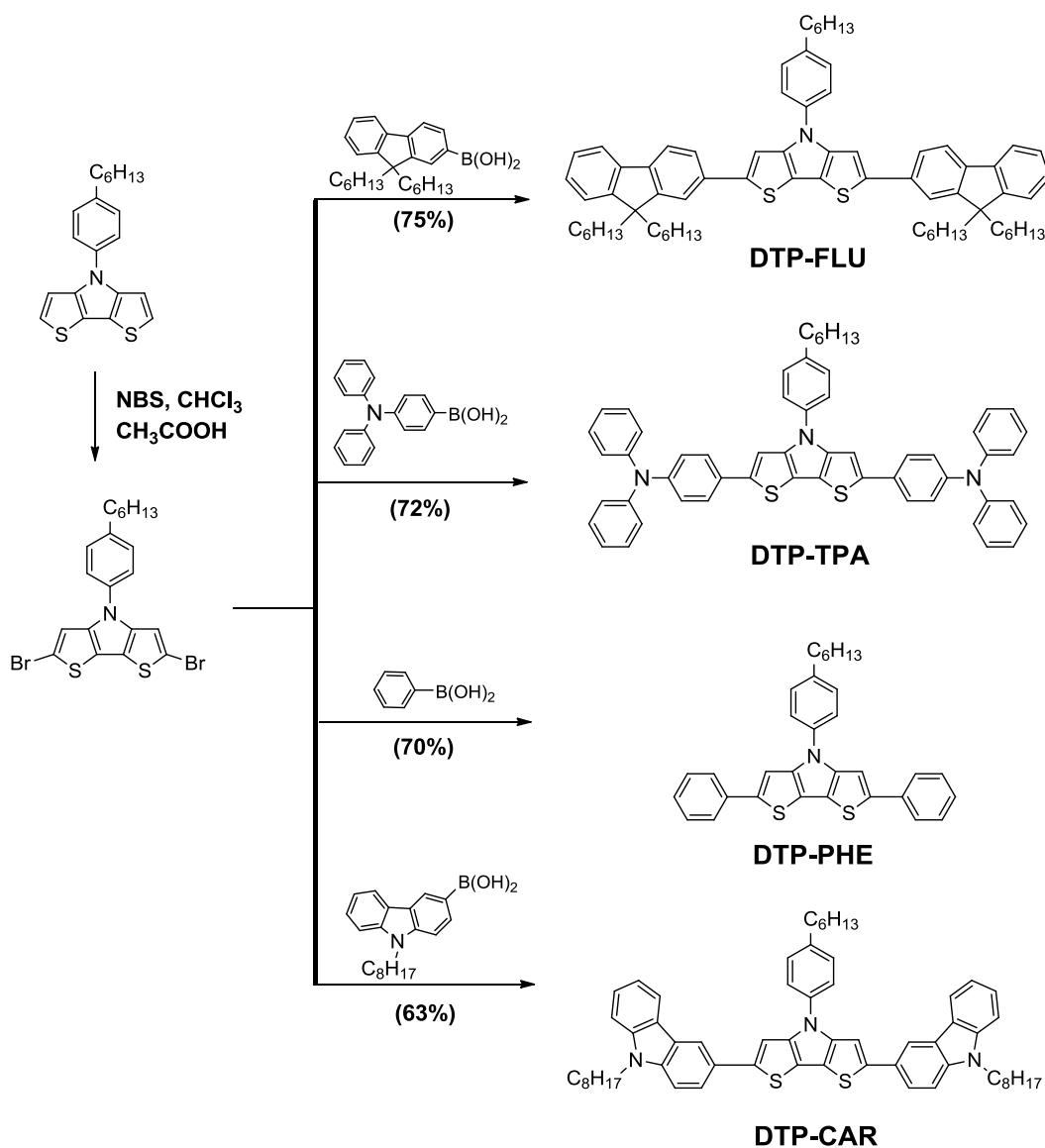
using atomic force microscopy (AFM) in tapping mode. The experiment was performed at room temperature using a commercial AFM Nanoscope IV (Dimension 3100, Digital Instruments). The electrochemical behavior of the oligomers was investigated with cyclic voltammetry (CV). The cyclic voltammograms were recorded with a computer controlled CHI Electrochemical Analyzer/Workstation CHI 600C at a constant scan rate of 100 mV/s. Measurements were performed in an electrolyte solution of 0.1 M tetrabutylammoniumhexafluorophosphate ( $n\text{Bu}_4\text{NPF}_6$ ) dissolved in degassed dichloromethane. An undivided three electrode configuration cell was used with Pt wire as working and counter electrode, and Ag/AgCl as the reference electrode. The potentials are calibrated with ferrocene/ferrocenium redox couple (0.47 V). Onset value of the oxidation wave ( $E_{\text{ox}}^{\text{onset}}$ ) was used to calculate HOMO energy level, using the relation  $E_{\text{HOMO}} = -(4.38 + E_{\text{ox}}^{\text{onset}})$ . LUMO levels were calculated from  $E_{\text{HOMO}}$  and optical band gaps ( $E_g$ ).

The mobilities of charge carriers were measured by using time-of-flight photoconductivity technique. The system was composed of a pulsed nitrogen ( $\text{N}_2$ ) laser (Oriol 79074), a pulse generator (SRS-DG535), a DC voltage source (Kenwood PWR18-2), and a digital oscilloscope (Agilent-Infiniium, 1 GHz, 4 Gsa/s). The  $\text{N}_2$  laser with pulse width  $< 4$  ns, and pulse repetition rate 1 Hz, was illuminated on the ITO side of the device. The photocurrent under the influence of applied electric field was monitored across a variable resistor using an oscilloscope. It was ensured that the time constant of the setup is less than the transit time ( $RC < t_{\text{tr}}$ ). The active area of the device was  $4 \text{ mm}^2$ . The sample was mounted in a temperature controlled continuous flow cryostat under vacuum of  $\sim 10^{-5}$  mbar for temperature dependant measurements. The charge mobilities

were calculated using the relation  $\mu = d^2/Vt_T$ , where  $d$  is the thickness of the film,  $V$  is the applied voltage and  $t_T$  is the transit time. The transit time was obtained either from the inflection points in a double logarithmic plot of photocurrent *versus* time or by the integration method.<sup>20</sup>

### 5.2.3. Synthesis procedure

**Scheme 5.1.** Synthesis of DTP oligomers



**Synthesis of *N*-(4-hexylphenyl)-dithieno[3,2-*b*:2',3'-*d*]pyrrole (DTP):**<sup>18</sup> To a 250 ml round-bottom flask, which was evacuated and back-filled with nitrogen, was added toluene (40 ml), Pd<sub>2</sub>(dba)<sub>3</sub> (887 mg, 1.54 mmol) and P(<sup>t</sup>Bu)<sub>3</sub>HBF<sub>4</sub> (448 mg, 1.54 mmol). After 10 minutes 3,3'-dibromo-2,2'-bithiophene (2.5g, 7.72 mmol), NaO<sup>t</sup>Bu (2.23 g, 23.15 mmol) and 4-hexylaniline (1.92 g, 10.08 mmol) was added consecutively. Reaction mixture was allowed to stir at reflux for 5 hours. After completion of reaction (monitored by TLC), reaction mixture was allowed to cool, extracted with ethyl acetate and washed with water (3 × 100 ml). Organic layer was dried with anhydrous sodium sulfate and concentrated at rotary evaporator. The crude product was finally purified by column chromatography to give DTP as pale orange solid (1.7 g, 65%). <sup>1</sup>H NMR (300 MHz, CDCl<sub>3</sub>, δ, ppm) 7.49 (d, J = 8.22 Hz, 2H, Ph-**H**), 7.32 (d, J = 8.22 Hz, 2H, Ph-**H**), 7.16 (s, 4H, Th-H), 2.68(t, J = 7.73 Hz, 2H, Ar-**CH**<sub>2</sub>), 1.67 (m, 2H, **CH**<sub>2</sub>), 1.35 (m, 6H, **CH**<sub>2</sub>), 0.91(t, J = 6.57, **CH**<sub>3</sub>); <sup>13</sup>C NMR (75.4 MHz, CDCl<sub>3</sub>, δ, ppm) 144.3, 141.2, 137.8, 129.9, 123.6, 122.8, 116.9, 112.6, 35.8, 32.1, 31.8, 29.4, 23, 14.5; HRMS *m/z* [M]<sup>+</sup> calcd for C<sub>20</sub>H<sub>21</sub>NS<sub>2</sub> 339.115, found 339.1113.

**Synthesis of 2,6-dibromo-*N*-(4-hexylphenyl)-dithieno[3,2-*b*:2',3'-*d*]pyrrole:**<sup>18</sup> To a 250 ml round-bottom flask DTP, glacial acetic acid and CHCl<sub>3</sub> were added. Reaction mixture was stirred 4°C for 5-10 minutes. *N*-Bromosuccinimide (2.5 eq.) was added in portions over 2 minutes. Reaction mixture was stirred at 4° C for 1.5 hours, and subsequently at room temperature for ½ hr. Reaction mixture was extracted with CHCl<sub>3</sub>/water twice and washed with saturated NaHCO<sub>3</sub> solution. The collected organic layer was dried over anhydrous sodium sulfate. The solvent was removed under reduced pressure and the crude product was purified by column chromatography to give 2,6-

dibromo-*N*-(4-hexylphenyl)-dithieno[3,2-*b*:2',3'-*d*]pyrrole (yield = 77 %).  $^1\text{H}$  NMR (300 MHz,  $\text{CDCl}_3$ ,  $\delta$ , ppm) 7.38 (d,  $J = 8.55$  Hz, 2H, Ph-**H**), 7.31 (d,  $J = 8.52$  Hz, 2H, Ph-**H**), 7.15 (s, 2H, Th-**H**), 2.67(t,  $J = 7.7$  Hz, 2H, Ar-**CH<sub>2</sub>**), 1.64 (m, 2H, **CH<sub>2</sub>**), 1.35 (m, 6H, **CH<sub>2</sub>**), 0.91(t,  $J = 6.57$ , **CH<sub>3</sub>**);  $^{13}\text{C}$  NMR (75.4 MHz,  $\text{CDCl}_3$ ,  $\delta$ , ppm) 141.9, 140.9, 136.5, 129.9, 127.4, 122.8, 115.4, 110.3, 35.5, 31.7, 31.4, 29, 22.6, 14.1; HRMS  $m/z$  [ $\text{M}$ ] $^+$  calcd for  $\text{C}_{20}\text{H}_{19}\text{NBr}_2\text{S}_2$  496.9305, found 494.9324.

**Representative synthesis of DTP oligomers:** 2,6-Dibromo-*N*-(4-hexylphenyl)-dithieno[3,2-*b*:2',3'-*d*]pyrrole (2 mmol) and corresponding monoboronic acid (4.2 mmol) were dissolved in 40 mL of dry THF under  $\text{N}_2$ . To this solution  $\text{K}_2\text{CO}_3$ (aq) (2 M, 30 mL;  $\text{N}_2$  bubbled before use) and  $\text{Pd}(\text{PPh}_3)_4$  (0.2 mmol) were added. After stirring for 6 hours at 80 °C, the reaction mixture was cooled and extracted with ethyl acetate. The combined organic layer was dried with anhydrous sodium sulfate, concentrated under reduced pressure, and purified by column using 99:1 hexane - ethyl acetate mixture as eluent.

**2,6-Bis[2-(9,9-dihexyl-9*H*-fluorene)]-*N*-(4-hexylphenyl)-dithieno[3,2-*b*:2',3'-*d*]pyrrole (DTP-FLU):** Yellow green solid (75 %).  $^1\text{H}$  NMR (300 MHz,  $\text{CDCl}_3$ ,  $\delta$ , ppm) 7.71-7.5 (m, 10H, Ar-**H**); 7.44-7.3 (b, 10H, Ar-**H**); 2.75 (t, 7.71 Hz, 2H, Ar-**CH<sub>2</sub>**), 2 (t, 7.4 Hz, 8H, Ar-**CH<sub>2</sub>**), 1.73 (m, 2H, **CH<sub>2</sub>**), 1.38 (m, 6H, **CH<sub>2</sub>**), 1.06 (b, 32H, **CH<sub>2</sub>**), 0.763 (b, 15H, **CH<sub>3</sub>**).  $^{13}\text{C}$  NMR (75.4 MHz,  $\text{CDCl}_3$ ,  $\delta$ , ppm) 151.6, 150.9, 144.4, 144.3, 141.4, 140.7, 140.6, 137.4, 134.3, 129.8, 127, 126.8, 124.3, 123.2, 122.9, 120.1, 119.7, 119.6, 116.1, 1.7.8, 55.2, 40.4, 35.7, 31.7, 31.5, 29.7, 29.1, 23.7, 22.6, 22.6, 14.1, 14; FAB-MS:  $m/z$  1003 ( $\text{M}^+$ ). Anal. Calcd for  $\text{C}_{70}\text{H}_{85}\text{NS}_2$ : C, 83.69; H, 8.53; N, 1.39; S, 6.38. Found: C, 83.74; H, 8.74; N, 1.34; S, 6.33.

**2,6-Bis[4-(*N,N*-diphenylamino)phenyl]-*N*-(4-hexylphenyl)dithieno[3,2-*b*:2',3'-*d*]pyrrole**



**(DTP-TPA):** Yellow solid (72 %).  $^1\text{H}$  NMR (300 MHz,  $\text{CDCl}_3$ ,  $\delta$ , ppm) 7.52 (d, 8.04 Hz, 3H, Ar-H), 7.35 (b, 9H, Ar-H), 7.25 (b, 4H, Ar-H), 7.14-7.05 (b, 18H, Ar-H), 2.7 (t, 7.56 Hz, 7.89 Hz, 2H, Ar- $\text{CH}_2$ ), 1.69 (m, 2H,  $\text{CH}_2$ ), 1.35 (m, 6H,  $\text{CH}_2$ ), 0.93 (t, 3H,  $\text{CH}_3$ );  $^{13}\text{C}$  NMR (75.4 MHz,  $\text{CDCl}_3$ ,  $\delta$ , ppm) 147.7, 147.5, 146.7, 141.2, 137.3, 129.7, 129.3, 128.7, 127.7, 127.3, 126.6, 124.9, 124.4, 124.3, 124.1, 123.9, 123, 122.8, 35.5, 31.7, 31.7, 31.5, 29.1, 22.6, 14.1; FAB-MS;  $m/z$  825 ( $\text{M}^+$ ) Anal. Calcd for  $\text{C}_{56}\text{H}_{47}\text{N}_3\text{S}_2\cdot\text{C}_4\text{H}_8\text{O}_2$ : C, 78.83; H, 6.06; N, 4.6; O, 3.5; S, 7.01. Found: C, 78.67; H, 6.85; N, 4.2; O, 3.52; S, 7.14.

**2,6-Diphenyl-*N*-(4-hexylphenyl)-dithieno[3,2-*b*:2',3'-*d*]pyrrole (DTP-PHE):** Yellow solid (70 %).  $^1\text{H}$  NMR (300 MHz,  $\text{CDCl}_3$ ,  $\delta$ , ppm) 7.89 (d,  $J = 7.89$  Hz, 4H, Ar-H), 7.54 (d,  $J = 8.37$ , 2H, Ar-H), 7.39 (m, 8H, Ar-H), 7.29 (m, 1H, Ar-H), 7.24 (m, 1H, Ar-H), 2.71 (t, 2H,  $J = 7.56$ , Ar- $\text{CH}_2$ ), 1.7 (m, 2H, - $\text{CH}_2$ ), 1.34 (m, 6H, - $\text{CH}_2$ ), 0.92 (t,  $J = 7$  Hz, 3H, - $\text{CH}_3$ );  $^{13}\text{C}$  NMR (75.4 MHz,  $\text{CDCl}_3$ ,  $\delta$ , ppm) 144.2, 142.5, 141.4, 137.2, 135.4, 129.8, 128.9, 127.3, 125.4, 122.9, 116.3, 108.2, 35.6, 31.7, 31.5, 29, 22.6, 14.1; EI-MS:  $m/z$  491 ( $\text{M}^+$ ). Anal. Calcd for  $\text{C}_{32}\text{H}_{29}\text{NS}_2$ : C, 78.16; H, 5.94; N, 2.85; S, 13.04. Found: C, 78.34; H, 6.39; N, 2.59; S, 12.74.

**2,6-Bis[3,6-(*N*-2-ethylhexylcarbazole)]-*N*-(4-hexylphenyl)dithieno[3,2-*b*:2',3'-*d*]pyrrole (DTP-CAR):** Yellow green solid (63 %).  $^1\text{H}$  NMR (300 MHz,  $\text{CDCl}_3$ ,  $\delta$ , ppm) 8.15 (d, 7.74Hz, 2H, Ar-H), 7.64 (d, 7.71Hz, 2H, Ar-H), 7.5-7.4 (m, 9H, Ar-H), 2.74 (t, 7.74 Hz, 7.71 Hz, 2H, Ar- $\text{CH}_2$ ), 2.1 (b, 2H, N- $\text{CH}_2$ ), 1.74 (m, 2H,  $\text{CH}_2$ ), 1.44-1.26 (b, 24H,  $\text{CH}_2$ ), 0.96-0.85 (b, 15H,  $\text{CH}_3$ );  $^{13}\text{C}$  NMR (75.4 MHz,  $\text{CDCl}_3$ ,  $\delta$ , ppm) 28.4, 26.4, 22.6, 22.4, 14.6, 14.2 (even after 30000 scans only a few peaks were observed). FAB-MS;  $m/z$  893 ( $\text{M}^+$ ). Anal. Calcd for  $\text{C}_{60}\text{H}_{67}\text{N}_3\text{S}_2$ : C, 80.58; H, 7.55; N, 4.7; S, 7.17. Found: C, 80.26; H, 7.75; N, 4.46; S, 7.04.

### 5.3. Result and discussion

#### 5.3.1. Synthesis

Scheme 5.1 represents synthetic route towards the target molecules. In literature, synthesis of DTP was successfully achieved by two routes. In the first route, DTP was synthesized from 3-bromothiophenes, using palladium catalyzed amination reaction followed by copper-catalyzed coupling.<sup>15</sup> In the second route, DTP is conveniently synthesized in good yields from 3,3'-dibromo-2,2'-bithiophene and alkyl/aryl amines, *via* amination reaction catalyzed by Pd<sub>2</sub>(dba)<sub>3</sub> and P(<sup>t</sup>Bu)<sub>3</sub>.<sup>18</sup> In order to incorporate different functional groups and stability of intermediates, we adopted the second strategy to synthesize the target compounds. Dibromo DTP was synthesized by brominating DTP with NBS in acetic acid-chloroform mixture. 9,9-Dihexyl-9*H*-fluorene-2-boronic acid<sup>21</sup> and *N*-(2-ethylhexyl)carbazole-2-boronic acid<sup>22</sup> were synthesized from 2-bromofluorene and carbazole, respectively by following the reported procedure. Target oligomers were synthesized in good yields (60 - 75%) by Suzuki coupling of corresponding boronic acids with dibromo DTP. All synthesized oligomers are stable and soluble in common organic solvents such as dichloromethane, chloroform, tetrahydrofuran and ethylacetate. <sup>1</sup>H NMR spectra, mass spectra, elemental analysis and X-ray single-crystal analysis confirmed the structure of oligomers.

#### 5.3.2. X-ray crystal structure

Single crystal of **DTP-TPA** suitable for single crystal X-ray diffraction were obtained as golden yellow crystals *via* slow evaporation of chloroform solution. Thermal ellipsoid plot of **DTP-TPA** is shown in Figure 5.2.

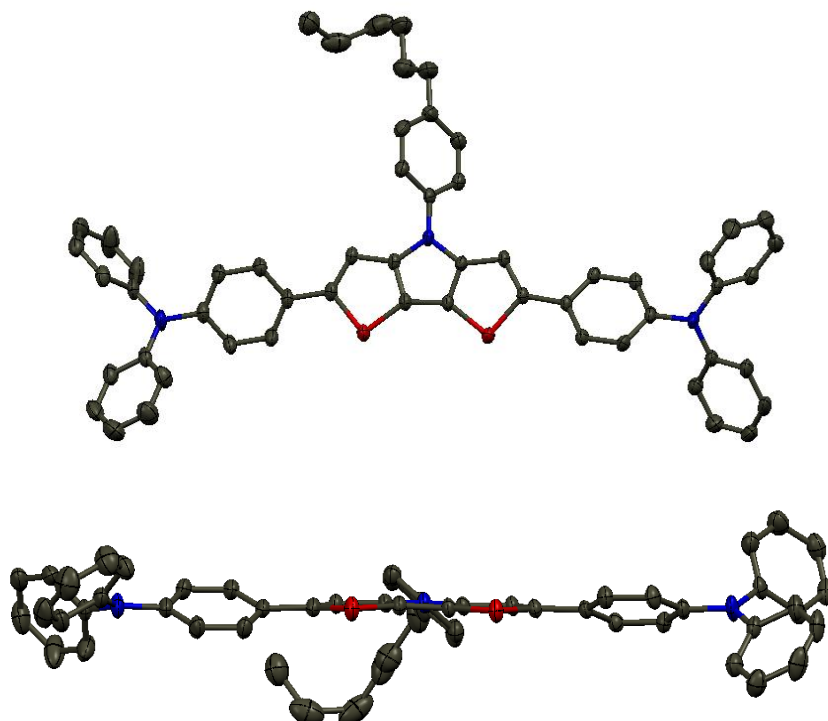


**Figure 5.2.** Thermal ellipsoid plot of **DTP-TPA**

This molecule was found to co-crystallize with ethyl acetate (workup solvent) in a triclinic lattice with unit cell parameters of  $a = 12.5499(5) \text{ \AA}$ ,  $b = 14.0994(6) \text{ \AA}$ ,  $c = 14.8676(6) \text{ \AA}$ ,  $\alpha = 88.6590(10)^\circ$ ,  $\beta = 71.1660(10)^\circ$  and  $\gamma = 80.8330(10)^\circ$ . The structures of these molecules are refined to final results of  $R1 = 0.0714$ , and goodness of fit of 1.093. It is observed that dithienopyrrole unit in **DTP-TPA** is planar with the pendant phenyl group twisted to  $41^\circ$  and the phenyl rings of two triphenylamine units are tilted by  $24^\circ$  and  $20^\circ$  relative to DTP plane. When compared to the crystal structure of parent *N*-(4-hexylphenyl)dithieno[3,2-*b*:2',3'-*d*]pyrrole,<sup>15</sup> S(1)-C(1), S(1)-C(4) and C(1)-C(2) bonds are slightly elongated by  $0.041 \text{ \AA}$ ,  $0.021 \text{ \AA}$  and  $0.02 \text{ \AA}$  respectively due to the substitution of triarylamine. The lengthening of C(1)-C(2) bond suggest an increase in delocalization of C=C within the  $\pi$ -system.

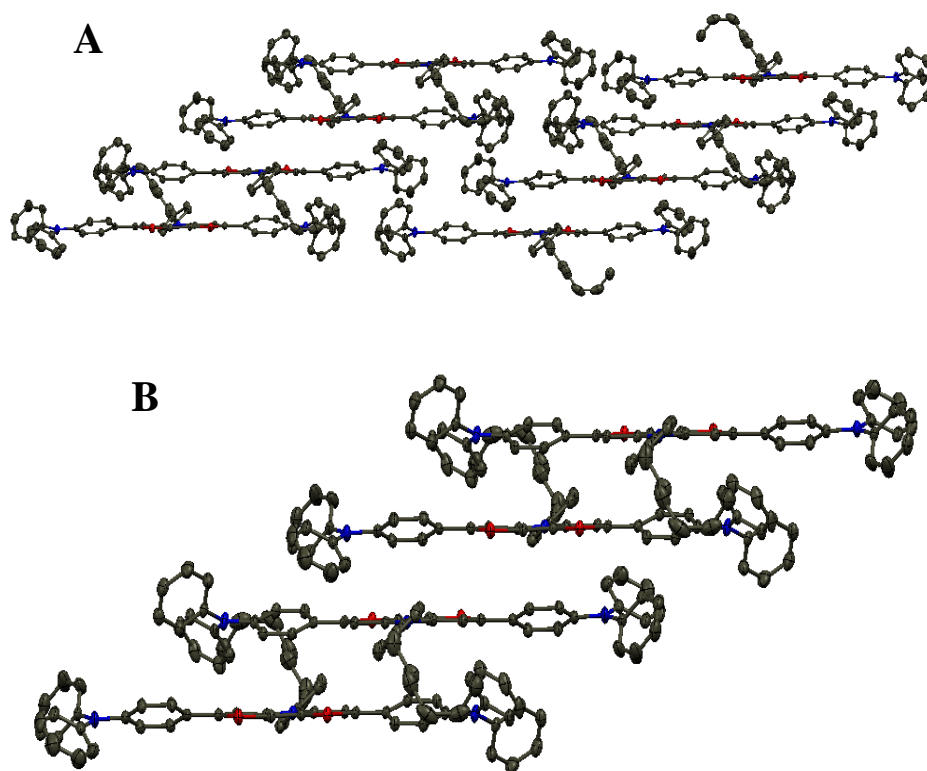


**Figure 5.3.** Crystal packing along *a*-axis (A) and packing of two adjacent columns (B) of **DTP-TPA**. Hydrogen atoms are removed for clarity

In solid state, **DTP-TPA** arrange in slipped  $\pi$ -stacked manner along *a*-axis with an internuclear distance of 3.37 Å, which equals the sum of van der Waals radii of carbon atoms (Figure 5.3). These  $\pi$ -stacked molecules are anti-cofacially arranged leading to a 1-dimensional structure. The phenyl group of triphenyl amine unit (attached to DTP) is involved in  $\pi$ -stacking with DTP core whereas the other two-phenyl groups interact with neighboring columns. Alkyl groups have no effect on overall packing of the molecule.

### 5.3.3. Optical properties

The UV-vis absorption spectra of all oligomers in solution as well as in thin film are shown in Figure 5.4 (A, B). All oligomers have strong absorption in the range of 380 - 420 nm. It is noted that in solution state the absorption maxima of all these oligomers are red shifted compared to the parent DTP ( $\lambda_{\text{max}} = 310$  nm) due to extension of conjugation.

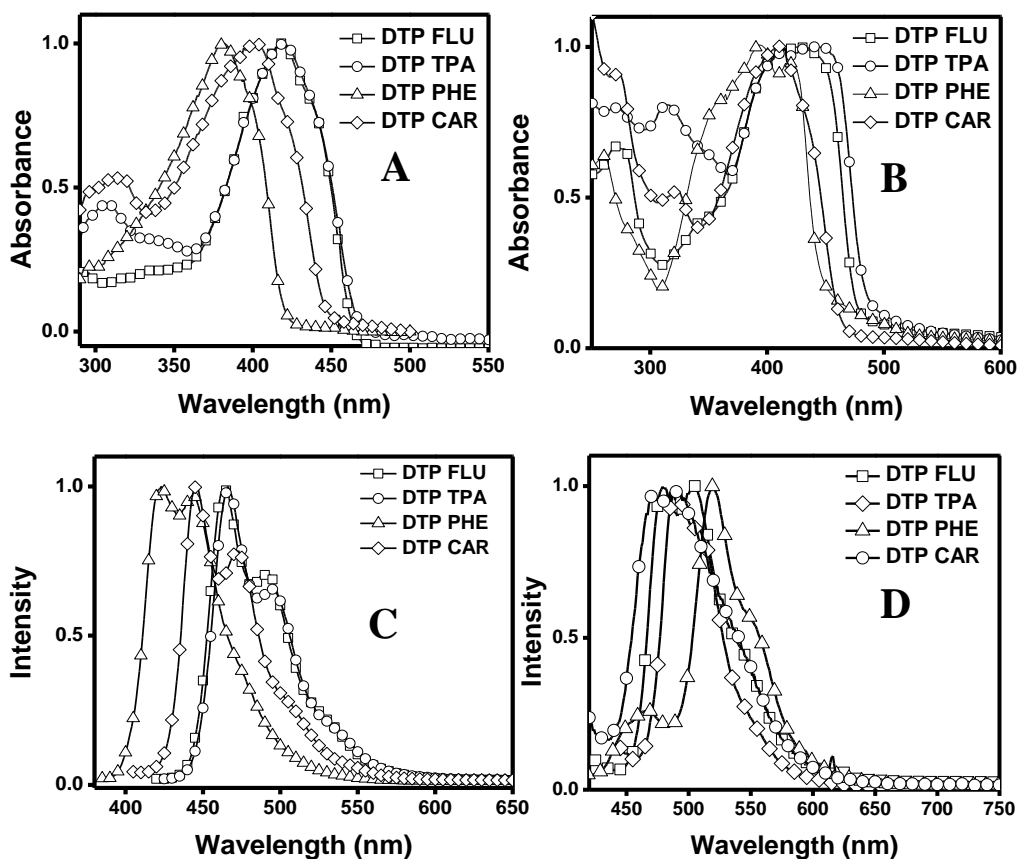


**Figure 5.4.** Normalized absorption spectra in solution state (THF) (A), in solid state (B) and emission spectra in solution state (THF) (C) and in solid-state (D) spectra of DTP oligomers

Relatively shorter wavelength absorption of **DTP-PHE** and **DTP-CAR** are expected due to shorter conjugation length of attached side group in the former and non-conjugated position of attachment in later. Transparent and uniform films were prepared

by spin coating the chloroform solution of oligomers on to a quartz substrate. Films of all oligomers were yellow-green in color except **DTP-PHE**, which was pale green in color. Broad peaks with bathochromic shift in absorption were observed for all oligomers in solid state (Figure 5.4B). Emission spectra of oligomers were also recorded in solution (THF) and film state (Figure 5.4C, D).

In solution state, all oligomers showed bluish green emission with emission maxima in the range of 440 - 490 nm. **DTP-PHE** showed blue emission at shorter wavelength than rest of the oligomers in the series. However, in solid state, **DTP-PHE** showed emission at a higher wavelength than rest of the oligomers. This can be attributed to the close packing of this molecule in the solid state compared to other members in the series. Emission spectra of other oligomers in the film state are also red shifted to give greenish-yellow emission. Interestingly, all synthesized DTP oligomers are emissive in nature. Solution state quantum yield of these compounds were calculated in THF with quinine sulfate as standard. **DTP-FLU** and **DTP-TPA** are the two highly fluorescent oligomers in the series with a solution state quantum yield of 75% and 70%, respectively. To the best of our knowledge, this is the highest solution state quantum yield reported for any DTP system. **DTP-PHE** and **DTP-CAR** exhibited a comparatively lower quantum yield of 57% and 52%, respectively.

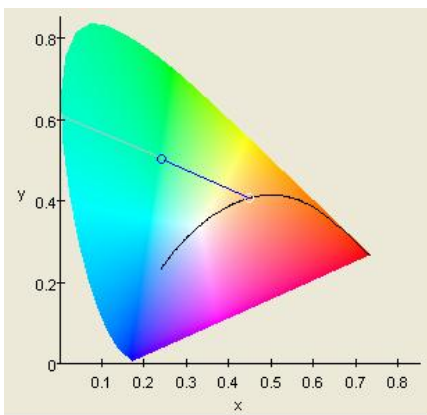


**Figure 5.5.** CIE coordinate in film sample of **DTP-FLU** ( $x=0.2422$ ,  $y=0.5019$ ,  $z=0.2559$ )

Unlike other known thiophene molecules, all oligomers showed emission in solid state.<sup>23</sup> The solid-state quantum yield of **DTP-FLU** and **DTP-TPA** were measured by using an integrating sphere.<sup>24</sup> **DTP-FLU** exhibited a solid-state quantum yield of 22%, while that of other emissive analogue **DTP-TPA** was 10%. The CIE coordinates of **DTP-FLU** and **DTP-TPA** are represented in Figure 5.5. From the initial study, it is noted that **DTP-FLU** and **DTP-TPA** exhibit similar photophysical properties. A detailed investigation of the excited state dynamics of these molecules will provide a better understanding of their photophysical properties. The low solid state quantum yield of **DTP-TPA** compared to **DTP-FLU** may be due to the  $\pi$ -stacking (also indicated by single crystal X-ray diffraction) which leads to the self-quenching of excited state species.<sup>25</sup> The optical properties of all compounds in solution as well as in film state are summarized in Table 5.1.

**Table 5.1.** Optical properties of DTP oligomers in solution and solid state

Oligomer	Absorption $\lambda_{\max}$ (nm)		Emission $\lambda_{\max}$ (nm)		QY (%)	
	Solution (THF)	Thin Film	Solution (THF)	Thin Film	Solution	Thin Film
DTP-FLU	416	422	464, 491	481, 505	75 %	22 %
DTP-TPA	418	438	466, 495	490, 509	70 %	10 %
DTP-PHE	379	400	423, 444	468, 520	57 %	nd
DTP-CAR	401	413	446, 473	485	52 %	nd
DTP <sup>a</sup>	310, 300, 293, 261	-	325	-	0.28 %	-

nd- not determined

<sup>a</sup>Ogawa, K.; Rasmuseen, S. C. *J. Org. Chem.* **2003**, 68, 2921.

### 5.3.4. Electrochemical properties

Electrochemical properties of all oligomers were investigated by cyclic voltammetry. Cyclic voltammogram of oligomers were recorded using Pt wire as working electrode in dichloromethane with 0.1 M *n*-Bu<sub>4</sub>NPF<sub>6</sub> as supporting electrolyte (Figure 5.6). The CV potentials were measured versus Ag/AgCl electrode, which was calibrated using ferrocene/ferrocenium redox couple. No significant changes in cyclic voltammograms were observed after repeated scanning. More than one quasi-reversible peaks were observed for all oligomers with oxidation peak potential in the range of 0.5 - 1.75 V vs Ag/AgCl electrode. **DTP-FLU** and **DTP-PHE** showed two oxidation waves at higher potential (FLU 0.8, 1.28 V, PHE 0.88, 1.7 V) than parent DTP (0.65, 1.1 V).<sup>15</sup> For DTP, the second oxidation potential was assigned to the coupling of thiophene radical cation, which



is not the case for substituted DTP oligomers as the substituent block the electroactive sites.

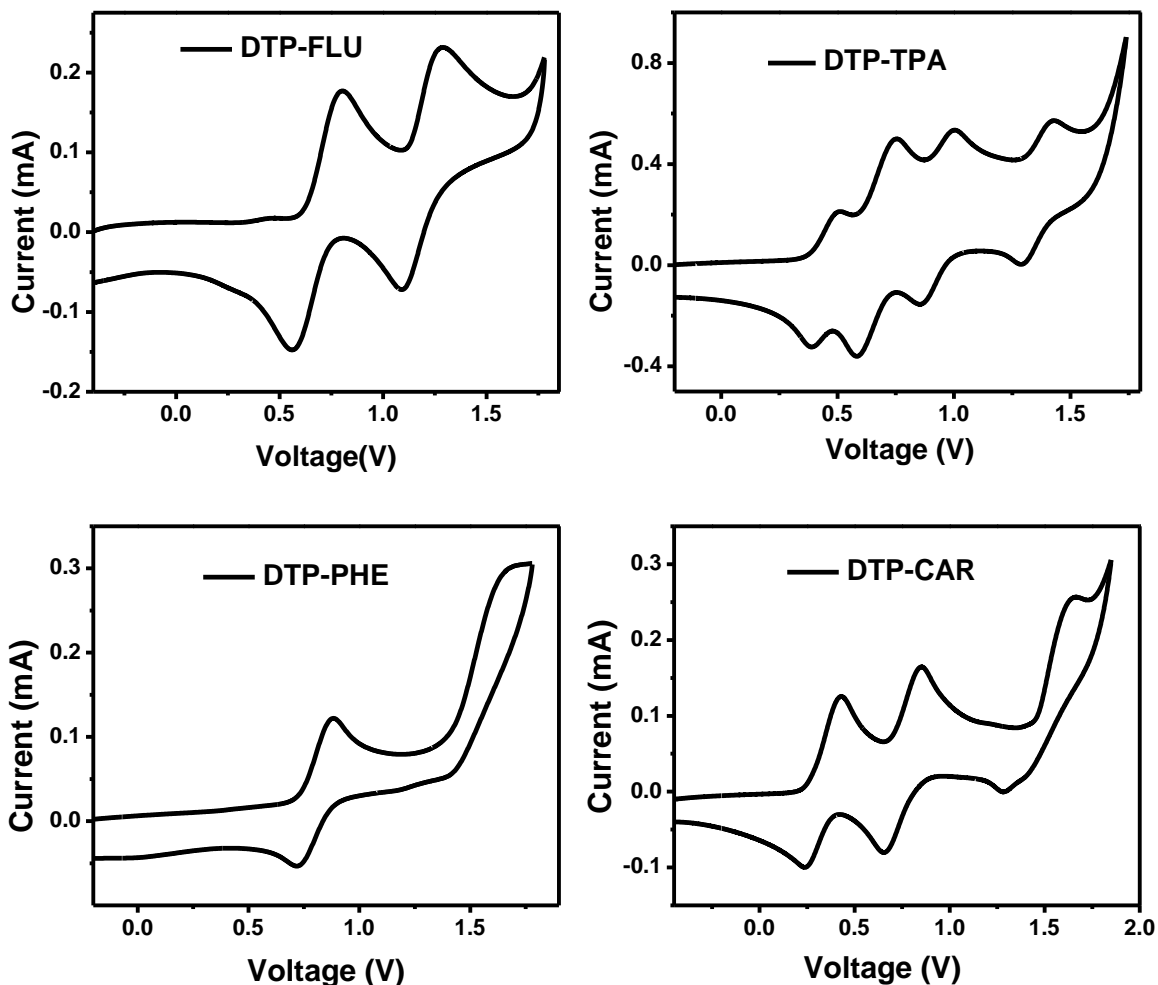


**Figure 5.6.** Cyclic voltammogram of DTP oligomers in dichloromethane containing 0.1 M  $n\text{-Bu}_4\text{NPF}_6$  at the scan rate of 100 mV/s

The first oxidation process of the oligomers involves DTP and subsequent process is likely to involve the side groups. In **DTP-FLU** and **DTP-PHE**, the second oxidation potential is due to the oxidation of fluorene and phenyl units.<sup>26</sup> Oligomers with nitrogen containing end groups (**DTP-CAR** and **DTP-TPA**) exhibited similar electrochemical behavior with multiple oxidation peaks which may be due to the oxidation of end groups.

The first oxidation potentials of **DTP-TPA** and **DTP-CAR** were observed at a lower value than the parent DTP, due to the increase in electron density of the system caused by the triphenylamine and carbazole end group, respectively.

All electrochemical data, the HOMO energy levels, optical band gap and calculated LUMO energy levels are summarized in Table 5.2. HOMO energy levels are obtained electrochemically from oxidation onset potential using the empirical formula,  $E_{\text{HOMO}} = - (E_{\text{ox}} + 4.38) \text{ eV}$ .<sup>27</sup> As we were not able to observe the reduction in these molecules in the scan range, LUMO values were calculated from  $E_{\text{HOMO}}$  and optical band gap ( $E_g$ ). The optical band gap varies from 2.81 eV (**DTP-PHE**) to 2.55 eV (**DTP-TPA**). **DTP-FLU** and **DTP-PHE** are found to have higher oxidation potential and lower HOMO level with increased stability as compared to other members in the series.

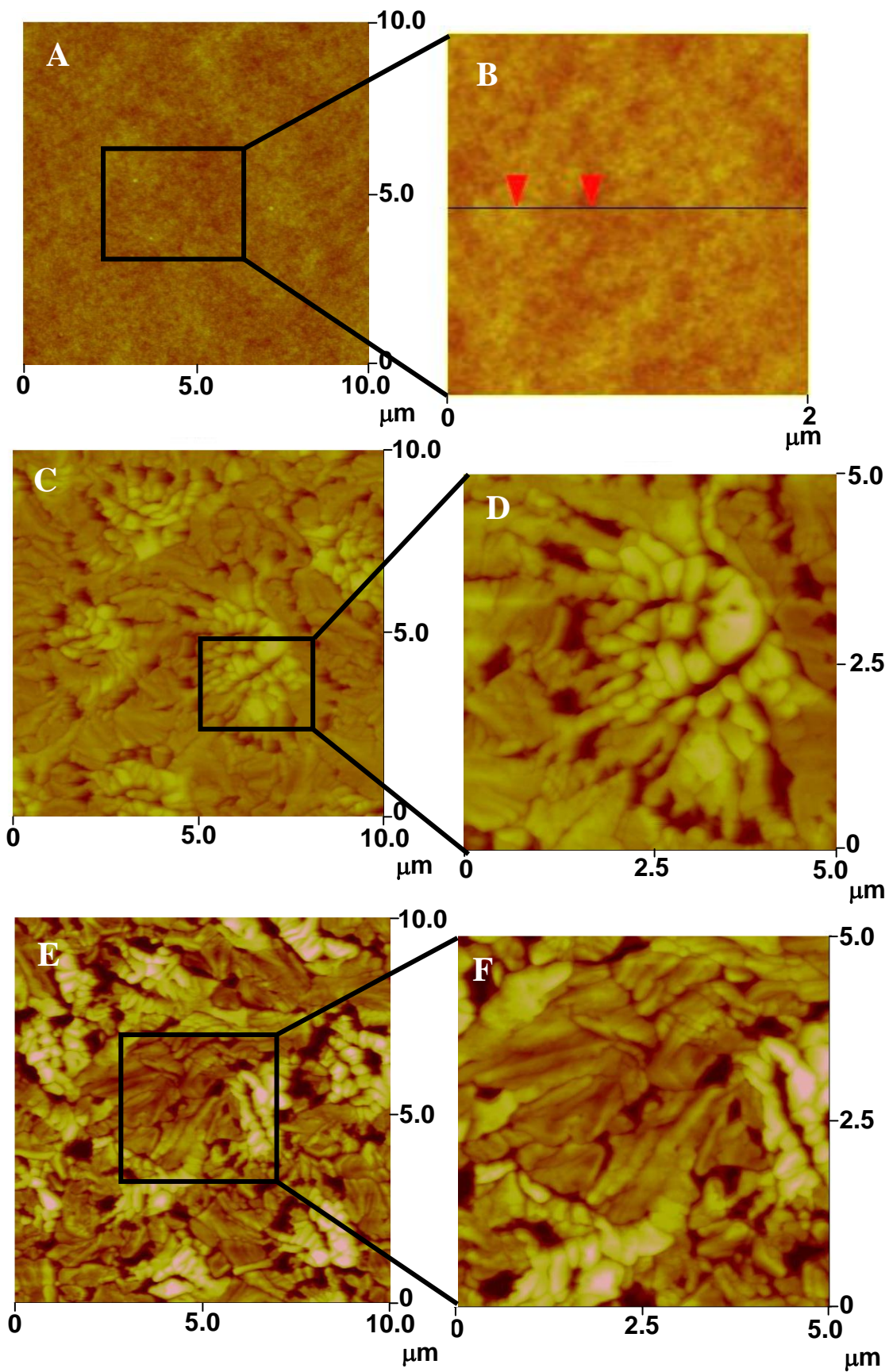
**Table 5.2.** Electrochemical properties of DTP-oligomers recorded in dichloromethane containing 0.1 M *n*-Bu<sub>4</sub>NPF<sub>6</sub> as supporting electrolyte

Oligomer	$E_{\text{oxid}}$ (V)	$E_{\text{oxid}}^{\text{onset}}$ (V)	$\Delta E$ (V)	$E_{\text{HOMO}}$ (eV)	$\lambda_{\text{onset}}$ (nm)	$E_g$ (eV)	$E_{\text{LUMO}}$ (eV)
DTP-FLU	0.8, 1.28	0.6	0.24, 0.19	-4.98	483	2.57	-2.41
DTP-TPA	0.49, 0.74, 0.99, 1.42	0.38	0.12, 0.17, 0.16, 0.14	-4.76	486	2.55	-2.21
DTP-PHE	0.88, 1.7	0.73	0.18, 0.19	-5.11	441	2.81	-2.3
DTP-CAR	0.5, 0.93, 1.73	0.37	0.19, 0.2, 0.38	-4.75	467	2.66	-2.09
DTP <sup>a</sup>	0.65, 1.1	-	-	-	-	-	-

<sup>a</sup>Ogawa, K.; Rasmussen, S. C. *J. Org. Chem.* **2003**, *68*, 2921.

### 5.3.5. Surface morphology

The morphology of the film sample was characterized by using atomic force microscopy (AFM). The film was prepared by spin coating the oligomer solution onto an ITO coated glass substrate. Figure 5.7 shows the tapping mode AFM images of DTP oligomers. **DTP-FLU**, **DTP-CAR** and **DTP-TPA** form a uniform film with rms roughness of about 1.619, 1.03 and 2.57 nm, respectively. It can be seen that **DTP-PHE** forms inter connected crystalline domains with grains of micrometer size. The average grain size was calculated to be around 0.8  $\mu\text{m}$ . It is observed that by annealing this sample (60 °C for 20 minutes) larger crystal domain or crystal grains (up to  $\sim 2\mu\text{m}$ ) are formed (see Figure 5.7E and F).



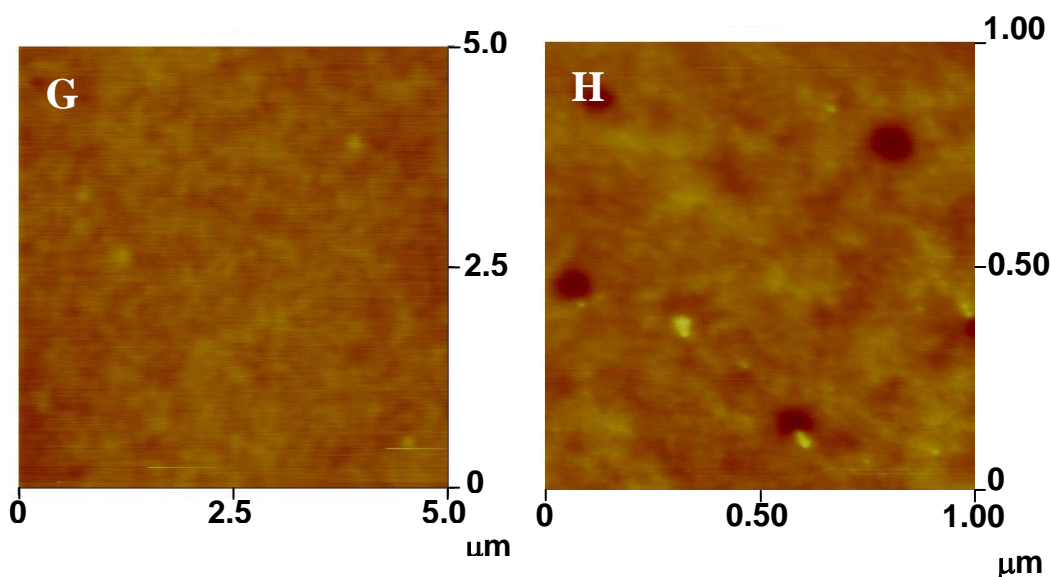


**Figure 5.7.** Tapping mode AFM images shows the surface morphology of the spin coated oligomers (A) **DTP-FLU** (10  $\mu\text{m} \times 10 \mu\text{m}$ ) and (B) Magnified image of A (5  $\mu\text{m} \times 5 \mu\text{m}$ ). (C) **DTP-PHE** (10  $\mu\text{m} \times 10 \mu\text{m}$ ) and (D) Magnified image of C (5  $\mu\text{m} \times 5 \mu\text{m}$ ), (E) the same sample after annealing at 60 $^{\circ}\text{C}$  for 20 minutes (10  $\mu\text{m} \times 10 \mu\text{m}$ ) and (F) Magnified image of E (5  $\mu\text{m} \times 5 \mu\text{m}$ ). (G) **DTP-CAR** (5  $\mu\text{m} \times 5 \mu\text{m}$ ) and (H) **DTP-TPA** (1  $\mu\text{m} \times 1 \mu\text{m}$ )

### 5.3.6. Charge transport properties

The charge mobility of the oligomers was measured by using conventional time-of-flight (TOF) photoconductivity technique. The device configuration used for the TOF measurement was ITO/DTP/Al. Film samples of DTP oligomers was prepared by drop casting the chloroform solution onto ITO coated glass substrate in a solvent saturated environment. The thickness of the oligomer film was measured by using a surface profiler. A 100 nm thick aluminum (Al) electrode was evaporated on to the DTP film by using Edwards's thermal evaporator. The charge mobilities were calculated using the relation  $\mu = d^2/Vt_T$ , where  $d$  is the thickness of the film,  $V$  is the applied voltage and  $t_T$  is the transit time. Figure 5.8A, B shows the linear plot of TOF hole transients obtained for **DTP-PHE** and **DTP-TPA**. All these oligomers are found to be hole transporting in

nature. Figure 5.8C, D represents the variation of hole mobility with applied electric field in **DTP-PHE** and **DTP-TPA**, respectively. In the case of **DTP-PHE**, the transit time was extracted by integration method<sup>28</sup> and in **DTP-TPA**; it was obtained from the log-log plot. For **DTP-PHE** and **DTP-TPA**, the hole mobility was found to be  $4.2 \times 10^{-6} \text{ cm}^2/\text{Vs}$  (field =  $2.6 \times 10^5 \text{ V/cm}$ ) and  $2.09 \times 10^{-6} \text{ cm}^2/\text{Vs}$  (field =  $4 \times 10^5 \text{ V/cm}$ ), respectively. The zero field mobility, which is a valuable parameter in many applications, was calculated from the Pool-Frenkel plot and it was found to be  $2.9 \times 10^{-6} \text{ cm}^2/\text{Vs}$  and  $4.6 \times 10^{-8} \text{ cm}^2/\text{Vs}$  for **DTP-PHE** and **DTP-TPA**. Figure 5.9 shows the linear plot of TOF hole transients obtained for **DTP-FLU** at 298K. It is clear from the figure that the initial decay in the photocurrent follows a constant current plateau. This appearance of constant current plateau is due to the non-dispersive nature of the hole transport. The subsequent decay in the current is due to the holes reaching the other electrode at which they are discharged. In this case the transit time, for the arrival of carriers was readily obtained from the inflection point in the double logarithmic plot of photocurrent versus time (see inset Figure 5.9).

The charge transport parameters of all the oligomers are summarized in Table 5.3. In the case of **DTP-CAR** the photocurrent was very weak, therefore it was difficult to obtain accurate hole mobility value. It is noteworthy that the hole mobilities of all DTP oligomers are in good agreement with the Pool-Frenkel relationship ( $\mu = \mu_{(E=0)} \exp(\gamma E^{1/2})$ ), where  $\mu_{(E=0)}$  is the zero field mobility and  $\gamma$  is the slope of the field dependence of charge mobility.<sup>29</sup>

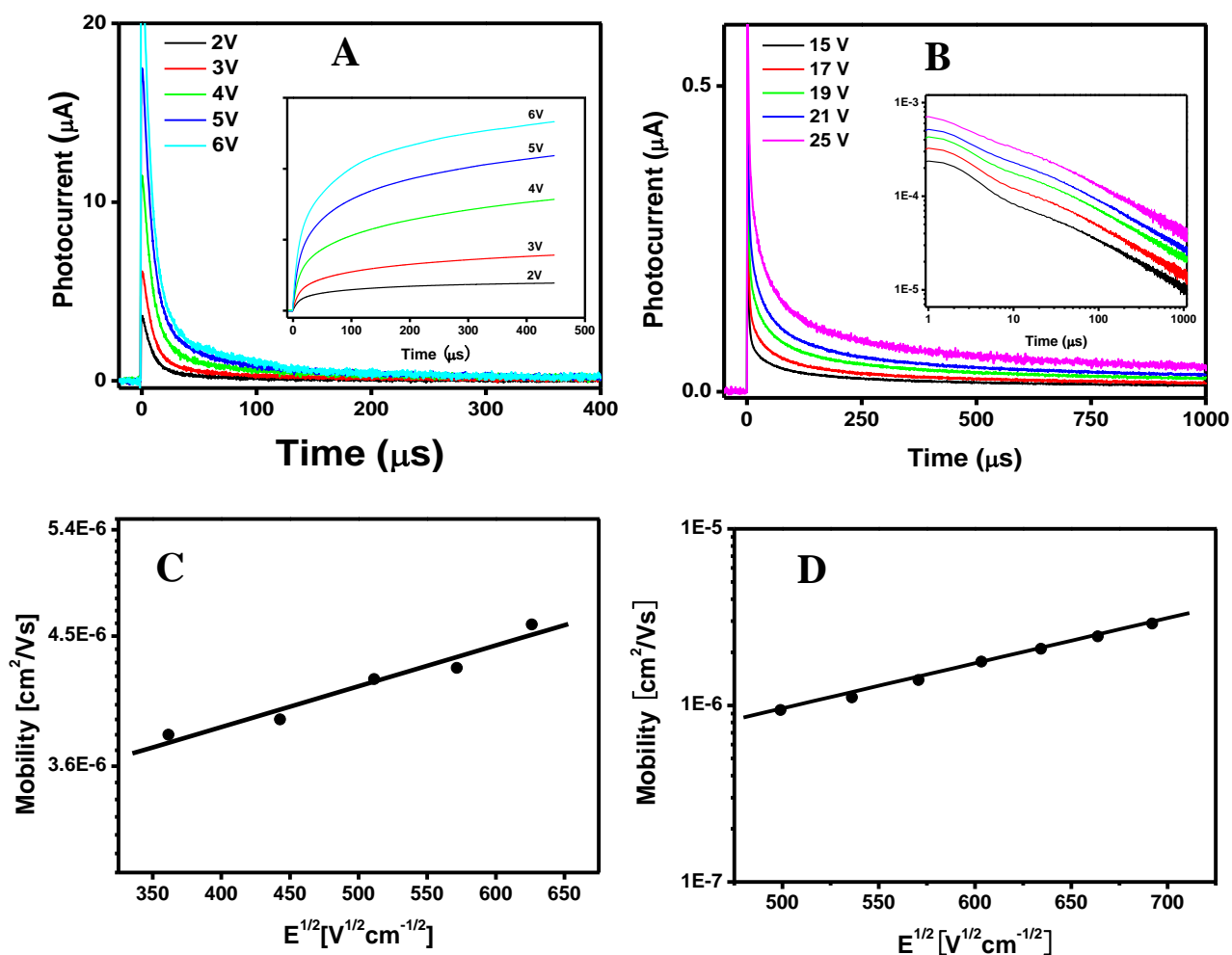


**Figure 5.8.** The linear plot of TOF hole transients for **DTP-PHE** (A) and **DTP-TPA** (B). The inset of A is the corresponding integrated plot of **DTP-PHE** and inset of B is the corresponding log-log plot of **DTP-TPA**. Variation of TOF hole mobility with applied electric field for **DTP-PHE** (C) and **DTP-TPA** (D), solid line is a linear fit with Pool-Frenkel equation

High solid-state fluorescence and reversible electrochemical property of **DTP-FLU** indicates the potential of this oligomer in various opto-electronic applications. Therefore, in order to get an in-depth knowledge of the transport property of **DTP-FLU**, a detailed investigation of its charge transport behavior was carried out. The dependence of hole mobility with applied electric field and temperature was studied in detail by analyzing the

experimental results using the Bassler's Gaussian disorder model and correlated disorder model.

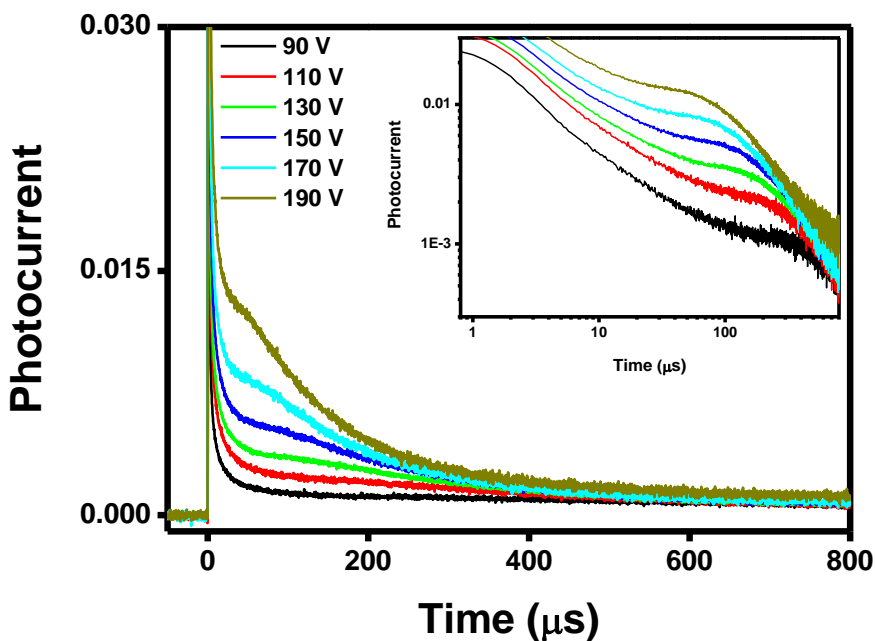


**Figure 5.9.** Linear plot of time-of-flight hole current transients for different applied voltage in DTP-FLU film at 298 K. The inset shows the corresponding double-logarithmic plot

**Table 5.3.** Hole mobility of DTP-oligomers

Oligomer	Mobility ( $\text{cm}^2/\text{Vs}$ )	Zero field Mobility	$\gamma$ ( $\text{cm}/\text{V}$ ) <sup>1/2</sup>
DTP-FLU	$7.7 \times 10^{-6}$ (Field: $2.9 \times 10^5$ V/cm)	$6.1 \times 10^{-7}$ $\text{cm}^2/\text{Vs}$	$2.04 \times 10^{-3}$
DTP-TPA	$2.09 \times 10^{-6}$ (Field: $4.0 \times 10^5$ V/cm)	$4.6 \times 10^{-8}$ $\text{cm}^2/\text{Vs}$	$2.6 \times 10^{-3}$
DTP-PHE	$4.2 \times 10^{-6}$ (Field: $2.6 \times 10^5$ V/cm)	$2.9 \times 10^{-6}$ $\text{cm}^2/\text{Vs}$	$3.04 \times 10^{-4}$
DTP-CAR	nd	nd	nd

nd-not determined



The charge carrier mobility of **DTP-FLU** was measured at a temperature range of 218 - 308K. The linear plot of TOF hole transients obtained at various temperatures are shown in Figure 5.10.

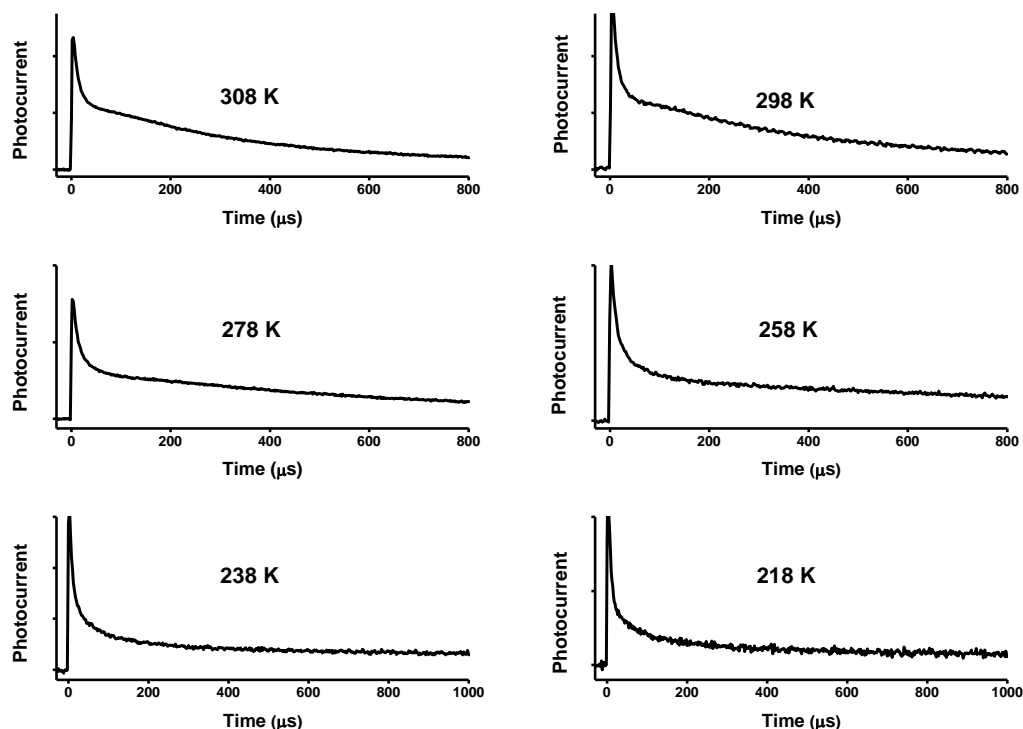


**Figure 5.10.** Linear plot of TOF photocurrent transients at various temperatures in **DTP-FLU** (Field:  $2.7 \times 10^5$  V/cm)

At 298 K, the hole mobility was found to be  $7.7 \times 10^{-6}$  cm<sup>2</sup>/Vs at an applied electric field of  $2.9 \times 10^5$  V/cm. It is noteworthy that at all temperatures, the field-dependences of the hole mobilities are in good agreement with the Pool-Frenkel relationship. The Pool-Frenkel plots of hole mobility in **DTP-FLU** at various temperatures are shown in Figure 5.11.

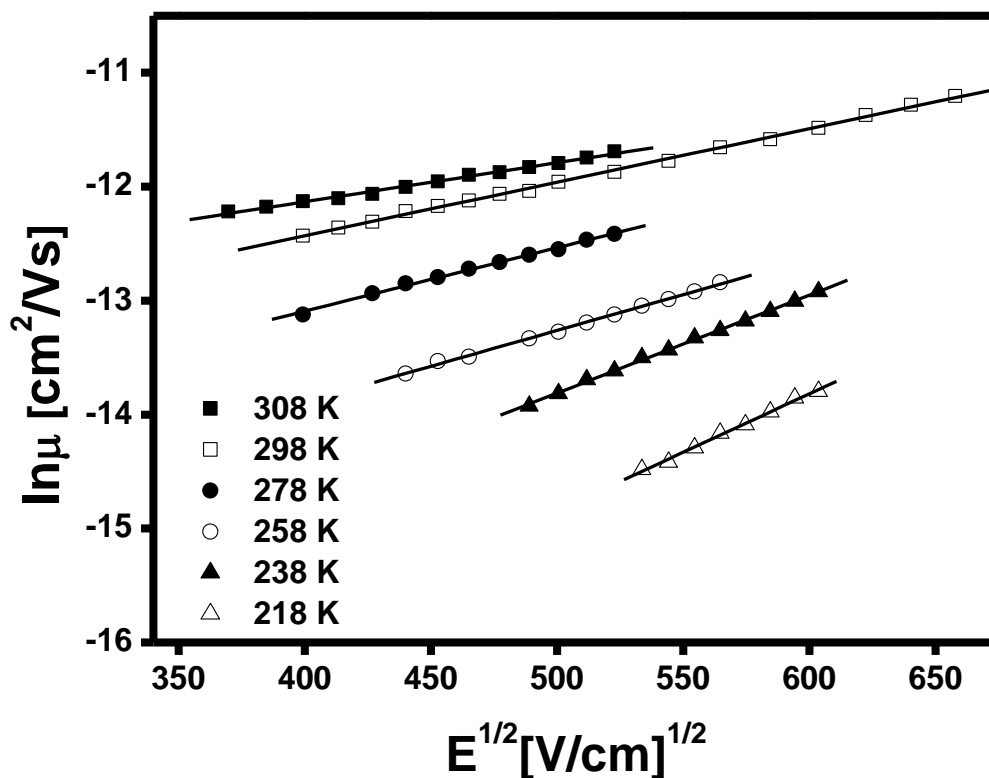


**Figure 5.11.** Poole–Frenkel plots of hole mobility in **DTP-FLU** at various temperatures

The hole mobility was found to be increasing with increase in temperature. At 238 K the hole mobility was found to be  $1.2 \times 10^{-6} \text{ cm}^2/\text{Vs}$  at an applied field of  $2.7 \times 10^5 \text{ V/cm}$ , but at 278 K the mobility was increased to  $4.1 \times 10^{-6} \text{ cm}^2/\text{Vs}$  and at 308 K it was found to be  $8.4 \times 10^{-6} \text{ cm}^2/\text{Vs}$  with the same applied electric field. The zero field mobility ( $\mu_{(E=0)}$ ) and the slope  $\gamma$  were extracted from this Pool-Frenkel plot and the zero-field mobility was plotted against temperature (Figure 5.12). It is clear from the plot that the zero-field mobility increases with increase in temperature and the slope,  $\gamma$  decreases with increase in temperature. This illustrates the typical hopping mechanism of charge transport in **DTP-FLU**. Generally in conjugated molecular solids the transport of charges proceeds by hopping between localized sites on individual molecules. It is known that the disorder in energies of these localized sites arises from variations in conjugation length,

conformation of the molecule or intermolecular interactions. This leads to a distribution of site energies and these distributions lead to a significant dispersion in the charge hopping times.

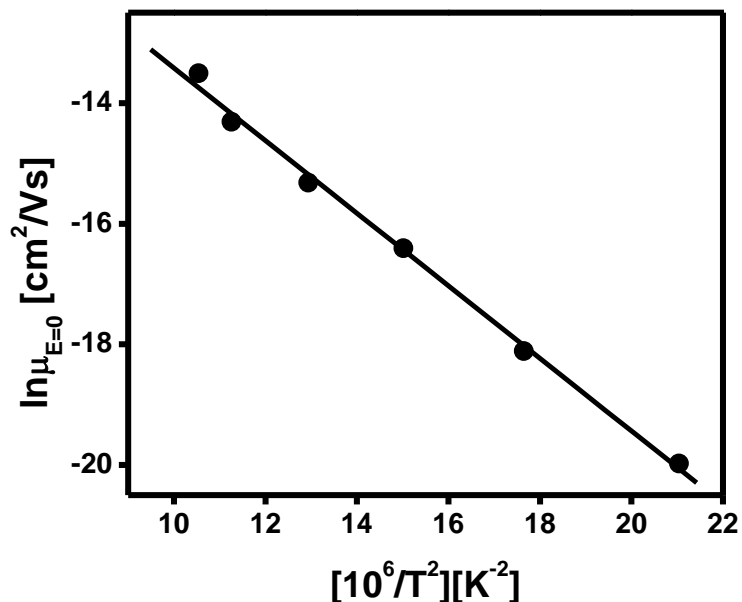


**Figure 5.12.** Temperature dependence of mobilities at zero-field in **DTP-FLU**

The mechanism of charge transport and the relation between the Gaussian energy distribution and the characteristics of time-of-flight transients in disordered organic materials was interpreted by various models. Gaussian disorder model (GDM), proposed by Bässler *et.al.* is one of the empirical expression which has been widely used to characterize the field and temperature dependence of charge transport in amorphous organic solids.<sup>30</sup> In GDM, it is assumed that the charge transport occurs through a hopping mechanism with Gaussian distributed energetic disorder of localized hopping sites and intermolecular positional disorder. According to Gaussian model, energetic disorder ( $\sigma$ ) and positional disorder parameter ( $\Sigma$ ) are the two crucial parameters, which influence the carrier mobility. The energetic disorder corresponds to the width of the

Gaussian density of states and it arises from the distribution of conjugation length. The positional disorder parameter arises from the fluctuations of intermolecular distances or mutual orientation of neighboring molecules. This GDM model also accounts for the crossover from nondispersive to dispersive transport at low temperatures.<sup>31</sup> In Gaussian model the dependence of hole mobility on electric field and temperature can be expressed by Equation 5.1.<sup>31a</sup>

$$\mu_{GDM} = \mu_{\infty} \exp\left[-\left(\frac{2\sigma}{3kT}\right)^2\right] \times \exp\left[C \left\{\left(\frac{\sigma}{kT}\right)^2 - \Sigma^2\right\} E^{1/2}\right] \quad (5.1)$$

Where  $\mu_{\infty}$  is the high temperature limit of the mobility,  $\sigma$  is the energetic disorder bandwidth,  $\Sigma$  is the parameter of positional disorder and C is the empirical constant. The empirical constant indicates the hopping distances that a charge carrier has to overcome to be transferred from one site to another. The energetic disorder parameter and high temperature limit of mobility was extracted from the plot of logarithmic zero field mobility *versus*  $1/T^2$  (Figure 5.12) and it was found to be  $\mu_{\infty} = 6.1 \times 10^{-4} \text{ cm}^2 / \text{V s}$  and  $\sigma = 100 \text{ meV}$ . Also the positional disorder parameter and the empirical constant C were extracted by plotting the slope of the field dependence ( $\gamma$ ) against  $(\sigma/kT)^2$  (see Figure 5.13A) and the values of  $\Sigma$  and C were obtained from the linear fit. It was found to be  $\Sigma = 2.4$  and  $C = 4.6 \times 10^{-4} (\text{cm} / \text{V})^{1/2}$ .

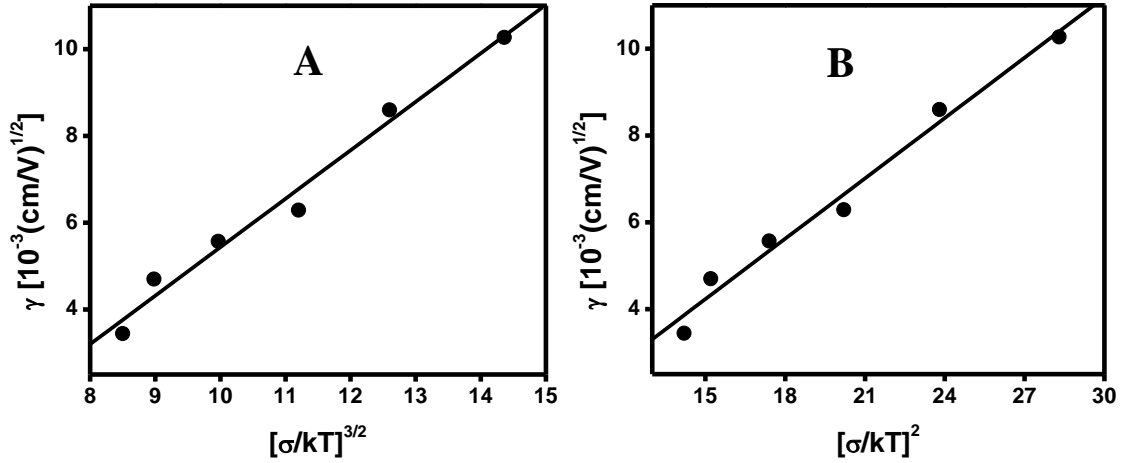


**Figure 5.13.** The slope of the field dependence of the logarithmic mobility *versus*  $(\sigma/kT)^2$  for DTP-FLU, the solid line is a linear fit according to equation 5.1 (A). The slope of the field dependence of the logarithmic mobility *versus*  $(\sigma/kT)^{3/2}$ , the solid line is a linear fit according to equation 5.2 (B)

It is reported that long range correlations due to charge-dipole interaction exists in disordered organic materials.<sup>32</sup> But in GDM model, the correlation between the sites is not accounted. This leads to the development of another model called correlated disorder model (CDM) which accounts for the charge-dipole interactions.<sup>33</sup> According to CDM the nondispersive mobility in correlated media can be represented by equation 5.2.

$$\mu_{CDM} = \mu_{\infty} \exp \left[ - \left( \frac{3\sigma}{5kT} \right)^2 \right] \times \exp \left[ 0.78 \left\{ \left( \frac{\sigma}{kT} \right)^{3/2} - 2 \right\} \sqrt{\frac{eaE}{\sigma}} \right] \quad (5.2)$$

In CDM carrier hopping among the sites are arranged on a cubic lattice with a cell spacing  $a$ . Also it is described that in CDM the high temperature limit of mobility may have additional temperature dependence due to other less correlated sources of energy disorder or polaron effects. The major difference between GDM and CDM is the predicted temperature dependence of  $\gamma$ . Figure 5.13B shows the variation of  $\gamma$  with

$(\sigma/kT)^{3/2}$  and the linear fit is according to CDM (equation 5.2). The average cell spacing (a) was obtained from this linear plot and it was found to be 1.4 nm. The energetic disorder parameter according to CDM model was also calculated from the plot of logarithmic zero field mobility *versus* temperature (Figure 5.12) and was found to be 111 meV. The localization length for the charges was calculated by using equation 5.3 with the derived values of energetic disorder parameter,  $\mu_\infty$  and average cell spacing.

$$\mu_\infty = \frac{ea^2\nu_{ph}}{\sigma} \exp\left(\frac{-2a}{L}\right) \quad (5.3)$$

where  $\nu_{ph}$  is the phonon frequency for hopping ( $\sim 10^{12} \text{ s}^{-1}$ ). The localization length was estimated to be 5 Å. The results obtained from both the models (GDM and CDM) are summarized in Table 5.4.

**Table 5.4.** Charge transport parameters of **DTP-FLU** calculated using Gaussian disorder model (GDM) and Correlated disorder model (CDM)

Gaussian disorder model	Correlated disorder model
$\mu_\infty, \text{GDM}: 6.1 \times 10^{-4} \text{ cm}^2 / \text{V s}$	$\mu_\infty, \text{CDM}: 6.1 \times 10^{-4} \text{ cm}^2 / \text{V s}$
$C: 4.6 \times 10^{-4} (\text{cm} / \text{V})^{1/2}$	$\sigma_{\text{CDM}}: 111 \text{ meV}$
$\sigma_{\text{GDM}}: 100 \text{ meV}$	$a: 1.4 \text{ nm}$
$\Sigma: 2.4$	$L: 5 \text{ \AA}$

The charge transport parameters obtained from the GDM/CDM analysis are similar to the established conjugated materials such as poly (*p*-phenylenevinylene)

(PPV), polyfluorene (PFO) etc.<sup>34</sup> It is interesting to note that the intersite hopping constant and energetic disorder obtained in the case of **DTP-FLU** is found to be similar to that in PFO (intersite hopping constant =  $2.4 \times 10^{-4} \text{ (cm / V)}^{1/2}$  and  $\sigma_{\text{GDM}} = 90 \text{ meV}$ ).<sup>35</sup> Also it is noteworthy that in the case of (2-methoxy-5-(2'-ethylhexyloxy)-1,4-phenylenevinylene)/C60 composite (MEH-PPV/C<sub>60</sub>)<sup>36</sup> system the intersite hopping constant was found to be in the  $10^{-4} \text{ cm}^{1/2} \text{ V}^{-1/2}$  which is very similar to that of **DTP-FLU**. Therefore it can be concluded that DTP based materials have similar transport properties as that of standard conjugated systems such as PFO, PPV *etc* which has potential for device applications. Therefore the charge transport parameters of DTP based molecules can be controlled and optimized which will enable us to fine tune and fabricate the optoelectronic devices.

#### 5.4. Conclusion

A new series of DTP-incorporated oligomeric system with phenyl, fluorene, triphenylamine and carbazole units are synthesized and characterized. Crystal structure and crystal packing of **DTP-TPA** was studied. **DTP-TPA** packs in the  $\pi$ -stacked manner with an intermolecular distance of 3.37 Å. The oligomer **DTP-PHE** showed a blue emission with the solution state quantum yield of 57%. All other oligomers showed green emission with quantum yield of 52 - 75%. **DTP-FLU** exhibit high solution quantum yield of 75% and solid-state quantum yield of 22%. Higher oxidation potential and low-lying HOMO of **DTP-FLU** and **DTP-PHE** compared to other two members in the series indicates the higher stability of these compounds. The materials are found to be hole transporting and the mobilities of the charge carriers were measured by using time-of-flight technique. The hole mobilities were found to be in the order of  $10^{-7}$

$6 \text{ cm}^2/\text{Vs}$ . Highly fluorescence nature of **DTP-FLU** and **DTP-TPA** in solid state and reversible electrochemical property indicates the potential of these oligomers in optoelectronic application such as organic light emitting field effect transistors (OLEFET). Due to their high crystalline nature **DTP-PHE** is a potential candidate for OFET applications. The charge transport property of **DTP-FLU** was investigated in detail. The hole mobilities were measured over a range of temperatures from 218 K to 308 K. The field and temperature dependence of mobility was analyzed by Gaussian disorder model and Correlated disorder model and the charge transport parameters were extracted. The results indicate that dithienopyrrole-based compounds are promising new material for various optoelectronic applications.



## 5.5. Reference

---

- (1) (a) Sirringhaus, H.; Tessler, N.; Friend, R. H. *Science* **1998**, *280*, 1741. (b) Garnier, F.; Hajlaoui, R.; Yassar, A.; Srivastava, P. *Science* **1994**, *265*, 1684.
- (2) (a) *Handbook of Oligo- and Polythiophene*; Fichou, D., Wiley-VCH: Weinheim, Germany, New York, 1999. (b) *Electronic Materials: The Oligomer Approach*; Müllen, K.; Wegner, G. Wiley-VCH: Weinheim, Germany, New York, 1998.
- (3) Roncali, J. In *Handbook of Conducting Polymers*, 2<sup>nd</sup> ed.; Skotheim, T. A., Elsenbaumer, R. L., Reynolds, J. R., Eds.; Marcel Dekker: New York, 1998; Chapter 12.
- (4) (a) Ohmori, Y.; Uchida, M.; Muro, K.; Yoshino, K. *Solid state commun.* **1991**, *80*, 605. (b) Braun, D.; Gustaffson, G.; McBranch, D.; Heeger, A. J. *J. Appl. Phys.* **1992**, *72*, 564. (c) Andersson, M. R.; Thomas, O.; Mammo, W.; Svensson, M.; theander, M.; Inganäs, O. *J. Mater. Chem.*, **1999**, *9*, 1933. (d) Gigli, G.; Barbarella, G.; Favaretto, L.; Cacialli, F.; Cingolani, R. *Appl. Phys. Lett.* **1999**, *75*, 439. (e) Perepichka, I. F.; Perepichka, D. F.; Meng, H.; Wudl, F. *Adv. Mater.* **2005**, *17*, 2281.
- (5) (a) Murphy, A. R.; Fréchet, J. M. J.; Chang, P.; Lee, J.; Subramanian, V. *J. Am. Chem. Soc.* **2004**, *126*, 1596. (b) Chang, P. C.; Lee, J.; Huang, D.; Subramanian, V.; Murphy, A. R.; Fréchet, M. J. *Chem. Mater.*, **2004**, *16*, 4783. (c) Letizia, J. A.; Facchetti, A.; Stern, C. L.; Ratner, . A.; Marks, T. *J. Am. Chem. Soc.* **2005**, *127*, 13476.
- (6) (a) Campos, L. M.; Tontchev, A.; Güness, S.; Sonmez, G.; Neugebauer, H.; Sariciftci, N. S.; Wudl, F. *Chem. Mater.* **2005**, *17*, 4031. (b) Sonmez, G. *Chem. Commun.* **2005**, 5251. (c) Wienk, M. M.; Turbiez, M. G. R.; Struijk, M. P.; Fonrodona, M.; Janseen, R. A. *J. Appl. Phys. Lett.* **2006**, *88*, 153511(1).
- (7) (a) Stoyanovioh, F. M. ; Federov, B. P. ; *Zh. Org. Khim.* **1965**, *1*, 1282. (b) Janssen, M. J. ; De Jong, F. ; *J. Org Chem.* **1971**, *36*, 1645.
- (8) Coppo, P.; Tuner, M. L. *J. Mater. Chem.* **2005**, *15*, 1123.
- (9) (a) Zanirato, P.; Spagnolo, P.; Zanardi, G. *J. Chem. Soc. Perkin Trans. I.* **1983**, 2551. (b) Berlin, A.; Pagani, G.; Zotti, G.; chiavon, G. *Makrokol. Chem.* **1992**, *193*, 399. (c) Beggiano, G.; Casalbore-Miceli, G.; Geri, A.; Berlin, A.; Pagani, G. *Synth. Met.* **1996**, *82*, 11. (d) Berlin, A.; Zotti, G.; Schiavon, G.; Zecchin, S. *J. Am. Chem. Soc.* **1998**, *120*, 13453. (e) Fujitsuka, M.; Sato, T.; Sezaki, F.; Tanaka, K.; Watanabe, A.; Ito, O.

- J. Chem. Soc., Faraday Trans.* **1998**, *94*, 3331. (f) Laks, B.; Del Nero, J. *Synth. Met.* **1999**, *101*, 379. (g) Zotti, G.; Berlin, A.; Schiavon, G.; Zecchin, S. *Synth. Met.* **1999**, *101*, 622. (h) Nero, J. D.; Laks, B. *J Mol Model* **2001**, 354.
- (10) Baumgartner, T. *J. Inorg. Organomet. Polym.* **2006**, *15*, 389.
- (11) (a) Li, X. -C.; Sirringhaus, H.; Garnier, F.; Holmes, A. B.; Moratti, S. C.; Feeder, N.; Clegg, W.; Teat, S. J.; Friend, R. H. *J. Am. Chem. Soc.* **1998**, *120*, 2206. (b) Coppo, P.; Tuner, M. L.; Cupertino, D. C.; Yeates, S. G. *Mater. Res. Soc. Symp. Proc.* **2003**, *771*, 61. (c) Sun, Y. M.; Ma, Y. Q.; Liu, Y. Q.; Lin, Y. Y.; Wang, Z. Y.; Wang, Y.; Di, C. A.; Xiao, K.; Chen, X. M.; Qiu, W. F.; Zhang, B.; Yu, G.; Hu, W. P.; Zhu, D. B. *Adv. Funct. Mater.* **2006**, *16*, 426. (d) Moulé, A. J.; Tsami, A.; Bünnagel, T.; Forster, M.; Kronenberg, N. M.; Scharber, M.; Koppe, M.; Morana, M.; Brabec, C. J.; Meerholz, K.; Scherf, U. *Chem. Mater* **2008**, *20*, 4045.
- (12) Berlin, A.; Pagani, G. A.; Sannicolò, F.; Schiavon, G.; Zotti, G. *Polymer* **1991**, *32*, 1841.
- (13) (a) Belcher, W. J.; Rasmussen, S. C.; Dastoor, P. C. *Polym. Prepr.* **2007**, *48*, 11. (b) Zhou, E.; Nakamura, M.; Nishizawa, T.; Zhang, Y.; Wei, Q.; Tajima, K.; Yang, C.; Hashimoto, K. *Macromolecules*, **2008**, *41*, 8302. (c) Steckler, T. T.; Zhang, X.; Hwang, J.; Honeyager, R.; Ohira, S.; Zhang, X-H.; Grant, A.; Ellinger, S.; Odom, S. A.; Sweat, D.; Tanner, D. B.; Rinzler, A. G.; Barlow, S.; Brédas, J. L.; Kippelen, B.; Marder, S. R.; Reynolds, J. R. *J. Am. Chem. Soc.* **2009**, *131*, 2824.
- (14) (a) Liu, J.; Zhang, R.; Sauvé, G.; Kowalewski, T.; McCullough, R. D. *J. Am. Chem. Soc.* **2008**, *130*, 13167. (b) Zhang, W.; Li, J.; Zhang, B.; Qin, J.; Lu, Z.; P. Y.; Mary, B.; Chan-Park, Li, C. M. *Macromolecules* **2008**, *41*, 8953.
- (15) Ogawa, K.; Rasmussen, S. C. *J. Org. Chem.* **2003**, *68*, 2921.
- (16) (a) Radke, K. R.; Ogawa, K.; Rasmussen, S. C. *Org. Lett.* **2005**, *7*, 5253. (b) Ogawa, D.; Rasmussen, S. C. *Macromolecules* **2006**, *39*, 1771. (c) Mo, H.; Rasmussen, S. C. *Polym. Prepr.* **2007**, *48*, 61. (d) Ogawa, K.; Mo, H.; Radke, K. R.; Rasmussen, S. C. *Polym. Prepr.* **2007**, *48*, 40.
- (17) Zhang, W.; Li, J.; Zhang, B.; Qin, J. *Macromol. Rapid Commun.* **2008**, *29*, 1603.
- (18) Odom, S. A.; Lancaster, K.; Beverina, L.; Lefler, K. M.; Thompson, N. J.; Coropceanu, V; Brédas, J -L.; Marder, S. R.; Barlow, S. *Chem. Eur. J.* **2007**, *13*, 9637.
- (19) Crosby, G. A.; Demas, J. N. *J. Phys. Chem.* **1971**, *75*, 991.
- (20) Vijila, C.; Balakrishnan, B.; Huang, C.; Chen, Z.-K.; Zhen, C.-G.; Auch, M. D. J.; Chua, S. J. *Chem. Phys. Lett.* **2005**, *414*, 393.

- (21) Perepichka, I. I.; Perepichka, I. F.; Bryce, M. R.; Palsson, L.-O. *Chem. Commun.*, **2005**, 3397.
- (22) (a) Feng, G. L.; Lai, W. Y.; Ji, S. J.; Huang, W. *Tetrahedron Lett.* **2006**, *47*, 7089. (b) Zhang, K.; Chen, Z.; Yang, C.; Zhang, X.; Tao, Y.; Duan, L.; Chen, L.; Zhu, L.; Qin, J.; Cao, Y. *J. Mater. Chem.* **2007**, *17*, 3451.
- (23) Beljonne, D.; Cornil, J.; Friend, R. H.; Janssen, R. A. J.; Bredas, J. L. *J. Am. Chem. Soc.* **1996**, *118*, 6453.
- (24) de Mello, J. C.; Wittmann, H. F.; Friend, R. H. *Adv. Mater.* **1997**, *9*, 230.
- (25) (a) Rothberg, L. J.; Yan, M.; Papadimitrakopoulos, F.; Galvin, M. E.; Kwock, E. W.; Miller, T. M. *Synth. Met.* **1996**, *80*, 41. (b) Peng, Z.; *Polym. News* **2000**, *25*, 185. (c) Ashraf, R. S.; Shahid, M.; Klemm, E.; Al-Ibrahm, M.; Senfuss, S. *Macromol. Rapid Commun.* **2006**, *27*, 1454.
- (26) Hapiot, P.; Lagrost, C.; Le Floch, F.; Raoult, E.; Berthelot, J. -R. *Chem. Mater.* **2005**, *17*, 2003.
- (27) (a) Leeuw, D. M.; Simenon, M. M. J.; Brown, A. R.; Einerhand, R. E. F. *Synth. Met.* **1997**, *87*, 53. (b) Cui, Y.; Zhang, X.; Jenkhe, S. A. *Macromolecules* **1999**, *32*, 3824. (c) Li, Y.; Ding, J.; Day, M.; Tao, Y.; Lu, J.; D'iorio, M. *Chem. Mater.* **2004**, *16*, 2165.
- (28) Campbell, A. J.; Bradley, D. D. C. *Appl. Phys. Lett.* **2001**, *79*, 2133.
- (29) Borsenberger, P. M.; Pautmeier, L.; Bässler, H. *J. Chem. Phys.* **1991**, *94*, 5447.
- (30) (a) Bässler, H. *Phys. Status Solidi B*, **1993**, *15*, 175. (b) Poplavskyy, D.; Nelson, J. *J. Appl. Phys.* **2003**, *93*, 341. (c) Laquai, F.; Wegner, G.; Im, C.; Bässler, H.; Heun, S. *J. Appl. Phys.* **2006**, *99*, 203712.
- (31) (a) Borsenberger, P. M.; Pautmeier, L. T.; Bässler, H. *Phys. Rev. B* **1992**, *46*, 12145. (b) Bässler, H.; Borsenberger, P. M.; *Chem. Phys.* **1994**, *177*, 763. (c) Borsenberger, P. M.; Schein, L. B. *J. Phys. Chem.* **1994**, *98*, 233.
- (32) Novikov, S. V.; Dunlap, D. H.; Kenkre, V. M.; Parris, P. E.; Vannikov, V. *Phys. Rev. Lett.* **1998**, *81*, 4472.
- (33) Martin, S. J.; Kambili, A.; Walker, A. B. *Phys. Rev. B* **2003**, *67*, 165214.
- (34) (a) Martens, H. C. F.; Brom, H. B.; Blom, P. W. M.; Schoo, H. F. M. *Phys. Stat. Sol.* (b) **2000**, *218*, 283. (b) Kreuzis, T.; Poplavskyy, D.; Tuladhar, S. M.; Campoy-Quiles, M.; Nelson, J.; Campbell, A. J.; Bradley, D. D. C. *Phys. Rev. B* **2006**, *73*, 235201.

(35) Khan, R. U. A.; Poplavskyy, D.; Kreuzis, T.; Bradley, D. D. C. *Phys. Rev. B* **2007**, *75*, 035215.

(36) Shi, Q.; Hou, Y.; Jin, H.; Li, Y. *J. Appl. Phys.* **2007**, *102*, 073108.

## ***Chapter 6***

# ***Thieno[3,4-d]imidazole-bithiophene: A Versatile Building Block for Low Bandgap Polymers***

***Publication from the chapter:***

**Balaji, G.;** Parameswaran, M.; Setyono, D.; Valiyaveetil, S. “*Thieno[3,4-d]imidazole-bithiophene – Versatile Building Block For Low Bandgap Polymers*”. (Submitted to *Org. Lett.*).

## 6.1. Introduction

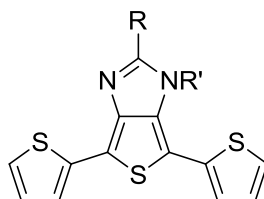
Among the  $\pi$ -conjugated materials oligo and polythiophenes evolved as one of the most prominent organic semiconducting materials.<sup>1</sup> In last few decades, many of these compounds had been successfully demonstrated for practical applications such as light-emitting diodes,<sup>2</sup> photovoltaic devices<sup>3</sup> and field-effect transistors.<sup>4</sup> Oligothiophenes are widely studied as it also serves as a model for understanding the properties of polythiophenes.<sup>5</sup> Bandgap is one of the important parameter that governs the intrinsic optical and electronic properties of conjugated materials.<sup>6</sup> Therefore tuning the bandgap is of fundamental importance for tuning the properties of the conjugated system. Low bandgap materials are of interest for full color or near-infrared light-emitting diodes<sup>7</sup> and high efficient photovoltaic devices.<sup>8</sup> Among thiophene-based polymers, the most efficient approach to lower the bandgap involves the tailoring of the monomer structure in order to increase the quinoid character at the outlay of its aromaticity. The strategy of annealing the aromatic groups at 3,4-position of thiophene ring has led to the reduction of bandgap.<sup>9</sup> Utilizing this strategy, many thiophene-based polymers are prepared and successfully applied for practical applications.

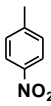
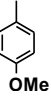
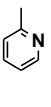
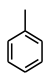
Polyisothionaphthene (PITN) is the first known low bandgap polymer, prepared by Wudl *et al.* utilizing this approach.<sup>10</sup> Electropolymerization of isothianaphthene resulted in PITN with a bandgap of 1 eV, which is lesser than that of thiophene (2 eV).<sup>11</sup> This low bandgap of PITN was achieved inspite of the reduced  $\pi$ -conjugation, resulted due to the steric hindrance between benzo-H and thiophene-S atoms of adjacent units. By replacing benzo-H with N-atom in PITN, the resulting polymer is expected to have a lower bandgap than PITN. Also based on theoretical calculation polythieno[3,4-*b*]-pyrazine was

predicted to have much smaller bandgap than PITN.<sup>12</sup> The electropolymerized thieno[3,4-*b*]pyrazine showed a very low bandgap of ca. 0.69 eV.<sup>13</sup> Terthienyl precursors draw considerable attention in preparing low bandgap polymers as 3,4- fused thiophene system in the middle of terthiophene unit utilize both donor-acceptor and fused ring concept to construct low bandgap materials.<sup>14</sup> Utilizing this, built in alternate donor-acceptor nature, many monomers like 1,3-di(2-thienyl)isothionaphene,<sup>15</sup> 4,6-di(2-thienyl)thieno[3,4-*c*][1,2,5]thiazole,<sup>16</sup> 4,6-di(2-thienyl)thieno[3,4-*b*]pyrazine<sup>17</sup> were synthesized to yield low bandgap polymers which are widely employed for organic photovoltaics (OPV) applications. However, PITN and polythienothiadiazole based polymers have poor processability and film-forming ability which limits their practical applications.<sup>18</sup> Among these fused systems, better OPV performance was demonstrated by thienopyrazine based polymers.<sup>19</sup> However, thienopyrazine based polymers are reported to undergo photodegradation which limits the lifetime of their devices.<sup>20</sup> Therefore, it is necessary to design and synthesize stable, tunable and soluble low bandgap systems for organic electronic applications. In this aspect, it is reasonable to expect that imidazole fused thiophene systems (thieno[3,4-*d*]imidazoles) will be a potential moiety to prepare low bandgap materials for electronic applications. Recently, perylene linked thienoimidazole monomer and polymers were reported, but the focus of the study was centered on perylene moiety.<sup>21</sup>

Herein, we report the synthesis and characterization of a new series of 5,7-di(2-thienyl)-thieno[3,4-*d*]imidazoles based oligomers and polymers with varied substituents (Figure 6.1). These substituents includes long alkyl chain, phenyl, substituted phenyl (electron donating and withdrawing), and heterocyclic (pyridine) groups. Their single

crystal structure, solid-state packing, photophysical and electrochemical properties are studied in detail. The cation and amino acid sensing ability of the pyridine substituted oligomer was also explored. These oligomers are electropolymerized to yield the corresponding low bandgap polymers. In addition, the charge mobility of the parent oligomers was measured using time-of-flight photoconductivity method.



Compounds	R	R'	Compounds	R	R'
T1	H	H	T5		H
T2	H	<i>n</i> -C <sub>6</sub> H <sub>13</sub>	T6		H
T3	<i>n</i> -C <sub>10</sub> H <sub>21</sub>	H	T7		H
T4		H			

**Figure 6.1.** Chemical structure of the newly synthesized dithienothieno[3,4-*d*]imidazole

## 6.2. Experimental

### 6.2.1. Materials and method

2,5-dibromo-3,4-dinitrothiophene was synthesized following the literature procedure.<sup>22</sup> All reactions were carried out under inert atmosphere (Nitrogen or Argon), unless specified otherwise. All reagents were purchased from Aldrich, Fluka or Merck



and used without further purification. All reactions were carried out with freshly distilled anhydrous solvents under inert atmosphere. Tetrahydrofuran (THF) was purified via distillation over sodium under nitrogen atmosphere. Chromatographic purification was carried out using silica gel (230 - 400 mesh).

### 6.2.2. Instrumentation

NMR spectra  $^1\text{H}$  (300 MHz) and  $^{13}\text{C}$  (75.4 MHz) were recorded on a Bruker AMX 300 spectrometer. The chemical shifts are reported in ppm and referenced to the residual solvent peak. The UV-vis spectra were measured on a Shimadzu UV-1601 PC spectrophotometer and fluorescence measurements were carried out on a RF-5301PC Shimadzu spectrofluorophotometer. The quantum yield of the compounds was measured using quinine sulfate (0.1 M  $\text{H}_2\text{SO}_4$ ) as reference.<sup>23</sup> The cyclic voltammograms were recorded with a computer controlled CHI electrochemical analyzer/workstation CHI-600C at a constant scan rate of 100 mV/s. Measurements were performed in an electrolyte solution of 0.1 M tetrabutylammonium hexafluorophosphate ( $\text{Bu}_4\text{NPF}_6$ ) dissolved in dichloromethane. An undivided three-electrode configuration cell was used with a platinum disc as working electrode, platinum wire as the counter electrode, and Ag/AgCl as the reference electrode. Electropolymerization was carried out using Indium tin oxide (ITO) as working electrode, Pt wire as counter electrode and Ag/AgCl as reference electrode. The charge mobility of **T1** was measured by using conventional time-of-flight technique (TOF). For TOF measurements **T1** film was prepared by spin coating (spin speed: 250 rpm for 180 sec) of the chloroform solution onto an indium tin oxide (ITO) patterned glass substrate. A 100 nm thick aluminum electrode was evaporated onto the **T1** film by an Edwards's thermal evaporator to get a device with an active area of 4 mm<sup>2</sup>.

The thickness of the film was determined using a surface profiler (KLA-Tencor P10 surface profiler). All measurements were performed in air at room temperature and no detectable degradation was observed under repeated measurements.

### 6.2.3. Synthesis procedure

**3',4'-Diamino-[2,2';5',2'']terthiophene (3):** Compound was prepared as previously described in the literature with small modification.<sup>24</sup> To a mixture of **2** (2.45 g, 7.24 mmol) in absolute ethanol (50 mL) and concentrated HCl (110 mL) was added tin metal (10.73 g, 90.4 mmol) in small portions. The resulting mixture was stirred at room temperature for 24 h. Ethanol was removed under vacuum. Reaction mixture was basified with saturated K<sub>2</sub>CO<sub>3</sub> solution until pH was adjusted to eight. White precipitate was filtered at the pump and washed with diethyl ether. Filtrate was collected and extracted with water. Organic layer was dried using anhydrous sodium sulfate and concentrated at rotary evaporator and purified by silica column with ethyl acetate/hexane system to afford **3** (1.1 g, 55%) as yellow brown solid. <sup>1</sup>H NMR (300 MHz, CDCl<sub>3</sub>, δ, ppm), 7.27 (dd, *J* = 1.5 Hz, 5.1 Hz, 2H, Th-**H**), 7.06-7.1 (m, 4H, Th-**H**), 3.73 (s, 4H, NH<sub>2</sub>); <sup>13</sup>C NMR (75.4 MHz, CDCl<sub>3</sub>, δ, ppm) 135.9, 133.6, 127.7, 124.0, 123.9, 110; MS (EI) *m/z* (rel. intensity, M+) 278.

**5,7-Di(2-thienyl)thieno[3,4-*d*]imidazole (T1):** Compound **3** (0.4 g, 1.44 mmol) was dissolved in 7 ml ethanol. Hydrochloric acid (30 ml, 4M) and formic acid (55 μl, ρ = 1.22 g/ml) were added and the reaction mixture was refluxed for 4 hours. The resulting mixture was cooled to room temperature, neutralized with K<sub>2</sub>CO<sub>3</sub> solution, and extracted with ethyl acetate. The combined organic layer (6 × 20 ml) was dried with anhydrous Na<sub>2</sub>SO<sub>4</sub> and concentrated at rotary evaporator and purified by column chromatography

using 30:70 ethyl acetate/hexane to afford 0.36 g of **T1** as brown solid (87%).  $^1\text{H}$  NMR (300 MHz, DMSO- $d_6$ ,  $\delta$ , ppm) 12.36 (s, 1H, N-**H**), 8.36 (s, 1H, N=C-**H**), 7.49 (d,  $J = 4.77$  Hz, 2H, Th-**H**), 7.42 (d,  $J = 7.23$  Hz, 2H, Th-**H**), 7.11-7.16 (m, 2H, Th-**H**);  $^{13}\text{C}$  NMR (75.4 MHz, DMSO- $d_6$ ,  $\delta$ , ppm) 135.1, 129, 128.3, 125.4, 124.5, 123.7, 123.6; MS (ESI)  $m/z$  (rel. intensity, M+) 289.2, (rel. intensity, M-) 287.2. Anal. Calcd. for  $\text{C}_{13}\text{H}_8\text{N}_2\text{S}_3$ : C, 54.14; H, 2.8; N, 9.71; S, 33.35. Found: C, 54.26; H, 2.29; N, 9.6; S, 33.51.

**5,7-Di(2-thienyl)-*N*-hexylthieno[3,4-*d*]imidazole (T2):** Compound **T1** (0.21 g, 0.7 mmol) and NaOH (0.1 g, 2.5 mmol) were dissolved in acetonitrile (15 ml). After an hour, 1-bromohexane (130  $\mu\text{l}$ , 0.84 mmol) was added and the reaction mixture was stirred at room temperature for 24 hours. The resulting mixture was extracted with ammonium chloride solution and ethyl acetate. The combined organic layer ( $3 \times 20$  ml) was dried with anhydrous  $\text{Na}_2\text{SO}_4$ , concentrated under reduced pressure, and separated on a silica gel column using 25:75 ethyl acetate/hexane to afford 0.2 g of viscous brown liquid (76%).  $^1\text{H}$  NMR (300 MHz,  $\text{CDCl}_3$ ,  $\delta$ , ppm) 7.84 (s, 1H), 7.43 (dd,  $J = 1.15$  Hz, 3.6 Hz; 1H, Th-**H**), 7.35 (dd,  $J = 1.3$  Hz, 5.1 Hz; 1H, Th-**H**), 7.27 (dd,  $J = 1.1$  Hz, 4.1 Hz; 1H, Th-**H**), 7.04-7.13 (m, 3 H, Th-**H**), 4.02 (t,  $J = 7.23$  Hz, 2H, Ar-**CH**<sub>2</sub>), 1.48-1.53 (m, 2H, **CH**<sub>2</sub>), 1.15-1.25 (m, 6H, **CH**<sub>2</sub>), 0.81 (m, 3H, **CH**<sub>3</sub>);  $^{13}\text{C}$  NMR (75.4 MHz,  $\text{CDCl}_3$ ,  $\delta$ , ppm) 152.9, 147.3, 135.1, 135, 133.3, 127.5, 127.5, 127.3, 126.2, 124.4, 123.6, 117.1, 102.4, 46.38, 31, 30.2, 25.8, 22.2, 13.8; MS (EI)  $m/z$  (rel. intensity, M+) 373.1. Anal. Calcd. for  $\text{C}_{19}\text{H}_{20}\text{N}_2\text{S}_3$ : C, 61.25; H, 5.41; N, 7.52; S, 25.82. Found: C, 61.24; H, 5.49; N, 7.3; 25.59.

**5,7-Di(2-thienyl)-2-decyl-thieno[3,4-*d*]imidazole (T3):** Undecanoic acid (0.13 g, 0.7 mmol) and  $\text{POCl}_3$  (5 ml) were added to a reaction flask followed by diamine **3** (0.12 g,

0.43 mmol). The reaction mixture was allowed to stir at room temperature for 30 minutes and at reflux for five hours. The resulting mixture was cooled to room temperature, poured carefully into cold water, and basified (to pH ~9) with aqueous ammonia. The solution was then extracted with ethyl acetate and the combined organic layer (3 × 20 ml) was dried with anhydrous Na<sub>2</sub>SO<sub>4</sub>. Ethyl acetate was removed under reduced pressure and separated by silica column using 15:85 ethyl acetate/hexane mixture to yield 0.11 g of brown liquid (60%). <sup>1</sup>H NMR (300 MHz, acetone-d<sub>6</sub>, δ, ppm) 7.4-7.35 (m, 4H, Th-**H**), 7.07 (dd, *J* = 1.5 Hz, 3.6 Hz; 2H, Th-**H**), 2.81 (t, *J* = 7.56 Hz, 2H, N=C-**CH**<sub>2</sub>), 1.82-1.86 (m, 2H, **CH**<sub>2</sub>), 1.26 (m, 14H, **CH**<sub>2</sub>), 0.86 (t, *J* = 6.9 Hz, 3H, **CH**<sub>3</sub>); <sup>13</sup>C NMR (75.4 MHz, acetone-d<sub>6</sub>, δ, ppm) 166.5, 135.4, 127.7, 123.5, 122.9, 115.4, 31.6, 29.52, 29.2, 29.2, 29, 28.7, 28.5, 28.2, 22.2, 13.3. MS (ESI) *m/z* (rel. intensity, M+) 429.3, (rel. intensity, M-) 427.3. Anal. Calcd. for C<sub>23</sub>H<sub>28</sub>N<sub>2</sub>S<sub>3</sub>: C, 64.44; H, 6.58; N, 6.53; S, 22.44. Found: C, 64.73; H, 6.93; N, 6.42; 22.24.

**General synthesis of 5,7-di(2-thienyl)-2-arylthieno[3,4-*d*]imidazole (T4-T7) (Method A):**

Compound **3** (0.1 g, 0.36 mmol) was dissolved in 10 ml of ethanol under nitrogen atmosphere. Corresponding aryl aldehyde and *p*-benzoquinone (0.04 g, 0.37 mmol) were then added. The reaction mixture was stirred at 95 °C for 6 hours, and then allowed to cool. The ethanol was evaporated and the mixture was extracted using ethyl acetate. The combined organic layer (3 × 20 ml) was dried over anhydrous Na<sub>2</sub>SO<sub>4</sub>, concentrated under reduced pressure and separated on a silica column using ethyl acetate/hexane mixture to yield the target compounds.

**General synthesis of 5,7-di(2-thienyl)-2-arylthieno[3,4-*d*]imidazole (T4-T7) (Method B):**

Amine compound **3** (250 mg, 0.9 mmol) was dissolved in 5ml of acetonitrile under nitrogen atmosphere. Aryl aldehyde (0.45 mmol) was added followed by bromodimethyl sulfonium bromide (BDMS) (1.3 mmol). Reaction mixture was stirred for 4 hours at room temperature. After completion of reaction (as monitored by TLC), acetonitrile was evaporated and the crude mass was extracted with ethyl acetate. Organic layer was separated and dried with anhydrous Na<sub>2</sub>SO<sub>4</sub> and evaporated using rotary evaporator. Column chromatography of the residue over silica gel using 80:20 hexane / ethyl acetate as eluent afforded the target compounds in good yield (75 – 85%).

**5,7-Di(2-thienyl)-2-phenylthieno[3,4-*d*]imidazole (T4):** Dark green solid; (40% yield, method A and 81% yield, method B). <sup>1</sup>H NMR (300 MHz, acetone-*d*<sub>6</sub>, δ, ppm) 8.26 - 8.29 (m, 2H), 7.51 - 7.56 (m, 5H), 7.4 - 7.42 (d, 2H), 7.11 - 7.14 (m, 2H); <sup>13</sup>C NMR (75.4 MHz, acetone-*d*<sub>6</sub>, δ, ppm) 161.8, 135, 130.8, 130.4, 129.9, 129, 128.4, 127.7, 127, 123.8, 123.4; MS (ESI) *m/z* (rel. intensity, M<sup>+</sup>) 365.3, (rel. intensity, M<sup>-</sup>) 363.4. Anal. Calcd. for C<sub>19</sub>H<sub>12</sub>N<sub>2</sub>S<sub>3</sub>: C, 62.61; H, 3.32; N, 7.69; S, 26.39. Found: C, 62.43; H, 3.29; N, 7.6; S, 26.59.

**5,7-Di(2-thienyl)-2-(4-nitrophenyl)thieno[3,4-*d*]imidazole (T5):** Black solid; yield: (44% yield, by method A and 84% by method B). <sup>1</sup>H NMR (300 MHz, THF-*d*<sub>8</sub>, δ, ppm) 10.83 (s, 1H, N-**H**), 8.39 (dd, J = 10.53 Hz, 8.04 Hz, 4H, Ar-**H**), 7.61(d, 3.6 Hz, 1H, Th-**H**), 7.36-7.33 (m, 3H, Th-**H**), 7.08 (m, 2H, Th-**H**); <sup>13</sup>C NMR (75.4 MHz, THF-*d*<sub>8</sub>, δ, ppm) 160.2, 149.8, 149.1, 137, 136.9, 136.3, 136.1, 136, 130.6, 128.6, 125.6, 128.2, 124.9, 124.6, 124.5, 124.4, 124.3, 116.9, 104.8. MS (ESI) *m/z* (rel. intensity, M<sup>+</sup>) 410.5, (rel. intensity, M<sup>-</sup>) 408.4. Anal. Calcd for C<sub>19</sub>H<sub>11</sub>N<sub>3</sub>O<sub>2</sub>S<sub>3</sub>: C, 55.73; H, 2.71; N, 10.26; S, 23.49. Found: C, 55.42; H, 2.89; N, 10; S, 23.93.

**5,7-Di(2-thienyl)-2-(4-methoxyphenyl)thieno[3,4-*d*]imidazole (T6):** Green solid; yield: 38 mg (27% yield by method A and 77% by method B).  $^1\text{H}$  NMR (300 MHz, acetone- $d_6$ ,  $\delta$ , ppm) 8.23 (d,  $J = 8.88$  Hz, 2H), 7.6 (d,  $J = 3.73$  Hz, 1H, Th-**H**), 7.42-7.4 (m, 3H, Th-**H**), 7.15-7.01 (m, 4H, Th-**H** and Ar-**H**), 3.91 (s, 3H, O-**CH**<sub>3</sub>);  $^{13}\text{C}$  NMR (75.4 MHz, THF- $d_8$ ,  $\delta$ , ppm) 162.8, 136.7, 129.5, 128.4, 128.3, 128.2, 128.2, 124.1, 124, 123.8, 114.8. MS (ESI)  $m/z$  (rel. intensity, M<sup>+</sup>) 395.3, (rel. intensity, M<sup>-</sup>) 393.2 Anal. Calcd for C<sub>20</sub>H<sub>14</sub>N<sub>2</sub>OS<sub>3</sub>: C, 60.89; H, 3.58; N, 7.1; O, 4.06; S, 24.38. Found: C, 60.95; H, 3.61; N, 7.21; O, 3.96; S, 25.2.

**5,7-Di(2-thienyl)-2-(2-pyrido)thieno[3,4-*d*]imidazole (T7):** Red solid; yield: 70 mg (53% yield by method A and 73% by method B).  $^1\text{H}$  NMR (300 MHz, acetone- $d_6$ ,  $\delta$ , ppm) 11.46 (b, 1H, N-**H**), 8.72 (d,  $J = 4.77$  Hz, 1H, Py-**H**), 8.45 (d,  $J = 7.89$  Hz, 1H, Py-**H**), 8.03 (t,  $J = 7.1$  Hz, 1H, Py-**H**), 7.64 (d,  $J = 3.63$  Hz, 1H, Th-**H**), 7.58-7.53 (m, 2H), 7.47-7.41 (m, 2H), 7.16-7.12 (m, 2H);  $^{13}\text{C}$  NMR (75.4 MHz, CDCl<sub>3</sub>,  $\delta$ , ppm) 159.9, 149.1, 148, 137.1, 128.1, 127.8, 125.2, 124.4, 124, 123.4, 122.4, 122.3; MS (ESI)  $m/z$  (rel. intensity, M<sup>+</sup>) 366.3, (rel. intensity, M<sup>-</sup>) 364.6. Anal. Calcd for C<sub>18</sub>H<sub>11</sub>N<sub>3</sub>S<sub>3</sub>: C, 59.15; H, 3.03; N, 11.5; S, 26.32. Found: C, 59.77; H, 3.64; N, 10.59; S, 25.5.

## 6.3. Results and discussion

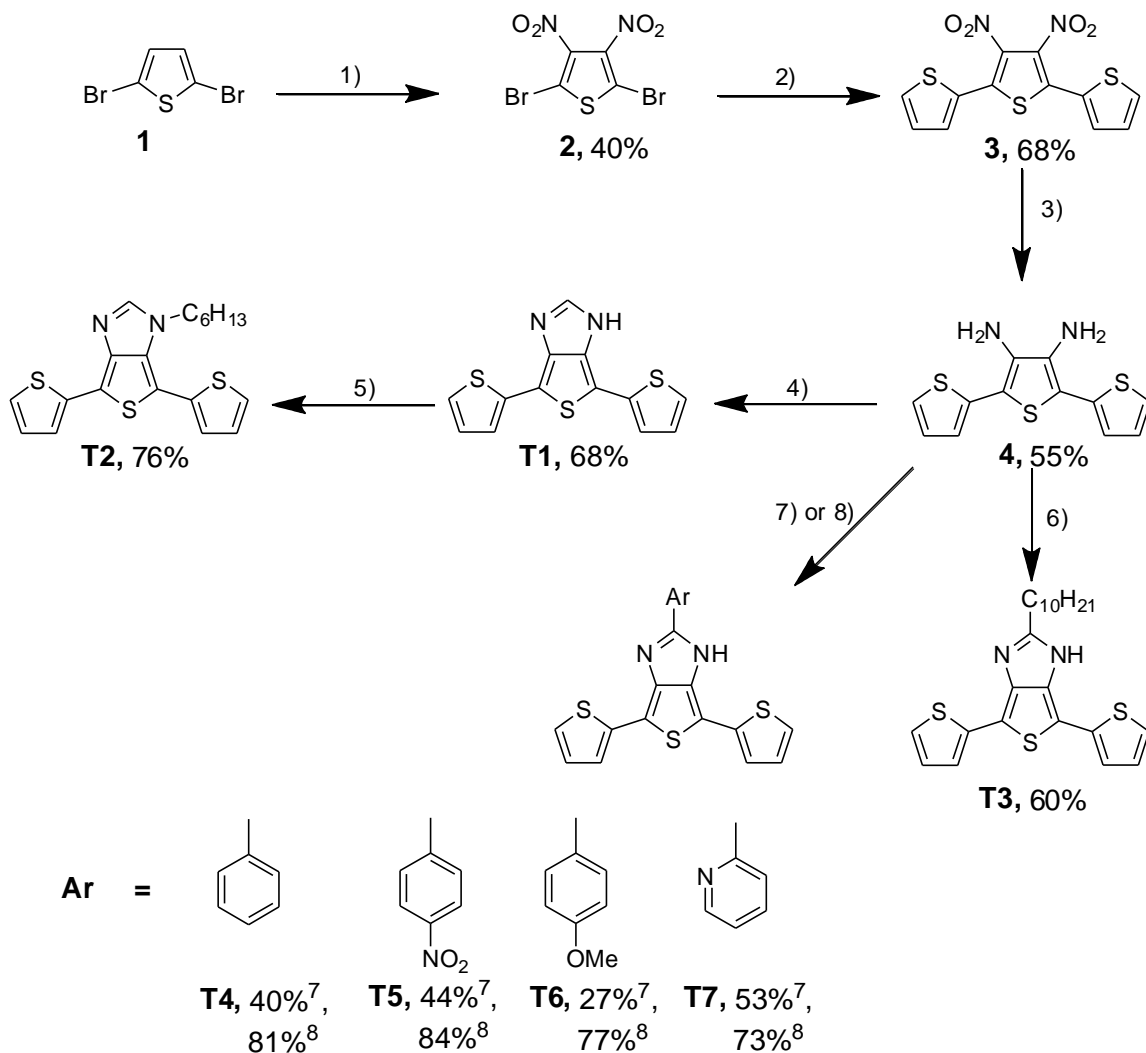
### 6.3.1. Synthesis

Thienoimidazole derivatives were synthesized starting from 2,5-dibromothiophene and the synthetic route is outlined in Scheme 6.1. 2,5-Dibromothiophene was nitrated with fuming nitric acid and fuming sulfuric acid following the literature procedure.<sup>22</sup> Suzuki coupling of 2,5-dibromo-3,4-dinitrothiophene with 2-thienylboronic acid gave 3',4'-dinitro-

2,2';5',2''terthiophene in 68% yield. The diamine **3** was prepared following the literature procedure with small modification.<sup>24</sup> The reduction of dinitro compound **2** was effected by tin in ethanol-hydrochloric acid to result in 3',4'-diamino-2,2';5',2''terthiophene in 55% yield. Thienoimidazoles are obtained by the reaction of diamine **3** with corresponding acid (in case of **T1** - **T3**) or aldehyde (in case of **T4** - **T7**). The parent compound **T1** was synthesized in good yield as a pale yellow-green solid by refluxing diamine (**4**) in formic acid, in presence of hydrochloric acid. The parent compound **T1** was alkylated with *n*-hexylbromide to afford *N*-hexyl derivative **T2** in 76% yield. The *C*-alkyl derivative **T3** was synthesized by heating undecanoic acid and phosphoryl chloride to afford viscous brown liquid in 60% yield. Aryl substituted thienoimidazole derivatives (5,7-di(2-thienyl)-2-arylthieno[3,4-*d*]imidazole) **T4** - **T7** were prepared by refluxing diamine **4** with corresponding aldehyde and *p*-benzoquinone in ethanol (39 - 53% yield). The poor stability of the diamine **3** at higher temperature leading to its decomposition was attributed to the lower yield of the reaction.<sup>22</sup> Carrying out the reactions at milder conditions (reaction at room temperature) will improve the yield, but the above reaction fails to yield the desired product at lower temperature. In order to carry out the reaction under milder condition, condensation was carried out in presence of bromodimethylsulfonium bromide (BDMS). The BDMS is a simple versatile reagent used to carry out variety of organic transformations.<sup>25</sup> Recently, benzimidazoles are synthesized from *o*-phenylenediamine and aldehyde using BDMS.<sup>26</sup> The BDMS is believed to facilitate oxidative dehydrogenation of cyclic intermediate at room temperature to form benzimidazole. Utilizing this milder method, thienoimidazole oligomers **T4** - **T7** were synthesized from diamine **3** by the treatment with aryl aldehyde

and BDMS at room temperature under nitrogen atmosphere. The reaction occurred smoothly within 4 hours with the good yields of 70 – 85%.

**Scheme 6.1.** Synthesis of target thienoimidazole based oligomers (**T1** - **T7**)<sup>a</sup>

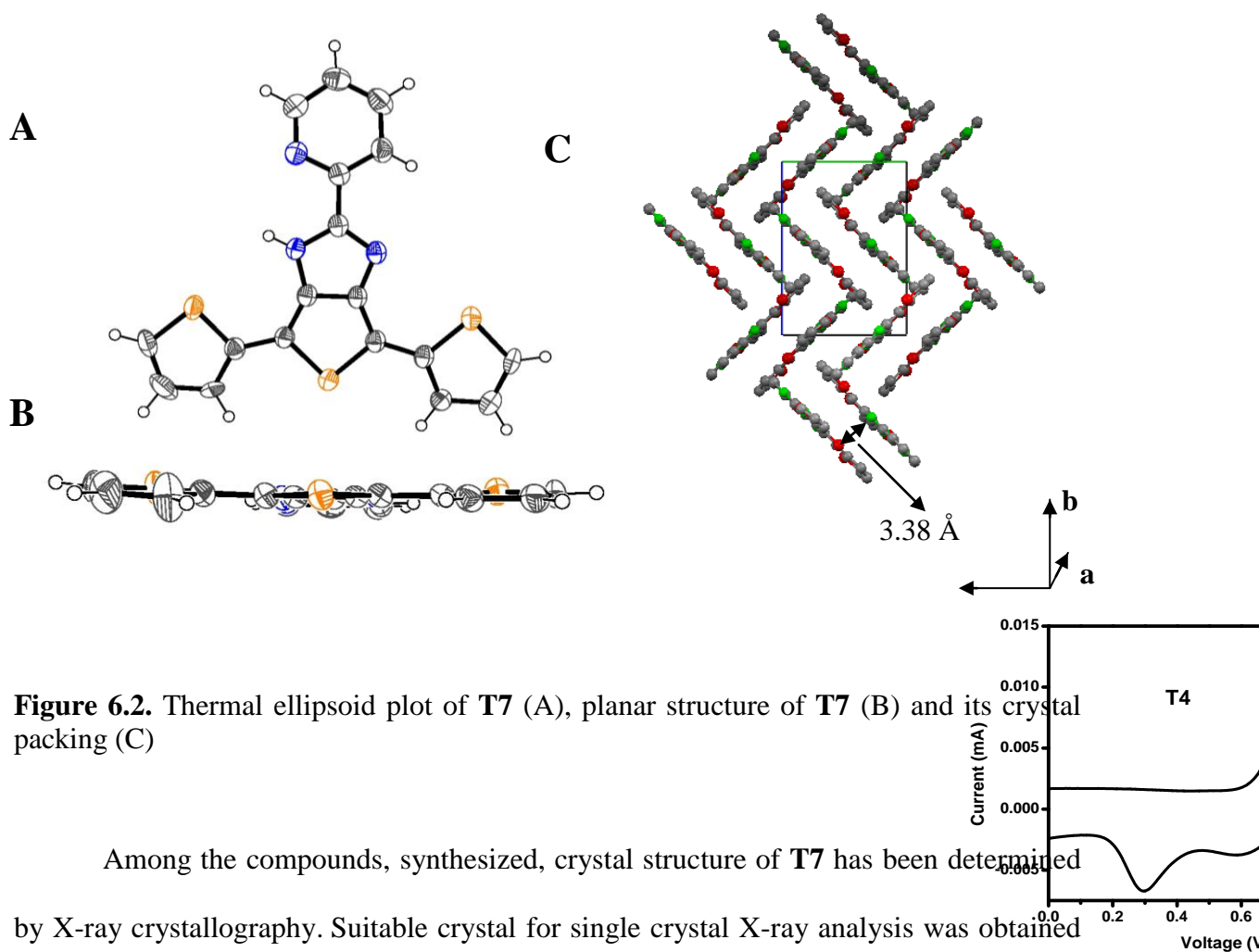


<sup>a</sup>Reagents and conditions. 1) Fuming sulfuric acid, fuming nitric acid, 3h. 2) 2-thiopheneboronic acid, K<sub>2</sub>CO<sub>3</sub> (aq), Pd(PPh<sub>3</sub>)<sub>4</sub>, THF, 75 °C, 12 h. 3) Sn, HCl, Ethanol, rt, 24 h. 4) HCOOH, HCl, Ethanol, reflux, 4 h. 5) C<sub>6</sub>H<sub>13</sub>Br, NaOH, CH<sub>3</sub>CN, rt, 24 h. 6) C<sub>10</sub>H<sub>21</sub>COOH, POCl<sub>3</sub>, reflux, 5 h. 7) aryl aldehyde, *p*-benzoquinone, ethanol, reflux, 6 h. 8) aryl aldehyde, BDMS, CH<sub>3</sub>CN, rt, 4 h.



The newly synthesized compounds are characterized by  $^1\text{H}$ ,  $^{13}\text{C}$  NMR spectroscopy, mass spectrometry, elemental analysis and single-crystal X-ray diffraction. The synthesized compounds are soluble in common organic solvents such as ethyl acetate, chloroform and tetrahydrofuran. All compounds are stable and stored in air for months without any decomposition.

### 6.3.2. Single crystal XRD



Among the compounds, synthesized, crystal structure of **T7** has been determined by X-ray crystallography. Suitable crystal for single crystal X-ray analysis was obtained by slow evaporation of **T7** from a mixture of chloroform and diethyl ether. **T7** was obtained as brown prism, to have monoclinic lattice with unit cell parameters of  $a = 13.0639(7) \text{ \AA}$ ,  $b = 9.4536(5) \text{ \AA}$ ,  $c = 13.8401(7) \text{ \AA}$  and  $\beta = 108.5220(10)^\circ$  and the

space group of P2(1)/n. Though the terminal thiophenes are disordered, crystal structure was resolved to a R1-value of 4% and goodness of fit (GOOF) of 1.034. As shown in Figure 6.2, **T7** is not strictly planar and thiophene rings are arranged in an anti-parallel conformation. In contrast to 1,3-di(2-thienyl)benzo[*c*]thiophene, no steric repulsion is observed between H-atom of imidazole with adjacent thiophene ring.<sup>27</sup> The torsional angles between thiophene and thienoimidazole units were found to be 5.41° and 3.14° and that of thienoimidazole and pyridine ring is 1.31°. These torsional angles are lesser compared to that of 1,3-di(2-thienyl)thieno[3,2-*b*]pyrazine (6.5° and 11.6°).<sup>17</sup> Shorter C-C distance between thiophene units (1.44 Å) and between imidazole-pyridine units (1.466 Å) illustrates the extended conjugation between the aryl units.

In the solid state, molecules arrange themselves in sandwich herringbone packing along *a*-axis with plane-to-plane distance of 3.38 Å between the dimer. These dimers are slipped with respect to their molecular plane and are anti co-facially packed. The molecular dimers in this molecule do not show any (S⋯S) contacts between chalcogen atoms. But like  $\alpha$ -terthiophene, **T7** show short S⋯S contact of 3.63 Å between sulfur atoms of edge to face overlapped thiophene units.<sup>28</sup> The edge to face overlapped molecules are arranged with a near perpendicular (herringbone) angle of 82.8°.

### 6.3.3. Absorption properties

The absorption spectrum of all the oligomers (**T1** - **T7**) recorded in THF is shown in Figure 6.3.

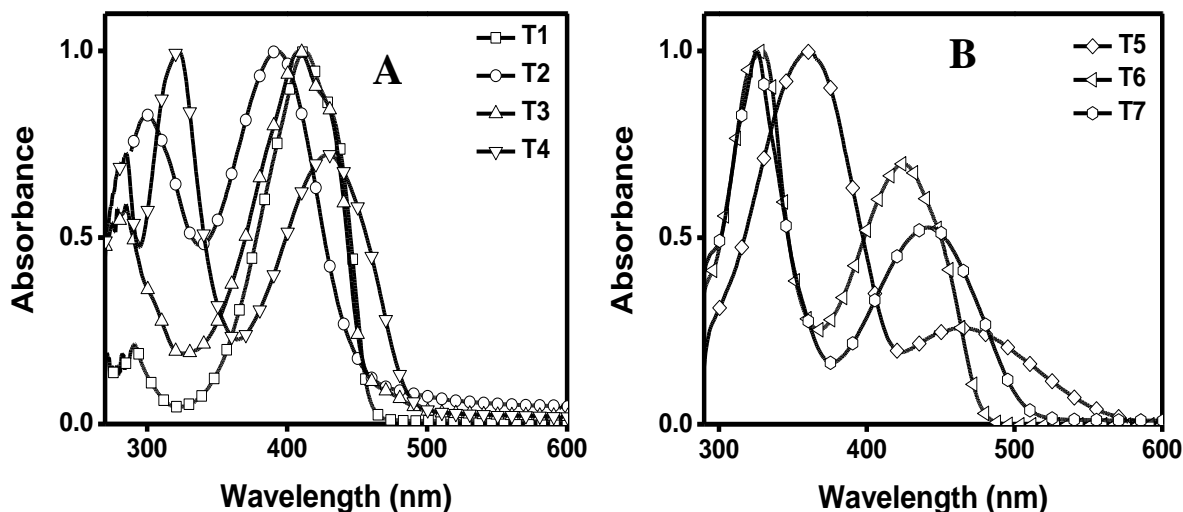


**Figure 6.3.** Normalized absorption spectra of dithienothienoimidazole (**T1** - **T7**) recorded in THF

It is observed that the oligomers (unsubstituted and with alkyl substituents) **T1** - **T3** showed two prominent absorption peaks. The high intensity peak with absorption maxima in the range of 390 - 415 nm and a low intensity peak centered around 278 nm. These high intensity bands corresponds the  $\pi$ - $\pi^*$  transitions of the extended oligomers. In the case of oligomers with an aryl substituents (**T4** - **T6**) an additional peak in the range of 313 - 328 nm is observed, which may be due to the  $\pi$ - $\pi^*$  transitions of thienoimidazole unit (central unit). It should be noted that in all the aryl substituted oligomers these are the peaks with higher molar extinction coefficient. However, in oligomers **T7** the absorption corresponds to thienoimidazole moiety was not observed which indicates the extensive conjugation in these systems. Compared to the parent oligomer **T1**, the alkyl substituted oligomers **T2** and **T3** suffers a blue shift in the absorption (20 and 4 nm respectively). The *N*-alkylated isomer **T2** suffers a comparatively higher blue shift due to the disruption of planarity caused by the steric hindrance of alkyl

group. But the aryl substituted oligomers **T4** - **T7** shows a red shift (10 - 55 nm) which may be due to the electron withdrawing nature of the phenyl ring which increases the electron delocalization along the back bone. This bathochromic shift may also be due to the charge transfer (CT) in these substituted thienoimidazole derivatives. It is noteworthy that the absorption maxima of all these dithienyl thienoimidazole are in between terthiophene (354 nm)<sup>29</sup> and dithienyl thienopyrazine (529 nm).<sup>17</sup>

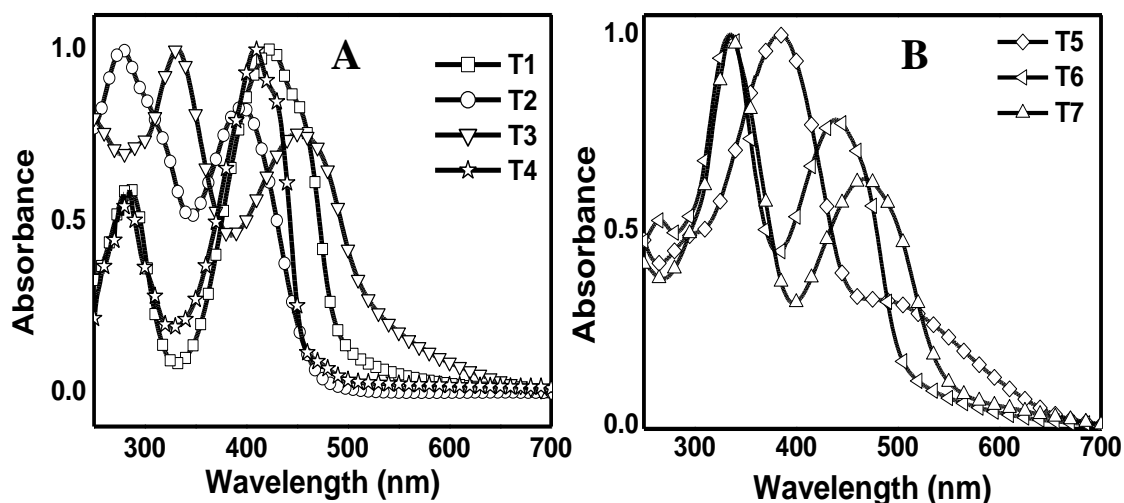


**Figure 6.4.** Thin film optical absorption spectra of dithienothienoimidazole (**T1** - **T7**) recorded in solid state

Figure 6.4 represents the solid-state absorption spectra of all oligomers (**T1** - **T7**). As a regular trend, in film state the absorption maxima are red shifted compared to that in solution for all oligomers. **T3** oligomer shows almost same  $\lambda_{\text{max}}$  in solution and in solid state.

### 6.3.4. Emission properties

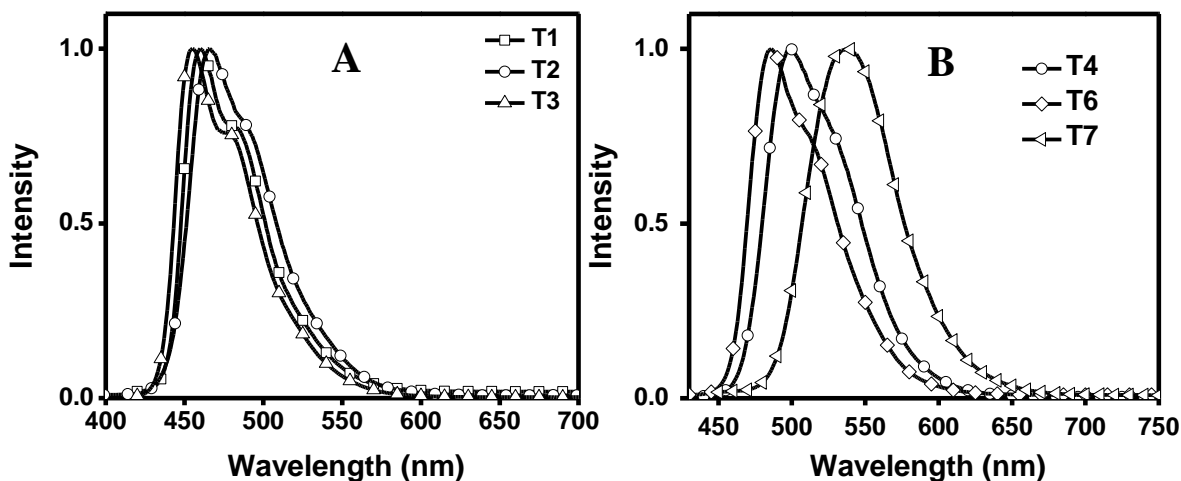


**Figure 6.5.** Normalized emission spectra of dithienothienoimidazole (**T1 - T7**) recorded in THF

Figure 6.5 shows the emission spectra of all oligomers obtained in THF solution. It is observed that these spectra were red shifted compared to terthiophene (407, 426 nm).<sup>29a</sup> This bathochromic shift increases with increase in electron-accepting nature of the substituents. The phenyl substituted moiety (**T4**) emits in the green region with an emission maximum at 500 nm. But the pyridyl substituted oligomer (**T7**) has orange red emission with maxima at 553 nm. All other oligomers (**T1 - T3** and **T6**) showed a blue-green emission with maxima in the range of 460 - 486 nm. In the case of nitro substituted oligomers (**T5**) very weak / no fluorescence was observed. This may be due to the efficient non-radiative decay pathways such as charge transfer.

Unlike the other members in the series pyridine substituted derivative (**T7**) exhibit a large Stoke's shift of 113 nm. It is also observed that the oligomer **T7** exhibit solvatochromic behavior with the emission maxima varies up to 15 nm depending on the nature of the solvent (Figure 6.6). Such higher Stoke's shift with solvent dependent

emission indicates the excited state intramolecular charge transfer (ICT) between pyridine (acceptor) and thiophene unit (donor). The solution state quantum yield (QY) of all oligomers is measured in THF. It is interesting to note that the unsubstituted dithienothienoimidazole (**T1**) exhibit a quantum efficiency ( $\Phi_F$ ) of 35% much higher compared to terthiophene in various solvents (benzene, dioxane, ethanol, acetonitrile, and methylcyclohexane), which are in the range of 5 - 7%.<sup>29a</sup> But **T2** and **T3** exhibit a reduced efficiency of 21% which is due to the increase in the deactivation pathways like internal conversion owing to the presence of alkyl chains.<sup>30</sup> It is observed that the  $\Phi_F$  values of oligomers decreases with increasing the electron-accepting strength of the substituents (see Table 6.1). A very high quantum yield of 51% was observed for **T6** which is one of the highest values reported for any terthiophene analogue. Benzo[*c*]thiophene based terthienyl system was reported to have a solution state quantum yield of 57% highest value for any thiophene based system.<sup>27</sup> The quantum yield reduces gradually to 31% for **T4** and the lowest of 7% for **T7**.

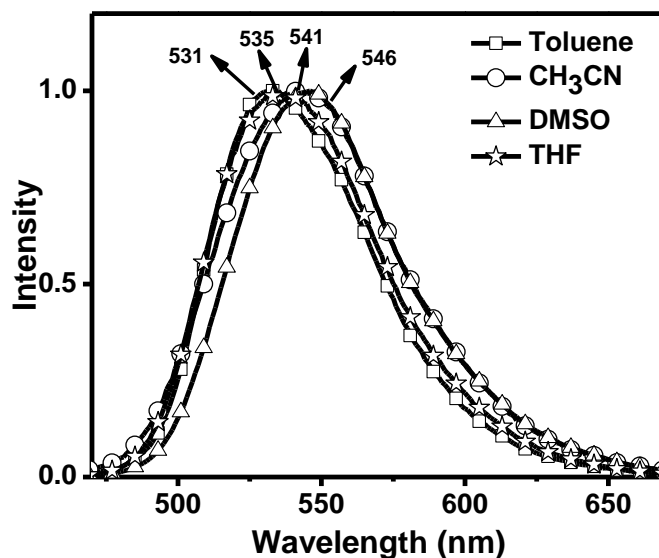


**Figure 6.6.** Emission spectra of **T7** oligomer in different solvents

The relaxation of the excited state can be strongly affected by the quenching of exciton by non radiative trapping centers and formation of excimers or charge transfer complex.<sup>31</sup> This will reduce the photoluminescence (PL) quantum yield of the materials. So in general if this non radiative pathway is not very efficient the PL QY will be high. Probably in **T5** this non radiative decay is prominent, so no emission is observed and in the case of **T6** it is weak and hence it is highly fluorescent. The complete photophysical data of all the oligomers are depicted in Table 6.1.

**Table 6.1.** Photophysical properties of dithienothieno[3,4-*d*]imidazole (**T1** - **T7**)

Compound	$\Phi_F$ (%)	$\lambda_{\text{abs}} / \text{nm}$ (THF)	$\lambda_{\text{abs}} / \text{nm}$ (Solid)	$\lambda_{\text{em}} / \text{nm}$ (THF)
<b>T1</b>	35.0	412.6	423	460
<b>T2</b>	21.0	392	396	466
<b>T3</b>	21.0	408.5	408.5	460
<b>T4</b>	31.0	430	452	500
<b>T5</b>	nd	467*, 360	491*, 384	nd
<b>T6</b>	51.6	425	439	486
<b>T7</b>	7.0	422	468	535
<b>Terthiophene<sup>a</sup></b>	8.0 <sup>⊥</sup>	349 <sup>⊥</sup>	-	429, 408 <sup>⊥</sup>
<b>1,3-di(2-thienyl)benzo[c]thiophene<sup>b</sup></b>	57 <sup>⊥</sup>	426 <sup>⊥</sup>	-	550, 490 <sup>⊥</sup>
<b>1,3-di(2-thienyl)thieno[3,4-b]pyrazine<sup>c</sup></b>	-	529 <sup>†</sup>	-	-

\* Shoulder peak, <sup>⊥</sup> Recorded in *n*-hexane. <sup>†</sup> Recorded in chloroform. nd- not determined.

<sup>a</sup>Ferraris, J. P.; Skiles, G. D. *Polymer* **1987**, 28, 179. Ferraris, J. P.; Andrus, R. G.; Hrnecir, D. C. *J. Chem. Soc. Chem. Commun.* **1989**, 1318. <sup>b</sup>Bäuerle, P.; Götz, G.; Emerle, P.; Port, H. *Adv. Mater.* **1992**, 4, 546. <sup>c</sup>Kitamura, C.; Tanaka, S.; Yamashita, Y. *Chem. Mater.* **1996**, 8, 570.

In solid state no fluorescence was observed for all oligomers which may be due to the  $\pi$  stacking of conjugated molecules in solid state which leads to self-quenching of excitons.<sup>29</sup>

### 6.3.5. Acid-Base sensing

It is observed that the absorption and emission spectra of dithienothieno[3,4-*d*]imidazoles were influenced by the addition of acid / base. All oligomer suffers a blue shift in absorption (4 to 26 nm) by the addition of CF<sub>3</sub>COOH (TFA) which may be due to the protonation of imine nitrogen of imidazole unit. However, in alkaline medium (in NaOH), except in *N*-alkylated oligomer (**T2**) the absorption bands of all other oligomers were red shifted (18 - 28 nm) compared to the absorption band in THF. This may be due to the deprotonation of imidazole moiety. Though TFA has marginal effect on the photoluminescence of oligomers, NaOH imparts a significant red shift (~ 20 nm) (Figure 6.7). The spectral characteristics of all the oligomers obtained by the addition of TFA and NaOH in THF are depicted in Table 6.2. The possible reaction taking place by the addition of sodium hydroxide and trifluoroacetic acid is indicated in Scheme 6.2.

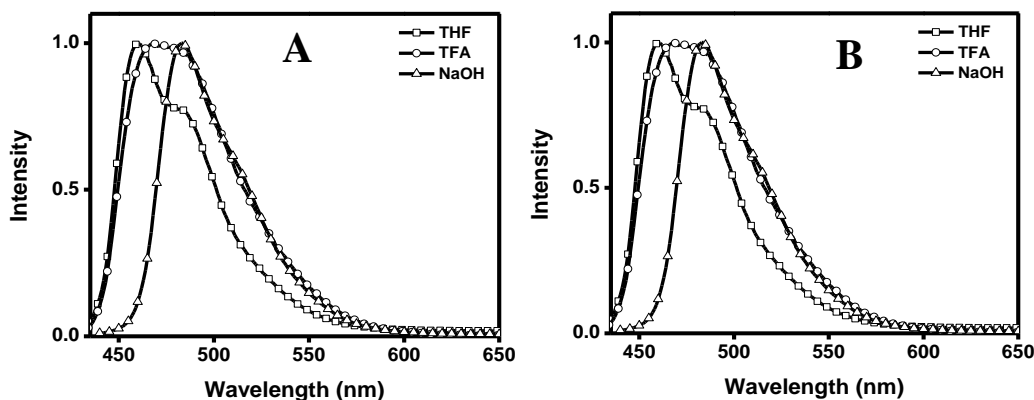


**Figure 6.7.** Absorption (A) and emission (B) spectra of **T1** upon addition of acid and base



**Scheme: 6.2.** Proposed reaction of **T1** with sodium hydroxide and trifluoroacetic acid

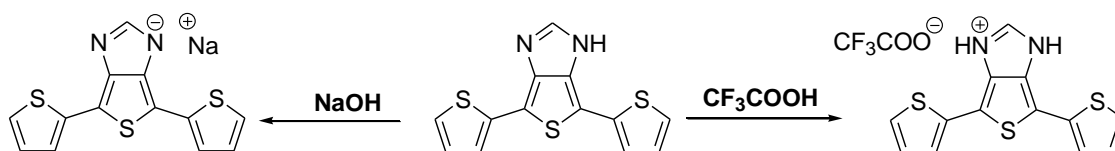


**Table 6.2.** The absorption and emission maxima of dithienothieno[3,4-*d*]imidazoles upon addition of  $\text{CF}_3\text{COOH}$  and  $\text{NaOH}$  in THF

Compound	$\lambda_{\text{abs}} / \text{nm}$			$\lambda_{\text{em}} / \text{nm}$		
	THF	TFA	NaOH	THF	TFA	NaOH
<b>T1</b>	412.6	402	434	460	468	484
<b>T2</b>	392	385	385	466	480	463
<b>T3</b>	408.5	402	428	460	455	499
<b>T4</b>	430	425	454	500	499	514
<b>T5</b>	360, 467*	354, 462*	396.5, 498*	nd	nd	nd
<b>T6</b>	425	406	446	486	485	506
<b>T7</b>	422	396	450	535	535	553

\* Shoulder peak. nd - not determined.

### 6.3.6. Electrochemical properties

Cyclic voltammetry of oligomers **T1** - **T7** were recorded using Pt working electrode in dichloromethane with 0.1 M *n*-Bu<sub>4</sub>NPF<sub>6</sub> as supporting electrolyte. Cyclic voltammogram of all oligomers are represented in Figure 6.8. All oligomers showed irreversible oxidation peaks with peak potential in the range of 0.8 – 1.0 V vs Ag/ AgCl which is less compared to terthiophene (1.08 V).<sup>32</sup> Among the oligomers *N*-alkyl derivative **T2**, exhibits highest oxidation potential of 0.94 V. When compared to structurally related compounds, the oxidation potential of dithienothienoimidazole oligomers is in between that of 1,3-di(2-thienyl)benzo[*c*]thiophene (0.64 V)<sup>33</sup> and 1,3-di(2-thienyl)thieno[3,4-*b*]pyrazine (1 V).<sup>34</sup> All substituted imidazoles except methoxy substituted **T6** are observed at higher potentials than the parent oligomer **T1**. Lower oxidation potential of **T6** is due to the electron-donating ability of methoxy group. HOMO energy levels are calculated from oxidation onset potential using the empirical formula  $E_{\text{HOMO}} = - (E_{\text{ox}} + 4.38) \text{ eV}$ .<sup>35</sup> LUMO energy levels are calculated from HOMO energy level and bandgap, calculated from the absorption onset of UV-vis spectra. The HOMO and calculated LUMO energy levels are summarized in Table 6.3. HOMO levels of **T1** - **T7** were in the range of -5.02 to -5.19 eV from vacuum level. HOMO energy level of **T2** is lower compared to **T1**, which suggests that *N*-alkylation of imidazole nitrogen improves the stability of thienoimidazole system.

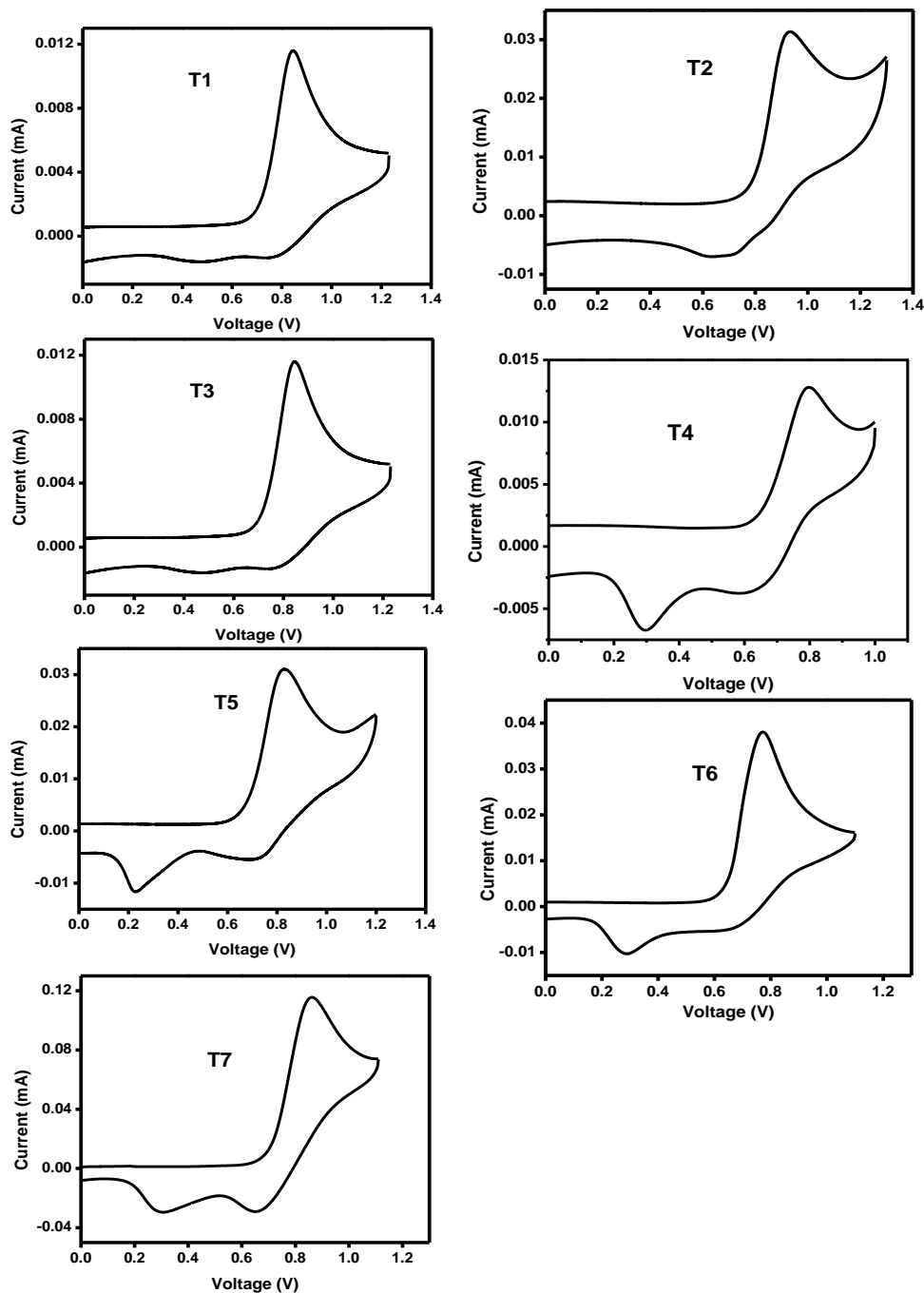


**Figure 6.8.** Cyclic voltammogram of dithienothieno[3,4-*d*]imidazole oligomers (T1 - T7) in dichloromethane containing 0.1M *n*-Bu<sub>4</sub>NPF<sub>6</sub> as supporting electrolyte at a scan rate of 100 mV s<sup>-1</sup>

**Table 6.3.** Electrochemical properties of dithienothieno[3,4-*d*]imidazole oligomers (T1 - T7)

Compounds	E <sup>a</sup> <sub>oxid</sub> (V)	E <sub>dedoping</sub> (V)	E <sup>a</sup> <sub>onset</sub> (V)	HOMO level <sup>b</sup> (eV)	Optical Bandgap <sup>c</sup> (eV)	LUMO level <sup>d</sup> (eV)
T1	0.82	0.73, 0.44	0.67	-5.05	2.7	-2.37
T2	0.94	0.67	0.79	-5.17	2.73	-2.46
T3	0.82	0.75, 0.4	0.65	-5.03	2.7	-2.35
T4	0.8	0.61, 0.3	0.62	-5.0	2.54	-2.48
T5	0.83	0.72, 0.23	0.68	-5.06	2.18	-2.9
T6	0.77	0.67, 0.29	0.63	-5.01	2.59	-2.44
T7	0.86	0.66, 0.29	0.68	-5.06	2.55	-2.53
Terthiophene <sup>I</sup>	1.08 <sup>e</sup>	-	-	-	-	-
1,3-di(2-thienyl)benzo[ <i>c</i> ]thiophene <sup>II</sup>	0.64 <sup>e</sup>	-	-	-	-	-
1,3-di(2-thienyl)thieno[3,4- <i>b</i> ]pyrazine <sup>III</sup>	0.99 <sup>e</sup>	-	-	-	-	-

<sup>I</sup>Ferraris, J. P.; Skiles, G. D. *Polymer* **1987**, 28, 179. Ferraris, J. P.; Andrus, R. G.; Hrcir, D. C. *J. Chem. Soc. Chem. Commun.* **1989**, 1318. <sup>II</sup>Bäuerle, P.; Götz, G.; Emerle, P.; Port, H. *Adv. Mater.* **1992**, 4, 546. <sup>c</sup> Kitamura, C.; <sup>III</sup>Tanaka, S.; Yamashita, Y. *Chem. Mater.* **1996**, 8, 570.

<sup>a</sup>Potentials (vs Ag/AgCl) calculated from cyclic voltammetry: 0.1 M Bu<sub>4</sub>NPF<sub>6</sub> in acetonitrile, Pt as working electrode under the scan rate of 100 mVs<sup>-1</sup>. <sup>b</sup> Calculated using the relationship E<sub>HOMO</sub> = -(E<sup>oxi</sup><sub>onset</sub> + 4.38) eV.<sup>35</sup> <sup>c</sup>Calculated from absorption onset wavelength. <sup>d</sup> Derived from optical bandgap and HOMO. <sup>e</sup>Potential values are corrected with respect to Ag/AgCl electrode.

### 6.3.7. Ionochromic effect of oligomers

Thiophene based oligomeric sensors are interesting since they can be easily polymerized which have wider applications. Pyridoimidazoles are ligands which are well known to complex with transition metals.<sup>36</sup> Owing to good complexing ability of the pyridine nitrogen and imidazolyl nitrogen, **T7** was expected to show responses to metal ions. Ionochromic effect of **T7** was studied with aliquots of metal salts like  $\text{Co}^{3+}$ ,  $\text{Fe}^{3+}$ ,  $\text{Ni}^{2+}$ ,  $\text{Cu}^{2+}$ ,  $\text{Zn}^{2+}$ ,  $\text{Pd}^{2+}$  and  $\text{Cd}^{2+}$  (as acetates) into a THF solution of **T7**. There was an apparent color change upon addition of  $\text{Zn}^{2+}$ ,  $\text{Cu}^{2+}$  and  $\text{Ni}^{2+}$ . Upon addition of  $\text{Cu}^{2+}$ , **T7** turns brown in color, with  $\text{Ni}^{2+}$  turns orange red and with  $\text{Zn}^{2+}$  color was pale orange red. Figure 6.9 represents the photograph of **T7** in solution without the metal ions and with  $\text{Ni}^{2+}$ ,  $\text{Cu}^{2+}$  and  $\text{Zn}^{2+}$  ions.

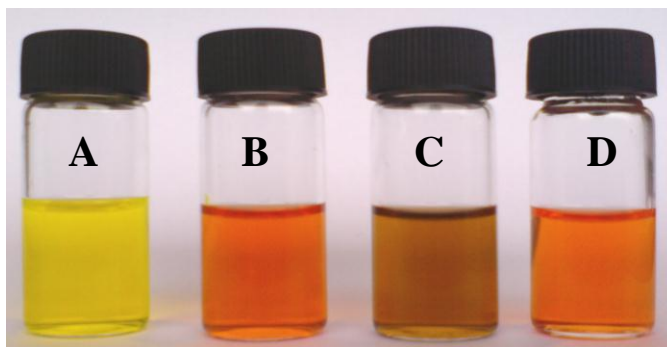


**Figure 6.9.** Visual features of **T7** (A) in THF upon addition of  $\text{Ni}(\text{OAc})_2$  (B),  $\text{Cu}(\text{OAc})_2$  (C) and  $\text{Zn}(\text{OAc})_2$  (D). (**T7** and salt concentrations are  $2.2 \times 10^{-5}$  M and  $10 \times 10^{-3}$  M)

The color changes are attributed to the formation of metal complexes due to the presence of (pyridyl) imidazole unit in **T7**. Upon titration of **T7** with metal salts, a decrease in absorbance maxima accompanied with a shift to longer wavelength is observed

[Figure 6.10(A - C)]. In case of Ni(II) and Cu(II) the shift is higher ( $\Delta\lambda_{\text{max}} = 20 - 38 \text{ nm}$ ) indicating a stronger binding compared to Zn(II) ( $\Delta\lambda_{\text{max}} = 5 - 8 \text{ nm}$ ). Three sharp isobestic points was observed ( $\lambda = 468, 400 \text{ and } 336 \text{ nm}$ ) for all the above mentioned metal ions indicating the formation of a new species out of **T7**.

It is also observed that the addition of metal acetates quenched the fluorescence of oligomers due to chelation enhancement of quenching (CHEQ) between the metal ion and **T7**.<sup>37</sup> There are two types of quenching processes, static and dynamic quenching. Static quenching is due to ground-state complexation and dynamic quenching resulting due to interaction of quencher with excited state species. In this case, static quenching is resulted due to complexation of metal ions with **T7**, which results in new absorption peaks and energy transfer process that favors nonradiative decay pathways. The quenching rate constant ( $K_{\text{sv}}$ ) was calculated using the Stern-Volmer relation.<sup>38</sup> Figure 6.10 (D - F) represent the change in emission spectra upon addition of copper acetate and the corresponding Stern-Volmer plots are represented in the inset of Figure 6.10(D - F).  $K_{\text{sv}}$  values were determined from linear Stern–Volmer plots and was found to be  $2.5 \times 10^5 \text{ M}^{-1}$  for  $\text{Ni}^{2+}$ ,  $1.6 \times 10^5 \text{ M}^{-1}$  for  $\text{Cu}^{2+}$  and  $3.1 \times 10^4 \text{ M}^{-1}$  for  $\text{Zn}^{2+}$ . It should be noted that the  $K_{\text{sv}}$  for  $\text{Zn}^{2+}$  is one order magnitude lower than that for  $\text{Cu}^{2+}$  and  $\text{Ni}^{2+}$ . It is observed that  $\text{Pd}^{2+}$  gives a color change with a long time delay (60 minutes) which may be due to its relatively larger size. It is noteworthy that the three metal ions ( $\text{Zn}^{2+}$ ,  $\text{Cu}^{2+}$  and  $\text{Ni}^{2+}$ ) responded with a sharp color change which is easily distinguishable from each other. It can be concluded that the divalent metal ion with four coordinate geometry having appropriate ionic size is the suitable candidate to complexes with **T7**.

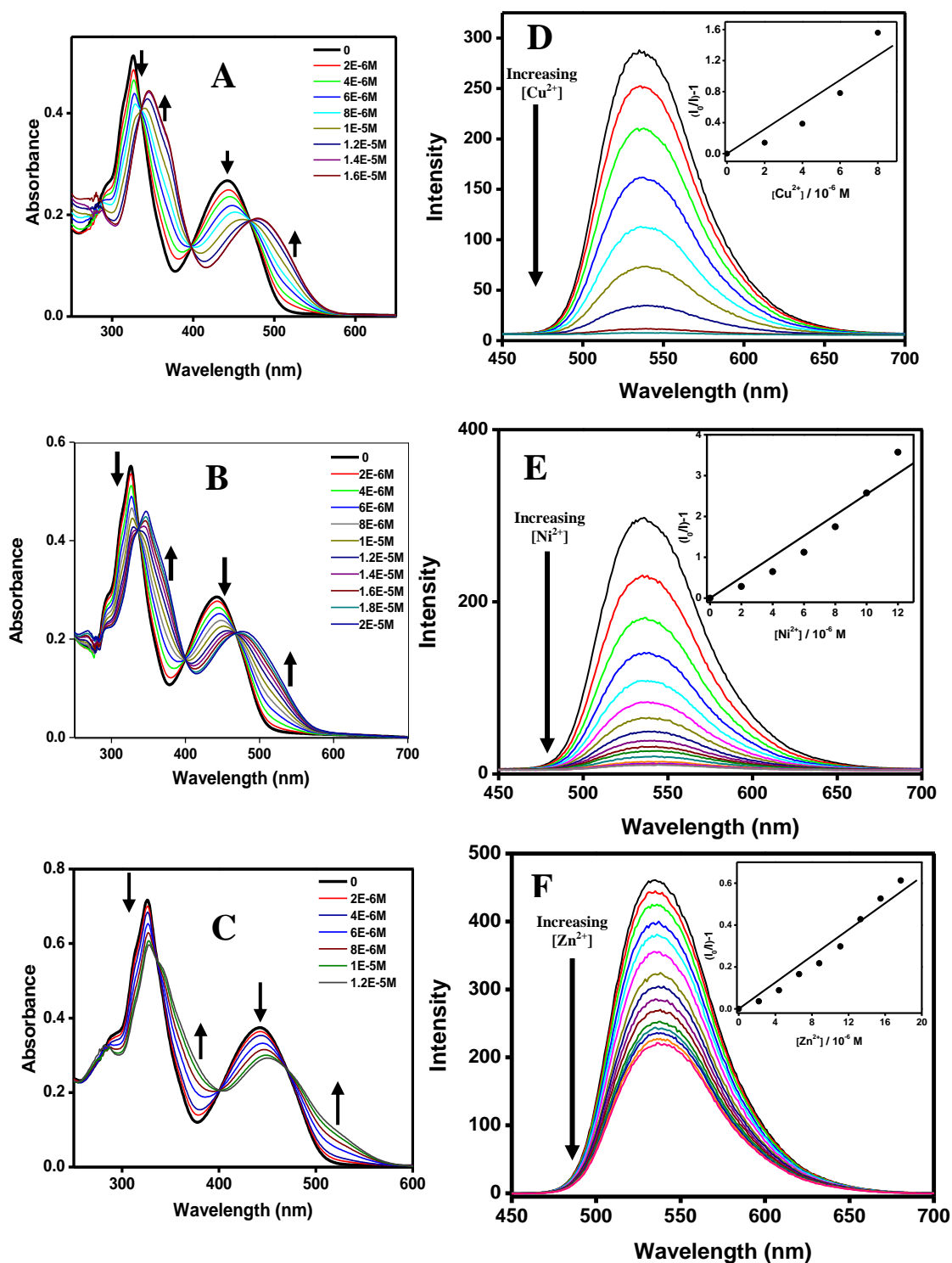


**Figure 6.10.** Absorption spectra of the spectrophotometric titration of solution of **T7** ( $2.2 \times 10^{-5}$  M) with metal salts ( $1 \times 10^{-2}$  M) Cu<sup>2+</sup> (A), Ni<sup>2+</sup> (B), Zn<sup>2+</sup> (C) in THF. The fluorescence emission spectra of **T7** in THF with successive addition of Cu<sup>2+</sup> (D), Ni<sup>2+</sup> (E), Zn<sup>2+</sup> (F). The inset of (D, E and F) is the Stern–Volmer plot of linear range in the low quencher concentration regime

### 6.3.8. Amino acid sensing

Recently, Li *et al*, reported an indirect method for detecting  $\alpha$ -amino acids using conjugated polymers.<sup>39</sup> The  $\text{Cu}^{2+}$  was used to quench the fluorescence of conjugated polymers, which was recovered upon the addition of  $\alpha$ -amino acids due to the complexation of  $\text{Cu}^{2+}$  with amino acids. As the fluorescence of pyrido-imidazole compound (**T7**) was quenched by the addition of metal ions ( $\text{Ni}^{2+}$ ,  $\text{Cu}^{2+}$  and  $\text{Zn}^{2+}$ ), their potentiality towards amino acid sensing was also explored. As expected, upon addition of amino acids (cystine, proline, and tryptophan) to **T7**- $\text{Cu}^{2+}$  solution, the fluorescence of **T7** was turned-on, with the fluorescence intensity recovered up to 68%. Figure 6.11 represents the effect of addition of  $\text{Cu}^{2+}$  and  $\alpha$ -amino acids on the emission property of **T7**. Unlike the previous report (where  $\text{Cu}^{2+}$  was used) other metal ions like  $\text{Zn}^{2+}$  and  $\text{Ni}^{2+}$  are also utilized to sense amino acids by this indirect method. The **T7**- $\text{Ni}^{2+}$  complex showed the fluorescence recovery of about 40-50% (53% for cystine, 41% for tryptophan and 41% for proline), where as  $\text{Zn}^{2+}$  (69% for cystine, 56% for tryptophan and 63% for proline) showed the recovery of more than 60% similar to  $\text{Cu}^{2+}$  (68% for cystine, 58% for tryptophan and 67% for proline). Scheme 6.3 represents the turn-off and turn-on sensing behavior of **T7** with metal ions and amino acids respectively. The  $\text{Cu}^{2+}$  and  $\text{Zn}^{2+}$  complexed **T7** are efficient in sensing amino acids compared to  $\text{Ni}^{2+}$  complex and this may be due to the weaker interaction of  $\text{Ni}^{2+}$  with amino acid.



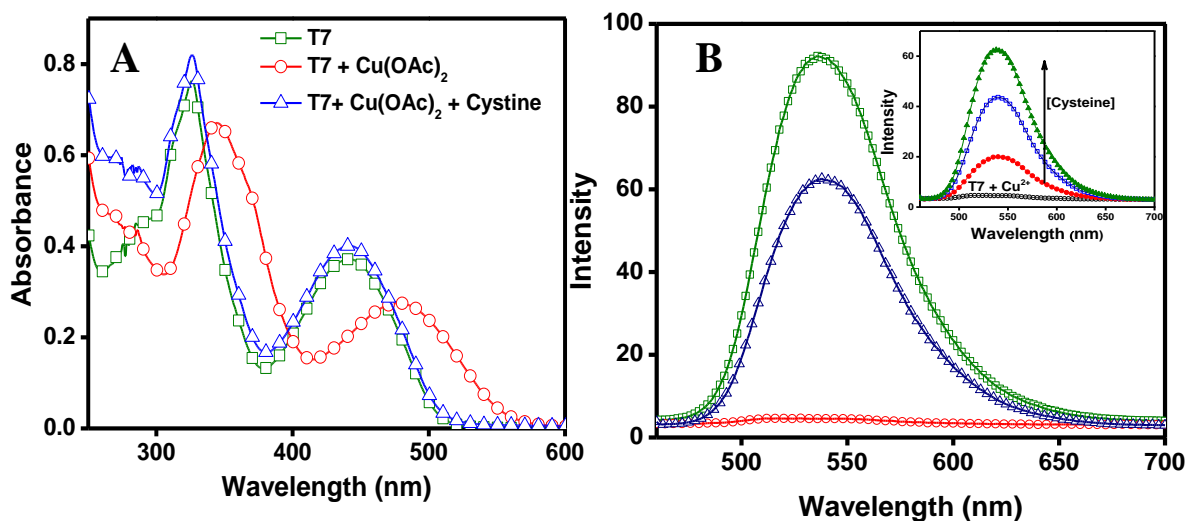
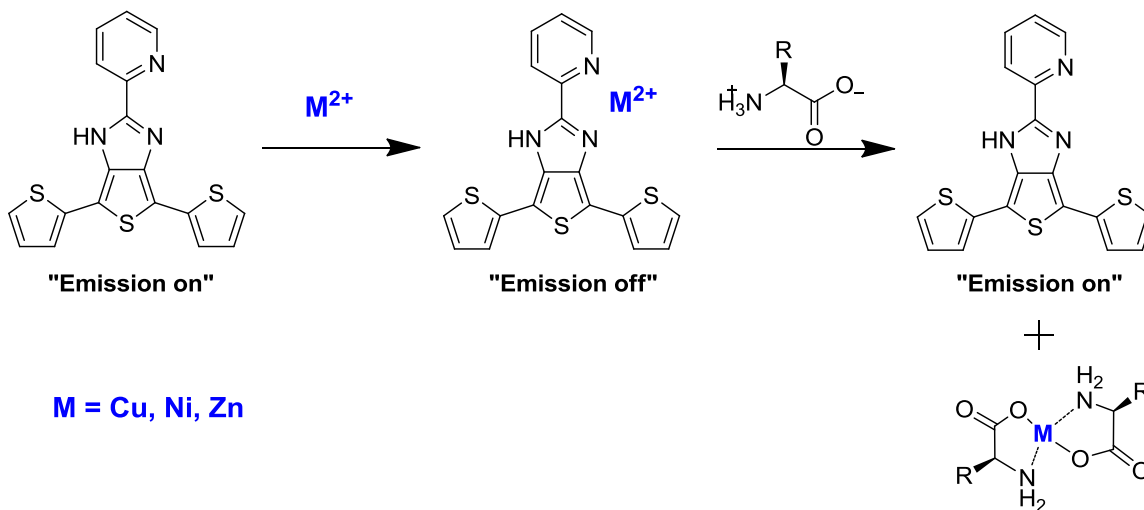


**Figure 6.11.** Change in Absorption (A) and Fluorescence spectra (B) of **T7** in THF ( $\square$ ) with the addition of  $\text{Cu}(\text{OAc})_2$  ( $\circ$ ) and with  $\text{Cu}(\text{OAc})_2$  and cystine ( $\Delta$ ). Inset: Fluorescence titration of **T7** containing  $\text{Cu}(\text{OAc})_2$  with cystine in THF

**Scheme 6.3.** Schematic representation of fluorescence turn-off and turn-on sensing behavior of **T7** towards metal ions and  $\alpha$ -amino acids



### 6.3.9. Charge mobility

The charge mobility of **T1** was measured by using conventional time-of-flight (TOF) technique. The TOF measurement system was composed of a pulsed nitrogen ( $\text{N}_2$ )

laser (Oriel 79074), a pulse generator (SRS-DG535), a DC voltage source (Kenwood PWR18-2), and a digital oscilloscope (Agilent-Infiniium, 1 GHz, 4 Gsa/s). The  $N_2$  laser with pulse width  $<4$  ns, and pulse repetition rate 1 Hz, was shot on the ITO side of the device. The photocurrent under the influence of applied electric field was monitored across a variable resistor using an oscilloscope. The mobilities of the charges were calculated using the relation  $\mu = d^2/Vt_{tr}$ , where  $d$  is the polymer film thickness,  $V$  is the applied voltage and  $t_{tr}$  is the transit time. The transit time was extracted by integration method.<sup>40</sup> The device architecture used was ITO/T1(0.11  $\mu\text{m}$ )/Al. The material was found to be hole transporting in nature. The transient photocurrent and variation of hole mobility with applied electric field is shown in Figure 6.12.

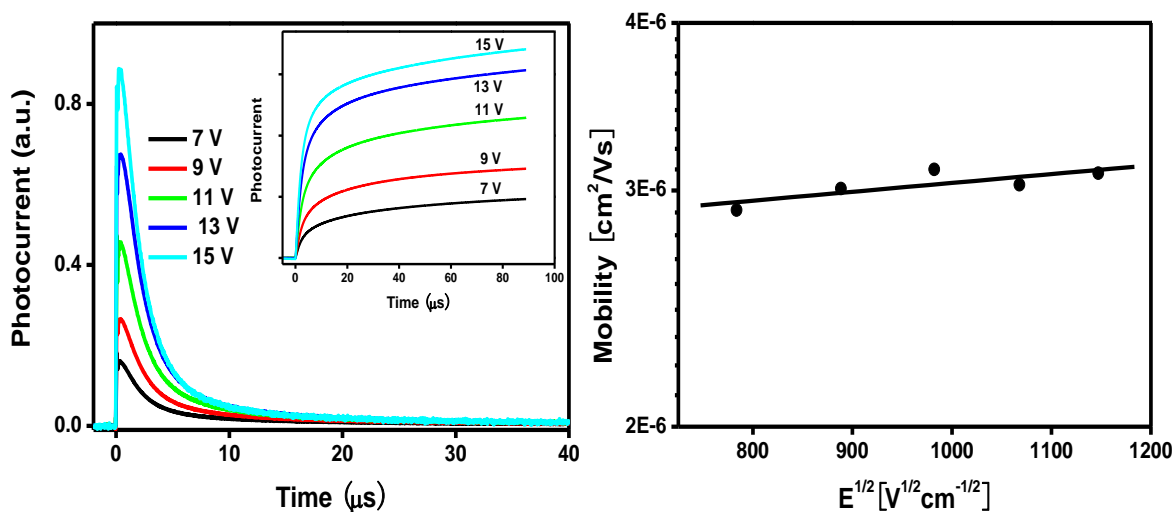


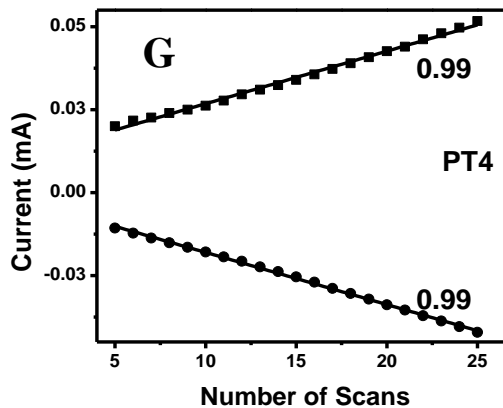
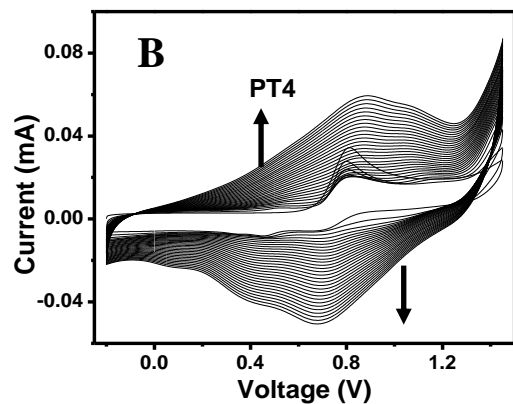
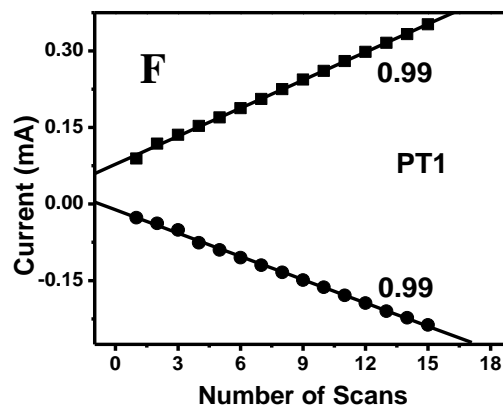
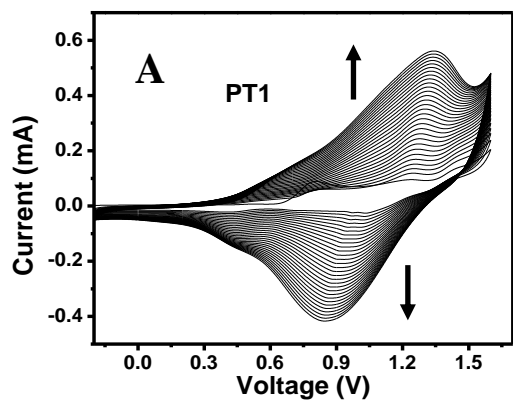
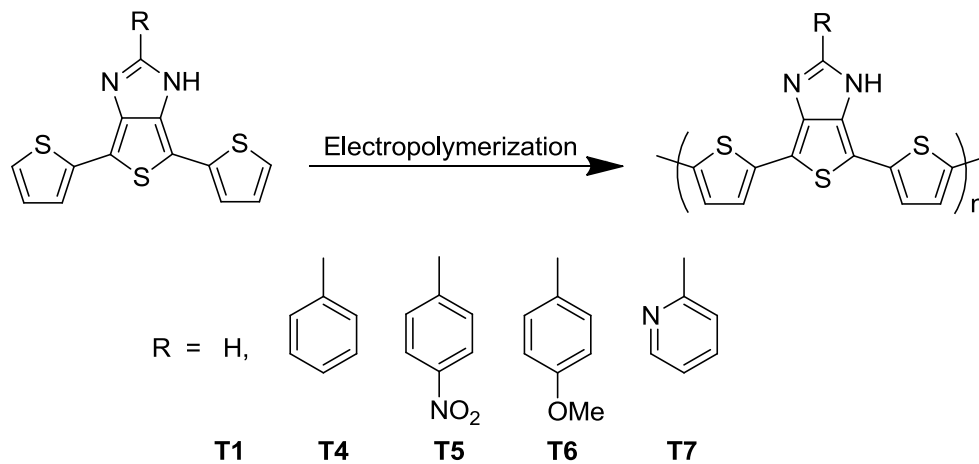
**Figure 6.12.** Linear plot of TOF hole transient for different applied voltages and inset shows the corresponding integrated plot (A). Variation of TOF hole mobility with applied electric field, solid line is a linear fit according to Pool-Frenkel equation (B)

It is clear from the Figure 6.12B that the hole mobility is not varying much with the electric field. The hole mobility was found to be  $3 \times 10^{-6} \text{ cm}^2/\text{V}$  at an applied electric field of  $1.14 \times 10^6 \text{ V/cm}$ . The zero field mobility was extracted from the Pool-Frenkel

relation ( $\mu = \mu_{(E=0)} \exp(\gamma E^{1/2})$  where  $\mu_{(E=0)}$  is the zero field mobility and  $\gamma$  is the slope of the field dependence of charge mobility)<sup>41</sup> and it was found to be  $2.6 \times 10^{-6} \text{ cm}^2/\text{Vs}$ .

### 6.3.10. Electropolymerization

All oligomers in the series except alkyl-substituted oligomers (**T2** and **T3**) are easily electropolymerized to form the corresponding low bandgap polymers (Scheme 6.4). The oligomers are polymerized from dichloromethane solution containing 0.1 M TBAPF<sub>6</sub> as supporting electrolyte. The polymerization was achieved by repetitive scanning of anodic potential in the range of -0.4 to 1.6 V. The potentiodynamic polymerization process of other monomers is shown in Figure 6.13. The polymerization occurred smoothly, which was evidenced by the appearance of new oxidation peak at a potential lower than the corresponding oligomers. The growth of polymer is indicated by a gradual increase in current during the potential cycle [Figure 6.13 (E - H)]. The polymerization resulted in a purple colored, uniform deposit of polymer on the working electrode. Electrodeposited polymer showed a homogenous coating and adhering to the electrode. The deposited polymer film was dedoped electrochemically and washed with dichloromethane to remove monomer and supporting electrolyte. The resulted polymer film was stable under ambient conditions. The oligomers **T2** and **T3** containing long alkyl chain showed lesser tendency to polymerize. This may due to the higher solubility of oxidized oligomers, which diffuse from the electrode surface preventing the formation of polymer.

**Scheme 6.4.** Electropolymerization of dithienothieno[3,4-*d*]imidazole based oligomers

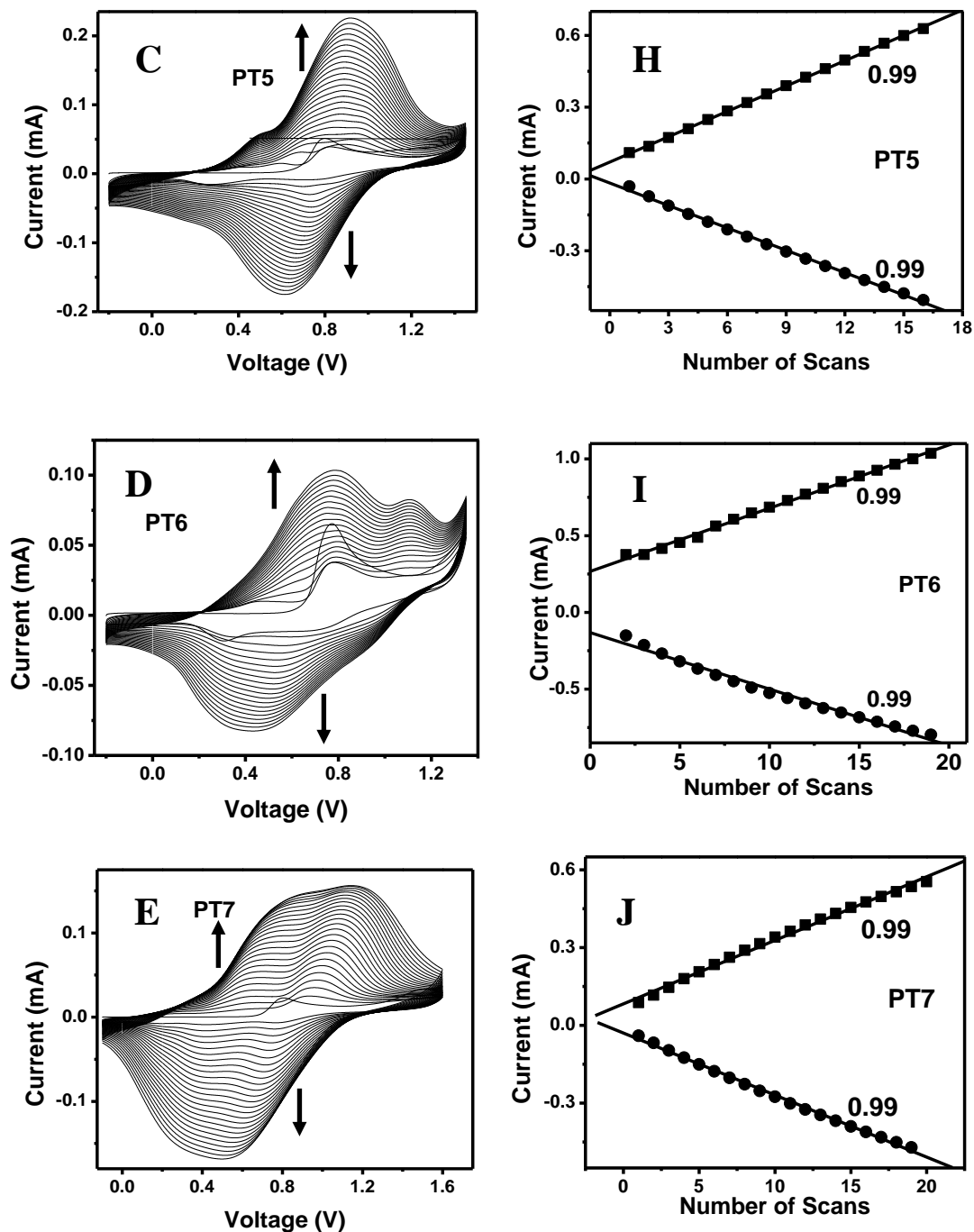


**Figure 6.13.** Electropolymerization of thieno[3,4-*d*]imidazole oligomers carried out at a scan rate of 100 mV/s, in dichloromethane containing 0.1 M TBAPF<sub>6</sub> as supporting electrolyte (A-E). Plot of current vs number of scans for the electropolymerization of thienoimidazole (F-J)

### 6.3.11. Optical and electrical properties of polymers

The absorption spectra of electropolymerised polymer films were recorded. All polymers showed a broad absorption in the visible region (Figure 6.14). Cyclic voltammogram of electropolymerised film on ITO electrode was recorded from monomer free electrolytic solution of dichloromethane (Figure 6.15). It is observed that these polymers show electrochromic behavior during anodic potential sweep. In these polymers electro-optic changes occurs in visible region with color switches from purple brown (neutral state) to sky blue (oxidized state) upon change in applied potential. All polymers showed broad quasi-reversible oxidation peak around 1.0 V. HOMO level calculated from oxidation onset and the calculated LUMO from absorption onset are represented in Table 6.4. Though HOMO of these polymers is low lying, they are stable in air. Poly **T1** showed very high lying HOMO compared all other aryl-substituted polymers. All polymers possess low bandgap (1.5 eV - 1.6 eV) and further their energy levels (HOMO and LUMO) are tuned by the substitution on imidazole ring.

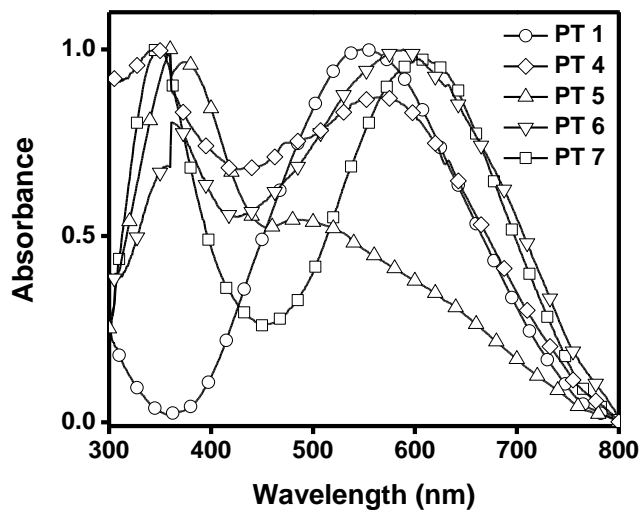


**Figure 6.14.** Absorption spectra of electropolymerized polymer film over ITO surface

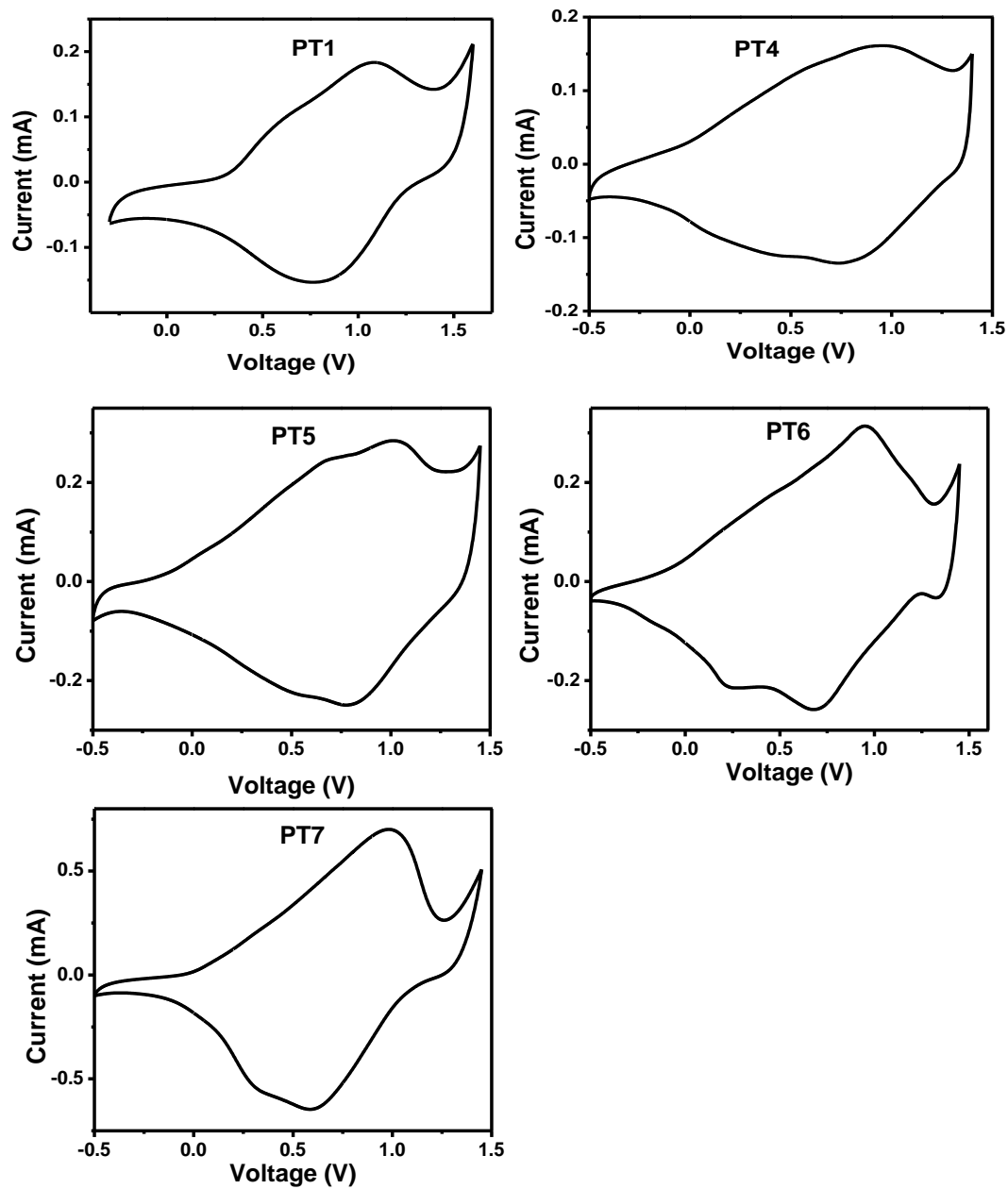


**Figure 6.15.** Cyclic voltammogram of electropolymerized films of poly(thieno[3,4-*d*]imidazole) in monomer free electrolyte at a scan rate of 100 mV/s

**Table 6.4.** Optoelectronic properties of electropolymerized dithienothieno[3,4-*d*]imidazole polymers

Polymers	$E_{\text{oxid}}$ (V)	$\lambda_{\text{max}}$ (nm)	$E_{\text{HOMO}}$ (eV)	$E_{\text{g}}$ (optical) (eV)	$E_{\text{LUMO}}^{\text{calc.}}$ (eV)	$E_{\text{onset oxid}}$ (V)	$\lambda_{\text{onset}}$ (nm)
<b>PT1</b>	1.1	550	-4.71	1.63	-3.08	0.31	760
<b>PT4</b>	0.95	565	-.427	1.61	-2.66	-0.13	770
<b>PT5</b>	1.02	488	-4.27	1.59	-2.68	-0.13	780
<b>PT6</b>	0.95	590	-4.27	1.58	-2.69	-0.135	786
<b>PT7</b>	1.0	609	-4.44	1.6	-2.84	0.04	775

#### 6.4. Conclusion

In summary, a new series of thiophene-based oligomers were synthesized and characterized in detail. The oligomers are highly planar and pyridine substituted oligomer (**T7**) arrange in close sandwich herringbone packing with a near perpendicular herringbone angle with a short contact of 3.38 Å. Oligomers are highly fluorescent with the solution state quantum yield ranging from 6% to 52 % depending on the substitution. Oligomers with electron donating substituents are highly fluorescent whereas with electron withdrawing substituents are less fluorescent / not emissive. The electronic spectra of these oligomers are sensitive to acid and base. A blue and red shift in absorption maxima was observed by the addition of TFA and sodium hydroxide respectively. Electrochemical properties conclude that these oligomers are highly stable with low-lying HOMO energy level with the bandgap in the range of 2.15-2.7 eV. Pyridine substituted oligomers (**T7**) sense metal ions like Ni<sup>2+</sup>, Cu<sup>2+</sup> and Zn<sup>2+</sup> with a



sharp color change. In addition, pyridine substituted oligomer in presence of metal ion sense amino acids. Preliminary charge transport studies on parent oligomer (**T1**) using time-of-flight photoconductivity method showed that the material is hole transporting in nature with a hole mobility of  $3 \times 10^{-6} \text{ cm}^2/\text{Vs}$  at an applied electric field of  $1.14 \times 10^6 \text{ V/cm}$ . Upon polymerization, these oligomers resulted in low band gap polymer with the band gap of around 1.6 eV. Incorporation of these polymers in organic photovoltaic application is also under progress.

## 6.5. References

---

- (1) (a) Zotti, G.; Zecchin, S.; Schiavon, G.; Vercelli, B.; Berlin, A.; Porzio, W. *Chem. Mater.* **2004**, *16*, 2091. (b) Meng, H.; Perepichka, D. F.; Wudl, F. *Angew. Chem.* **2003**, *115*, 682; *Angew. Chem. Int. Ed.* **2003**, *42*, 658. (c) Westenhoff, S.; Abrusci, A.; Feast, W. J.; Henze, O.; Kilbinger, A. F. M.; Schenning, A. P. H. J.; Silva, C. *Adv. Mater.* **2006**, *18*, 1281. (d) Henze, O.; Feast, W. J.; Gardebien, F.; Jonkheijm, P.; Lazzaroni, R.; Leclère, P.; Meijer, E. W.; Schenning, A. P. H. J. *J. Am. Chem. Soc.* **2006**, *128*, 5923. (e) Jeffries-EL, M.; Sauv e, G.; McCullough, R. D. *Adv. Mater.* **2004**, *16*, 1017.
- (2) (a) Mitschke, U.; B auerle, P. *J. Mater. Chem.* **2000**, *10*, 1471. (b) Rothberg, L. J.; Lovinger, A. J. *J. Mater. Res.* **1996**, *11*, 3174. (c) J ustel, T.; Nikol, H.; Ronda, C. *Angew. Chem.* **1998**, *110*, 3251; *Angew. Chem.; Int. Ed.* **1998**, *37*, 3084.
- (3) (a) Sariciftci, N. S.; Smilowitz, L.; Hegger, A. J.; Wudl, F. *Science* **1992**, *258*, 1474. (b) Wohrle, D.; Meissner, D. *Adv. Mater.* **1991**, *3*, 129. (c) Hall, J. J. M.; Walsh, C. A.; Greenham, N. C.; Marseglia, E. A.; Friend, R. H.; Morattii, S. S.; Holmes, A. B. *Nature*, **1995**, *376*, 498. (d) Videlot, C.; El Kassmi, A.; Ficou, D. *Solar Energy Mater. Solar Cells* **2000**, *63*, 69. (e) Fichou, D. *J. Mater. Chem.* **2000**, *10*, 571. (f) Norma, N.; Tsuzuki, T.; Shirota, Y. *Adv. Mater.* **1995**, *7*, 647.
- (4) (a) Forrest, S. R. *Chem. Rev.* **1997**, *97*, 1793. (b) Bao, Z.; Lovinger, A. J.; Brown, J. J. *J. Am. Chem. Soc.* **1998**, *120*, 207. (c) Horowitz, G.; Garnier, F.; Yassar, A.; Hajlaoui, R.; Kouki, F. *Adv. Mater.* **1996**, *8*, 52. (d) Dimitrakopoulos, C. D.; Malenfant, P. *Adv. Mater.* **2002**, *14*, 99. (e) Katz, H. E.; Lovinger, A. J.; Laquindanum, J. G. *Chem. Mater.* **1998**, *10*, 457. (e) Garnier, F.; Hajlaoui, R.; El Kassmi, A.; Harowitz, Laigre, L.; Porzio, W.; Armanini, M.; Provasoli, F. *Chem. Mater.* **1998**, *10*, 3334.
- (5) *Handbook of Oligo- and Polythiophene*; Fichou, D., Wiley-VCH: Weinheim, Germany, New York, 1999.
- (6) Roncali, J. *Chem. Rev.* **1997**, *97*, 173.
- (7) Baigent, D. R.; Hamer, P. J.; Friend, R. H.; Moratti, S. C.; Holmes, A. B. *Synth. Met.* **1995**, *71*, 2175.
- (8) Bundgaard, E.; Krebs, F. C. *Sol. Energy Mater. Sol. Cells* **2007**, *91*, 954.
- (9) (a) van Mullekom, H. A. M.; Vekemans, J. A. J. M.; Havinga, E. E.; Meijer, E. W. *Materials Science and Engineering* **2001**, *32*, 1. (b) Delgado, M. C. R.; Hern andez, V.; Navarrete, J. T. L.; Tanaka, S.; Yamashita, Y. *J. Phys. Chem. B* **2004**, *108*, 2516.
- (10) Wudl, F.; Kobayashi, M.; Heeger, A. J. *J. Org. Chem.* **1984**, *49*, 3382.

- (11) (a) Colaneri, N.; Kobayashi, M.; Heeger, A. J.; Wudl, F. *Synth. Met.* **1986**, *14*, 45. (b) Kobayashi, M.; Colaneri, N.; Boysel, M.; Wudl, F.; Heeger, A. J. *J. Chem. Phys.* **1985**, *82*, 5717.
- (12) Nayak, K.; Marynick, D. S. *Macromolecules* **1990**, *23*, 2237.
- (13) Kenning, D. D.; Rasmussen, S. C. *Macromolecules* **2003**, *36*, 6298
- (14) Roncali, J. *Chem. Rev.* **1992**, *92*, 711.
- (15) (a) Lorcy, D.; Cava, M. P. *Adv. Mater.* **1992**, *4*, 562. (b) Musinanni, S.; Ferraris, J. P. *J. Chem. Soc., Chem. Commun.* **1993**, 172. (c) Hoogmartens, I.; Adriaensens, P.; Carleer, R.; Vanderzande, D.; Martens, H.; Gelan, J. *Synth. Met.* **1992**, *51*, 219.
- (16) Tanaka, S.; Yamashita, Y. *Synth. Met.* **1993**, *55-57*, 1251. (b) A.K. Bakhshi, H. Ago, K. Yoshizawa, K. Tanaka, T. Yamabe, *J. Chem. Phys.* **1996**, *104*, 5528.
- (17) Kitamura, C.; Tanaka, S.; Yamashita, Y. *J. Chem. Soc., Chem. Commun.* **1994**, 1585.
- (18) Shaheen, S. E.; Vangeneugden, D.; Kiebooms, R.; Vanderzande, D.; Fromherz, T.; Padinger, F.; Brabec, C. J.; Sariciftci, N. S. *Synth. Met.* **2001**, *121*, 1583.
- (19) (a) Mammo, W.; Admassie, S.; Gadisa, A.; Zhang, F.; Inganäs, O.; Andersson, M. *Solar Energy Materials & Solar Cells*, **2007**, *91*, 1010. (b) Zhang, F. L.; Perzon, E.; Wang, X. J.; Mammo, W.; Andersson, M. R.; Inganäs, O. *Adv. Funct. Mater.* **2005**, *15*, 745. (c) Campos, L. M.; Tontcheva, A.; Günes, S.; Sonmez, G.; Neugebauer, H.; Sariciftci, N. S.; Wudl, F. *Chem. Mater.*, **2005**, *17*, 4031.
- (20) Kulkarni, A. P.; Zhu, Y.; Jenekhe, S. A. *Macromolecules*, **2008**, *41*, 339.
- (21) Blanco, R.; Gómez, R.; Seoane, C.; Segura, J. L.; Mena-Osteritz, E.; Bäuerle, P. *Org. Lett.* **2007**, *9*, 2171.
- (22) Kenning, D. D.; Mitchell, K. A.; Calhoun, T. R.; Funfar, M. R.; Sattler, D. J.; Rasmussen, S. C. *J. Org. Chem.* **2002**, *67*, 9073.
- (23) Crosby, G. A.; Demas, J. N. *J. Phys. Chem.* **1971**, *75*, 991.
- (24) Xia, Y.; Luo, J.; Deng, X.; Li, X.; Li, D.; Zhu, X.; Yang, W.; Cao, Y. *Macromol. Chem. Phys.* **2006**, *207*, 511.
- (25) Choudhury, L. H.; Parvin, T.; Khan, A. T. *Tetrahedron* **2009**, *65*, 9513.
- (26) Das, B.; Holla, H.; Srinivas, Y. *Tet. Lett.* **2007**, *48*, 61.
- (27) Bäuerle, P.; Götz, G.; Emerle, P.; Port, H. *Adv. Mater.* **1992**, *4*, 564.

- (28) van Bolhuis, F.; Winberg, H.; Havinga, E. E.; Meijer, E. W.; Staring, E. G. J. *Synth. Met.* **1989**, *30*, 381.
- (29) (a) Becker, R. S.; de Melo, J. S.; Macanita, A. L.; Elisei, F. *Pure Appl. Chem.* **1995**, *67*, 9. (b) Peng, Z.; *Polym. News* **2000**, *25*, 185.
- (30) (a) Barbarella, G.; Favaretto, L.; Sotgi, G.; Zambianchi, M.; Fattori, V.; Cocchi, M.; Cacialli, F.; Gigli, G.; Cingolani, R. *Adv. Mater.* **1999**, *11*, 1374. (b) Berlman, I. B. *J. Phys. Chem.* **1970**, *74*, 3085.
- (31) (a) Becker, R. S.; de Melo, J. S.; J. S.; Macanita, A.L.; Elisei, F. *J. Phys. Chem.* **1996**, *100*, 18683. (b) Rothberg, L. J.; Yan, M.; Papadimitrakopoulos, F.; Galvin, M. E.; Kwock, E. W.; Miller, T. M. *Synth. Met.* **1996**, *80*, 41.
- (32) (a) Ferraris, J. P.; Skiles, G. D. *Polymer* **1987**, *28*, 179. (b) Ferraris, J. P.; Andrus, R. G.; Hrcir, D. C. *J. Chem. Soc. Chem. Commun.* **1989**, 1318.
- (33) Bäuerle, P.; Götz, G.; Emerle, P.; Port, H. *Adv. Mater.* **1992**, *4*, 546.
- (34) Tanaka, S.; Yamashita, Y. *Chem. Mater.* **1996**, *8*, 570.
- (35) (a) Li, Y.; Ding, J.; Day, M.; Tao, Y.; Lu, J.; D'iorio, M. *Chem. Mater.* **2004**, *16*, 2165. (b) Leeuw, D. M.; Simenon, M. M. J.; Brown, A. R.; Einerhand, R. E. F. *Synth. Met.* **1997**, *87*, 53. (c) Cui, Y.; Zhang, X.; Jenkhe, S. A. *Macromolecules* **1999**, *32*, 3824.
- (36) (a) Yue, S, -M.; Xu, H, -B.; Ma, J, -F.; Su, Z, -M.; Kan, Y, -H.; Zhang, H, -J. *Polyhedron*, **2006**, *25*, 635-644. (b) Pachhunga, K.; Therrien, B.; Kreisel, K. A.; Yap, G. P. A.; Kollipara, M. R. *Polyhedron*, **2007**, *26*, 3638-3644.
- (37) (a) Czarnik, A. W.; *Fluorescent Chemosensors for Ion and Molecule Recognition*, American Chemical Society, Washington, DC, **1993**. (b) A. P. De Silva, A. P.; Gunaratne, H. Q. N.; Gunnlaugsson, T.; Huxley, A. J. M.; McCoy, C P.; Rademacher, J, T.; Rice, T. E. *Chem. Rev.* **1997**, *97*, 1515.
- (38) (a) Lakowicz, J. R. *Principles of Fluorescence Spectroscopy*, 2<sup>nd</sup> ed.; Plenum Press: New York, **1999**. (b) C. B. Murphy, C. B.; Zhang, Y.; Troxler, T.; Ferry, V.; Martin, J. J.; Jones Jr., W. E. *J. Phys. Chem. B.* **2004**, *108*, 1537-1543.
- (39) Li, Z.; Lou, X.; Li, Z.; Qin, J. *ACS Appl. Mater. Interfaces*, **2009**, *1*, 232.
- (40) Campbell, A, J.; Bradley, D. D. C. *Appl. Phys. Lett.*, **2001**, *79*, 2133.
- (41) Borsenberger, P, M.; Pautmeier, L.; Bässler, H. *J. Chem. Phys.* **1991**, *94*, 5447.

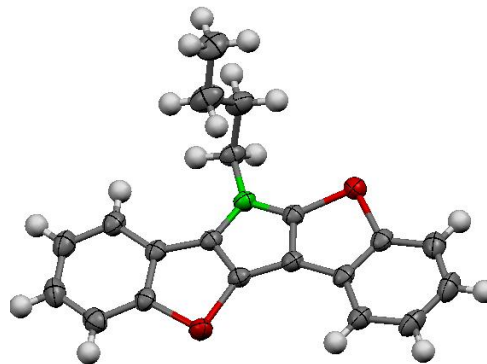
# ***APPENDIX***

## CRYSTALLOGRAPHIC INFORMATION

## CHAPTER 2

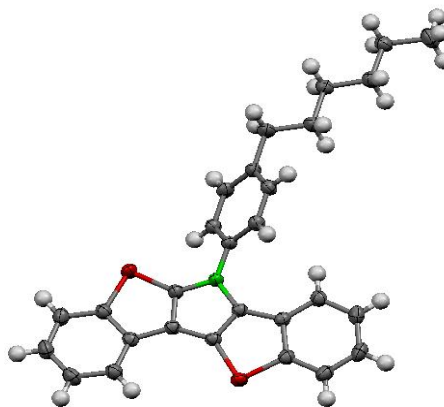
## Crystal data for compound 1a:

Empirical formula	C <sub>20</sub> H <sub>17</sub> N S <sub>2</sub>
Formula weight	335.47
Temperature	223(2) K
Wavelength	0.71073 Å
Crystal system	Orthorhombic
Space group	Pbca
Unit cell dimensions	a = 9.6873(6) Å    α = 90°. b = 17.8299(11) Å    β = 90°. c = 18.9630(11) Å    γ = 90°.
Volume	3275.4(3) Å <sup>3</sup>
Z	8
Density (calculated)	1.361 Mg/m <sup>3</sup>
Absorption coefficient	0.323 mm <sup>-1</sup>
F(000)	1408
Crystal size	0.46 × 0.34 × 0.16 mm <sup>3</sup>
Theta range for data collection	2.15 to 27.50°.
Index ranges	-11 ≤ h ≤ 12, -23 ≤ k ≤ 22, -23 ≤ l ≤ 24
Reflections collected	21892
Independent reflections	3761 [R(int) = 0.0444]
Completeness to theta = 27.50°	100.0 %
Absorption correction	Sadabs, (Sheldrick 2001)
Max. and min. transmission	0.9501 and 0.8655
Refinement method	Full-matrix least-squares on F <sup>2</sup>
Data / restraints / parameters	3761 / 0 / 210
Goodness-of-fit on F <sup>2</sup>	1.047
Final R indices [I > 2σ(I)]	R1 = 0.0620, wR2 = 0.1508
R indices (all data)	R1 = 0.0754, wR2 = 0.1592
Largest diff. peak and hole	1.223 and -0.306 e.Å <sup>-3</sup>



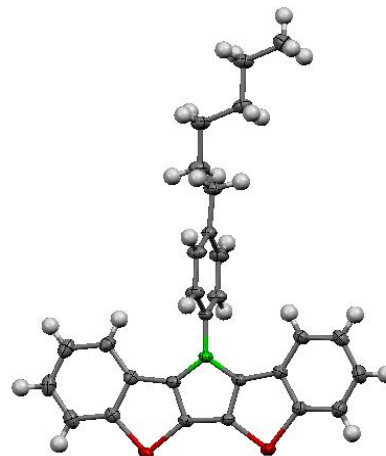
**Crystal data for compound 1b:**

Empirical formula	C <sub>28</sub> H <sub>25</sub> N S <sub>2</sub>
Formula weight	439.61
Temperature	223(2) K
Wavelength	0.71073 Å
Crystal system	Triclinic
Space group	P-1
Unit cell dimensions	a = 8.3728(5) Å    α = 102.4620(10)°. b = 11.6125(7) Å    β = 100.0360(10)°. c = 12.3650(7) Å    γ = 102.8830(10)°.
Volume	1112.69(11) Å <sup>3</sup>
Z	2
Density (calculated)	1.312 Mg/m <sup>3</sup>
Absorption coefficient	0.255 mm <sup>-1</sup>
F(000)	464
Crystal size	0.70 × 0.40 × 0.30 mm <sup>3</sup>
Theta range for data collection	1.73 to 27.49°.
Index ranges	-10 ≤ h ≤ 8, -14 ≤ k ≤ 15, -12 ≤ l ≤ 16
Reflections collected	7854
Independent reflections	5061 [R(int) = 0.0185]
Completeness to theta = 27.49°	99.4 %
Absorption correction	Sadabs, (Sheldrick 2001)
Max. and min. transmission	0.9273 and 0.8414
Refinement method	Full-matrix least-squares on F <sup>2</sup>
Data / restraints / parameters	5061 / 0 / 281
Goodness-of-fit on F <sup>2</sup>	1.067
Final R indices [I > 2σ(I)]	R1 = 0.0404, wR2 = 0.1132
R indices (all data)	R1 = 0.0453, wR2 = 0.1185
Largest diff. peak and hole	0.359 and -0.261 e.Å <sup>-3</sup>



**Crystal Data for compound 2b**

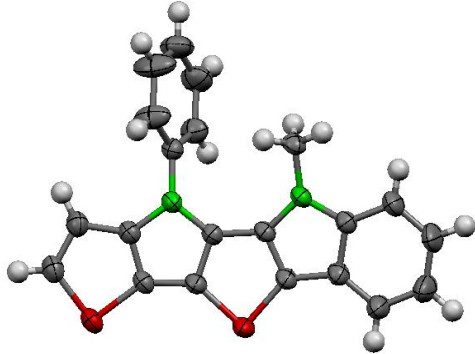
Empirical formula	C <sub>28</sub> H <sub>25</sub> N S <sub>2</sub>	
Formula weight	439.61	
Temperature	223(2) K	
Wavelength	0.71073 Å	
Crystal system	Triclinic	
Space group	P-1	
Unit cell dimensions	a = 10.4421(6) Å	α = 81.7120(10)°.
	b = 11.0184(6) Å	β = 68.1210(10)°.
	c = 11.3293(6) Å	γ = 66.5690(10)°.
Volume	1109.85(11) Å <sup>3</sup>	
Z	2	
Density (calculated)	1.315 Mg/m <sup>3</sup>	
Absorption coefficient	0.256 mm <sup>-1</sup>	
F(000)	464	
Crystal size	0.60 × 0.46 × 0.22 mm <sup>3</sup>	
Theta range for data collection	1.94 to 27.50°.	
Index ranges	-13 ≤ h ≤ 13, -14 ≤ k ≤ 14, -14 ≤ l ≤ 14	
Reflections collected	14495	
Independent reflections	5101 [R(int) = 0.0236]	
Completeness to theta = 27.50°	99.9 %	
Absorption correction	Sadabs, (Sheldrick 2001)	
Max. and min. transmission	0.9458 and 0.8615	
Refinement method	Full-matrix least-squares on F <sup>2</sup>	
Data / restraints / parameters	5101 / 0 / 281	
Goodness-of-fit on F <sup>2</sup>	1.045	
Final R indices [I > 2σ(I)]	R1 = 0.0386, wR2 = 0.1012	
R indices (all data)	R1 = 0.0415, wR2 = 0.1038	
Largest diff. peak and hole	0.351 and -0.412 e.Å <sup>-3</sup>	





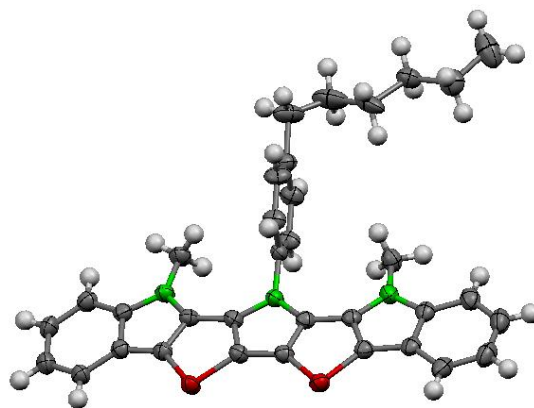
## CHAPTER 3

## Crystal data for compound 9b:

Empirical formula	$C_{22.75} H_{18} Cl_{0.5} N_2 S_2$	
Formula weight	401.24	
Temperature	223(2) K	
Wavelength	0.71073 Å	
Crystal system	Monoclinic	
Space group	C2/c	
Unit cell dimensions	$a = 29.2045(15) \text{ \AA}$ $\alpha = 90^\circ$ $b = 13.3826(7) \text{ \AA}$ $\beta = 99.7000(10)^\circ$ $c = 11.4733(6) \text{ \AA}$ $\gamma = 90^\circ$	
Volume	$4420.0(4) \text{ \AA}^3$	
Z	8	
Density (calculated)	$1.206 \text{ Mg/m}^3$	
Absorption coefficient	$0.310 \text{ mm}^{-1}$	
F(000)	1672	
Crystal size	$0.38 \times 0.26 \times 0.10 \text{ mm}^3$	
Theta range for data collection	2.37 to $27.50^\circ$	
Index ranges	$-37 \leq h \leq 33$ , $-11 \leq k \leq 17$ , $-14 \leq l \leq 14$	
Reflections collected	15417	
Independent reflections	5077 [R(int) = 0.0295]	
Completeness to theta = $27.50^\circ$	99.9 %	
Absorption correction	Semi-empirical from equivalents	
Max. and min. transmission	0.9696 and 0.8912	
Refinement method	Full-matrix least-squares on $F^2$	
Data / restraints / parameters	5077 / 11 / 263	
Goodness-of-fit on $F^2$	1.101	
Final R indices [I > 2sigma(I)]	R1 = 0.0696, wR2 = 0.2045	
R indices (all data)	R1 = 0.0800, wR2 = 0.2147	
Largest diff. peak and hole	0.865 and $-0.366 \text{ e.\AA}^{-3}$	

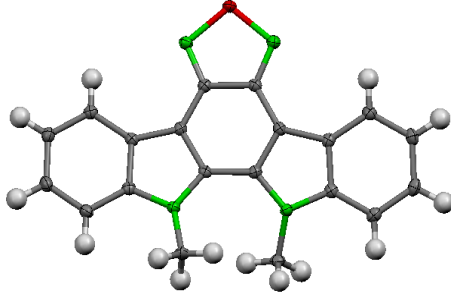
**Crystal data of compound 10a:**

Empirical formula	$C_{34}H_{31}N_3S_2$
Formula weight	545.74
Temperature	223(2) K
Wavelength	0.71073 Å
Crystal system	Triclinic
Space group	P-1
Unit cell dimensions	$a = 10.8111(6)$ Å $\alpha = 95.1190(10)^\circ$ . $b = 11.6692(6)$ Å $\beta = 102.5780(10)^\circ$ . $c = 11.6801(6)$ Å $\gamma = 103.2940(10)^\circ$ .
Volume	$1384.49(13)$ Å <sup>3</sup>
Z	2
Density (calculated)	$1.309$ Mg/m <sup>3</sup>
Absorption coefficient	$0.221$ mm <sup>-1</sup>
F(000)	576
Crystal size	$0.56 \times 0.36 \times 0.16$ mm <sup>3</sup>
Theta range for data collection	$1.81$ to $27.50^\circ$ .
Index ranges	$-14 \leq h \leq 14$ , $-15 \leq k \leq 15$ , $-15 \leq l \leq 15$
Reflections collected	18102
Independent reflections	6353 [R(int) = 0.0353]
Completeness to theta = $27.50^\circ$	99.8 %
Absorption correction	Empirical
Max. and min. transmission	0.9654 and 0.8860
Refinement method	Full-matrix least-squares on F <sup>2</sup>
Data / restraints / parameters	6353 / 7 / 373
Goodness-of-fit on F <sup>2</sup>	1.032
Final R indices [I > 2sigma(I)]	R1 = 0.0561, wR2 = 0.1423
R indices (all data)	R1 = 0.0677, wR2 = 0.1507
Largest diff. peak and hole	$0.569$ and $-0.396$ e.Å <sup>-3</sup>



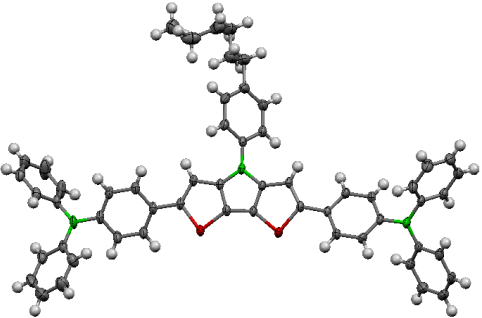
## CHAPTER 4

## Crystal data for compound 5a:

Empirical formula	$C_{20}H_{14}N_4S$	
Formula weight	342.41	
Temperature	100(2) K	
Wavelength	0.71073 Å	
Crystal system	Monoclinic	
Space group	P2(1)/c	
Unit cell dimensions	$a = 8.9001(4)$ Å	$\alpha = 90^\circ$
	$b = 11.3943(5)$ Å	$\beta = 91.9020(10)^\circ$
	$c = 14.9742(7)$ Å	$\gamma = 90^\circ$
Volume	$1517.70(12)$ Å <sup>3</sup>	
Z	4	
Density (calculated)	1.499 Mg/m <sup>3</sup>	
Absorption coefficient	0.224 mm <sup>-1</sup>	
F(000)	712	
Crystal size	0.74 x 0.70 x 0.30 mm <sup>3</sup>	
Theta range for data collection	2.25 to 27.49°	
Index ranges	$-10 \leq h \leq 11$ , $-11 \leq k \leq 14$ , $-18 \leq l \leq 19$	
Reflections collected	10499	
Independent reflections	3486 [R(int) = 0.0189]	
Completeness to theta = 27.49°	100.0 %	
Absorption correction	Sadabs, (Sheldrick 2001)	
Max. and min. transmission	0.9359 and 0.8519	
Refinement method	Full-matrix least-squares on F <sup>2</sup>	
Data / restraints / parameters	3486 / 0 / 228	
Goodness-of-fit on F <sup>2</sup>	1.045	
Final R indices [I > 2sigma(I)]	R1 = 0.0368, wR2 = 0.0962	
R indices (all data)	R1 = 0.0382, wR2 = 0.0972	
Largest diff. peak and hole	0.402 and -0.283 e.Å <sup>-3</sup>	

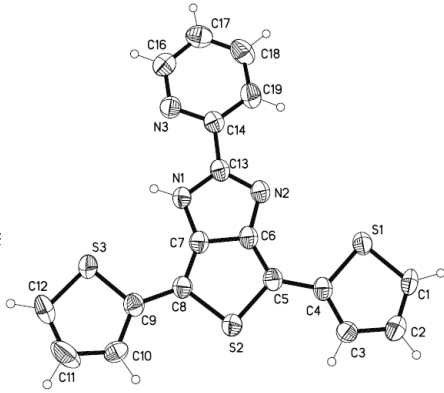
## CHAPTER 5

## Crystal data for DTP-TPA

Empirical formula	C <sub>60</sub> H <sub>55</sub> N <sub>3</sub> O <sub>2</sub> S <sub>2</sub>	
Formula weight	914.19	
Temperature	223(2) K	
Wavelength	0.71073 Å	
Crystal system	Triclinic	
Space group	P-1	
Unit cell dimensions	a = 12.5499(5) Å      α = 88.6590(10)° b = 14.0994(6) Å      β = 71.1660(10)° c = 14.8676(6) Å      γ = 80.8330(10)°	
Volume	2457.00(17) Å <sup>3</sup>	
Z	2	
Density (calculated)	1.236 Mg/m <sup>3</sup>	
Absorption coefficient	0.156 mm <sup>-1</sup>	
F(000)	968	
Crystal size	0.60 x 0.20 x 0.10 mm <sup>3</sup>	
Theta range for data collection	1.46 to 27.50°	
Index ranges	-16 ≤ h ≤ 16, -18 ≤ k ≤ 18, -19 ≤ l ≤ 19	
Reflections collected	32075	
Independent reflections	11283 [R(int) = 0.0354]	
Completeness to theta = 27.50°	99.9 %	
Absorption correction	Semi-empirical from equivalents	
Max. and min. transmission	0.9846 and 0.9124	
Refinement method	Full-matrix least-squares on F <sup>2</sup>	
Data / restraints / parameters	11283 / 31 / 605	
Goodness-of-fit on F <sup>2</sup>	1.093	
Final R indices [I > 2σ(I)]	R1 = 0.0714, wR2 = 0.1847	
R indices (all data)	R1 = 0.0847, wR2 = 0.1942	
Largest diff. peak and hole	0.921 and -0.437 e.Å <sup>-3</sup>	

## CHAPTER 6

## Crystal data for compound T7

Empirical formula	$C_{18} H_{11} N_3 S$	
Formula weight	365.48	
Temperature	223(2) K	
Wavelength	0.71073 Å	
Crystal system	Monoclinic	
Space group	P2(1)/n	
Unit cell dimensions	$a = 13.0639(7)$ Å	$\alpha = 90^\circ$ .
	$b = 9.4536(5)$ Å	$\beta = 108.5220(10)^\circ$ .
	$c = 13.8401(7)$ Å	$\gamma = 90^\circ$ .
Volume	$1620.73(15)$ Å <sup>3</sup>	
Z	4	
Density (calculated)	1.498 Mg/m <sup>3</sup>	
Absorption coefficient	0.461 mm <sup>-1</sup>	
F(000)	752	
Crystal size	0.60 x 0.40 x 0.12 mm <sup>3</sup>	
Theta range for data collection	1.87 to 27.50°.	
Index ranges	$-16 \leq h \leq 16$ , $-11 \leq k \leq 12$ , $-17 \leq l \leq 17$	
Reflections collected	11176	
Independent reflections	3703 [R(int) = 0.0266]	
Completeness to theta = 27.50°	99.7 %	
Absorption correction	Sadabs, (Sheldrick 2001)	
Max. and min. transmission	0.9467 and 0.7694	
Refinement method	Full-matrix least-squares on F <sup>2</sup>	
Data / restraints / parameters	3703 / 94 / 277	
Goodness-of-fit on F <sup>2</sup>	1.034	
Final R indices [I > 2sigma(I)]	R1 = 0.0414, wR2 = 0.1074	
R indices (all data)	R1 = 0.0461, wR2 = 0.1115	
Largest diff. peak and hole	0.336 and -0.299 e.Å <sup>-3</sup>	

## LIST OF PUBLICATIONS

1. **Balaji, G.**; Phua, D. I.; Shim, W. L.; Valiyaveettil, S. “*Synthesis and Characterization of Unsymmetric Indolodithienopyrrole and Extended Diindolodithienopyrrole*”, *Org. Lett.* **2010**, *12*, 232.
2. **Balaji, G.**; Shim, W. L.; Parameswaran, M.; Valiyaveettil, S. “*Thiadiazole Fused Indolo[2,3-a]carbazole Based Oligomers and Polymer*”, *Org. Lett.* **2009**, *11*, 4450-4453.
3. **Balaji, G.**; Valiyaveettil, S. “*Synthesis and Properties of Symmetric and Unsymmetric Dibenzothienopyrroles*”, *Org. Lett.* **2009**, *11*, 3358-3361.
4. Parameswaran, M.; **Balaji, G.**; Jin, T. M.; Vijila, C.; Vadukumpully, S.; Furong, Z.; Valiyaveettil, S. “*Charge Transport Studies in Fluorene - Dithieno[3,2-b:2',3'-d]pyrrole Oligomer using Time-of-Flight Photoconductivity Method*”, *Org. Electron.*, **2009**, *10*, 1534-1540.
5. **Balaji, G.**; Parameswaran, M.; Jin, T. M.; Vijila, C.; Furong, Z.; Valiyaveettil, S. “*Synthesis and Hole-transporting Properties of Highly Fluorescent N-aryl Dithieno[3,2-b:2',3'-d]pyrrole Based Oligomers*”. *J. Phys. Chem. C* **2010**, *114*, 4628.
6. **Balaji, G.**; Parameswaran, M.; Setyono, D.; Valiyaveettil, S. “*Thieno[3,4-d]imidazole-bithiophene – Versatile Building Block For Low Bandgap Polymers*”. (Submitted to *Org. Lett.*).

## MANUSCRIPT UNDER PREPARATION

7. **Balaji, G.**; Parameswaran, M.; Jin, T. M.; Vijila, C.; Valiyaveettil, S. “*Synthesis and Transport Properties of N-Aryl Dithieno[3,2-b;2,3-d]Pyrrole Based Polymers*”. (Manuscript under preparation).
8. **Balaji, G.**; Parameswaran, M.; Valiyaveettil, S. “*Thenieno[3,4-d]Imidazole Based Low Band Gap Polymers*”. (Manuscript under preparation).
9. **Balaji, G.**; Parameswaran, M.; Jin, T. M.; Vijila, C.; Valiyaveettil, S. “*Synthesis and Transport Properties of Phenylene-Bithiophene Based Co-Polymers*”. (Manuscript under preparation).
10. Basheer, C.; **Balaji, G.**; Hui, C. S.; Lee, H. K.; Valiyaveettil, S. “*Novel On-Site Sampling Procedure Using Functional Polymer-Coated Multi Fibers Microextraction of Organophosphorus Pesticides in Sea Water*”. (To be submitted to *Journal of Chromatography: A*).

## NON-REFERRED ARTICLES

11. **Balaji, G.**; Vajiravelu, S.; Valiyaveetil, S. “*Light Emitting Conjugated Polymers Incorporating Thiophene-Phenylene Monomers*”, *Polymer Preprints* **2008**, 49, 738.
12. Vajiravelu, S.; **Balaji, G.**; Valiyaveetil, S. “*Interaction of Carbazole Substituted Unsymmetrical Coronene Oligomers with Perylene Bisimide Molecules*”, *Polymer Preprints* **2008**, 49, 628.

## CONFERENCES

1. **Balaji, G.**; Valiyaveetil, S. “*Synthesis and Characterization of Thienopyrrole Based Heteroacenes*” Proc. 6<sup>th</sup> Singapore International Chemical Conference (SICC-6), Singapore Dec. 15-18 2009.
2. **Balaji, G.**; Twan, C. H.; Valiyaveetil, S. “*Swivel-Cruciform Oligothiophene Trimer*” Proc. 6<sup>th</sup> Singapore International Chemical Conference (SICC-6), Singapore Dec. 15-18 2009.
3. **Balaji, G.**; Parameswaran, M.; Setyono, D.; Valiyaveetil, S. Oligothieno[3,4-*d*]imidazoles for Electronic and Sensing Applications Proc. International Conference on Materials for Advanced Technologies (ICMAT), **Singapore, July - 2009. (Oral Presentation)**
4. **Balaji, G.**; Valiyaveetil, S. Synthesis, Structure and Properties of Symmetric and Asymmetric Dibenzothienopyrroles, Proc. 4<sup>th</sup> Mathematical and Physical Sciences Graduate Congress (MPSGC), **Singapore, Dec – 2008.**
5. **Balaji, G.**; Khanijou, J. K.; Sivaraman, J.; Valiyaveetil, S. Extraction and Characterization of Novel Bioactive Compounds from *Ehretia Buxifolia*, 13<sup>th</sup> Biological Sciences Graduate Congress (BSGC), **Singapore, Dec - 2008.**
6. **Balaji, G.**; Vajiravelu, S.; Valiyaveetil, S. Light Emitting Conjugated Polymers Incorporating Thiophene-Phenylene Monomers, Proc. 236<sup>th</sup> ACS National Meeting, Philadelphia, PA, **United States, Aug - 2008.**
7. Vajiravelu, S.; **Balaji, G.**; Valiyaveetil, S. Interaction of Carbazole Substituted Unsymmetrical Coronene Oligomers with Perylene Bisimide Molecules, Proc. 236<sup>th</sup> ACS National Meeting, Philadelphia, PA, **United States, Aug - 2008.**
8. **Balaji, G.**; Valiyaveetil, S. Light Emitting Conjugated Polymers Incorporating Thiophene-Phenylene Monomers, Proc. International Conference on Advanced Materials (ICAM), **India, Feb - 2008.**
9. **Balaji, G.**; Valiyaveetil, S. Interesting Series of Light Emitting Conjugated Polymers Incorporating Thiophene-Phenylene Monomers, Proc. 3<sup>rd</sup> Mathematical and Physical Sciences Graduate Congress (MPSGC), Kuala Lumpur, **Malaysia, Dec - 2007.**